ADSORPTION ON GOLD: EFFECTS ON SURFACE MORPHOLOGY AND REACTIVITY

A thesis presented by

THOMAS ARTHUR BAKER

to

The Department of Chemistry and Chemical Biology

in partial fulfillment of the requirements

for the degree of

Doctor of Philosophy

in the subject of

Chemical Physics

HARVARD UNIVERSITY

Cambridge, Massachusetts

May 2009

Dissertation Advisors: Professors Efthimios Kaxiras and Cynthia M. Friend

Thomas Arthur Baker

ADSORPTION ON GOLD: EFFECTS ON SURFACE MORPHOLOGY AND REACTIVITY

ABSTRACT

Computational tools are used in conjunction with experiments to understand adsorption and reactions on gold surfaces. We focus on systems important for oxidation, a class of reactions gold can perform quite readily. Experimental results have illustrated that the structure of gold is sensitive to adsorbate type and coverage, temperature, and many other factors. We find the adsorption of atomic oxygen and chlorine can significantly affect the morphology of the surface, either by favorably interacting with defects on the surface or by incorporating gold into the adsorbate layer, a process that is energetically favorable at higher coverages. The adsorbate-gold interaction becomes more covalent upon gold incorporation, which lowers the partial negative charge on the adsorbate, allowing for closer packing on the surface. The temperature dependence on the oxygen-gold interaction motivated the use of *ab-initio* molecular dynamics to model the dynamic surface modification during adsorption of atomic oxygen. We successfully match calculated vibrational spectra with experimental high-resolution electron energy loss spectroscopy results and suggest chemisorbed oxygen (oxygen bound in a locally flat three-fold coordination site) as the reactive species for oxidation on the surface. Since reactivity is closely related to surface morphology we studied the reaction of propene

with atomic oxygen on different defect covered gold surfaces. Reaction barriers for allylic hydrogen abstraction and oxametallacycle formation can differ by at least a factor of two and different pathways can be selected by modifying the surface structure. Furthermore, we find the correct pathway for phenol formation on cyclohexene and use *ab-initio* molecular dynamics to model the oxygen-covered gold surface for the oxidation of CO. We qualitatively reproduce experimental trends in reactivity and gain insight into the mechanism of CO oxidation on the oxygen-covered gold surface, confirming our previous result that chemisorbed oxygen is the reactive species on the surface.

TABLE OF CONTENTS

PART III – APPENDIX

ACKNOWLEDGEMENTS

‘To give anything less than your best, is to sacrifice the gift’

-Steve Prefontaine

It *is* quite a gift. But I do not mean a natural physical talent or intellect, but rather the gift of great teachers, friends, co-workers, family, and mentors who were extremely instrumental in my growth as a scientist.

I’ve been truly blessed to have some incredible mentors. Brett Criswell (Central Columbia High School) inspired me to study science, cultivated my interest, gave me room to explore, and was always willing to discuss new ideas with me as I grew during those important times as an adolescence. Ronald See (Indiana University of Pennsylvania) introduced me to a rigorous treatment of science and chemistry. He taught me most of the fundamental concepts of chemistry and how to apply those to solving a scientific problem. He taught me to believe in myself and he never seemed to think there was a ceiling to my potential. Along with being a wonderful advisor, he was a great friend, teaching me some of the finer points of life. Cynthia Friend and Tim Kaxiras (Harvard University) have been incredible advisors during my Ph.D work. They have taught me how to *do* science and how to make an impact. I have learned a great deal from them. I have been extremely lucky that they are dedicated advisors who care deeply about the well-being of their students. Any extremely busy professor who offers to buy you groceries when you have been deathly ill for a week is ok in my book. I also appreciate the help of Alán Aspuru-Guzik (Harvard University) who has been almost a third advisor, going incredibly out of his way to offer advice, write letters, and look out for me. I can’t thank him enough for all his help.

I have had the pleasure of working with people a lot smarter than me from whom I have learned a great deal: Lauren Benz, Anne Co, Xingyi Deng, Maria Fyta, Weiwei Gao, Jan Haubrich, Stephen Jensen, Byoung-Koun Min, Andreas Klust, Xiaoying Liu, Sheng Meng, Yina Mo, Dilini Pinnaduwage, Su Ying Quek, Ryan Quiller, Mike Stopa, Weili Wang, Bingjun Xu, Ling Zhou, and Wenguang Zhu. I thank everyone for all the help over the years.

I thank the following organizations for their financial or computational support; this is your tax dollars at work: National Science Foundation (Graduate School Fellowship and MRSEC), Department of Energy, National Nanotechnology Infrastructure Network, Teragrid, Harvard SEAS HPC, and Harvard FAS HPTC.

Finally, I thank some of my closer friends (Brian and Chun) for their support and humor. I thank Dilini for being a passionate and great friend who has always been there for me. I thank my family for their support and belief in me and finally I thank again all those who have helped and inspired me (and apologize for those I failed to mention) to complete this thesis.

GLOSSARY OF ACRONYMS

AIMD	*Ab-initio* Molecular Dynamics
BOMD	Born-Oppenheimer Molecular Dynamics
CN	Coordination Number
DFT	Density Function Theory
HREELS	High-Resolution Electron Energy Loss Spectroscopy
GGA	Generalized Gradient Approximation
KS	Kohn-Sham
LDA	Local Density Approximation
LEED	Low Energy Electron Diffraction
ML	Monolayer
PDOS	Partial Density of States
PBE	Perdew-Burke-Ernzerhof exchange-correlation functional
PW91	Perdew-Wang 91 exchange-correlation functional
RPBE	Revised-Perdew-Burke-Ernzerhof exchange-correlation functional
STM	Scanning Tunneling Microscopy
VASP	Vienna *Ab-initio* Simulation Package
XPS	X-ray Photoelectron Spectroscopy

CHAPTER 1

INTRODUCTION

It can be argued that for any heterogeneous system, **all** the important science occurs at the interface or the surface between two phases. Corrosion of a metal occurs at the metal-air (or liquid) interface, ion-channels located in the protein lipid bilayer at the surface of a cell regulate salt content, and even the interface between land and the ocean is typically prime real estate. The interesting processes occurring at interfaces, however, present challenges for experimentalists and theorists to explore, model, and describe. For example, a statistical mechanical treatment reserved for the bulk of a material can fail at the important interface. Often a thermodynamic equilibrium is not established at an interface because of the dynamic chemical and physical phenomena occurring at the surface. Nevertheless, both experimental and theoretical tools have been developed and are routinely used to understand and study important surfaces.

We use such tools in this thesis to understand the surface of gold. Gold is typically thought as a 'noble' metal: unreactive and stable. However in the 1980s, Haruta and co-workers discovered that Au could be reactive and used as a heterogeneous catalyst, specifically for the oxidation of CO[1] and propene[2]. However the exact nature of gold's catalytic activity and the mechanism by which gold can oxide reagents is not completely known. To understand the reactivity of gold, this work is split into two parts.

In the first part, *Fundamental Understanding of Adsorption*, we study the adsorption of chlorine and oxygen on the Au(111) surface. We gain a fundamental understanding in Chapter 3 of the type of bond created between chlorine and the gold

surface, finding that the interaction is covalent in nature, in contrast to the binding of most other halogens on metal surfaces. In chapter 4, we study the adsorption of chlorine on gold defects. The motivation for this is the importance of defects such as steps, adatoms, and vacancies on Au(111), especially since it is known that a wide variety of atoms can lift the herringbone reconstruction and pull gold atoms from the surface. In this chapter, we find that chlorine prefers to bind with defects and can stabilize vacancies that are formed on the surface. In chapter 5, we combine experimental results and density functional theory calculations to study the formation of surface chlorine structures. We find that gold incorporation into the chlorine overlayer depends on the coverage, with coverages above ~0.33 ML producing gold adatoms. In chapters 6-8, we turn our attention to oxygen adsorption and compare our results with those for chlorine adsorption, bringing forth similarities and key differences between the two. In chapter 6, we observe a favorable interaction of oxygen with defects such as steps and vacancies, similar to what was observed for chlorine. However, in contrast to chlorine, oxygen does not favorability interact with adatoms or a high number of gold vacancies. In chapter 5, we find that chlorine can form well-ordered, stable structures as evidenced by STM. The adsorption of oxygen, on the other hand, is very chaotic, disordered, and dynamic. This motivated the use of *ab-initio* molecular dynamics in chapter 7 to model the dynamic surface modification during adsorption of atomic oxygen. In this chapter we successfully calculate vibrational spectra consistent with experimental HREELS results and suggest that chemisorbed oxygen is the reactive species for oxidation on the surface. In the final chapter of Part I we improve our fundamental understanding of gold incorporation into a chlorine or oxygen adsorbate layer. We use charge density and partial density of states

plots to understand stabilization and bonding characteristics of chlorine and oxygen at higher coverages.

In the second part of this thesis, *Applications to Reactivity and Catalysis*, we apply understanding gained from the first part towards reactions on gold surfaces. In chapters 4 and 6 we learned that defects can affect the adsorption of chlorine and oxygen. In chapter 9, we study the affect of these same defects on the reaction of propene on oxygen covered Au(111). Not surprisingly, defects can play a significant role and we find that reaction barriers can differ by at least a factor of two depending on the nature of the defect. In chapter 10, we study phenol formation on cyclohexene. Finally in chapter 11, we use AIMD to study the oxygen-covered Au(111) surface, concentrating on the oxidation of CO. We are able to qualitatively reproduce experimental trends and gain insight into the mechanism of CO oxidation on the oxygen-covered gold surface.

References:

[1] M. Haruta, N. Yamada, T. Kobayashi, S. Iijima, *J. Catal.* **1989**, *115*, 301.

[2] T. Hayashi, K. Tanaka, M. Haruta, *J. Catal.* **1998**, *178*, 566.

CHAPTER 2

THEORETICAL APPROACH

The theoretical modeling of processes occurring at surfaces is extremely important. This modeling can help explain and interpret results obtained experimentally, test properties not attainable directly by experiments, and predict the characteristics of a nearly infinite set of new systems. However, doing so requires a careful and accurate treatment of the system under study.

Most processes occurring at surfaces are atomic scale in nature and involve complicated chemical interactions. Typically bonds are broken or formed and adsorbates cause subtle changes to the electronic structure of the surface. These and many other interactions on the surface require an accurate quantum mechanical treatment. The development of density functional theory (DFT) has resulted in a tool for accurately yet computationally cheaply solving the electronic structure of a system. The electronic structure can provide very useful information including: adsorption energies, surface energies, global and local minima structure configurations, charges and charge transfer, vibrational frequencies, reaction barriers, and many other properties. In the remainder of chapter 2, we will briefly describe DFT along with molecular dynamics which are two methods that are extensively employed in the work described in this thesis.

2.1 Schrödinger Equation

Solving the electronic structure of a system ultimately hinges upon an approximate solution to the many-body Schrödinger equation[1,2]:

$$\hat{H}\Psi = \hat{E}\Psi \tag{2.1.1}$$

where Ψ is the many-body wave function and $\hat{H}$ is the many-body Hamiltonian. For a molecular system this Hamiltonian is comprised of several parts including the kinetic energy of the ions and electrons, the nuclei-nuclei interactions, the electron-electron interactions, and the electron-nuclei interaction (commonly called the external potential). The Hamiltonian split into these terms is:

$$\hat{H} = \hat{T}_I + \hat{T}_i + \hat{V}_{I,I} + \hat{V}_{i,i} + \hat{V}_{\text{ext}} \tag{2.1.2}$$

where uppercase *I* represents nuclei and lowercase *i* represents electrons. However, because the motion of the nuclei is much slower compared to the motion of electrons, we will employ the Born-Oppenheimer approximation and disregard nuclear motion[3]. Our Hamiltonian now only contains terms important for solving the electronic structure:

$$\hat{H} = \hat{T} + \hat{V}_{i,i} + \hat{V}_{\text{ext}} \tag{2.1.3}$$

where the subscripts on $\hat{T}$ have been removed since it is clear that we are now only dealing with electrons. The terms in the above Hamiltonian are given as:

$$\hat{T} = \frac{\hbar}{2m}\sum_i \nabla_i^2 \tag{2.1.4}$$

$$\hat{V}_{i,i} = \frac{e^2}{2}\sum_i \sum_{j,i\neq j} \frac{1}{\left|\mathrm{r}_i - \mathrm{r}_j\right|} \tag{2.1.5}$$

$$\hat{V}_{\text{ext}} = e^2 \sum_I \sum_i \frac{Z_I}{\left|\mathrm{R}_I - \mathrm{r}_i\right|} \tag{2.1.6}$$

where lowercase **r** represents the location of electrons and uppercase **R** the location of nuclei. In practice, it is nearly impossible to solve the many-body Schrödinger equation analytically. However approximations, such as replacing the many-body equation with single-particle states or describing the electron exchange and correlation with a functional of the density, make finding the solution of the electronic structure a tractable problem. We will describe one of these approaches, density functional theory, in the following section.

2.2 Density Functional Theory

Density functional theory is comprised of two main approximations: (1) the representation of the many-body electron wave function by single particle states and (2) the ability to express the energy as a function of the density[4].

The root of the second approximation is Thomas-Fermi theory, where the energy of an electronic system can be calculated exclusively in terms of the electronic density[5,6]. Thomas and Fermi proposed a method to calculate the energy of an inhomogeneous electron system, comprised of kinetic, exchange, and correlation energy components, by using knowledge from the homogeneous system, where these components are known:

$$E_{\mathrm{ih}}[\rho] = \int \rho(\mathrm{r})\varepsilon_{\mathrm{h}}[\rho(\mathrm{r})]\mathrm{dr} \qquad (2.2.1)$$

where E_{ih} is the energy of the inhomogeneous system and ε_{h} is a functional of the density derived from the homogeneous system. In this *local density approximation*, the energy of the inhomogeneous system can be found by knowing the density of the system and assuming the value at each 'local point' is equal to that of the homogeneous system. While this approximation works well for systems that are similar to a homogeneous

electron gas (for example, a simple metal), problems arise for more complicated molecular systems, especially where exchange and correlation become important. These problems prompted the development of modern DFT.

The Thomas-Fermi concept of writing the energy exclusively in terms of the electronic density was not formally proven until 1964 by Honhenberg and Kohn[4]. They first showed that there is a unique electronic density that satisfies a certain external potential which is found from the ground state wave function by solving the full many-body Schrödinger equation. Secondly, in a variational type approach, they showed that the ground state density minimizes the total electronic energy of the system. Thus, for some electron density, ρ, the energy is equal to:

$$E[\rho] = \left\langle \Phi[\rho] \middle| \hat{T} + \hat{V}_{i,i} \middle| \Phi[\rho] \right\rangle + \int \rho(\mathrm{r}) \hat{V}_{\mathrm{ext}}(\mathrm{r}) d\mathrm{r} \qquad (2.2.2)$$

and therefore, for any density other than the exact ground state density the following inequality is true:

$$E_0 < E[\rho] \qquad (2.2.3)$$

It is important to note that the first term in Eq. 2.2.2 is a universal functional, in that it only depends on the electronic density.

There are several problems with solving Eq. 2.2.2. First, there is no method for solving the first term $\left\langle \Phi[\rho] \middle| \hat{T} \middle| \Phi[\rho] \right\rangle$, since an explicit expression of the kinetic energy in terms of electron density is not known. However, Kohn and Sham approached this problem by considering the fact that a system of non-interacting electrons is exactly described by an antisymmetric wave function of a Slater determinant type, made up of one-electron orbitals[7]. The exact expression for the kinetic energy of non-interacting electrons is:

$$\hat{T} = -\frac{\hbar^2}{2m}\sum_i f_i \langle \varphi_i | \nabla^2 | \varphi_i \rangle \tag{2.2.4}$$

where f_i are the occupation numbers of each orbital, φ_i. Kohn and Sham suggested that if a system of non-interacting electrons could produce a density that was similar to the interacting system (Eq. 2.2.2), then the kinetic energy could be easily calculated. This is done by utilizing a potential, called the *reference potential* (v_R), which uses the single particle Hamiltonian to reproduce an electron density that represents the true interacting many-body system:

$$\hat{H}_R = \sum_i^N \left[-\frac{\hbar^2}{2m}\nabla_i^2 + v_R(\mathrm{r}) \right] \tag{2.2.5}$$

The non-interacting system can be used to rewrite Eq. 2.2.2 using electron densities and Eq. 2.2.4 to find what is called the Kohn-Sham (KS) functional:

$$E_{KS}[\rho] = \hat{T}[\rho] + \int \rho(\mathrm{r}) v_{ext}(\mathrm{r}) d\mathrm{r} + \frac{1}{2}\iint \frac{\rho(\mathrm{r})\rho(\mathrm{r}')}{|\mathrm{r}-\mathrm{r}'|} d\mathrm{r} d\mathrm{r}' + \widetilde{E}_{XC}[\rho] \tag{2.2.6}$$

The term, $\widetilde{E}_{XC}[\rho]$, accounts for both the electron-electron exchange and correlation that is missing in Eq. 2.2.6 and the kinetic correlation missing in the first term since we assumed non-interacting electrons. Approximations for this functional will be discussed later in this chapter.

The goal of DFT is to find a reference potential that will match the density found from the non-interacting single particle Kohn-Sham orbitals to the true electron density. To do so, we can apply the variational principle to minimize the ground-state density:

$$\frac{\delta}{\delta\rho(\mathrm{r})}\left(E_{KS}[\rho] - \mu \int \rho(\mathrm{r}) d\mathrm{r} \right) = 0 \tag{2.2.7}$$

where μ is the chemical potential. Substituting Eq. 2.2.6. into Eq. 2.2.7 gives:

$$\frac{\delta T_R[\rho]}{\delta\rho(\mathrm{r})} + v_{\mathrm{ext}}(\mathrm{r}) + \int \frac{\rho(\mathrm{r}')}{|\mathrm{r}-\mathrm{r}'|} dr' + \frac{\delta \widetilde{E}_{\mathrm{XC}}[\rho]}{\delta\rho(\mathrm{r})} = \mu \tag{2.2.8}$$

The first term in Eq. 2.2.8 can be found by using the non-interacting Hamiltonian with the reference potential in Eq. 2.2.5:

$$E_{v_R}[\rho] = \hat{T}_R[\rho] + \int \rho(\mathrm{r}) v_R(\mathrm{r}) d\mathrm{r} \tag{2.2.9}$$

in which we assumed that the reference potential produced an electron density of the ground-state interacting system, even though the Hamiltonian is non-interacting. Since $E_{v_R}[\rho] \geq E_0$ (with the equality only true for the ground state density), the functional derivative of $E_{v_R}[\rho]$ should vanish for the ground state density. By applying the variational principle to the energy, we arrive at:

$$\frac{\delta T_R[\rho]}{\delta\rho(\mathrm{r})} + v_{\mathrm{R}}(\mathrm{r}) = \mu_{\mathrm{R}} \tag{2.2.10}$$

where μ_{R} is the chemical potential of the non-interacting system, which we assume will correspond to that of the interacting system. We can substitute Eq. 2.2.10 into Eq. 2.2.8 to arrive at the important expression for the reference potential:

$$v_{\mathrm{R}}(\mathrm{r}) = v_{\mathrm{ext}}(\mathrm{r}) + \int \frac{\rho(\mathrm{r}')}{|\mathrm{r}-\mathrm{r}'|} d\mathrm{r}' + \frac{\delta \widetilde{E}_{\mathrm{XC}}[\rho]}{\delta\rho(\mathrm{r})} \tag{2.2.11}$$

Since the reference potential depends on solutions of the one-electron Schrödinger equation (Eq. 2.2.5), the equation must be solved self-consistently.

To complete the solution, we must find approximations for the exchange and correlation, $\widetilde{E}_{\mathrm{XC}}[\rho]$. While a variety of different methods exist for treating this term, we will briefly discuss two established and widely used approximations, the local density approximation (LDA) and generalized gradient approximation (GGA).

The local density approximation starts with a well-known system, the homogeneous electron gas[7]. In a similar fashion to Thomas-Fermi theory, the electron exchange-correlation of an inhomogeneous system is treated as a local homogeneous electron gas, whose exchange and correlation are known to an excellent accuracy:

$$\widetilde{E}_{\mathrm{XC}}^{\mathrm{LDA}}[\rho] = \int \rho(\mathrm{r})\widetilde{\varepsilon}_{\mathrm{XC}}^{\mathrm{LDA}}[\rho(\mathrm{r})]d\mathrm{r} \tag{2.2.12}$$

The LDA energy functional term can be split into two components, exchange and correlation:

$$\widetilde{\varepsilon}_{\mathrm{XC}}^{\mathrm{LDA}} = \varepsilon_{\mathrm{X}}^{\mathrm{LDA}} + \widetilde{\varepsilon}_{\mathrm{C}}^{\mathrm{LDA}} \tag{2.2.13}$$

in which the exchange part is given exactly by Dirac's expression[8] and the correlation is given by several accurate numerical approximations[9-11].

Inhomogeneities in the electronic density create an obvious problem for a purely local approximation such as LDA. A natural extension is to carry out an expansion of the density in terms of the gradient and higher order derivatives. This allows for the energy to be written as:

$$E_{\mathrm{XC}}[\rho] = \int \rho(\mathrm{r})\varepsilon_{\mathrm{XC}}[\rho(\mathrm{r})]G_{\mathrm{XC}}[\rho(\mathrm{r}), \nabla\rho(\mathrm{r}), \nabla^2\rho(\mathrm{r}), ...]d\mathrm{r} \tag{2.2.14}$$

where the function G_{XC} is an enhancement factor which modifies the LDA expression to include the effect of variation of the density. Exchange-correlation functionals that employ these techniques are named generalized gradient approximations (GGA). A variety of different types exist, usually created by taking two approaches: 1. deriving expressions based on theoretical methods which fulfill formal conditions and 2. fitting functional forms and parameters to experimental results from a molecular training set[12]. Generally GGA provides an improvement over LDA and is mainly used in calculations presented in this thesis.

2.3 Molecular Dynamics

Solving the electronic structure of an atomic system can provide a wealth of useful information. However, a major drawback is the fact that the information gained from the simulation is, for the most part, static in nature. While there are techniques for extracting kinetic information from the static potential energy surface, ultimately the ability to track the dynamic motion of atoms is important in fully understanding the system.

Molecular dynamics (MD) is a powerful yet simple tool in theory (although in practice and when integrating with quantum mechanics, the method can become much more complicated) for following the dynamics of a system. In a MD simulation, the trajectories of particles with a position (**q**) and momentum (**p**) or velocity (**v**) are propagated through time following Newtonian mechanics[13]. The position of a particle after a certain amount of time, Δt, is simply:

$$\mathrm{q}(t+\Delta t) = \mathrm{q}(t) + \frac{\mathrm{p}(t)}{m}\Delta t \qquad (2.3.1)$$

It is important to note, however, that Eq. 2.3.1 is an approximation (Euler), a result of the fact that to perform the calculation, an infinitesimally small time-step cannot be used. The choice of this time-step is important since using too large of a time-step will cause the trajectory to waver far from the correct trajectory, while too small of a time-step will be to computationally costly. The Euler approximation is quite simple and as a result it is not very stable. Improvements are made by including higher order terms from a Taylor expansion. A popular method which is used in our work (named Verlet), uses sums of

Taylor expansions that correspond to forward and reverse time steps[14]. Positions are updated according to:

$$q(t+\Delta t) = 2q(t) - q(t-\Delta t) + a(t)\Delta t^2 \qquad (2.3.2)$$

where **a** is the acceleration. A variety of other techniques exist but regardless of the method used, with a set of initial positions and velocities, and a procedure for calculating the forces acting on any particle, we now have a method for following the dynamics of the system over time.

As mentioned above, molecular dynamics requires an accurate description of the forces acting on the particle in the simulation. If forces are ill-described, the calculated trajectory can 'steer' far from the correct trajectory. Forces can be calculated in a variety of ways, one popular approach for a simple system is to use a classical potential. But classical or empirical potentials are difficult to use when describing the behavior of a chemically complex system. We desire a more accurate approach which can be achieved by using quantum mechanical methods. There are a variety of methods for coupling quantum mechanical calculations with molecular dynamics. Rigorously, the time dependent Hamiltonian of a system incorporates quantum effects of nuclei, electrons, and the complete coupling between the two. A full quantum mechanical treatment is nearly impossible but approximations can be made by keeping the nuclear motion classical. Even within this context a variety of approaches exist, but we will focus on one such approach employed in our work, named Born-Oppenheimer Molecular Dynamics (BOMD) or *ab-initio* Molecular Dynamics (AIMD)[12]. In this approach, forces on atoms are calculated from ground-state DFT, the nuclei are propagated with some time-step, and the ground state electronic structure and forces acting on the nuclei are recalculated. This

approach, in contrast to other methods, uses a static time-independent electronic description, so that the electronic structure must be recalculated at each step. Newton's equation of motion for this method simply becomes:

$$m\mathrm{a}(t) = -\nabla \min\left\{\left\langle \Psi_0 \left| \hat{H}_{KS} \right| \Psi_0 \right\rangle\right\} \tag{2.3.3}$$

which is merely a mathematical representation of what is stated above.

Since temperature is an important parameter affecting the structure and reactivity of gold surfaces, it is important to model the surface in the canonical ensemble (constant number of particles, volume, and temperature, NVT). The treatment of the number of particles and volume is relatively easy to control within the context of our simulations, but care must be taken to control the temperature dependence. To do so, we employed Nóse dynamics[15]. In this approach connections are made between what Nóse calls a 'virtual' system and the physical system. His approach is to relate the microcanonical partition function of an extended virtual system (extended indicates that additional degrees of freedom are added) to the canonical partition function of the physical system, thus:

$$Z_{\mathrm{NVE}}^{\mathrm{virt}} = C(E,T,Q,q) Z_{\mathrm{NVT}}^{\mathrm{phys}} \tag{2.3.4}$$

where $C(E,T,Q,q)$ is a calculable number that depends on energy, temperature, and other parameters (Q,q) that are used to define the Hamiltonian of the extended system. The relationships between the virtual (unprimed) and physical (primed) systems are:

$$\mathrm{q}_i = \mathrm{q}_i', \quad \mathrm{p}_i = s\mathrm{p}_i' \tag{2.3.5}$$

where s is a fictitious mass related by:

$$m_i = s^2 m_i' \tag{2.3.6}$$

The Hamiltonian of the virtual extended system now becomes:

$$\hat{H} = \sum_i \frac{\mathrm{p}_i^2}{2m_i' s^2} + V(\{\mathrm{q}_i\}) + \frac{p_s^2}{2Q} + gkT \ln s \qquad (2.3.7)$$

where V is the potential of the physical system, Q is the mass of the additional degree of freedom s, and g is a parameter depending on the number of particles and the choice of time scaling. Time is scaled such that $dt' = dt/s$.

Nóse used Eq. 2.3.4, which has been proved[16,17], to assert that for any function A, the canonical and microcanonical averages over the respective physical and extended virtual phase spaces are equal:

$$\left\langle A(\mathrm{q}', \mathrm{p}') \right\rangle_{\mathrm{NVT}}^{\mathrm{phys}} = \left\langle A(\mathrm{q}, \mathrm{p}/s) \right\rangle_{\mathrm{NVE}}^{\mathrm{virt}} \qquad (2.3.8)$$

Thus in conclusion, if the Hamiltonian equation (Eq. 2.3.7) of the virtual system generates ergodic dynamics, then any physical quantity in this system can be related to the physical canonical ensemble average of this quantity.

In the following chapters of this thesis, we will employ techniques discussed in this chapter to understand adsorption and reactions on gold surfaces.

2.4 References

[1] E. Schrödinger, *Ann. D. Physik* **1926**, *79*, 361.

[2] E. Kaxiras, *Atomic and Electronic Structure of Solids* [University Press: Cambridge, **2003**].

[3] M. Born, J.R. Oppenheimer, *Ann. D. Physik* **1927**, *84*, 457.

[4] P. Hohenberg, W. Kohn, *Phys. Rev.* **1964**, *136*, B864.

[5] L.H. Thomas, *Proc. Cambridge Phil. Soc.* **1927**, *23*, 542.

[6] E. Fermi, *Z. Phys.* **1928**, *48*, 73.

[7] W. Kohn, L. Sham, *Phys. Rev.* **1965**, *14*, A1133.

[8] P.A.M. Dirac, *Proc. Cambridge Phil. Soc.* **1930**, *26*, 376.

[9] U. van Barth, L. Hedin, *J. Phys. C.* **1972**, *5*, 1629.

[10] S.H. Vosko, L. Wilk, M. Nusair, *Can. J. Phys.* **1980**, *58*, 1200.

[11] J.P. Perdew, A. Zunger, *Phys. Rev. B.* **1981**, *23*, 5048.

[12] J. Johanoff, *Electronic Structure Calculations for Solids and Molecules* [Cambridge University Press: Cambridge, **2006**].

[13] C.J. Cramer *Essentials of Computational Chemistry: Theories and Models* [John Wiley & Sons: West Sussex, **2004**].

[14] L. Verlet, *Phys. Rev.* **1967**, *159*, 98.

[15] S. Nose, *J. Chem. Phys.* **1984**, *81*, 511.

[16] H.C. Andersen, *J. Chem. Phys.* **1980**, *72*, 2384.

[17] W.G. Hoover, *Phys. Rev. A.* **1985**, *31*, 1695.

CHAPTER 3

NATURE OF Cl BONDING ON THE AU(111) SURFACE

3.1 Abstract

We report theoretical evidence from first-principles density functional theory (DFT) calculations that the bonding between Cl and the Au(111) surface is primarily covalent in character, which is in contrast to the generally held view that the bonding of halogens to metal surfaces is ionic. We observe the transfer of charge density into the region between interacting Au and Cl atoms, which would not be expected in case of Cl- anion formation (symmetric charge accumulation on Cl). Importantly, we also find a clear directionality of d_{z2} orbitals of the Au atoms pointing to the adsorbed Cl, and the mixing of electronic states between the gold surface and adsorbed chlorine.

This work was published as a communication in the *Journal of American Chemistry Society*: T.A. Baker, C.M. Friend, and E. Kaxiras. **2008**, *130*, 3720.

3.2 Introduction

Bonding of strongly electronegative halogen atoms on metal surfaces is of fundamental importance in understanding surface adsorption and has been studied extensively with experimental[1-4] and theoretical[5-8] tools. A particularly interesting case is the interaction of chlorine on the Au(111) surface[9-12], which has advantages for various applications: Gold (III) chloride is used as a homogenous catalyst for several important organic reactions including intramolecular cyclizations and cross-cycloisomerization reactions[13,14]. In heterogeneous chemistry, chlorinating reagents with gold can be used, for instance, to remove mercury emissions from coal-fired boilers[15]; chlorine also

increases the selectivity of styrene epoxidation on Au(111)[16] and acts as a poison for CO oxidation on supported gold particles[17,18].

We report theoretical evidence from first-principles density functional theory (DFT) calculations that the bonding between Cl and the Au(111) surface is primarily covalent in character. This is in contrast to the generally held view that the bonding of halogens to metal surfaces is ionic: Doll et al.[7] concluded from their theoretical studies that the interaction of Cl on Ag(111) is mainly ionic based on the finding that there is only a small overlap population between Cl and Ag and the chlorine charge is larger in the orbitals that are the most separated from silver. Bagus et al.[5] and Rubio et al.[8] used cluster calculations and found that a halogen atom on silver and mercury surfaces has a net charge of one electron. However, Quattrucci et al.[19] reported that they "do not observe significant charge transfer to the Cl [adsorbed on Au(111)]". Experimentally, the change in the work function can be used to measure the charge of an adsorbate.[20] Theoretical work predicts[21] a positive work function change (indicating a negatively charged adsorbate) for chlorine adsorption on the (001) surfaces of Cu, Ag and Au and a negative change (indicating a positively charged adsorbate) on Rh, Pt, and Pd. While the general conclusion is chlorine ionically bonds on all of these metal surfaces, these theoretical results show that the experimental work function changes should be treated with caution in interpreting the adsorbate charge.

3.3 Calculational Details

The DFT results were obtained with the VASP code[22] using the GGA-PW91 functional to model electron exchange and correlation[23]. Ultrasoft pseudopotenitals were

used using the default plane-wave cutoffs taken from the GGA ultrasoft-pseudopotential database[24,25].

The surface was modeled by a slab consisting of 12 layers in the (111) direction, with a $\sqrt{3}\times\sqrt{3}$ primitive unit cell; the six uppermost layers of the slab were allowed to relax, with the rest fixed at the ideal bulk positions. The bulk positions were taken from the calculated lattice constant of 4.17 Å which is in good agreement with the experimental value 4.08 Å[26]. A large vacuum region between the slabs of ~20 Å was used to insure that the dipole created by the chlorine adsorption did not artificially interact in neighboring unit cells. A Monkhorst-Pack Γ-centered 6x6x1 k-point sampling of reciprocal space is used. Spin polarized calculations were used as a test, but no significant effect on the energy comparisons was found.

The charge on the adsorbed Cl molecule is calculated by integrating the charge in a sphere of radius r_{Cl} centered at the nucleus of the atom. The length of r_{Cl} is determined by the distance from Cl to the minimum in the density on the line connecting to the closest Au neighbor. The net charge on Cl is the difference in the integrated charge using r_{Cl} for the adsorbed Cl on Au(111) and a gas phase Cl atom using the same r_{Cl} from the respective surface structure.

3.4 Results and Discussion

In the present work we use periodic slabs and GGA-PW91 to model the surface and electron exchange and correlation in the context of DFT calculations, and examine the nature of Cl bonding on Au(111). Our choice of surface supercell is a $(\sqrt{3}\times\sqrt{3})R30^\circ$ structure relative to the ideal bulk-terminated plane, with one adsorbed Cl atom per unit cell, which corresponds to Cl coverage of 0.33 monolayer (ML). The Cl atom is placed

either on top of a surface Au atom or at the three-fold hollow fcc site; in a previous report[12] we showed that the latter is the preferred binding site of Cl on this surface. Calculations were done at higher chlorine coverages, with similar results. One of the most important characteristics of a covalent bond is the localization of electronic density between the two atoms participating in the bond[27] whereas ionic character is assigned to a bond involving a transfer of electrons without localization between the atoms. We will employ electron density plots to examine the bonding between Au and Cl on the Au(111) surface.

To isolate the interaction between the Au surface and the adsorbed Cl atom, we calculate the difference in electronic density between the combined system (Cl adsorbed on the Au(111) surface) and the separate isolated components (free surface and free Cl atom) with atomic positions frozen at the optimized surface geometry with the adsorbate. This charge density difference for the two positions of the adsorbate is shown in Fig. 1: there is an accumulation of electronic density in the region between the chlorine atom and its nearest neighbor Au atom in both cases. Since Cl is a highly electronegative atom, we can expect it to attract electrons from the Au substrate. A purely ionic interaction would result in an increase of the electronic density of chlorine in a symmetric fashion around the chlorine atom. Figure 3.1, in contrast, shows that electron density is removed from the region around the Cl atom and is added in the region between the chlorine and nearest neighbor Au atom. The degree of electron density accumulation between the chlorine and gold are more pronounced when Cl is bound on top of the gold atom (Fig. 3.1a). When the coordination of chlorine decreases the bond distance decreases (from 2.69 Å at the three-fold hollow fcc site to 2.39 Å at the top site) and the electron density between Cl

and the nearest Au neighbor increases, Table 3.1. Electron density is removed from the spherical region located around both the chlorine and gold atom to contribute to the bond. This effect is reduced when Cl is situated at the hollow fcc site because of the higher coordination in this case. Figure 3.1 also shows a significant perturbation of the electronic density in the first layer of the gold substrate.

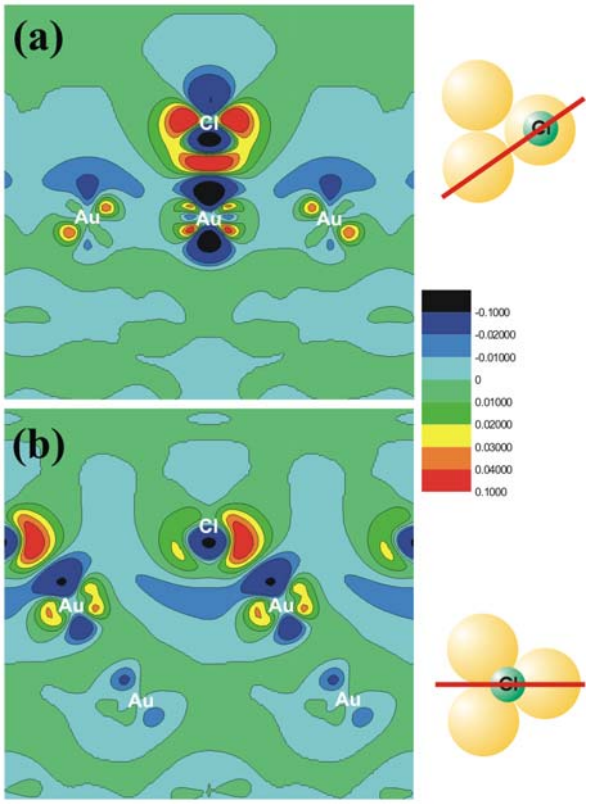

Figure 3.1: Charge density difference between the adsorbate system and the isolated components (gold surface and Cl atom), for Cl at the (a) the top position, (b) the hollow fcc site (shown in the geometries on the right, with red line indicating the plane of the charge difference plot). Positive values indicate accumulation of electronic charge, negative values correspond to depletion of charge. Each plot is 100 $Å^2$.

Table 3.1: Summary of results for Cl bound on different sites on Au(111). ρ_{min} is the amount of electron density located at the minimum in the density between Cl and its nearest neighbor Au atom.

Cl type	Au-Cl bond (Å)	Cl radius (Å)	Au radius (Å)	ρ_{min}	Cl charge
top	2.39	1.18	1.21	0.570	-0.22
bridge	2.58	1.27	1.31	0.392	-0.27
HCP	2.70	1.33	1.39	0.314	-0.33
FCC	2.69	1.35	1.34	0.319	-0.34

The degree of mixing between Au and Cl electronic states serves as another piece of evidence for covalent bonding between the Au substrate and the adsorbed Cl atom. Figure 3.2 shows the *p* electron partial density of states (*p*-PDOS) of Cl and Au as a function of energy for Cl at the hollow fcc site. The presence of common peaks in the Cl and Au *p*-PDOS suggests strong mixing of the two sets of electronic states characteristic of covalent bonding. The most pronounced feature in the Cl *p*-PDOS is a peak at ~1.8 eV, which does not correspond to a major peak in the Au *p*-PDOS. To understand the nature of this peak, the electronic density of states around this energy value is shown in Figure 3. A significant covalent interaction between Au and Cl is evident, with electronic density extending over both the chlorine site and the top layer of the gold surface. The Cl orbital is a symmetric, ring shaped orbital parallel to the surface. The surface gold atoms participate in this bond through d_z2 atomic orbitals pointing towards the Cl position at the three-fold hollow fcc site, in a different direction from their usual orientation on the clean surface, which is perpendicular to the surface plane. The directionality of these orbitals and the mixing of Au and Cl states at this energy is strong evidence of the covalent nature of the Cl-Au interaction.

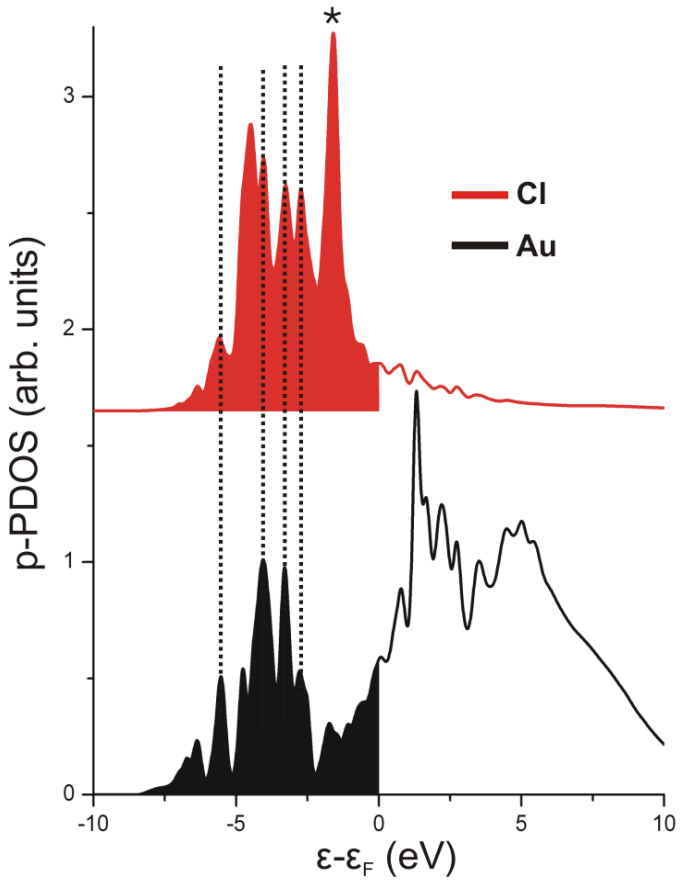

Figure 3.2: Density of states as a function of energy for p-electrons of Cl and Au for Cl adsorbed on at the hollow fcc site on the Au(111) surface. The zero energy is the Fermi level and filled states have shading below curve. The electron density corresponding to states in the largest peak of the Cl *p*-PDOS (identified by the asterisk) is shown in Fig. 3.3.

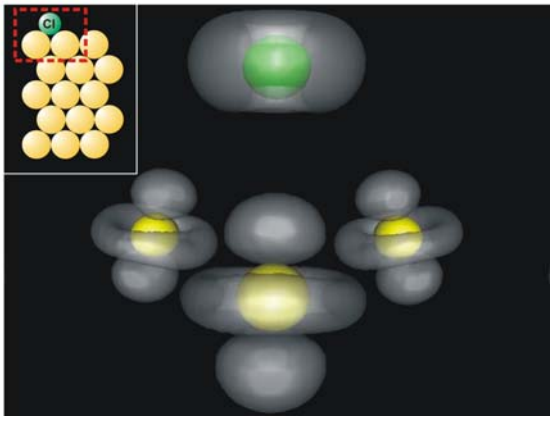

Figure 3.3: Electron density at the energy indicated by the asterisk in Figure 3.2 for Cl adsorbed at the hollow fcc site on Au(111). The inset shows a side view of the surface and the adsorbed Cl atom, with the area of the larger figure indicated by the red dotted line.

Our results are at variance with the generally accepted view concerning the adsorption of halogens on metal surfaces. In general, the interaction of chlorine with metals is indeed ionic in nature, but the Au/Cl system appears to be an exception. The adsorption of chlorine on gold is unusual because gold has the highest Pauling electronegativity[26] of all transition metals, making it the most likely to form a covalent bond with the highly electronegative halogens. The difference in electronegativity between Au and Cl is 0.76, apparently small enough to lead to formation of covalent bonds.

Our results do not contradict previous theoretical studies[5-8], which concerned the interaction of chlorine with the surfaces of other noble metals, such as silver and mercury. For example, the electronegativity difference between chlorine and silver or mercury is 1.23, considerably larger than that for the Cl-Au pair, justifying the more ionic character of the Cl-Ag and Cl-Hg interactions. Our results are particularly interesting in

the context of olefin oxidation reactions, suggesting that the bonding and functionality of Cl used as a promoter is different on Ag and on Au surfaces; specifically, the degree of charge separation in the two cases may lead to a smaller perturbation in the bonding of oxygen on the Au surface vs. on the Ag surface.

3.6 References

[1] A.G. Shard, V. R. J. Dhanak, *Phys. Chem. B.* **2000**, *104*, 2743-2748.

[2] A. G. Shard, V. R. Dhanak, A. Santoni, *Surf. Sci.* **2000**, *445*, 309-314.

[3] A. G. Shard, V. R. Dhanak, A. Santoni, *Surf. Sci.* **1999**, *429*, 279-286.

[4] M. F. Kadodwala, A. A. Davis, G. Scragg, B. C. C. Cowie, M. Kerkar, D. P. Woodruff, R. G. Jones, *Surf. Sci.* **1995**, *324*, 122-132.

[5] P. S. Bagus, G. Pacchioni, M. R.Philpott, *J. Chem. Phys.* **1989**, *90*, 4287-4295.

[6] K. Doll, N. M. Harrison, *Chem. Phys. Lett.* **2000**, *317*, 282-289.

[7] K. Doll, N. M. Harrison, *Phys. Rev. B.* **2001**, *63*, 6.

[8] J. Rubio, J. M. Ricart, J. Casanovas, M. Blanco, F. Illas, *J. Electroanal. Chem.* **1993**, *359*, 105-113.

[9] N. D. Spencer, R. M. Lambert, *Surf. Sci.* **1981**, *107*, 237-248.

[10] G. N. Kastanas, B. E. Koel, *Appl. Surf. Sci.* **1993**, *64*, 235-249.

[11] D. Lemoine, J. G. Quattrucci, B. Jackson, *Phys. Rev. Lett.* **2002**, *89*, 4.

[12] W. W. Gao, T.A. Baker, L. Zhou, D.S. Pinnaduwage, E. Kaxiras, C.M. Friend, *J. Am. Chem. Soc.* **2008**, *130*, 3560.

[13] A. S. K. Hashmi, L. Schwarz, J. H. Choi, T. M. Frost, *Angew. Chem., Int. Ed.* **2000**, *39*, 2285-2288.

[14] A. Stephen, K. Hashmi, T. M. Frost, J. W. Bats, *J. Am. Chem. Soc.* **2000**, *122*, 11553-11554.

[15] Y. X. Zhao, M. D. Mann, J. H. Pavlish, B. A. F. Mibeck, G. E. Dunham, E. S. Olson, *Environ. Sci. Technol.* **2006**, *40*, 1603-1608.

[16] D. S. Pinnaduwage, L. Zhou, W. W. Gao, C. M. Friend, *J. Am. Chem. Soc.* **2007**, *129*, 1872.

[17] P. Broqvist, L. M. Molina, H. Gronbeck, B. Hammer, *J. Catal.* **2004**, 227, 217-226.

[18] H. S. Oh, J. H. Yang, C. K. Costello, Y. M. Wang, S. R. Bare, H. H. Kung, M. C. Kung, *J. Catal*. **2002**, *210*, 375-386.

[19] J. G. Quattrucci, B. Jackson, D. Lemoine, *J. Chem. Phys.* **2003**, *118*, 2357.

[20] N.D. Lang, W. Kohn, *Phys. Rev. B.* **1971**, *3*, 1215.

[21] A. Migani, C. Sousa, F. Illas, Surf. Sci. **2005**, *574*, 297-305.

[22] G. Kresse, J. Hafner, *Phys. Rev. B.* **1993**, *47*, 558-561.

[23] J. P. Perdew, Y. Wang, *Phys. Rev. B.* **1992**, *45*, 13244-13249.

[24] G. Kresse, J. Hafner, *J. Phys - Cond. Mat.* **1994**, *6*, 8245-8257.

[25] D. Vanderbilt, *Phys. Rev. B* **1990**, *41*, 7892-7895.

[26] CRC Handbook of Chemistry and Physics; 77 ed.; D. R. Lide, Ed. [CRC Press: New York, **1996**].

[27] L. Pauling, *The Nature of the Chemical Bond and the Structure of Molecules and Crystals; An Introduction to Modern Structural Chemistry* 3rd ed. [Cornell University Press: Cornell, **1960**].

CHAPTER 4

CHLORINE INTERACTION WITH DEFECTS ON THE AU(111) SURFACE

4.1 Abstract

Chlorine is an important element in promoting oxidation on noble metal surfaces. Here, we report a comprehensive theoretical study of chlorine interaction with defects on the Au(111) surface, using density functional theory calculations and periodic slabs to model the surface. We find that chlorine binds preferentially on steps, vacancies, and gold adatoms. The increase in binding energy per chlorine atom, compared to binding on the flat, defect-free surface, is 0.29 eV when the chlorine atom is on top of a gold adatom, 0.38 eV when it is at the edge of a step, and 0.19 eV when it is next to a single surface vacancy. An extensive study of chlorine interaction with different numbers of surface gold vacancies revealed that chlorine interacts the strongest with three vacancies.

This work was published as an article in the *Journal of Chemical Physics*: T.A. Baker, C.M. Friend, and E. Kaxiras. **2008**, *129*, 104702.

4.2 Introduction

Gold has recently become important as a catalytic material[1-3]. Supported gold nanoparticles can be used to catalyze many reactions including the reduction of NO_x by hydrocarbons[4,5], the oxidation of CH_4 [6,7], CO[8] and propene[9], and the epoxidation of propylene.[10] Chlorine increases the selectivity of certain heterogeneous reactions including ethylene epoxidation on Ag/α-Al_2O_3[11] and olefin partial oxidation on Au(111)[12]

by dispersing and redistributing surface oxygen[13]. Despite these indications, the details of how chlorine and oxygen co-adsorb on the surface and the role that this plays in oxidation is not understood. This issue is actually one of broader interest. Namely, finding the active site of a heterogeneous catalyst is crucial in understanding how the catalyst can be effective and how it might be improved[14]. The active site is closely related to stable and metastable positions of a reactant on a surface, like chlorine on Au(111), whose adsorption is often the first step in a corrosion or catalytic reaction cycle.

The rich chemistry and physics between the interaction of chlorine and gold also makes this an important system from a fundamental viewpoint. Gold (III) chloride is used as homogenous catalyst for a number of important organic reactions including intramolecular cyclizations and cross-cycloisomerization reactions[15,16]. Chlorine is used as a lixiviant for gold[17] and the chorine adsorption on the Au(111) electrode has been studied electrochemically[18]. Chlorine also plays an important role in the contact between gold and semiconductor electrodes[19]. The adsorption of chlorine on Au(111) is dynamical in nature, involving many different structures and types of Cl bonding to Au[20,21]. Depending on Cl coverage, it involves initial release of gold atoms from the herringbone reconstruction, a chemisorbed overlayer, and further release of gold atoms to form a gold chloride[22].

Potential binding sites of chlorine on a gold surface include flat terrace sites and different types of defect sites. Defects and undercoordinated gold atoms are especially important to understand in catalysis, since these sites are thought to be more reactive and are often the active sites on a surface. For example, step edge sites of MoS_2 nanoparticles were found to be the active site for electrochemical H_2 evolution[23]. Undercoordinated Au

atoms could be possible sites for binding or even dissociation of O_2 for CO oxidation on Au nanoparticles[24-26]. Using STM, Biener *et. al.* showed that small AuS clusters preferentially nucleated at defect sites upon the adsorption of sulfur on Au(111)[27]. Chlorine, an electronegative species like sulfur and oxygen, may exhibit the same properties: the relevant stable and metastable chlorine positions could be on a step, an island, a terrace, or at the interface between a nanoparticle and the metal-oxide support[28].

In this work, we report a set of comprehensive calculations based on density functional theory (DFT) for the adsorption of chlorine on a Au(111) surface. Specifically, we investigate the interaction of chlorine with defects on this surface including a gold adatom, a step edge, and terrace vacancies. By comparing the adsorption energy of Cl on various sites on the defective surfaces, we found that Cl binds to all three of these defects stronger than it binds to the flat, defect-free Au(111) surface.

4.3 Calculational Details

The DFT results were obtained using the VASP code[29] with the GGA-PW91[30] functional to describe electron exchange and correlation. Ultrasoft pseudopotenitals are employed with the default plane-wave cutoff (219.471 eV) taken from the GGA ultrasoft-pseudopotential database[31,32] and a 7×7×1 k-point sampling was used. A high number of k-points were necessary to accurately describe the stepped surface. The surface was modeled by a slab consisting of 4 layers in the (111) direction, with a 4×4 primitive unit cell in the lateral directions; only the two uppermost layers of the slab were allowed to relax, with the rest fixed at the ideal bulk positions. By changing computational parameters (such as reciprocal-space sampling or slab thickness) we found small changes in relative energies; from these, we estimate that energy differences, on which all

physical conclusions are based, include error bars no greater than 0.1 eV, small enough to not affect any of the conclusions we draw.

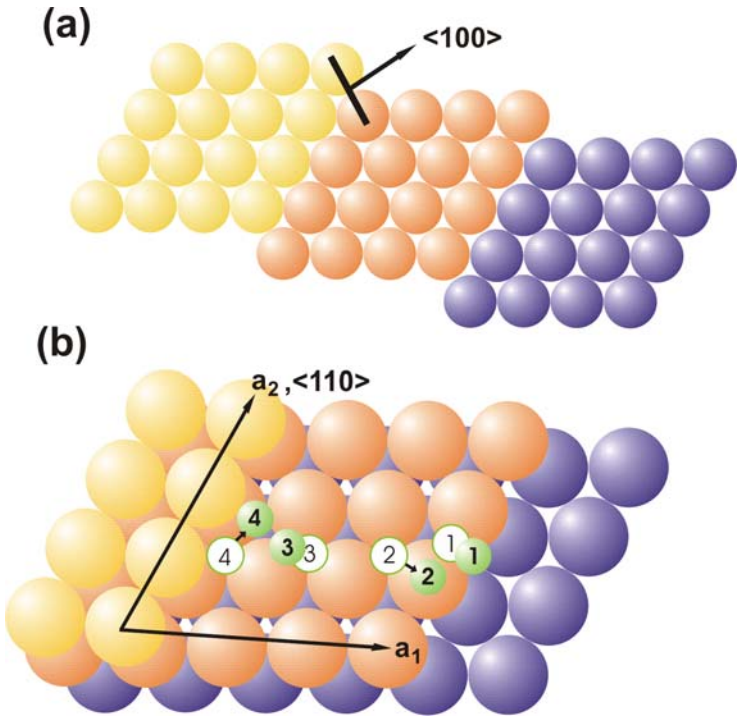

Figure 4.1: The model of the stepped <110>/{100} Au(533) surface employed in the calculations: (a) side view of the slab with each unit cell shown in a different color; (b) top view of stepped surface. Each unit cell contains 4 (111) layers and is offset to create a step. Yellow circles are the gold atoms that make up the upper step, orange circles represent the terrace, and purple circles are the layer of the lower step. White circles represent initial starting positions and solid green circles the final positions of the chlorine atom after relaxation. The vector normal to the plane of the step edge, <100>, is shown in (a) and the lattice unit cell vectors a_1 and a_2 are shown in (b).

The bulk positions were taken from the calculated lattice constant of 4.17 Å which is in good agreement with the experimental value 4.08 Å[33]. Spin-polarized calculations were also preformed for the entire adsorption system, but had no substantial effect on the results.

To study the interaction of chlorine with defects, three different Au(111) substrates were considered: a stepped surface, <110>/{100} Au(533), where <110> is the direction along the step edge and {100} is the plane of the step edge, a surface containing a single gold adatom, and a surface containing vacancies. In all of the calculations a single chlorine atom was adsorbed on the surface, corresponding to a 1/16 monolayer (ML) coverage. The stepped surface consisted of (111) terraces with each unit cell offset to create a step, shown in Fig. 1(a), the adatom surface had an additional gold adatom sitting on a three-fold site on the top layer of gold, and the vacancy surface had gold atoms removed from the top layer of the gold substrate; the number of removed gold atoms ranged from 1 to 13.

4.4 Results and Discussion

The reference configuration in this work is the adsorption of atomic chlorine on the flat, defect-free Au(111) surface. The adsorption energy was calculated for three different sites: on top of a gold atom (coordination number, CN = 1), on the bridge site (CN=2), and on a three-fold site (CN=3). The adsorption energy is defined relative to the chemical potential of Cl_2 gas:

$$E_{ads}(Cl) = -[E(Au/Cl) - E(Au) - 1/2E(Cl_2)] \quad (4.4.1)$$

where E(Au/Cl) is the total energy of a gold substrate with the chlorine atom adsorbed, E(Au) is the energy of the gold substrate, and $E(Cl_2)$ is the energy of a Cl_2 molecule. The

clean (1×1) Au(111) surface is a good reference point for two reasons: first, the experimentally observed herringbone reconstruction of the clean Au(111) surface is lifted upon initial chlorine adsorption, and second, the difference in surface energy between the ideal (1×1) surface and the surface with the herringbone reconstruction is actually quite small, ~0.02 eV per surface Au atom[34]. In this definition, a positive value for the adsorption energy means that the structure with the adsorbed Cl atom on the Au surface is energetically preferred over the bare surface plus Cl in molecular form far from the surface. The calculated bond length and binding energy for the Cl_2 molecule using the PW91 functional are 2.02 Å and 2.68 eV respectively; the corresponding experimental values are 1.99 Å and 2.51 eV[33]; these values calculated with the RPBE functional are 2.00 Å and 2.54 eV[35].

Chlorine adsorbed on the three-fold site was found to be the most stable, with an adsorption energy of E_{ads}= 0.99 eV, followed by adsorption to the bridge site with E_{ads}= 0.94 eV, and on the top site with E_{ads} = 0.78 eV. Previous DFT calculations also found the three-fold site to be the preferred binding site of chlorine on Au(111), with nearly the same Au-Cl distance and an adsorption energy at 1/2 ML coverage that was 0.48 eV lower than our value[36]. Since the adsorption energy of chlorine decreases with increasing coverage, and our adsorption energy was calculated at 1/16 ML coverage, we considered this to be reasonable agreement. All of the adsorption energies are positive, agreeing with the experimental observation that chlorine dissociation occurs on the Au(111) surface. The Au-Cl bond length increases with increasing CN, being 2.41 Å on the top site, 2.59 Å on the bridge site, and 2.66 Å on the three-fold site. These distances are all slightly longer that the Au-Cl distances found in bulk gold (III) chloride. The crystal of

bulk chloride contains planer Au_2Cl_6 molecules in a herringbone arrangement. The experimental bond distance for chlorine bonded to one gold atom and two gold atoms is 2.23 Å and 2.33 Å respectively[37].

The small difference in adsorption energy between the three-fold site and bridge site suggests that the diffusion barrier for chlorine on the surface is very low and the barrier to 'hop' from one three-fold site to another through the bridge site is approximately $\varepsilon_d = 0.05$ eV. This is consistent with the order-disorder transition that occurs as a function of temperature for the adsorption of chlorine on gold. Based on low energy electron diffraction studies[21], Cl forms ordered structures at 230 K. This is corroborated by recent STM studies showing that a disordered, mobile phase is present when Cl is adsorbed at 300 K, whereas highly ordered structures are formed upon subsequently cooling and observation at 120 K[13]. The calculated diffusion barrier implies that at 300 K the chlorine atoms are reasonably free to move on the surface, while at 120 K chlorine gets trapped in an ordered phase as the barrier to diffuse on the surface is too high to overcome at this temperature.

The first gold defect used to test the adsorption of chlorine was a single gold adatom on the unreconstructed Au(111) surface. Gold adatoms can play an important role on the Au(111) surface, especially when considering the initial adsorption on a clean surface. The clean Au(111) surface reconstructs in the so-called 'herringbone' pattern, resulting in an excess of 4.5% Au atoms on the top layer compared to the bulk (111) plane[38-40]. The presence of several adsorbed molecules lifts the reconstruction, thus releasing gold adatoms onto the surface[27,41,42]; making it is reasonable to use the unreconstructed surface as a reference point. Figure 4.2 shows multiple locations for the

adsorption of chlorine on the Au(111) surface with a gold adatom present. Many different configurations were tested; the ones shown in Figure 4.2 are final configurations after the system was relaxed, each position being a local minimum on the potential energy surface (PES). For configuration 1 (chlorine bound on top of the gold adatom) and 2 (chlorine bound to both the adatom and a gold atom on the substrate) the adsorption energy is 1.28 and 1.18 eV respectively, which is 0.29 and 0.18 eV higher (stronger adsorption) than chlorine on a three-fold site on the defect-free surface. The increase in the strength in binding can be seen in the bond length, for example the Au_{adatom}-Cl bond distance for configuration 1 is 2.30 Å, which is 0.11 Å shorter than Cl on top of an Au atom on the defect-free surface.

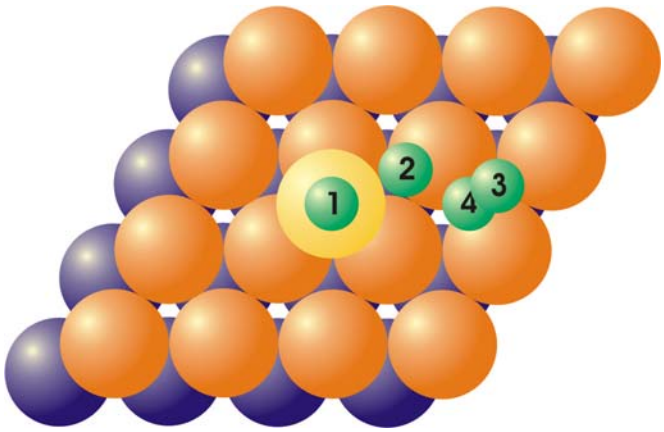

Figure 4.2: Chlorine adsorption sites on the Au(111) surface with a Au adatom. Orange circles represent the top layer of the gold, the yellow circle is the gold adatom, and smaller numbered green circles indicate the relaxed chlorine positions.

The interaction between the Au adatom and the Cl is short range, on the order of < ~4 Å, since placing the chlorine away from the gold adatom had no significant effect

on the adsorption energy compared to that of the defect-free surface. For example, in configuration 4 the adsorption energy is 0.92 eV, nearly the same as the adsorption energy found for chlorine on a bridge site of the defect-free surface. The same is true for configuration 3 whose adsorption energy is 0.93 eV, essentially the same as the adsorption energy for Cl on the hcp three-fold site on a defect-free surface, 0.94 eV. Therefore, there appears to be no long-range effect of the gold-adatom on Cl adsorption. Similar short range effects have been observed for the co-adsorption of CO and O on Pt(111)[43] and for CO and S on Rh(111)[44].

There are two important implications of these results. First, since the adsorption of chlorine is stronger to a gold adatom than any site on a flat (111) surface, even the three-fold site on the terrace, the initial chlorine atoms that are deposited on the surface will interact with adatoms that are present on the surface. Second, the presence of chlorine will lower the energy cost to create a gold adatom on the surface. The energy cost required to create an adatom is defined as:

$$E_{\text{Au cost}} = E(\text{Au}_{\text{surface+adatom}}) - E(\text{Au}_{\text{atom in bulk}}) - E(\text{Au}_{\text{surface}}) \qquad (4.4.2)$$

where $E(\text{Au}_{\text{surface+adatom}})$ is the total energy for the gold substrate with the Au adatom adsorbed on a three-fold site, $E(\text{Au}_{\text{atom in bulk}})$ is the energy of a gold atom in the bulk crystal, and $E(\text{Au}_{\text{surface}})$ is the energy of the gold substrate with a clean, defect-free surface. The energy cost to create a gold adatom without chlorine present is 0.61 eV while the energy cost with chlorine adsorbed on top of a gold adatom is 0.21 eV.

The second gold substrate investigated was the Au(533) stepped surface. The adsorption energy of chlorine was tested at various different sites. The starting and ending points of the geometry relaxation are shown in Figure 4.1b, illustrating that

chlorine prefers to interact with both the edge of a step and ledge of a step where the terrace meets the upper edge. Chlorine atoms relax away from the terrace either moving towards the edge of the step or towards the ledge depending on their starting location. The adsorption energies for the four configurations, shown in Figure 4.1b are 1.37, 0.97, 0.80, and 0.99 eV, in order. The configuration with the highest adsorption energy is the one with chlorine at the edge of the step, 'hanging' over the step and coordinated to two gold atoms. The binding energy for chlorine at the edge of the step is 0.38 eV higher than that of a defect-free surface. The Au-Cl distance at the step edge is 2.50 Å, 0.09 Å shorter than the Au-Cl distance for Cl on a bridge site of the defect-free surface. Chlorine prefers to bind on a step edge, consistent with the general trend that atoms bind more strongly to step edges[45]; for example, atomic oxygen (an electronegative species like Cl) also prefers to bind on a step of a Au(111) surface[46,47]. Upon the adsorption of chlorine at 300 K in experiments, dynamic STM images show serrated step edges, indicating an etching or migration of atoms at the step edge, which is in agreement with our calculations that chlorine shows a strong preference for these sites.

Experiments show that upon the adsorption of chlorine on Au(111), pits of atomic height begin to form on the surface[22]. It is unclear, however, if Cl is interacting or adsorbed near these pits on the surface. To investigate this phenomenon and at the same time test another type of surface defect as potential Cl attractor, the adsorption of chlorine was tested on a surface that contained gold vacancies. These vacancies are created by removing atoms from the top layer of the gold substrate and the adsorption energy was calculated for Cl residing at a three-fold site. The results are shown in Figure 4.3. Much like the other defect surfaces, the adsorption energy of chlorine is higher on a surface

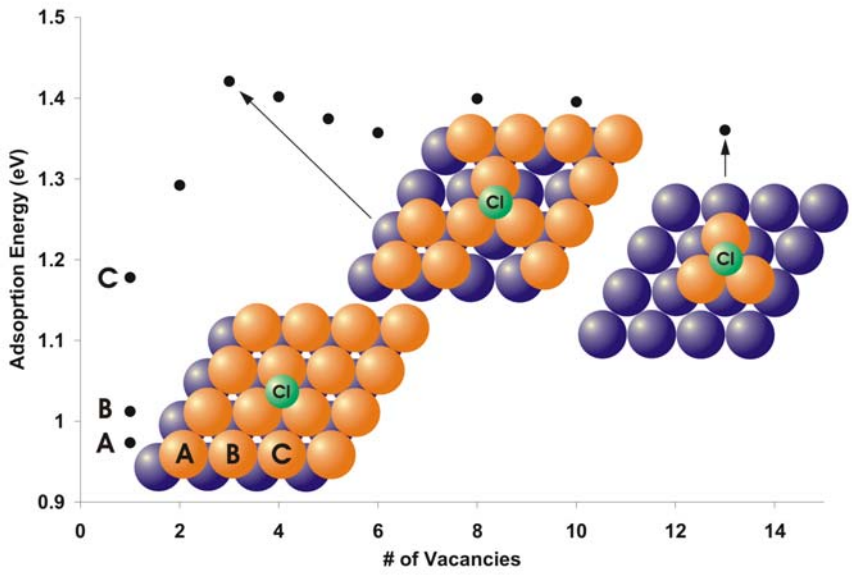

Figure 4.3: Adsorption energy of atomic chlorine as a function of number of vacancies on Au(111). Orange circles represent the top layer of gold and purple circles the second layer of gold. With only one vacancy there are three different configurations we considered: the gold atom removed to create the vacancy and the corresponding energy value are labeled A, B, and C. The optimal structure (with highest absorption energy) corresponds to three gold vacancies and the chlorine atom at the three-fold site on top of the remaining top-layer gold atoms, shown in the middle configuration. The structure with the highest number of vacancies (13) and its energy are shown on the right.

containing gold vacancies than on the clean, defect-free surface. The effect of the vacancy is greater when the gold atom removed is coordinated with two of the gold atoms to which the chlorine atom is bound. The adsorption energy also increases as the number of vacancies increases but only up to three vacancies. With more than three vacancies, the adsorption energy slowly starts to decrease. There is a clear interaction between the chlorine atom and the vacancy since in many of the configurations the

chlorine relaxes towards the vacancy. For example, in a configuration containing one vacancy (the gold atom labeled *B* in Figure 4.3 having been removed), the chlorine is shifted towards the vacancy site with the shortest Au-Cl distance being 2.61 Å and the next two Au-Cl distances being 2.68 Å and 2.77 Å. With three vacancies, the chlorine sits in the middle of a three-fold site with a shortest Au-Cl distance of 2.60 Å, which is 0.06 Å shorter than the Au-Cl distance on a defect-free surface, indicating a stronger interaction.

The results from each type of defect illustrate how the adsorption of chlorine can contribute to the release of gold atoms from the surface. Generally, strongly electronegative adsorbates can release gold from the surface, some examples on Au(111) being NO_2[48], S[49], CH_3SH[50,51], and O[52,53]. In fact, recent experimental work showed that at higher coverages of chlorine it is energetically favorable to incorporate gold atoms in the adsorbate adlayer[22]. The release of gold from the substrate upon adsorption is the result of either (or both) of two processes occurring: (a) the adsorbate interacts favorably with the gold atoms released, or (b) the adsorbate interacts favorably with a vacancy that is left behind after the gold atom is released. In the case of Cl on Au(111), our calculations show that chlorine stabilizes both adatoms and vacancies, suggesting that this is the driving force for the Au atom release that is observed experimentally at higher coverages.

Finally, we will use charge difference density plots to elucidate the bonding of Cl to different defect surfaces. Figure 4a is the charge difference plot for the preferred adsorption site of chlorine on the vacancy surface, the bridge site adjacent to the vacancy. The plot is the difference in the electron density for the adsorbed system and the gold

substrate with the gold atoms frozen in the positions from the adsorbed system. The figure shows this difference in the plane through the top layer of gold. There is a large negative region of charge in the middle of the plot corresponding to the location of the vacancy. When the vacancy is created, charge density is removed from what appears to be d-orbitals around each neighboring gold atom and accumulates on the edge of the vacancy. A vacancy created without the adsorption of chlorine results in the symmetric accumulation of charge around the vacancy (results not shown). The adsorption of chlorine creates a slightly asymmetric charge redistribution, with more charge facing the vacancy on the side opposite to the chlorine adsorption site. The adsorbed chlorine must polarize charge density in and around the vacancy to create this asymmetry. Interestingly, the adsorption of chlorine not only affects the charge density of the gold atoms to which it is coordinated, but also gold atoms much farther away; for example, atoms on the other side of the vacancy which are nearly two lattice constants away (~ 6 Å). This effect is more pronounced on the surface with vacancies compared to the ideal surface.

Figures 4.4b and 4.4c illustrate the bonding of chlorine on the vacancy and adatom gold surface. In these plots the charge of the frozen gold substrate and free Cl atom is subtracted from the charge of the total absorbated system including the substrate. A large localization of charge directly between the chlorine and gold atoms is evident in both cases, suggesting a strong covalent interaction. The amount of charge is much greater and localized than on the clean surface. Figure 4.4c also illustrates that a small amount of electron density is added between the gold adatom and the first layer of the gold. This may help stabilize the gold adatom and strengthen its interaction with the top

layer of gold. This effect, combined with the stronger covalent interaction, leads to the stronger binding of chlorine to the gold surfaces with vacancies or adatoms.

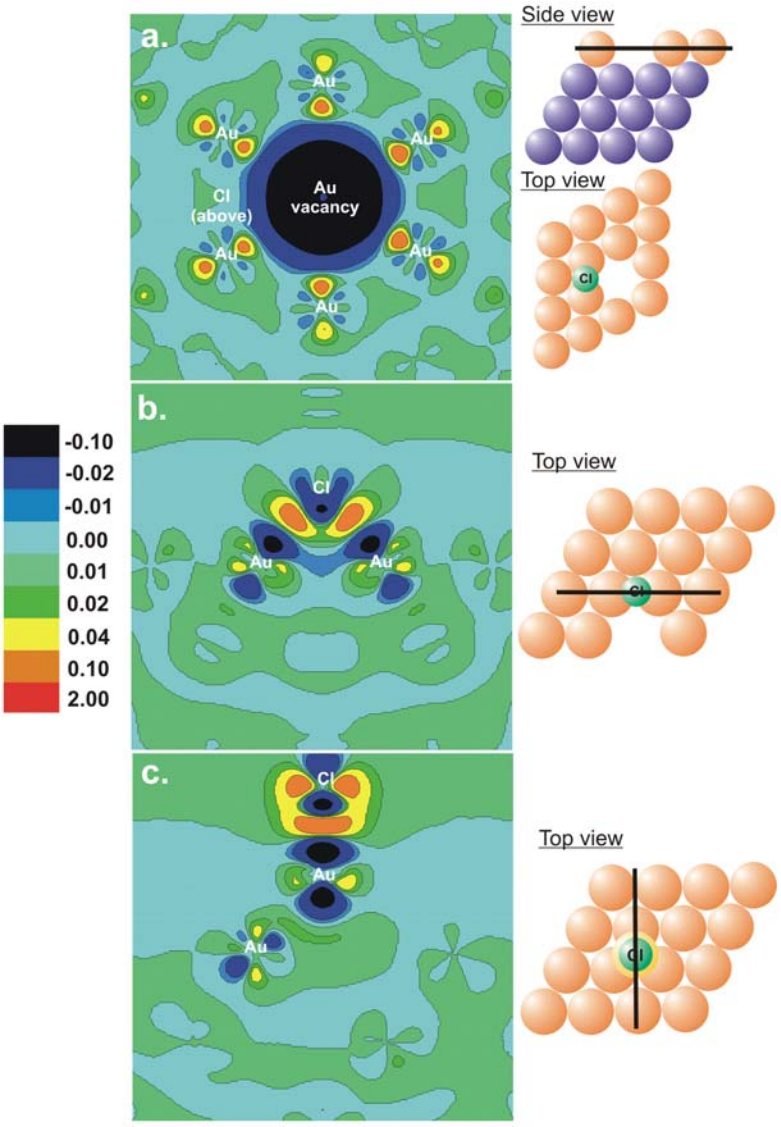

Figure 4.4: Charge difference plots for (a),(b) chlorine bound next to a gold vacancy and (c) chlorine bound on top of a gold adatom. Structural figures on the side of each plot indicate the atomic arrangements; the black line in each case indicates the plane on which the charge difference is plotted. Each plot corresponds to an area of 100 $Å^2$.

4.5 Conclusions

Our extensive set of DFT calculations show that atomic chlorine favorably interacts with defects on a gold surface. The adsorption of chlorine is stronger for a chlorine atom interacting with gold adatoms, steps, and vacancies. We expect that for a process that involves chlorine, the active sites on gold surfaces, such as those of a supported gold nanoparticle, will be near the defects (adatoms, steps, and vacancies) rather than sites on the flat terraces. These results also shed some light onto the interaction of chlorine with surface defects and the experimentally observed release of gold atoms upon the adsorption of chlorine. This mechanism may also be related to the effect of chlorine on the selectivity of olefin partial oxidation on Au(111), and other similar catalytic systems[54-56].

4.6 References

[1] M. Haruta, M. Date, *Appl. Catal. A.* **2001**, *222***,** 427.

[2] M. Haruta, *Chem. Rec.* **2003**, *3*, 75.

[3] R. Meyer, C. Lemire, S.K. Shaikhutdinov, H. Freund, *Gold Bull.* **2004**, *37*, 72.

[4] D. W. Lee, J. H. Ryu, D. H. Jeong, H.S. Lee, K. M. Chun, K. Y. Lee, *J. Ind. Eng. Chem.* **2003**, *9*, 102.

[5] B. W. Jang, J. J. Spivey, M. C. Kung, and H. H. Kung, *Energy Fuels* **1997**, *11*, 299.

[6] R. J. H. Grisel, P. J. Kooyman, and B. E.Nieuwenhuys, *J. Catal.* **2000**, *191*, 430.

[7] R. J. H. Grisel, B. E. Neiuwenhuys, *Catal. Today* **2001**, *64*, 69.

[8] M. Haruta, N. Yamada, T. Kobayashi, S. Iijima, *J. Catal.* **1989**, *115*, 301.

[9] T. Hayashi, K. Tanaka, M. Haruta, *J. Catal.* **1998**, *178*, 566.

[10] E. E. Stangland, K. B. Stavens, R. P. Andres, W. N. Delgass, *J. Catal.* **2000**, *191*, 332.

[11] R. M. Lambert, R. L. Cropley, A. Husain, M. S. Tikhov, *Chem. Comm.* **2003**, 1184.

[12] D. S. Pinnaduwage, L. Zhou, W.W. Gao, C. M. Friend, *J. Am. Chem. Soc.* **2007**, *129*, 1872.

[13] W. W. Gao, L. Zhou, D. S. Pinnaduwage, C. M. Friend, *J. Phys. Chem. C.* **2007**, *111*, 9005.

[14] T. Zambelli, J. Wintterlin, J. Trost, G. Ertl, *Science* **1996**, *273*, 1688.

[15] A. Stephen, K. Hashmi, T. M. Frost, J. W. Bats, *J. Am. Chem. Soc.* **2000**, *122*, 11553.

[16] A. S. K. Hashmi, L. Schwarz, J. H. Choi, T. M. Frost, *Angew. Chem. Int. Ed.* **2000**, *39***,** 2285.

[17] C. C. Nesbitt, E. B. Milosavljevic, J. L. Hendrix, *Ind. Eng. Chem. Res.* **1990**, *29***,** 1696.

[18] Z. C. Shi, S. J. Wu, J. Lipkowski, *J. Electroanal. Chem.* **1995**, *384*, 171.

[19] R. H. Williams, V. Montgomery, R. R. Varma, A. McKinley, *J. Phys. D.* **1977**, *10*, L253.

[20] N.D. Spencer, R. M. Lambert, *Surf. Sci.* **1981**, *107*, 237.

[21] G. N. Kastanas, B. E. Koel, *Appl. Surf. Sci.* **1993**, *64*, 235.

[22] W. W. Gao, T.A. Baker, L. Zhou, D. S. Pinnaduwage, E. Kaxiras, C. M. Friend, *J. Am. Chem. Soc.* **2008**, *130*, 3560.

[23] T. F. Jaramillo, K. P. Jorgensen, J. Bonde, J. H. Nielsen, S. Horch, I. Chorkendorff, *Science* **2007**, *317*, 100.

[24] I. N. Remediakis, N. Lopez, J. K. Norskov, *Appl. Catal. A.* **2005**, *291*, 13.

[25] C. Lemire, R. Meyer, S. K. Shaikhutdinov, H. J. Freund, *Surf. Sci.* **2004**, *552*, 27.

[26] T. V. W. Janssens, A. Carlsson, A. Puig-Molina, B. S. Clausen, *J. Catal.* **2006**, *240*, 108.

[27] M. M. Biener, J. Biener, C. M. Friend, *Langmuir* **2005**, *21*, 1668.

[28] C. Stampfl, M. V. Ganduglia-Pirovano, K. Reuter, M. Scheffler, *Surf. Sci.* **2002**, *500*, 386.

[29] G. Kresse, J. Hafner, *Phys. Rev. B* **1993**, *47*, 558.

[30] J. P. Perdew, Y. Wang, *Phys. Rev. B* **1992**, ***45***, 13244.

[31] D. Vanderbilt, *Phys. Rev. B* **1990**, *41*, 7892.

[32] G. Kresse, J. Hafner, *J. Phys. – Cond. Matter.* **1994,** *6*, 8245.

[33] CRC Handbook of Chemistry and Physics; 77 ed.; D. R. Lide, Ed. [CRC Press: New York, **1996**].

[34] Y. Wang, N. S. Hush, J. R. Reimers, *Phys. Rev. B.* **2007**, *75***,** 233416.

[35] P. Broqvist, L. M. Molina, H. Gronbeck, B. Hammer, *J. Catal.* **2004**, *227*, 217.

[36] D. Lemoine, J. G. Quattrucci, B. Jackson, *Phys. Rev. Lett.* **2002**, *89*, 4.

[37] E. S. Clark, D. H. Templeton, C. H. MacGillavry, *Acta. Cryst.* **1958**, ***11***, 284.

[38] S. Narasimhan, D. Vanderbilt, *Phys. Rev. Lett.* **1992**, *69***,** 1564.

[39] C. E. Bach, M. Giesen, H. Ibach, T. L. Einstein, *Phys. Rev. Lett.* **1997**, *78*, 4225.

[40] H. Ibach, *J. Vac. Sci. Technol. A.* **1994**, *12***,** 2240.

[41] H. Ibach, C. E. Bach, M. Giesen, A. Grossmann, *Surf. Sci.* **1997**, *375*, 107.

[42] D. Sander, U. Linke, H. Ibach, *Surf. Sci.* **1992**, *272*, 318.

[43] K. Bleakley, P. Hu, *J. Am. Chem. Soc.* **1999**, *121*, 7644.

[44] C. J. Zhang, P. Hu, M. H. Lee, *Surf. Sci.* **1999**, ***432***, 305.

[45] H. Ishida, A. Liebsch, *Phys. Rev. B* **1992**, *46*, 7153.

[46] Y. Xu, M. Mavrikakis, *J. Phys. Chem. B* **2003**, *107*, 9298.

[47] Z. P. Liu, P. Hu, A. Alavi, *J. Am. Chem. Soc.* **2002**, *124*, 14770.

[48] S. M. Driver, T. F. Zhang, D. A. King, *Angew. Chem. Int. Ed.* **2007**, *46*, 700.

[49] S. Y. Quek, M. M. Biener, J. Biener, J. Bhattacharjee, C. M. Friend, U. V. Waghmare, E. Kaxiras, *J. Phys. Chem. B.* **2006**, *110*, 15663.

[50] P. Maksymovych, D. C. Sorescu, D. Dougherty, J. T. Yates, *J. Phys. Chem. B.* **2005**, *109*, 22463.

[51] L. M. Molina, B. Hammer, *Chem. Phys. Lett.* **2002**, *360*, 264.

[52] B. K. Min, X. Deng, D. S. Pinnaduwage, R. Schalek, C. M. Friend, *Phys. Rev. B.* **2005**, *72*, 4.

[53] J. Biener, M. M. Biener, T. Nowitzki, A. V. Hamza, C. M. Friend, V. Zielasek, M. Baumer, *Chem. Phys. Chem.* **2006**, *7*, 1906.

[54] I. Sobczak, A. Kusior, J. Grams, M. Ziolek,, *J. Catal.* **2007**, *245*, 259.

[55] J. M. C. Soares, M. Hall, M. Cristofolini, M. Bowker, *Catal. Lett.* **2006**, *109*, 103.

[56] Y. X. Zhao, M. D. Mann, J. H. Pavlish, B. A. F. Mibeck, G. E. Dunham, E. S. Olson, *Environ. Sci. Technol.* **2006**, *40*, 1603.

CHAPTER 5

CHLORINE ADSORPTION ON AU(111): CHLORINE OVERLAYER OR SURFACE CHLORIDE?

5.1 Abstract

We report the first scanning tunneling microscope (STM) investigation, combined with density functional theory calculations, to resolve controversy regarding the bonding and structure of chlorine adsorbed on Au(111). STM experiments are carried out at 120 K to overcome instability caused by mobile species upon chlorine adsorption at room temperature. Chlorine adsorption initially lifts the herringbone reconstruction. At low coverages (<0.33 ML), chlorine binds to the top of Au(111)-(1 × 1) surface and leads to formation of an overlayer with $\sqrt{3} \times \sqrt{3}$ R30° structure at 0.33 ML. At higher coverages, packing chlorine into an overlayer structure is no longer favored. Gold atoms incorporate into a complex superlattice of an Au−Cl surface compound.

This work was published as an article in the *Journal of the American Chemical Society*: W.W. Gao, T.A. Baker, L. Zhou, D. S. Pinnaduwage, E. Kaxiras, and C. M. Friend, **2008**, *130*, 3560 with the experimental work completed by W.W. Gao, L. Zhou, and D. S. Pinnaduwage.

5.2 Introduction

Chlorine adsorption on gold has been considered as an important gas−solid interaction system[1-4], especially with recent studies on Au catalysis where both gold and chlorine are

often involved[5,6]. For example, gold is found to be especially active toward catalytic oxidation of mercury by chlorine[5] and has shown potential commercial applications in environmental mercury removal[7]. However, the role of gold, especially how gold interacts with Cl and Hg, is still unclear[5]. Gold is also an active catalyst in olefin partial oxidation[8,9]. Recent studies on Au(111) show that chlorine can disperse and redistribute surface oxygen and hence increases the reaction selectivity[6,10]. Although this dispersion effect has been clearly revealed, the structure of chorine and oxygen coadsorbed on gold is still unclear[10]. To answer these fundamental questions that are raised during development of gold toward practical applications, it is crucial to first elucidate the adsorption and structure of chlorine on gold.

Furthermore, previous studies of chlorine adsorption on Au have generated debate about the bonding and structure of the overlayer. Spencer and Lambert[1] reported that a lower-temperature Cl_2 desorption peak at 650 K would start to develop in temperature-programmed reaction only after a higher-temperature peak at 800 K saturated, suggesting a tightly bound layer formed first. They proposed that gold chloride ($AuCl_3$), possibly multiple layers, directly forms upon chlorine adsorption on Au(111). Kastanas and Koel[2] subsequently studied chlorine adsorption on Au(111) over a wider temperature range and observed a $\sqrt{3} \times \sqrt{3}$ R30° low-energy electron diffraction (LEED) pattern at temperatures below 230 K. Furthermore, they did not detect a Cl 2p binding energy shift in X-ray photoelectron spectroscopy (XPS) as a function of increasing chlorine coverage. Since there is no evidence of chloride formation, they concluded that only a chemisorbed chlorine overlayer was present. They also proposed an overlayer structure, where chlorine is bound to the top of Au(111)-(1 × 1) surface, based on the $\sqrt{3} \times \sqrt{3}$ R30°

periodicity in LEED pattern, which corresponded to a coverage of 1.33 monolayers (ML) of Cl. With the obvious inconsistency in two studies, the nature of Cl−Au interaction and the structure of Cl on Au(111) remain unsolved[11].

In this article, we report the first scanning tunneling microscope (STM) studies of Cl_2 adsorption on Au(111). The STM work in combination with density functional theory (DFT) calculations and XPS are used to demonstrate that chlorine interaction with Au(111) is a dynamic process involving multiple stages at different chlorine coverages. Initially at low Cl coverage (below 0.33 ML), Au atoms are released from the herringbone reconstruction to relieve surface stress. Continuous chlorine adsorption leads Cl atoms to bind on top of a Au(111)-(1 × 1) layer, ultimately leading to the Au(111)-$\sqrt{3} \times \sqrt{3}$ R30°-Cl overlayer at 0.33 ML coverage. At higher coverage, more Au atoms are removed from the surface and a surface chloride compound that contains Au atoms forms. Interestingly, the charge on the chemisorbed Cl is similar to the gold (III) chloride, based on our theoretical results, accounting for the absence of a Cl 2p binding energy shift. Our study demonstrates the delicate balance between charge transfer and formation of a compound overlayer on the surface. We place our studies of Cl on Au(111) in a more general context.

5.3 Experimental Details

Experiments were carried out in a two-chamber ultrahigh vacuum (UHV) system with a base pressure of 2×10^{-10} Torr. The Au single crystal with (111) orientation was cleaned in a preparation chamber by repeated Ar^+ ion sputtering and annealing to 900 K. Auger electron spectroscopy (AES) and LEED confirmed that the surface was clean and the herringbone reconstruction was present. Temperature-programmed desorption (TPD)

experiments were also carried out in the preparation chamber, with heating rate ~10 K/s. Chlorine (Matheson Tri Gas Inc., research grade) was background dosed through a leak valve attached to the preparation chamber.

The STM images were acquired in the second UHV chamber using a commercial, variable-temperature STM (RHK Technology, Inc.). The scanner was calibrated using atomically resolved images of the clean Au(111) surface and the Au(111) step height for the lateral and vertical directions, respectively. In this article, all STM images were collected with the bias voltage of +0.3 V (sample biased, empty states) and a tunneling current of 1 nA.

The X-ray photoelectron spectra were obtained in a separate UHV system equipped with LEED, quadrupole mass spectrometer (Balzers), a dual anode X-ray source (Perkin-Elmer 04-548), and a hemispherical energy analyzer (SPECS EA-10-plus). Core-level spectra were excited 1253.6 eV Mg Kα_1, α_2 radiation. To quantify the coverages using intensities measured in XPS, the Shirley background was subtracted[12]. Sulfur-covered Au(111) is prepared by exposing Au to 1×10^{-5} Torr SO_2 for 30 min at 300 K, followed by flashing the sample to 550 K[13,14]. A split $\sqrt{3} \times \sqrt{3}\ R30°$ LEED pattern was observed after this procedure, which corresponds to a sulfur coverage of 0.28 ML[13,15]. The split spots signify that there are three equivalent domains on the surface.

5.4 Calculations Details

The DFT results were obtained with the VASP code[16] using the GGA-PW91 functional[17] to model electron exchange and correlation. Ultrasoft pseudopotentials were used with the default plane-wave cutoffs for different elements taken from the GGA ultrasoft pseudopotential database[18]. Calculations were done with a 12-layer slab of a

$\sqrt{3} \times \sqrt{3}$ R30° unit cell of Au(111), with the bottom six layers remaining fixed in their bulk positions and the top six layers allowed to relax. A large vacuum region between the slabs of 20 Å was used to ensure that the dipole created by the chlorine adsorption did not artificially interact in neighboring unit cells. A Monkhorst-Pack Γ-centered 6 × 6 × 1 k-point sampling was used. Spin-polarized calculations were used to test each set of data and were found to have no significant effect on the energy comparisons.

The charge on chlorine was found by integrating the amount of electronic density in a sphere centered at the chlorine nucleus. The radius for the sphere was determined by finding the minimum in the density between the line connecting a chlorine and the closest gold atom the chlorine is bound to. The distance from the chlorine nucleus to this midpoint was used as the radius. The charge was then found by comparing the number of electrons in this sphere compared to the electrons in a sphere (using the same radius) of a free gas phase chlorine atom.

All the calculations reported in this work were also tested with the RPBE functional. The RPBE functional was considered since it has been shown to provide a better description of the chemisorption energetics for adsorbates on transition metal surfaces[18]. When using the GGA-RPBE functional, planeaugmented wave pseudopentials[19] were used, again using the plane-wave cutoffs taken from the database. The RPBE functional agreed with the PW91 functional except for one structure, the 1/3 ML chlorine bound on a bridge site of a surface with 1/3 ML gold vacancies. For this structure, the energy gain (0.61 eV) is enough to overcome the cost of creating the vacancies (0.53 eV). However, using the PBE functional, with plane-augmented wave pseudopentials, the conclusion agrees with PW91 since the energy gain in adsorption

energy is 0.60 eV while the energy cost is 0.65 eV. We believe that the PW91 and PBE functionals provide the correct conclusion, since the RPBE functional underestimates both the cohesive energy of a bulk Au atom and the Au(111) surface energy. Using a functional that can correctly account for Au-Au binding is important in this work, since we are concerned about the differences in energy between a flat and adatom covered gold surface. In general, it is known that DFT-GGA calculations will underestimate cohesive energies of metals. We find that the underestimation is most extreme with the RPBE functional; the cohesive energy was calculated using the PW91, PBE, and RPBE functional and found to be -3.02, -2.99, and -2.38 eV. The experimental cohesive energy is -3.81 eV[20] and a previous calculation found the energy using PW91 (RPBE) functional -3.08 (-2.46)[21]. The same trend is observed in surface energy which was calculated using the PW91, PBE, and RPBE functional and was found to be 0.0437, 0.0381, and 0.0153 eV/Å^2, respectively. An experimental value[22] has been found to be 0.0936 eV/Å^2, while past theoretical results have used a variety of techniques, including a Green's-function linear-muffin-tin-orbitals method[23] which found a value of 0.10 eV/Å^2, an embedded-atom-method[24] which found 0.0493 eV/Å^2. Since RPBE greatly underestimates the cohesive energy and surface energy, it most likely underestimates the cost of creating a gold atom or vacancy and this is reason why we are cautious about conclusions from using this functional.

5.5 Experimental Results

At room temperature, chlorine adsorption on Au(111) causes corrosion and formation of mobile species. To overcome the instability induced by mobile species, STM experiments were carried out at 120 K. Clean Au(111) reconstructs to the so-called

herringbone structure, such that the surface contains ~4% more atoms than the same plane in the bulk. The strain created by the mismatch between the top layer and the underlying bulk is minimized by the zigzag arrangement of soliton walls[25] (Figure 5.1a).

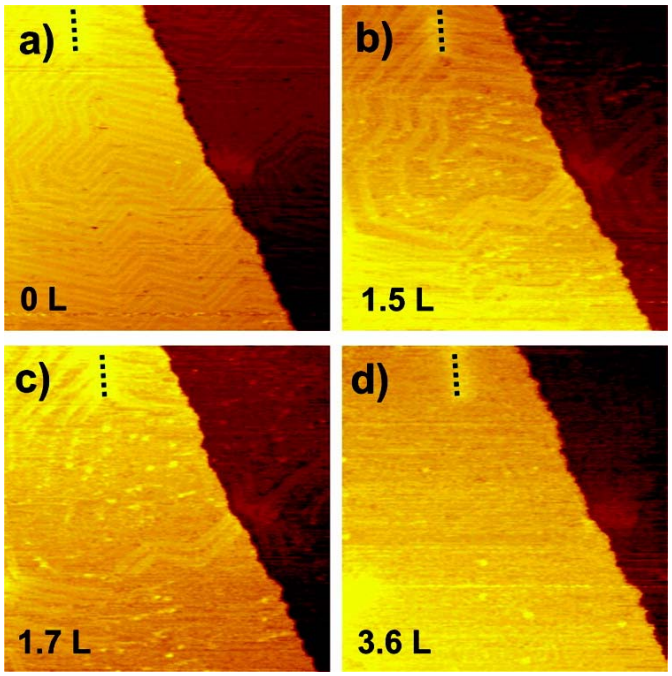

Figure 5.1: STM images recorded during Cl adsorption on Au(111), all from the same area of 150 × 150 nm^2. The dashed line marks a screw dislocation as a position reference. Cl_2 pressure is 4×10^{-9} Torr. Cl_2 dosing and STM imaging are at 120 K.

Adsorption of Cl_2 leads to the obvious disturbance and partial disappearance of the herringbone structure (Figure 5.1b,c). The surface reconstruction is lifted, and excess Au atoms on the surface layer are ejected, as indicated by the particles observed in the images. Because the surface temperature is low in these data, the Au released from the herringbone has limited mobility; thus, some particles are formed on the terraces. When the Cl_2 dosage reaches 3.6 L, no soliton wall can be observed using STM (Figure 5.1d).

Previous LEED studies also showed that, upon dosing chlorine, Au(111) reconstruction spots disappeared and only sharp (1 × 1) spots were observed[1,2]. The reversal of the herringbone reconstruction and ejection of Au atoms from the surface also occurs upon oxygen[26], sulfur[13,26], NO_2[27], and styrene[28] adsorption on Au(111). The strong charge transfer between gold and electronegative species presumably serves as the driving force for this process; however, the nature of the structures formed in these various cases depends on the specific surface−adsorbate interaction.

Accurate determination of the chlorine coverage is essential for further understanding the structures formed on Au(111). By measuring AES and XPS signal intensities, Kastanas and Koel used oxygen adsorption on platinum as the reference to derive oxygen and further chlorine coverages on Au(111)[2]. This method introduced several variables that resulted in a large discrepancy between their coverage estimates (2.9 and 0.8 ML) obtained from AES and XPS, respectively.

Herein, we use sulfur on Au(111) as a reference to determine the Cl coverage using intensities measured using XPS. Previous studies precisely determined the coverage of specific ordered structures of S on Au(111) using radioactive tracer techniques employing ^{35}S[14,29]. Since no chlorine diffusion into the bulk is observed on Au(111)[1,2], the chlorine coverage can be quantified with XPS using the split $\sqrt{3} \times \sqrt{3}$ *R*30° LEED pattern (inset, Figure 5.2) for sulfur ($\theta_S \approx 0.3$ ML) on Au(111) as a standard. The corresponding sulfur 2p spectrum and Cl 2p spectrum at the saturated Cl coverage are plotted in Figure 2. The integrated areas under the spectra are first normalized to the Au 4f peaks and then divided by the corresponding sensitivity factors of Cl and S (0.48 and 0.35, respectively)[30]. The ratio of chlorine to sulfur intensity is

measured to be 3.2:1. Because the sulfur coverage is known as ~0.3 ML, the saturation Cl coverage on Au(111) is therefore ~1 ML.

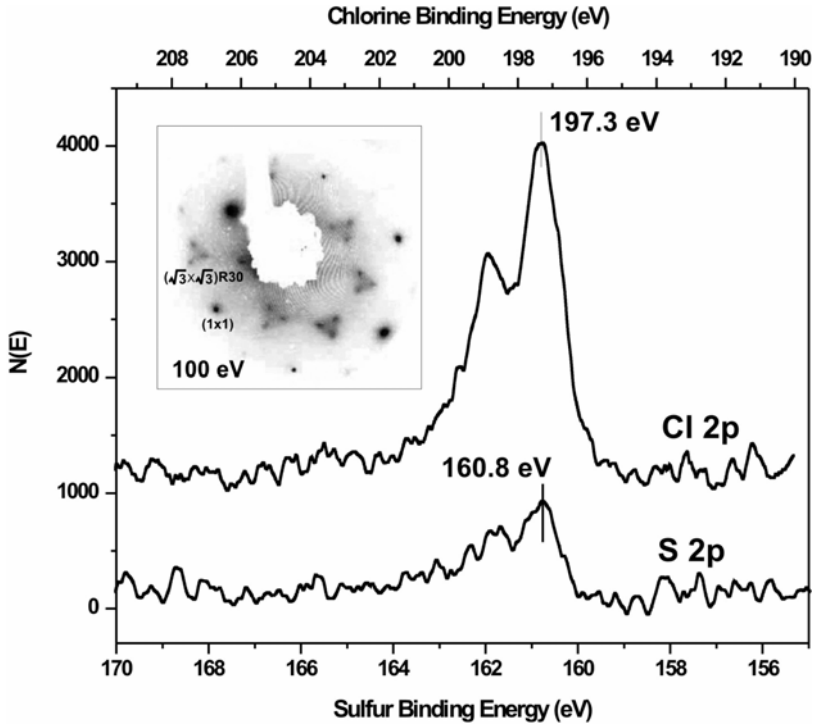

Figure 5.2: Inset shows LEED pattern obtained on Au(111) after exposing to 5×10^{-5} Torr SO_2 for 30 min at 300 K, followed by flashing sample to 500 K. After LEED, sulfur 2p XPS is obtained. Chlorine 2p spectrum is obtained after dosing 5×10^{-8} Torr Cl_2 at 300 K to saturation. The Cl and S spectra are plotted on shifted energy scales so as to overlap for the convenience of comparing intensities.

To further obtain structural information of chlorine on Au(111), Cl_2 was first dosed at 300 K and STM images were collected at 120 K. The chlorine coverage was estimated by comparing the area under the Cl_2 desorption trace relative to that of saturation coverage. When the chlorine coverage reaches ~0.33 ML, STM images in

Figure 5.3a and the corresponding zoom-in image in Figure 5.3b show a $\sqrt{3} \times \sqrt{3}\ R30°$ structure, which is consistent with the observed LEED pattern (inset of Figure 5.3a). It is also noticed that, with varying bias voltages from +0.3 to −2 V, there is no distinguishable contrast change observed in STM. Previous studies have also shown that chlorine adsorption on most fcc (111) surfaces form $\sqrt{3} \times \sqrt{3}\ R30°$ structure at coverage of 0.33 ML, and it is often attributed to Cl located at threefold hollow sites[11].

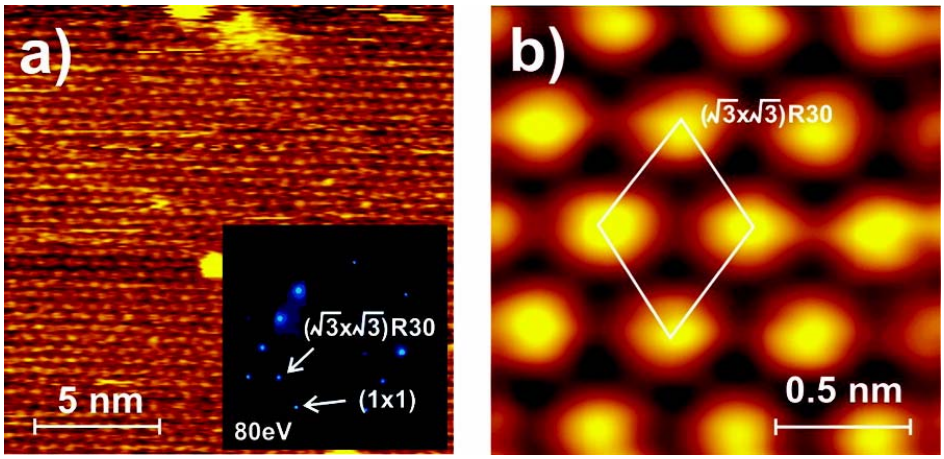

Figure 5.3: (a) STM images recorded at ~0.3 ML chlorine on Au(111). (b) Zoom-in image of (a), showing a $\sqrt{3} \times \sqrt{3}\ R30°$ atomic arrangement. Inset in (a) shows LEED pattern of the surface. Cl_2 is dosed at 300 K. STM imaging and LEED are carried out at 120 K.

Upon further dosing of chlorine at 300 K to 0.8 ML and imaging at 120 K, the surface transforms into a "honeycomb" structure, as shown in Figure 5.4a. The inset of Figure 5.4a shows a closeup of this "honeycomb" structure. It is observed that each honeycomb hexagon is composed of six units, and each unit adopts a dimer structure.

Indeed, gold chloride is found to exist as dimers in both solid and gas phases[31-33]. Therefore, this structural similarity implies that, at this high chlorine coverage, Au atoms incorporate into the adsorbate layer and form surface compound.

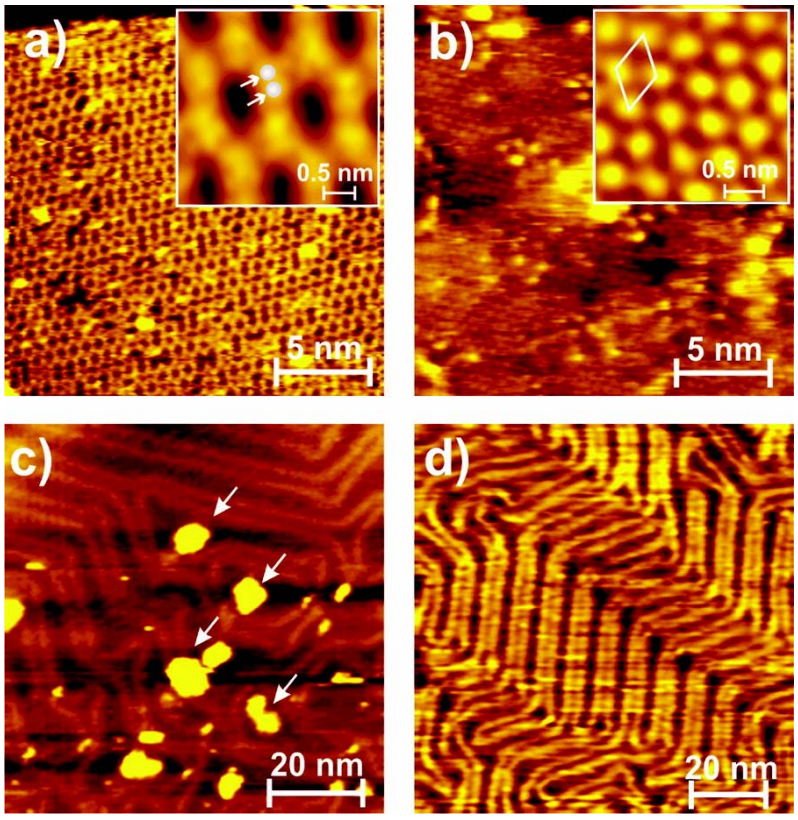

Figure 5.4: STM images of (a) ~0.8 ML chlorine on Au(111) showing the honeycomb structure. The inset shows that each unit in the hexagon adopts a dimer structure. (b) Flashing (a) to 750 K. (c) Annealing (a) at 750 K for 1 min. (d) Annealing (a) at 750 K for 5 min. Cl_2 is dosed at 300 K. All STM images were collected at 120 K.

We unequivocally demonstrate that gold atoms from the surface are incorporated into the Cl structure at high coverage by the observed change in surface morphology upon desorption of a fraction of the Cl from the surface. As reported previously[1,2], Cl_2

evolves from Au(111) with a broad peak centered at ~640 K and a high-temperature peak at ~790 K. By flashing the "honeycomb" structure to 750 K using a heating rate similar to the TPD experiments, only ~0.16 ML chlorine is left on the surface, as estimated from TPD (Supporting Information). At this stage, STM images obtained at 120 K show patches of $\sqrt{3} \times \sqrt{3}$ *R*30° structure and disordered particles (Figure 5.4b). Longer annealing at 750 K for 1 min desorbs all the chlorine. At this stage, both particles and partially re-formed soliton walls can be observed (Figure 5.4c). These particles have Au(111) single atomic height and cover ~6% of the surface area; therefore, these particles must include Au atoms derived from the bulk structure, *not* just the excess atoms that would be incorporated into the herringbone. Notably, in the STM image, the herringbone structure is already partially manifested, so that the total amount of Au originally associated with the Au−Cl surface compound is greater than 6%. After the sample is annealed at 750 K for 5 min, all Cl is removed from the surface; the particles disappear (Figure 5.4d) and the characteristic herringbone structure re-forms, further indicating that gold is released from a complex during chlorine desorption. No Au desorption was detected in any of our desorption experiments, indicating that the Au released remains on the surface. Therefore, the STM results at different annealing stages demonstrate that, at coverages above 0.33 ML, Au atoms incorporate into the absorbate layer to form a surface compound.

5.6 Calculations Results

Experimentally, we have unambiguous evidence that Au atoms incorporate into a chloride structure at high coverage (>0.33 ML), but no evidence for Au incorporation into $\sqrt{3} \times \sqrt{3}$ R30° structure. Below 0.33 ML, Au initially released from the herringbone

reconstruction mainly appears to migrate to step edges and incorporate into a (1 × 1) Au structure under the Cl overlayer. DFT calculations were used to test possible structures for the 0.33 ML Cl on Au(111) and to test model systems that incorporate Au adatoms so as to gain physical insight into the driving forces for this phenomenon. The adsorption of chlorine is tested on three different Au(111) substrates: clean Au(111)-(1 × 1) surface and surfaces covered with 0.33 and 0.67 ML of Au adatoms (Figure 5.5).

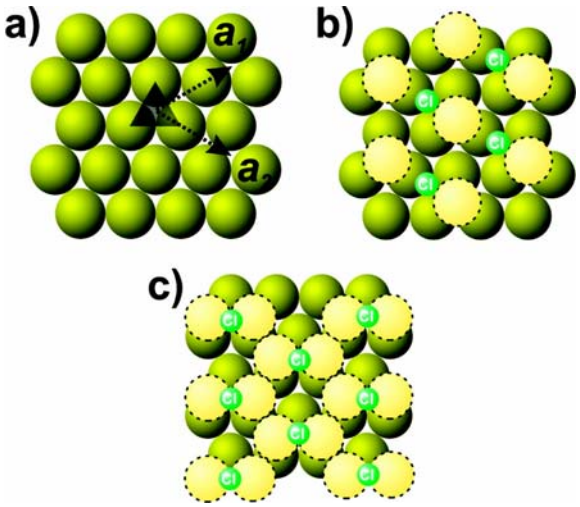

Figure 5.5. Different configurations to test Cl adsorption on Au(111) with DFT. (a) Clean $\sqrt{3}\times\sqrt{3}\,R30°$ Au(111) surface with the unit cell and lattice vectors a_1 and a_2. (b) 0.33 ML Cl on the "side" of the 0.33 ML Au adatoms. (c) 0.33 ML Cl on "bridge sites" of the 0.67 ML Au adatoms. The dark large circles represent the underlying gold, whereas the lighter large circles represent Au adatoms, and the small green circles are chlorine atoms.

We restrict ourselves to only testing structures with $\sqrt{3}\times\sqrt{3}$ R30° unit cell, according to periodicity observed in both LEED and STM at 0.33 ML Cl coverage (Figure 5.5a). One layer in the unit cell only contains three gold atoms; therefore, 0.33 and 0.67 ML of

adatoms represent all the possible substrates that could result in gold incorporation upon the adsorption of chlorine.

We calculate the energies of Cl bound to the Au using the Au(111)-(1 × 1) surface as a reference to evaluate the relative stability of the various structures tested. The energies for the chlorine adsorbed system are defined relative to the breaking of a Cl−Cl bond and the cost required to create adatoms on the surface in the relevant cases:

$$E(\mathrm{Cl}) = E(\mathrm{Cl/Au}) - 1/2E(\mathrm{Cl_2}) + E_{\mathrm{Au\ cost}} - E(\mathrm{Au}) \qquad (5.6.1)$$

where E(Cl/Au) is the total electronic energy of a chlorine bound on the gold substrate, E(Au) is the energy of the Au(111)-(1 × 1) substrate, $E(\mathrm{Cl_2})$ is the energy of $\mathrm{Cl_2}$ molecule, and $E_{\mathrm{Au\ cost}}$ is the energy for creating n gold adatoms, which is defined as:

$$E_{\mathrm{Au\ cost}} = E(\mathrm{Au_{surface+adatom}}) - nE(\mathrm{Au_{atom\ in\ bulk}}) - E(\mathrm{Au}) \qquad (5.6.2)$$

where $E(\mathrm{Au_{surface+adatom}})$ is the total energy of the Au(111) substrate with the adatom, and $E(\mathrm{Au_{atom\ in\ bulk}})$ is the energy of a gold atom in the bulk. This energy cost was calculated for 0.33 and 0.67 ML of adatoms on the top layer of the $\sqrt{3} \times \sqrt{3}\ R30°$ unit cell and found to be 0.75 and 0.65 eV, respectively. The calculated bond length and binding energy for $\mathrm{Cl_2}$ using the PW91 functional was found to be 2.02 Å and 2.68 eV, respectively, where the experimental values are 1.99 Å and 2.48 Ev[34]. These values were also previously calculated using the RPBE functional and found to be 2.00 Å and 2.54 eV[35].

On Au(111)-(1 × 1), the binding of a single chlorine (0.33 ML coverage) was tested at four different sites: top, bridge, and the hcp and fcc threefold sites (Table 5.1). The threefold hollow sites are found to be the lowest in energy, and a very small advantage in energy was found for the adsorption of chlorine at an fcc site. The very small energy differences between the fcc, hcp, and bridge site (0.04 eV) indicate a very

small energy barrier for chlorine migration on Au(111) surface. Previous DFT calculations also found the threefold site to be the preferred binding site for chlorine on Au(111), with nearly the same Au−Cl distance and an adsorption energy at 0.5 ML coverage that was 0.40 eV higher in energy (due to increased repulsive interactions at higher coverage) than our value[4]. The adsorption of Cl on Ag(111) also prefers the threefold site and is slightly stronger than the Au−Cl interaction (E_{ads} = −1.63 eV at 0.33 ML coverage)[36]. The bond enthalpy of diatomic AuCl is −3.56 eV[37].

Table 5.1. Energies Calculated Using the PW91 Functional for 0.33 ML Cl Bound to Three Different Surfaces: Clean Au(111), Au(111) with 0.33, and 0.67 ML Au Adatoms

Surface	**site**	**energy (eV)**
Au(111)	top	−0.65
	bridge	−0.87
	hcp	−0.88
	fcc	−0.91
Au(111)+0.33 ML Au adatom	top	−0.43
	side	−0.47
Au(111)+0.67 ML Au adatom	bridge	−0.81
	vacancy	−0.24

In previous studies of chlorine structure on Au(111), Kastanas and Koel suggested a model in which 1.33 ML chlorine are packed on Au(111) surface to form a flat overlayer[2]. Our coverage calibration ruled out this model[11]. Nevertheless, we also tested this model with DFT by first allowing all degrees of freedom of the chlorine atoms to relax on a flat $\sqrt{3} \times \sqrt{3}\,R30°$ unit cell of Au. However, it was found that the chlorine did not remain bound on a flat surface. The Cl atoms were then constrained in the *z*-direction (perpendicular to the surface), and the energy was found for different distances from the

surface. Using the PW91 functional, no energy gain is found for packing this many chlorine atoms on the surface. Therefore, a coverage of 1.33 ML Cl overlayer on a flat Au (1 × 1) surface, as proposed by Kastanas and Koel[2], is unfavorable.

With an additional 0.33 ML Au adatoms located on threefold sites of Au(111), the adsorption of 0.33 ML Cl was tested on various sites on the surface of the $\sqrt{3} \times \sqrt{3}\, R30°$ unit cell of Au(111)-(1 × 1). Chlorine bound on the side of an adatom resulted in the lowest energy (Figure 5.5b). It was found that the binding of Cl on both top and the side of an adatom is stronger than that of chlorine on Au(111)-(1 × 1) surface as overlayer. But this stronger interaction cannot compensate for the cost of creating the adatom covered surface (0.75 eV), and Au incorporation would result in a higher total energy than the chlorine overlayer (Table 5.1).

When the surface contains 0.67 ML Au adatoms (equivalently, 0.33 ML of vacancies), the energy cost of creating this surface is 0.65 eV. The adsorption of chlorine was tested on various sites on the substrate, and the energy was the lowest for chlorine on a bridge site coordinated to two gold adatoms (Figure 5.5c). Chlorine bonded in the vacancy is found to be much higher in energy than the bridge site. Similar to the previous case, the energy gain for adsorbing chlorine to adatoms is not enough to compensate the energy cost of creating adatoms (Table 5.1). Therefore, the DFT calculations indicate that gold atoms are *not* incorporated into $\sqrt{3} \times \sqrt{3}\, R30°$ structure at 0.33 ML Cl coverage.
In the above discussions, “overlayer” and “chloride” are mainly referred to the geometric arrangement of adsorbed Cl atoms. However, this definition may not be accurate to describe, from an electronic point of view, the nature of Cl−Au bonding. Upon the adsorption of 0.33 ML chlorine overlayer, we found the charge on the chlorine atom was

−0.33. In fact, gold (III) chloride (Au_2Cl_6) adopts a planer dimer structure[31,32] (Figure 5.6). The experimental (calculated) bond distance for chlorine bonded to one gold atom and two gold atoms in the dimer is 2.23 Å (2.30 Å) and 2.33 Å (2.39 Å), respectively. The charge for bridge Cl (bonded to two Au atoms) was found to be −0.33, whereas the charge found for terminal Cl (bonded to one Au atom) was −0.22. Compared with that of the Au(III) chloride compound, the similar charge of Cl in 0.33 ML Cl overlayer suggests a significant charge transfer from the gold substrate to the chlorine atom[38-40].

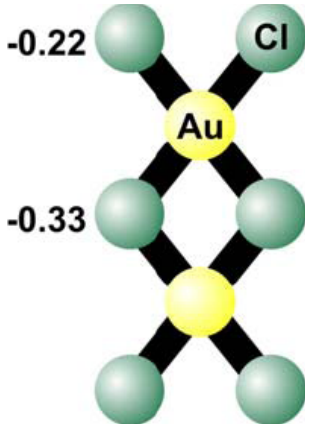

Figure 5.6. Gold (III) chloride structure adopted from Ref. 31 and 32. The charge of terminal Cl is found to be -0.22 and that of the bridge Cl is found to be -0.33.

The fact that the charge on the Cl in the overlayer is similar to the gold (III) chloride indicates chloride-like bonding even without Au adatom incorporation. This may be responsible for the contradictory interpretations of spectroscopic results to discriminate chemisorbed Cl and chloride on Au(111)[1,2]. For example, the absence of a Cl 2p binding energy shift with coverage change[2], therefore, cannot conclusively rule out the possibility of chloride formation. Indeed, a small increase (~0.4 eV) in Cl 2p binding energy from coverage of 0.26 ML to saturation is observed in our XPS data. But because of the very

small binding energy shift and limited instrument resolution, we do not attempt to assign specific chlorine species. In this case, synchrotron-based high-resolution XPS may be able to provide more valuable information[41]. On the other hand, the strong interaction between gold and chlorine in the overlayer also suggests that the overlayer formation can cause large electronic disturbance to the Au(111) substrate. One needs to be cautious in halogen adsorption studies because models in which substrate is treated as an undisturbed surface can be oversimplified. We are currently trying to address this point using additional DFT studies.

5.7 Conclusions

Our results reveal a dynamic process of chlorine adsorption on Au(111). Chlorine initially lifts the herringbone reconstruction. At low coverages (<0.33 ML), chlorine binds to the top of Au(111)-(1 × 1) surface and leads to formation of an overlayer with $\sqrt{3} \times \sqrt{3}\, R30°$ structure at 0.33 ML. At higher coverages, gold atoms are removed from Au(111)-(1 × 1) and form a complex superlattice of a Au−Cl surface compound.
The picture of chlorine interaction with gold revealed by STM studies can provide insight into the mechanism of surface reactions[3]. However, important questions still remain in this system: What is the microscopic mechanism of transformation from chlorine overlayer to surface compound? What is the structure of surface gold chloride? Halogenation is a complex process that involves multiple mechanistic aspects, as indicated by tremendous studies and continuing effort on other transition-metal surfaces. Moreover, the gold chloride structure has been considered as a challenge in both

experimental and theoretical studies[42,43]. Therefore, we believe our results will initiate further studies on this system.

5.8 References

[1] N. D. Spencer, R. M. Lambert, *Surf. Sci.* **1981**, *107*, 237.

[2] G. N. Kastanas, B. E. Koel, *Appl. Surf. Sci.* **1993**, *64*, 235.

[3] C. T. Rettner, D. J. Auerbach, *Science* **1994**, *263*, 365.

[4] D. Lemoine, J. G. Quattrucci, B. Jackson, *Phys. Rev. Lett.* **2002**, *89*, 268302.

[5] Y. X. Zhao, M. D. Mann, J. H. Pavlish, B. A. F. Mibeck, G. E. Dunham, E. S. Olson, *Environ. Sci. Technol*. **2006**, *40*, 1603.

[6] D. S. Pinnaduwage, L. Zhou, W. Gao, C.M. Friend, *J. Am. Chem. Soc.* **2007**, *129*, 1872.

[7] R. Burks, *Chem. Eng. News* **2007**, *85*, 87.

[8] M. Haruta, M. Date, *Appl. Catal. A.* **2001**, *222*, 427.

[9] X. Deng, C. M. Friend, *J. Am. Chem. Soc.* **2005**, *127*, 17178.

[10] W. Gao, L. Zhou, D.S. Pinnaduwage, R.J. Madix, C.M. Friend, *J. Phys. Chem. C.* **2007**, *111*, 9005.

[11] E. I. Altman, M. Bienfait, H. P. Bonzel, H. Brune, R. Diehl, M. Y. L. Jung, V. G. Lifshitz, M. E. Michel, R. Miranda, R. McGrath, K. Oura, A. A. Saranin, E. G. Seebauer, P. Zeppenfeld, A. V. Zotov, in *Physics of Covered Solid Surfaces*; H. P. Bonzel, Ed.; *Adsorption on Surfaces and Surface Diffusion of Adsorbates* [Springer-Verlag: New York, **2001**; Vol. 42, p 421].

[12] D. A. Shirley, *Phys. Rev. B.* **1972**, *5*, 4709.

[13] M. M. Biener, J. Biener, C. M. Friend, *Langmuir* **2005**, *21*, 1668.

[14] M. M. Biener, J. Biener, C. M. Friend, *Surf. Sci.* **2007**, *601*, 1659.

[15] M. Yu, H. Ascolani, G. Zampieri, D. P. Woodruff, C. J. Satterley, R. G. Jones, V. R. Dhanak, *J. Phys. Chem. C* **2007**, *111*, 10904.

[16] G. Kresse, J. Hafner, *Phys. Rev. B.* **1993**, *47*, 558.

[17] J. P. Perdew, Y. Wang, *Phys. Rev. B.* **1992**, *45*, 13244.

[18] G. Kresse, J. Hafner, *J. Phys.: Condens. Matter* **1994**, *6*, 8245.

[19] C. Nordling, J. Osterman, *Physics Handbook*; [Lund: **1987**].

[20] C. Kittel, *Introduction to solid state physics*; [Wiley: New York, **1996**].

[21] L. M. Molina, B. Hammer, *Phys. Rev. B* **2004,** *69*, 155425.

[22] F. R. d. Boer, R. Boom, W. C. M. Mattens, A. R. Miedema, A. K. Niessen, I *Cohesion in Metals*; [North-Holland: Amsterdam, **1988**].

[23] H. L. Skriver, N. M. Rosengaard, *Phys. Rev. B* **1992,** *46, 7157.*

[24] S. M. Foiles, M. I. Baskes, M. S. Daw, *Phys. Rev. B* **1986,** *33, 7983.*

[25] C. Woll, S. Chiang, R. J. Wilson, P. H. Lippel, *Phys. Rev. B* **1989**, *39*, 7988.

[26] B. K. Min, A. R.Alemozafar, M. M. Biener, J. Biener, C. M. Friend, *Top. Catal.* **2005**, *36*, 77.

[27] S. M. Driver, T. F. Zhang, D. A. King, *Angew. Chem., Int. Ed.* **2007**, *46*, 700.

[28] A. E. Baber, S. C. Jensen, E. V. Iski, E. C. H. Sykes, *J. Am. Chem. Soc.* **2006**, *128*, 15384.

[29] M. Kostelitz, J. L. Domange, J. Oudar, *Surf. Sci.* **1973**, *34*, 431.

[30] *Handbook of X-ray Photoelectron Spectroscopy;* C. D. Wagner, W. M. Riggs, L. E. Davis, J. F. Moulder, G. E. Muilenberg, Eds.; [Perkin-Elmer Corp.: Eden Prairie, MN, **1979**.]

[31] E. S. Clark, D. H. Templeton, C. H. Macgillavry, *Acta Crystallogr.* **1958**, *11*, 284.

[32] B. Reffy, M. Kolonits, A. Schulz, T. M. Klapotke, M. Hargittai, *J. Am. Chem. Soc.* **2000**, *122*, 3127.

[33] I. J. Blackmore, A. J. Bridgeman, N. Harris, M. A. Holdaway, J. F. Rooms, E. L. Thompson, N. A. Young, *Angew. Chem., Int. Ed.* **2005**, *44*, 6746.

[34] K. P. Huber, G. Herzberg, *Molecular Spectra and Molecular Structure Constant of Diatomic Molecules*; [Van Nostrand: New York, **1979**].

[35] P. Broqvist, L. M. Molina, H. Gronbeck, B. Hammer, *J. Catal.* **2004**, *227*, 217.

[36] N. H de Leeuw, C. J. Nelson, C. R. A. Catlow, P. Sautet, W. Dong, *Phys. Rev. B* **2004**, *69*, 045419.

[37] CRC Handbook of Chemistry and Physics; 77 ed.; D. R. Lide, Ed. [CRC Press: New York, **1996**].

[38] K. Doll, N. M. Harrison, *Chem. Phys. Lett.* **2000**, *317*, 282.

[39] K. Doll, N. M. Harrison, *Phys. Rev. B* **2001**, *63*, 165410.

[40] A. Migani, C. Sousa, F. Illas, *Surf. Sci.* **2005**, *574*, 297.

[41] H. Piao, M. C. N. Enever, K. Adib, J. Hrbek, M.A. Barteau, *Surf. Sci.* **2004**, *571*, 139.

[42] M. Hargittai, A. Schulz, B. Reffy, M. Kolonits, *J. Am. Chem. Soc.* **2001**, *123*, 1449.

[43] D. J. Gorin, F. D. Toste, *Nature* **2007**, *446*, 395.

CHAPTER 6

ATOMIC OXYGEN ADSORPTION ON AU(111) SURFACE WITH DEFECTS

6.1 Abstract

We study the equilibrium structures for the adsorption of atomic oxygen on Au(111) surfaces containing defects such as vacancies and steps, using first-principles density-functional-theory calculations. We considered the gold-oxygen interaction as a function of surface vacancy concentration, the interaction with 1,2 and 4 gold adatoms (the latter number arranged in groups that represent 2D or 3D gold islands), the interaction at steps, and finally, the effect of strain. We find that there is an attractive interaction between oxygen atoms and vacancies on the surface, which lowers the cost to create a surface vacancy by 0.20 eV, but the interaction between oxygen and gold adatoms is repulsive. We conclude that the strength of the oxygen-gold interaction is correlated with the coordination number of the gold atom to which the oxygen is bound.

The work was published as an article in *Journal of Physical Chemistry C.*: T.A. Baker, C.M. Friend, and E. Kaxiras. **2009.** ***113,*** 3232.

6.2 Introduction

While Au is often valued for its relative inertness, Haruta and co-workers discovered that Au nanoparticles supported on reducible metal oxides are active for the catalytic oxidation[1-3] of CO[4] and propene[5]. Supported gold nanoparticles also promote a

range of other reactions, including the hydrogenation of acetylene[6], reduction of NO_x by hydrocarbons[7], and the oxidation of CH_4[8] and NO[9]. Au has also proven very useful in the oxidation of CO because Pt catalysts are not effective below 200^{O}C, resulting in the production of CO during cold-start-up[10,11].

There are several proposed explanations and factors that control the catalytic activity of gold nanoparticles on oxide supports. Studies have shown that the size of the Au nanoparticle on supported metal oxides has a substantial effect on the catalytic activity[12-14]. Other important factors impacting the catalytic activity include the nature of the metal oxide support, the oxidation state of Au, and the method by which the catalyst was prepared[15]. Recent results, however, indicate that the oxide support or nano-sized gold may not be needed for the reaction. For example, unsupported bulk gold powder and nanoporous gold foams are active for CO oxidation[16-18], and CO oxidative amination[15]. Single crystal gold has also been found to be reactive for a variety of oxidation reactions[19-21].

The mechanism for low-temperature CO oxidation is not clearly understood; undercoordinated Au could be possible sites for binding or even dissociation of O_2, which is an important step in the catalytic process[22-24]. Moreover, adsorption of CO and O is stronger on a surface where undercoordinated Au atoms exist[12]. It is therefore important to understand how undercoordinated atoms can be created on the surface and under what conditions they are stable. For example, supported gold catalysts will often deactivate over time under typical catalytic conditions, which is attributed to the agglomeration of Au particles (sintering) or the poisoning of active sites by accumulation of by-products[25].

Understanding how gold atoms are released from a gold surface and the how islands are formed will help elucidate the mechanism of sintering.

The release of metal atoms from a surface is of deep fundamental importance to many areas of surface chemistry, especially catalysis and surface reactivity. Since changes in metal-metal bonding can have a dramatic effect on the stability of intermediates and the energies of transition states, it is important to account for the release of atoms from the surface during adsorption or reaction in theoretical models.

Herein, we investigate the effect of adsorbed oxygen atoms on the release of Au atoms from the Au(111) surface using calculations based on density-functional-theory, in order to address recent experimental results. Kinetically, the release of atoms from Au(111) is expected to be facile because the clean surface reconstructs to form the 'herringbone' structure, which has an excess of 4.5% Au atoms compared to the bulk-terminated (111) plane. Dislocations at the 'elbow' sites[26-28] form to relieve strain from lattice mismatch. Atoms at the dislocations are more weakly bound and, therefore, readily released from the surface. In fact, adsorbed species—for example, sulfur[29,30], oxygen[31], NO_2[32], methanethiol[33,34], styrene[35] — lift (reverse) the herringbone reconstruction and release gold adatoms on the surface[36].

Experiments show that atomic oxygen can release gold atoms from the Au(111) substrate[31]. In recent theoretical work, Shi *et. al.* have also predicted that the energetically most favorable configuration of oxygen on Au(111) is a "surface-oxide-like" structure that has gold incorporated in its structure[37]. To do so, the atomic oxygen must either have an attractive interaction with the gold adatom once it is released from the surface, or the oxygen must have an attractive interaction with the vacancy left behind

after the gold atom is released from the surface site. Based on this assumption, we study the interaction of oxygen with gold adatoms and vacancies on the Au(111) surface, and determine the energy cost for removing gold from different possible sites both with and without oxygen present. We find that atomic oxygen, at low coverages, has a repulsive interaction with adatoms and an attractive interaction with vacancies, this latter interaction being responsible for the release of gold atoms from the surface in the presence of oxygen.

6.3 Computational Details

The computations in the work were performed using the VASP code[38], both with the GGA-PW91[39] and the GGA-RPBE[40] exchange-correlation functionals. The RPBE functional was used because it provides a better description of the chemisorption energies for adsorbates on transition metal surfaces[40]. Ultrasoft pseudopotenitals were employed with the default plane-wave cutoffs for different elements taken from the GGA ultrasoft-pseudopotential database[41,42] and 7x7x1 k-point sampling was used. The surface was modeled by a slab consisting of 4 layers in the (111) direction, with a primitive 4x4 unit cell in the lateral directions; only the two uppermost layers of the slab were allowed to relax, with the rest fixed at the ideal bulk positions. The bulk gold positions of the bottom two layers were taken from the calculated lattice constant of 4.17 Å which is in good agreement with the experimental value 4.08 Å[43]. Spin-polarized calculations were also considered, but had no substantial effect on the reported results.

The relative energy differences on which we base our conclusions agree well when the two different exchange-correlation functionals are used, and we will quote only

the results from the PW91 functional. In the few cases where there were small differences, both sets of data are presented and the differences are discussed.

Vibrational frequencies were calculated using the force-constant approach implemented within the VASP code. To save computational cost, all vibrational results were calculated with 4x4x1 Monkhorst-Pack k-point sampling. Test cases were calculated with 7x7x1 k-point sampling but found to change the resulting frequencies by no more than 1 cm^{-1}. The adsorbate and the gold atoms directly bound to the adsorbate are displaced by a step of 0.025 Å to calculate the mass-weighted dynamical (Hessian) matrix. The eigenvalues and eigenvectors of this matrix equal the vibrational frequencies and direction of each normal mode vibration, respectively.

6.4 Results and Discussion

The reference calculation used in this work is the binding of oxygen on a clean , defect-free Au(111)-(1x1) surface. All energies in the tables are reported as relative adsorption energies, with a positive relative energy indicating a weaker oxygen adsorption compared to adsorption on the (1x1) surface. All calculations were performed using a *p*(4x4) unit cell of Au(111), thus one adsorbed oxygen corresponds to an 1/16 ML coverage. The adsorption energy for oxygen is defined as:

$$E_{ads} = E_{O/Au} - E_{Au} - E_{O} \qquad (6.4.1)$$

where $E_{O/Au}$ is the total energy of an oxygen atom bound to the gold substrate, E_{Au} is the energy of the gold substrate, and E_{O} is the energy of atomic oxygen. Oxygen prefers to bind on an FCC three-fold hollow site and its adsorption energy is E_{ads} = -3.08 eV (-2.69 eV) with an Au-O bond distance of 2.16 Å (2.17 Å) using the PW91 (RPBE) functional.

This agrees well with past literature; Gajdos *et. al.* found using the PBE functional found an energy of -2.78 eV and Au-O bond distance of 2.16 Å for an 1/9 ML coverage[44]. Due to the repulsive nature of atomic oxygen on the surface, our calculated adsorption energies are lower because we looked at a lower coverage (1/16 ML). The experimental Au-O bond length for gold coordinated to three Au atoms in bulk gold (III) oxide is 2.04 Å[45].

Since oxygen prefers a three-fold site and the bridge site is the second lowest in energy site on the surface, diffusion of oxygen should proceed from a FCC hole (three-fold site) to a bridge site (two-fold) to an HCP hole (three-fold). The diffusion barrier for oxygen, defined as:

$$E_d = E_{bridge} - E_{fcc} \tag{6.4.2}$$

is $E_d = 0.49$ eV. The diffusion barrier for a gold adatom through the same path is much lower, only 0.11 eV. For comparison, the calculated diffusion barrier for Au using the embedded atom method with potentials developed by Adams, Foiles, and Wolfer[46] and by Voter and Chen[47] is 0.021 and 0.038 eV, respectively[48]. It is interesting to note that the ratio between the diffusion barrier and the adsorption energy are very different for oxygen and Au adatom on Au(111): 0.160 and 0.046, respectively.

6.4.1. Interaction of Gold with Adatoms

The adsorption of atomic oxygen was studied on a surface containing one and two gold adatoms, Figure 6.1. The system was allowed to relax including all degrees of freedom of the two layers of Au(111), the gold adatom, and oxygen bound to the surface. The results are summarized in Table 6.1.

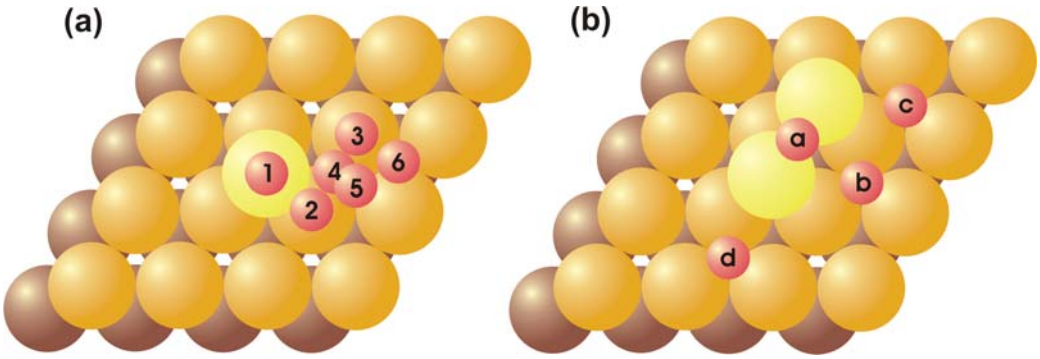

Figure 6.1: Starting configurations used to study the adsorption of atomic oxygen on an Au(111) surface containing one (a) and two (b) gold adatoms. The dark spheres are the underlying *p*(4x4) Au(111) surface, the orange spheres are the top layer of gold, and the yellow spheres are gold adatoms. The smaller red circles label the oxygen atom.

Table 1: Relative adsorption energies (E_{rel}, versus 1/16 ML coverage of oxygen in three-fold sites on the Au(111)-(1x1) surface) of atomic oxygen on the one (Figure. 6.1a) and two (Figure. 6.1b) gold adatom covered surface.

One Au adatom		Two Au adatoms	
Site	E_{rel} (eV)	Site	E_{rel} (eV)
1	0.92	a	-0.07
2	0.60	b	0.08
3	0.52	c	0.23
4	0.18	d	0.18
5	0.06		
6	0.27		

Oxygen is adsorbed more strongly on the clean (1x1) surface compared to adsorption next to a single gold adatom (Table 6.1). All of the tested configurations have a higher relative adsorption energy except for the configurations where the oxygen is

placed away from the adatom. For example, in configuration 5 there is essentially no interaction between the adatom and the oxygen since the adsorption energy of oxygen is nearly equal to oxygen on a clean surface. When oxygen is placed in an HCP hole and relaxed (configuration 6), both the gold adatom and adsorbed oxygen stay in their three-fold site. The relative adsorption energy of this configuration (compared to oxygen on a defect-free surface) is 0.27 eV. However, this difference is a result of the energy cost of having an oxygen atom in an HCP three-fold site compared to the more favorable FCC three-fold site. On a clean surface, the difference in the adsorption energies for an oxygen in an FCC compared to an HCP three-fold site is 0.24 eV.

Given the relative calculated diffusion barriers for a gold adatom vs. an adsorbed oxygen atom, we anticipate the optimization of the oxygen bonding to the surface in a system that contains both gold and oxygen adatoms. For example, when the forces were relaxed in configuration 2, the gold adatom moved away from the oxygen atom to a spot in between the neighboring three-fold and bridge site. The oxygen atom is shared between the gold adatom and a gold atom in the surface. Interestingly, the gold atom in the first layer was pulled out of the plane of the other gold atoms in the first layer by ~ 1 Å (Figure. 6.2). The distance between oxygen and both the gold adatom and gold atom that was lifted out of the surface is 2.03 Å. In configuration 3 the gold adatom was brought out of its three-fold site towards the oxygen and the oxygen drifted slightly from the top of the Au adatom resulting in a similar Au_{adatom}-O distance of 2.04 Å.

We also studied models with two Au adatoms (Figure 6.1b) and found that the Au dimer also relaxes in response to the oxygen atom. For example, in configuration *b*, which shows the starting configuration, the two gold adatoms both moved away from the

oxygen on the neighboring threefold site resulting in an Au_{adatom}-O distance of 4.58 Å. In configuration *c* and *d,* the Au adatoms stayed in their original configurations, resulting in a shorter distance between the oxygen and gold adatoms and a higher relative adsorption energy for oxygen.

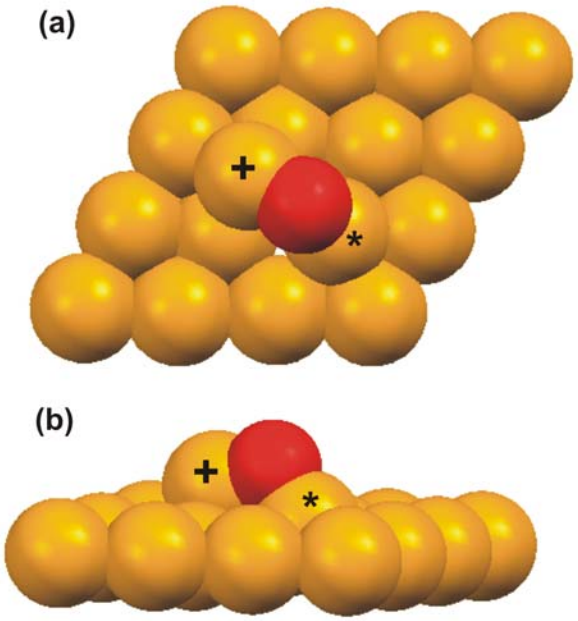

Figure 6.2: Top (a) and side (b) view of relaxed configuration 2. The orange spheres are gold atoms while the red sphere is oxygen. The gold atom with the plus (+) symbol is the gold adatom, while the gold atom with the asterisk (*) is pulled nearly 1 Å out of the plane of surface gold atoms. Note that only one layer underneath the adsorbed oxygen is shown; however, four layers were used in the calculation.

Our calculations lead us to conclude that there is generally not a favorable interaction of oxygen with gold adatoms. The adsorption energy for oxygen with a gold adatom present only becomes equal to oxygen on a clean surface when the adatom and oxygen are well-separated. Oxygen prefers the coordination of the three-fold site and it

is not energetically favorable to gain coordination from additional gold atoms. However, the adsorption of oxygen can be slightly stronger compared to the (1x1) surface if it is bound in the two-fold site between two gold adatoms; configuration a, Figure 6.1(b). This point is consistent with the results calculated with the RPBE functional (-0.20 eV) suggesting that oxygen indeed has a slightly favorable interaction in the 2-fold site defined by the gold adatom dimer. This result indicates that oxygen may prefer to bind with a gold atom that is missing coordination to other gold atoms. This possibility will be investigated later in this report.

Our calculations further indicate that oxygen will assume a configuration on the surface so as to achieve a coordination as close to 3 Au atoms as possible by either moving towards other gold adatoms or shortening its bond to surface gold atoms. Configurations 3 and 4 in Figure 6.1a illustrate this effect. In both cases, the O is coordinated to fewer than three Au centers in the (111) plane and in both cases the lowest energy configuration with the Au adatom present involves rearrangement that brings the gold adatom in closer proximity to the oxygen. The resulting Au_{adatom}-O distance was smaller when the oxygen was on a top site versus a bridge site since the oxygen on the top was missing coordination to other gold atoms.

6.4.2. Interaction of Gold with Vacancies

Oxygen *does* interact more strongly with Au vacancies compared to the (1x1) surface, in contrast to the effect of Au adatoms. In order to evaluate the interaction of oxygen with Au vacancies, we calculated the relative adsorption energy of the oxygen with a vacancy and the energy cost for creating *n* vacancies. The energy cost of creating *n* vacancies is defined as:

$$E_{cost}(n) = E_{vacancy} + nE_{bulk} - E_{full} \quad (6.4.3)$$

where $E_{vacancy}$ is the total energy of the surface with n gold atoms removed, E_{bulk} is the energy of a gold atom in the bulk crystal, and E_{full} is the energy of the surface without the removal of gold atoms used to make the vacancy.

The most striking result is that the adsorption of oxygen in three-fold sites near the vacancy is more favorable compared to the (1x1) surface. This energy gained from oxygen bonding to this surface, however, is not sufficient to offset the cost of making the vacancy. For example, the adsorption energy for oxygen on a three-fold site adjacent to the vacancy (site 2 in Figure 6.3) has an adsorption energy 0.20 eV lower than adsorption on the (1x1) surface, but the energetic cost to create the vacancy is 0.60 eV (Table 6.2). The oxygen does not sit exactly in the center of the three-fold site, but rather is shifted slightly towards the vacancy. The distance between the gold atom next to the vacancy and the oxygen is 2.14 Å while the distance from the oxygen to the other gold atoms in the three-fold site is 2.19 Å. Surprisingly, the adsorption energy of oxygen *in* the vacancy (site 3) is higher than for O in a 3-fold site on the (1x1) surface.

Table 6.2: Relative oxygen adsorption energy (E_{rel}) and energy cost to create a gold vacancy (E_{cost}) for different adsorption sites on the vacancy covered surface as shown in Fig. 3.

Site	E_{rel} (eV)	E_{cost} (eV)
no oxygen	-	0.60
1	-0.02	0.58
2	-0.20	0.41
3	0.21	0.81

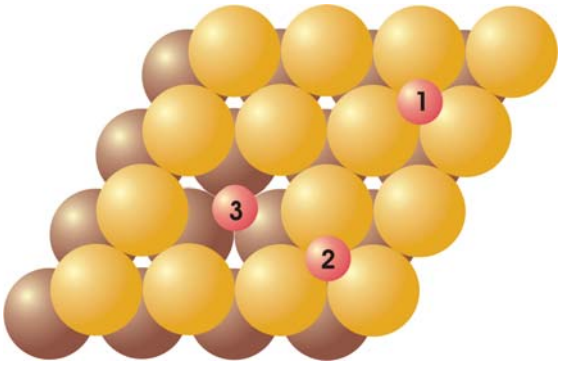

Figure 6.3: Adsorption sites for atomic oxygen on a Au(111) surface containing one vacancy. The orange spheres represent the top layer of gold, while dark spheres represent the second layer of gold atoms.

6.4.3. Interaction of Oxygen with Steps and Other Structures

The prevalence of steps on extended surfaces and particle edges render them important binding sites to consider for oxygen. Previous studies by Liu et al.[49] reported that atomic oxygen is bound more strongly to the stepped Au(211) and Au(221) surface than the flat Au(111) surface by several tenths of an eV. The most favorable site for oxygen adsorption was reported to be the bridge site at the edge of the step (site 2 in Figure 6.4b) using the GGA-PBE functional. Xu and Mavrikakis[50] also found that atomic oxygen is more strongly bound to an Au(211) surface; however, they found that the most favorable adsorption site is a hanging fcc site at the edge of a step (site 1 in Figure 6.4b) using the GGA-PW91 functional. Our objective was to isolate the effect of the step by using a bigger unit cell, Au(533), and to specifically investigate the ability of oxygen to remove gold atoms from the step.

In our work, the stability of the oxygen decreased as the adsorption site moves away from under-coordinated gold atoms at the step edge and towards a site with a

coordination greater than three against the ledge of a step (Configurations 1 and 5, Fig. 4b, Table 3). This conclusion is based on a comparison of the binding energy of oxygen at various positions relative to the step edge (Figure 6.4, Table 6.3).

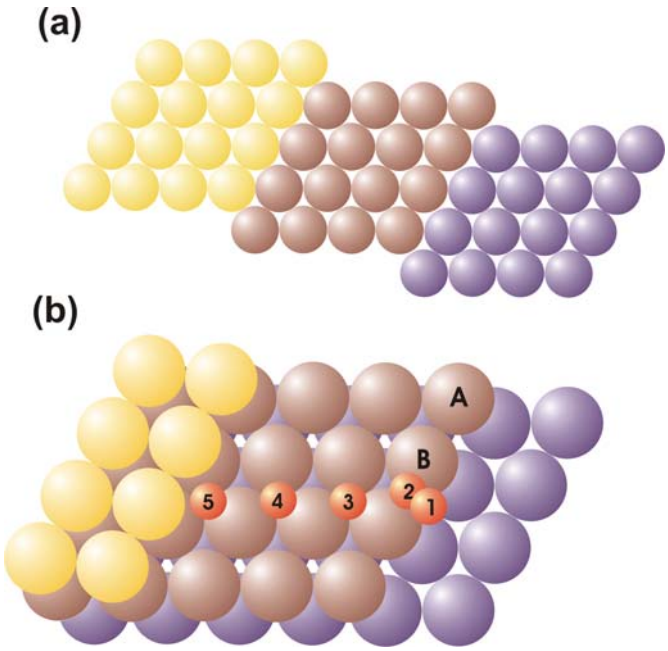

Figure 6.4: Model of stepped <110>/{100} Au(533) surface, where <110> is the direction along the step edge and {100} is the plane of the step edge: (a) side view of step; (b) top view. Yellow spheres are gold atoms that make up the upper step, the dark spheres comprise the middle terrace, and the blue spheres are the gold layer of the lower step. The red numbered circles represent different binding sites of oxygen. The gold atoms with capital letters are removed to create a step vacancy.

We found that oxygen was essentially equally stable at the "hanging fcc" site at the edge of a step (site 1), bridge site (site 2), and the fcc site at the edge of the step (site 3). The oxygen that started on the bridge site (site 2), relaxed towards (but not completely) to the hanging fcc site (site 1). With the PW91 functional, however, the adsorption of oxygen

at the step is not stronger than oxygen adsorption on the (1x1) surface, as was found in the literature with the PBE functional. Our results indicate that adsorption in the middle of terrace is weaker than at the edge of the step, but because of the small size of the terrace in our step calculations and contradiction with previous work that used a different exchange-correlation functional, we cannot conclude convincingly that the adsorption of oxygen is stronger on a step-edge. As a comparison, the same set of calculations were done using the RPBE functional. Nearly the same trends and values were found.

A second role of oxygen bonding at step edges is that it facilitates the removal of Au from the step edge. In particular, oxygen adsorbed on a three-fold site at the edge of a step (Site 3, Figure 6.4) lowered the cost of removing a gold atom from the step (Table 6.3).

The adsorption for oxygen in a three-fold site is stronger on a small 2D-island of Au (by -0.21 eV) than a flat (1x1) surface. This effect is illustrated by our study of four gold adatoms forming a cluster adsorbed on top of the Au(111) surface (Figure 6.5). Furthermore, the presence of oxygen lowers the cost to remove the fourth adatom in the 2D-island by 0.10 eV.

In contrast to the 2-D island, oxygen's interaction with 3-D islands (Figure 6.6) is weaker compared to the (1x1) surface. The 3-D island consists of 4 gold adatoms that form a pyramid on top of the Au(111) surface. While it is an unphysical system, it can serve as a model to understand the interaction of oxygen to different gold species. Two different adsorption sites for oxygen were tested, one is a three-fold site on the side of the 3-D island (labeled as site 1 in Figure 6.6) and the second is on the side of the bottom layer of the 3-D island (labeled as site 2). In both cases, oxygen is more weakly bound

than in the case of oxygen on a flat surface, the relative adsorption energy for site 1 and 2 is 0.63 and 0.32 eV, respectively.

Table 6.3: Relative oxygen adsorption energy (E_{rel}) and energy cost to create a gold vacancy (E_{cost}) for oxygen bound on the stepped surface as shown in Figure 6.4. The number indicates the location of the oxygen, while the letter represents which gold atom was removed to create a vacancy (Figure 6.4b). Calculations were done with both the PW91 and RPBE functional.

Site	PW91 E_{rel} (eV)	RPBE E_{rel} (eV)
1	0.09	0.00
2	0.08	0.00
3	0.12	0.07
4	0.26	0.23
5	0.35	0.35
	E_{cost} (eV)	E_{cost} (eV)
no oxygen	0.19	0.16
2a	0.31	0.25
3a	0.03	0.01
3b	0.23	0.23

The energy cost to remove the gold atom on top of the 3-D island without any oxygen present is -0.48 eV. If the oxygen from site 1 is allowed to "roll" into the three-fold site as in 2D-island, the energy cost becomes -1.42 eV, which is a gain in energy of almost 1 eV. Since the adsorption of atomic oxygen on a 3D-island is weak, the energetic gain for destroying the 3D-island is large.

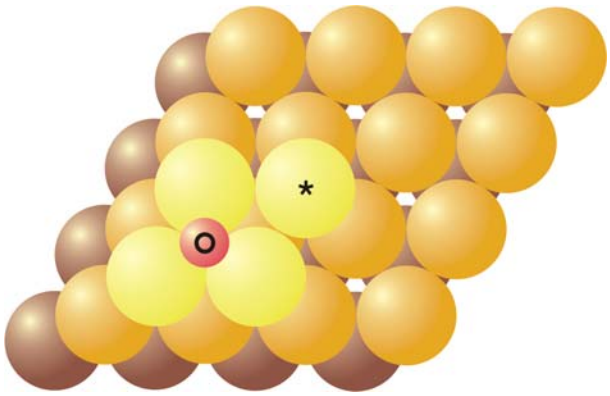

Figure 6.5: Diagram of 2D-island. Dark spheres represent the underlying Au(111) surface, orange spheres are top layer of gold, and yellow spheres are adatoms that make up the 2D-island. The oxygen is adsorbed on an fcc three-fold site of the gold adatoms and is labeled by red sphere with an O. The cost to remove a gold adatom was calculated for the atom labeled with an asterisk.

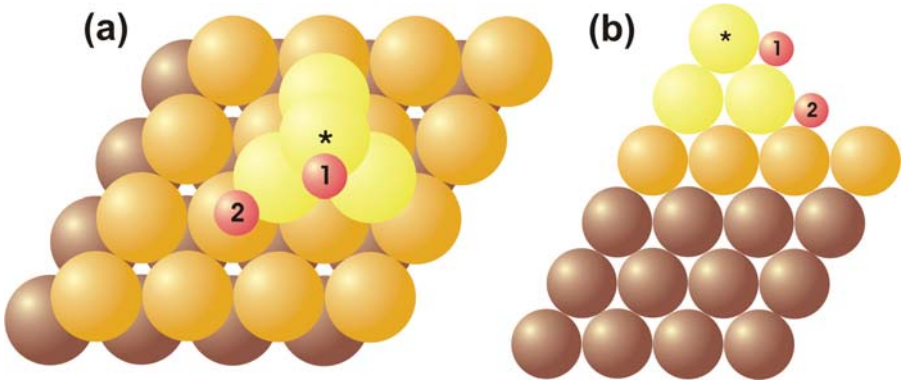

Figure 6.6: Top (a) and side (b) diagram of 3D-island. Dark spheres represent the underlying Au(111) surface, orange spheres are top layer of gold, and yellow spheres are adatoms that make up the 3D-island. The location of the adsorbed oxygen atom is labeled with a smaller red sphere. The gold atom on top of the pyramid with the asterisk is removed to create the vacancy.

6.4.4. Oxygen Adsorption on a Strained Surface

Previous studies have suggested that surface strain plays an important role in the reactivity of Au catalysts. For example, it was found that strain is induced in gold particles by interaction with the MgO support[51] . The DFT studies of Xu and Mavrikakis[52] also found that Au(111) and Au(211) surfaces with elongated Au-Au bond lengths led to an increase in the adsorption energy of both atomic oxygen and molecular oxygen. Accordingly, we investigated the effect of stretching and compressing Au-Au bonds on the bonding of atomic oxygen. All the layers of the gold were held fixed in these calculations to avoid buckling of the surface. The results are summarized in Figure 6.7.

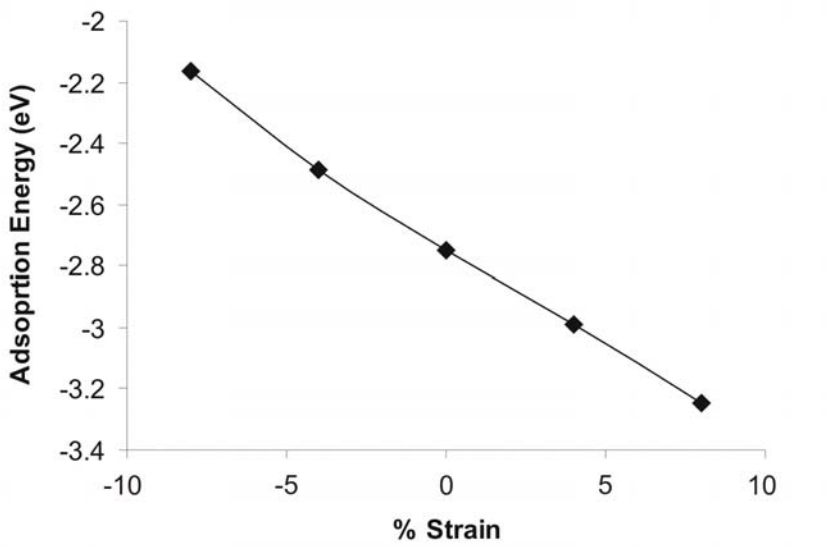

Figure 6.7: Adsorption energy of atomic oxygen on the strained surface versus the percent of strain. The percent of strain is the percent change in the unit cell vectors, where 0% represents the ideal unit cell lengths of the gold surface.

The adsorption of oxygen on the 3-fold site becomes stronger as the gold surface is stretched. As the gold substrate is stretched, the effective coordination of each gold atom is lowered. The stronger adsorption of oxygen on the stretched surface is consistent with our other results that showed stronger oxygen binding in a site adjacent to a gold vacancy and at an edge of a step. On the other hand, compression of the Au-Au lattice destabilizes the O-Au bonding in the 3-fold site, again agreeing with the trend that oxygen does not prefer a higher coordination of gold. This illustrates an important correlation between the strength of the binding of oxygen with the coordination of the gold atoms to which the oxygen is bound too.

6.4.5. Adsorption Dependence on Number of Vacancies

There are two important factors that determine the binding energy of oxygen to gold: (1) the number of gold atoms the oxygen is bound to and (2) the coordination of the gold atoms to which the oxygen is bound. On the (1x1) surface it is clear that atomic oxygen prefers to be bound to three gold atoms, while two and one gold atoms become increasingly less favorable. There can be favorable two-fold coordination of oxygen to gold but the gold must have a different coordination to other gold atoms. Examples include the ability of oxygen to bind on a bridge site at a step edge or on two gold adatoms.

To further understand how the coordination of gold can affect the adsorption energy of oxygen, a systematic study was done to calculate the adsorption energy with respect to the number of vacancies on the surface. Atomic oxygen was bound on a three-fold site and different gold atoms were removed to create vacancies on the surface (Figure 6.8).

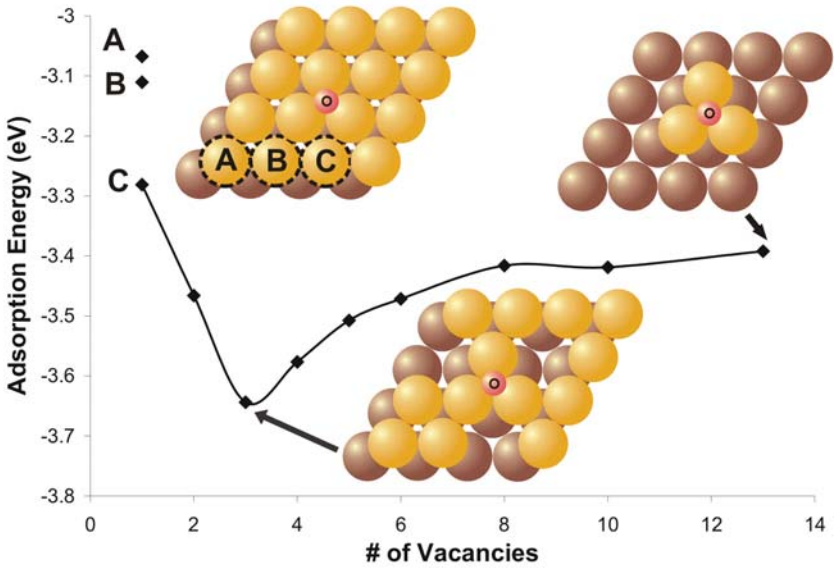

Figure 6.8: Adsorption energy of atomic oxygen as a function of the number of vacancies on Au(111). With only one vacancy there are three different configurations tested. The gold atom removed to create the vacancy is labeled (A,B, or C) on the model in the figure and its corresponding data point is also labeled. Models also show the atoms removed to create three vacancies and the final configuration with the maximum number of vacancies. Lighter yellow and darker brown large circles represent the top and second layer of gold, respectively.

The results show that the adsorption energy of oxygen on the surface can be decreased with the presence of vacancies, but interestingly, there is a minimum of this energy at three vacancies. Furthermore, oxygen lowers the cost to creating vacancies on the surface. Figure 6.9 shows the cost of creating vacancies as a function of the number of vacancies. Throughout the entire range of vacancies, the cost of creating a vacancy is always lower when oxygen is present. The cost is lowered from 0.20 eV (for 1 vacancy) to up to 0.56 eV (for 3 vacancies).

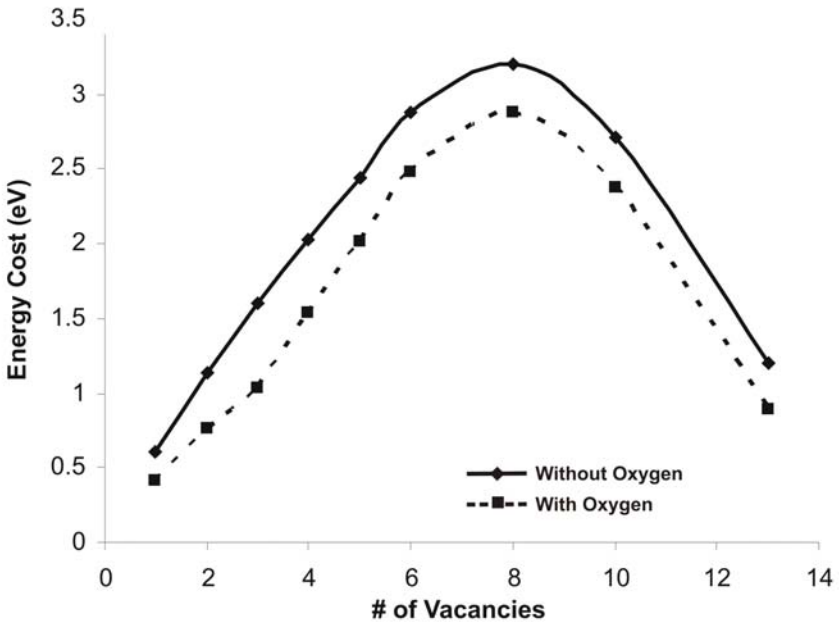

Figure 6.9: Energetic cost to create Au vacancies as a function of the number of vacancies. The solid top line is the cost without oxygen and the dotted line is with oxygen.

6.4.6. Vibrational Spectra

In order to compare our results with experimental data for oxygen bound to Au(111), we calculated the vibrational frequencies of several bonding configurations. The adsorption of atomic oxygen following ozone decomposition on Au(111) results in several oxygen species that have been studied with a variety of techniques[19,53]. Min et al. identified two prominent species on the surface as chemisorbed oxygen and gold oxide. Chemisorbed oxygen was observed in XPS at low oxygen coverages for ozone decomposition at 200 K, and oxidic oxygen is prevalent at higher coverages, > 0.5 ML, or when ozone is dosed on the surface at 400 K resulting in an ordered oxide. Both the work of N. Saliba *et al.*[53] and in our lab (unpublished) clearly observe at least two peaks

with high resolution electron energy loss spectra (HREELS): one at ~380 cm^{-1} and the other ~580 cm^{-1}. In our experimental work, we attribute the lower frequency peak at ~380 cm^{-1} to chemisorbed oxygen; however, the experiments are not able to determine the specific binding sites populated.

The calculated vibrational frequencies are in a range consistent with the experimental measurements for the "chemisorbed" oxygen formed on Au(111) and associated with a very defective surface (Table 6.4). Specifically, the calculated frequency for oxygen adsorption on a fcc site on the (1x1) surface is 405 cm^{-1}. Bonding in a site adjacent to a single vacancy shifts the stretch frequency to 370 cm^{-1} while binding to a 2-D island shifts the frequency up to 422 cm^{-1}. Surface strain also leads to shifts: compression leads to an upshift of ~20 cm^{-1} whereas elongation leads to very little change.

Table 6.4: Calculated vibrational frequencies for various systems. Only the highest frequency is listed because lower frequencies were significantly lower in intensity than the highest frequency and are generally at too low of a frequency to be resolved with most experimental HREELS systems. The motion corresponding to these frequencies is typically of the oxygen atom vibrating normal to the surface.

System	ν (cm-1)
FCC	405.5
Top of single adatom (Fig. 1a, site 1)	674.9
FCC on 2D island (Fig. 5)	421.9
Edge of Step (Fig. 4b, site 1)	452.5
Next to one vacancy (Fig. 3, site 2)	370.3
Bridge on 2 Au adatoms (Fig. 1b, site a)	491.9
FCC on Au strained -8%	442.5
FCC on Au strained 8%	405.9

The most significant change in frequency was calculated for oxygen bound atop a single adatom. The vibrational frequency is significantly higher than either of the major vibrational peaks observed; however, there is some intensity in this region of the spectrum, suggesting that there may be a minor amount of O-Au adatom bonding. Notably, none of the models described herein are consistent with the peak associated with the "2-D oxide", which forms at higher coverage and has an ordered structure. This result indicates that the oxide is fundamentally different in its bonding than the low-coverage structures studied herein, which is consistent with experimental studies showing that the "oxide" is much less reactive than the lower coverage structures[19].

6.5 Conclusions

It is known experimentally that atomic oxygen will release gold atoms from the Au(111) surface[31]. The cause for the evolution of this release of atoms is unknown. Our DFT calculations have shown that oxygen prefers to bind on three-fold sites on the Au(111)-(1x1) surface and will not interact with single gold adatoms. The number of gold atoms to which the oxygen is bound to has a significant effect on its stability. The fact the oxygen prefers a three-fold coordination is consistent with the noble nature of gold. There is only one known crystal of a stable gold oxide, Au_2O_3, and its synthesis is extremely difficult, requiring hydrothermal conditions with pressures of several 1000 atm[54].

The coordination of the gold atoms to which oxygen is bound to is an important factor in the energetics of oxygen adsorption. Oxygen interacts favorably with semi-undercoordinated gold in the form of terrace vacancies, steps, and 2D-islands but not with single adatoms or 3D-islands. This result suggests that atomic oxygen could break

up bigger islands leaving just oxygen bound to 2D-islands with three atoms, since oxygen bound to a three fold site is more stable. This agrees well with the experimental STM observation that the adsorption of oxygen results in a roughened gold surface[31].

Our calculations also show that oxygen can lower the thermodynamic cost for creating a vacancy by stabilizing (by at least 0.14 eV) the resulting vacancy left behind after the gold is released, in agreement with experimental results[55]. Table 6.5 summarizes the different systems and the cost for creating the vacancy with and without oxygen. This gain in energy could drive the release of gold atoms on Au(111) upon the adsorption of atomic oxygen.

Table 6.5: Summary of cost of creating a gold vacancy in various configurations both with and without oxygen adsorbed.

Au(111)	No Oxygen E_{cost} (eV)	Oxygen E_{cost} (eV)	Δ in E_{cost} (eV)
Terrace (one vacancy)	0.61	0.41	-0.20
Terrace (three vacancies)	1.60	1.03	-0.57
Step	0.19	0.03	-0.16
2D-Island	-0.21	-0.31	-0.10

Deciphering how adsorbates interact and release gold atoms that lead to a rough surface on Au(111) is crucial in understanding its catalytic properties. The interaction of oxygen with Au is critical for all oxidative catalysis. In general electronegative atoms and molecules can convert lattice Au atoms to Au adatoms. Generally understanding electronegative atoms on gold is not just important for atomic oxygen but other atoms including chlorine, which has been shown to enhance the selectivity toward olefin

epoxidation on Au(111)[56]. Future work in this direction will attempt to resolve issues related to the process by which gold is released, such as the energy barrier for this release, and the interaction of gold vacancies and adatoms with other electronegative species.

6.6 References

[1] M. Haruta, *Chem. Rec.* **2003**, *3*, 75.

[2] M. Haruta, M. Date, *Appl. Catal, A.* **2001**, *222*, 427-437.

[3] R. Meyer, C. Lemire, S. K. Shaikhutdinov, H. Freund, *Gold Bulletin* **2004**, *37*, 72.

[4] M. Haruta, N. Yamada, T. Kobayashi, S. Iijima, *J. Catal.* **1989**, *115*, 301.

[5] T. Hayashi, K. Tanaka, M. Haruta, *J. Catal.* **1998**, *178*, 566.

[6] R. J. H. Grisel, B. E. Neiuwenhuys, *Catal. Today* **2001**, *64*, 69.

[7] D. W. Lee, J. H. Ryu, D. H. Jeong, H. S. Lee, K. M. Chun, K. Y. Lee, *J. Ind. Eng. Chem.* **2003**, *9*, 102.

[8] R. J. H. Grisel, P. J. Kooyman, B. E. Nieuwenhuys, *J. Catal.* **2000**, *191*, 430.

[9] B. W. L. Jang, J. J. Spivey, M. C. Kung, H. H. Kung, *Energy Fuels* **1997**, *11*, 299.

[10] C. T. Campbell, *Science* **2004**, *306*, 234.

[11] C. W. Corti, R. J. Holliday, D. T. Thompson, *Appl. Catal, A.* **2005**, *291*, 253.

[12] N. Lopez, T. V. W. Janssens, B. S. Clausen, Y. Xu, M. Mavrikakis, T. Bligaard, J. K. Norskov, *J. Catal.* **2004**, *223*, 232.

[13] M. Valden, X. Lai, D. W. Goodman, *Science* **1998**, *281*, 1647.

[14] M. Valden, S. Pak, X. Lai, D. W. Goodman, *Catal. Lett.* **1998**, *56*, 7.

[15] B. L. Zhu, R. J. Angelici, *J. Am. Chem. Soc.* **2006**, *128*, 14460.

[16] Y. Iizuka, T. Tode, T. Takao, K.Yatsu, T. Takeuchi, S. Tsubota, M. Haruta, *J. Catal.* **1999**, *187*, 50.

[17] V. Zielasek, B.Jurgens, C. Schulz, J. Biener, M. M. Biener, A. V. Hamza, M. Baumer, *Angew. Chem., Int. Ed.* **2006**, *45*, 8241.

[18] C. X. Xu, J. X. Su, X. H. Xu, P. P. Liu, H. J. Zhao, F. Tian, Y. Ding, *J. Am. Chem. Soc.* **2007**, *129*, 42.

[19] B. K. Min, A. R. Alemozafar, D. Pinnaduwage, X. Y. Deng, C. M. Friend, *J. Phys. Chem. B.* **2006**, *110*, 19833.

[20] X. Y. Deng, B. K. Min, X. Y. Liu, C. M. Friend, *J. Phys. Chem. B.* **2006**, *110*, 15982.

[21] X. Y. Deng, C. M. Friend, *J. Am. Chem. Soc.* **2005**, *127*, 17178.

[22] I. N. Remediakis, N. Lopez, J. K. Norskov, *Appl. Catal, A.* **2005**, *291*, 13.

[23] C. Lemire, R. Meyer, S. K. Shaikhutdinov, H. J. Freund, *Surf. Sci.* **2004**, *552*, 27.

[24] T. V. W. Janssens, A. Carlsson, A. Puig-Molina, B. S. Clausen, *J. Catal.* **2006**, *240*, 108.

[25] M. M. Schubert, V. Plzak, J. Garche, R. J. Behm, *Catal. Lett.* **2001**, *76*, 143.

[26] S. Narasimhan, Vanderbilt, D. *Phys. Rev. Lett.* **1992**, *69*, 1564.

[27] C. E. Bach, M. Giesen, H. Ibach, T. L. Einstein, *Phys. Rev. Lett.* **1997**, *78*, 4225.

[28] H. Ibach, *J. Vac. Sci. Technol., A.* **1994**, *12*, 2240.

[29] M. M. Biener, J. Biener, C. M. Friend, *Langmuir* **2005**, *21*, 1668.

[30] S. Y. Quek, M. M. Biener, J. Biener, J. Bhattacharjee, C. M. Friend, U. V. Waghmare, E. Kaxiras, *J. Phys. Chem. B.* **2006**, *110*, 15663.

[31] B. K. Min, X. Y. Deng, D. Pinnaduwage, R. Schalek, C. M. Friend, *Phys. Rev. B.* **2005**, *72*, 4.

[32] S. M. Driver, T. F. Zhang, D. A. King, *Angew. Chem., Int. Ed.* **2007**, *46*, 700.

[33] P. Maksymovych, D. C. Sorescu, D. Dougherty, J. T. Yates, *J. Phys. Chem. B.* **2005**, *109*, 22463.

[34] L. M. Molina, B. Hammer, *Chem. Phys. Lett.* **2002**, *360*, 264.

[35] A. E. Baber, S. C. Jensen, E. V. Iski,; E. C. H. Sykes, *J. Am. Chem. Soc.* **2006**, *128*, 15384.

[36] D. Sander, U. Linke, H. Ibach, *Surf. Sci.* **1992**, *272*, 318.

[37] H. Shi, C. Stampfl, *Phys. Rev. B.* **2007**, *76*, 075327.

[38] G. Kresse, J. Hafner, *Phys. Rev. B.* **1993**, *47*, 558.

[39] J. P. Perdew, Y. Wang, *Phys. Rev. B.* **1992**, *45*, 13244.

[40] B. Hammer, L. B. Hansen, J. K. Norskov, *Phys. Rev. B.* **1999**, *59*, 7413-7421.

[41] D. Vanderbilt, *Phys. Rev. B.* **1990**, *41*, 7892.

[42] G. Kresse, J. Hafner, *J. Phys. Condens. Matter* **1994**, *6*, 8245.

[43] CRC Handbook of Chemistry and Physics; 77 ed.; D. R. Lide, Ed. [CRC Press: New York, **1996**].

[44] M. Gajdos, J. Hafner, A. Eichler, *J. Phys. Condens. Matter* **2005**, *18*, 13.

[45] P. G. Jones, H. Rumpel, E. Schwarzmann, G. M. Sheldrick, *Acta Crystallogr.* **1979**, *B35*, 1435.

[46] J. B. Adams, S. M. Foiles, W. G. Wolfer, *J. Mater. Res.* **1989**, *4*, 102.

[47] A. F. Voter, S. Chen, *Mater. Res. Soc. Symp. Proc.* **1987**, *82*, 175.

[48] C. L. Liu, J. M. Cohen, J. B. Adams, A. F. Voter, *Surf. Sci.* **1991**, *253*, 334.

[49] Z. P. Liu, P. Hu, A. Alavi, *J. Am. Chem. Soc.* **2002**, *124*, 14770.

[50] M. Mavrikakis, P. Stoltze, J. K. Norskov, *Catal. Lett.* **2000**, *64*, 101.

[51] S. Giorgio, C. Chapon, C. R. Henry, G. Nihoul, J. M. Penisson, *Philos. Mag. A.* **1991**, *64*, 87.

[52] Y. Xu, M. Mavrikakis, *J. Phys. Chem. B.* **2003**, *107*, 9298.

[53] N. Saliba, D. H. Parker, B. E. Koel, *Surf. Sci.* **1998**, *410*, 270.

[54] N. Weiher, E. A. Willneff, C. Figulla-Kroschel, M. Jansen, S. L. M. Schroeder, *Solid State Commun.* **2003**, *125*, 317.

[55] J. Biener, M. M. Biener, T. Nowitzki, A. V. Hamza, C. M. Friend, V. Zielasek, M. Baumer, *Chemphyschem* **2006**, *7*, 1906.

[56] D. S. Pinnaduwage, L. Zhou, W. W. Gao, C. M. Friend, *J. Am. Chem. Soc.* **2007**, *129*, 1872.

CHAPTER 7

ATOMIC OXYGEN ON AU(111): AN HIGH-RESOLUTION ELECTRON ENERGY LOSS SPECTROSCOPY AND AB-INITIO MOLECULAR DYNAMICS STUDY

7.1 Abstract

The Au(111) surface is the prototypical inert metal substrate, whose interaction with oxygen remains a controversial issue. Here, we study the effect of dosing temperature and coverage on the absorption of atomic oxygen on this surface, using *ab initio* molecular dynamics and high-resolution electron energy loss spectroscopy. Two vibrational peaks are observed experimentally at 380 and 580 cm^{-1}. The lower frequency peak is predominant at low oxygen coverages, while the higher frequency peak grows more pronounced with increasing oxygen coverage. Our simulations reproduce these results and show that oxygen chemisorbed on the surface is the primary species at low coverages or low surface temperatures. An oxide-like species, both on the surface and under the top layer of gold, becomes dominant at higher coverages or temperatures. These results elucidate the nature of oxidation of the Au(111) surface and answer long-standing questions, such as what is the active species for oxidation on Au(111).

The work is submitted as a letter to *Journal of Physical Chemistry C.*: T.A. Baker, X. Bingjun, L. Xiaoying, C.M. Friend, and E. Kaxiras. **2009.**

7.2 Introduction

The Au(111) surface has long been considered the prototypical inert metal substrate and a detailed understanding of the interaction of oxygen with this surface has become an important issue because oxidized Au(111) is a model for understanding chemical processes relevant to heterogeneous catalysis. The potential use of Au as a material for low-temperature selective oxidation catalysis has received renewed interest since the discovery of Haruta and others that gold nanoparticles supported on reducible metal oxides are active for such processes[1-7]. The adsorption of oxygen on gold is a complex process that has been studied both experimentally[8-11] and theoretically[12-15], but leading to contradictory conclusions concerning the nature and structure of the adsorbed oxygen. Several different species of atomic oxygen on the surface have been proposed and observed including chemisorbed oxygen[9] and various forms of gold oxide[8, 10, 11].

From the point of view of understanding the catalytic activity of gold, it is crucial to determine which oxygen species and structure prevails under different conditions. This can contribute toward improving and designing gold catalysts. Min et al.[16] found that the dosing temperature of atomic oxygen with ozone on Au(111) has a significant effect on the surface reactivity and selectivity to oxidation. Scanning tunneling microscopy (STM) studies revealed differences in the surface morphology depending on the temperature used for oxidation and the final coverage of oxygen; based on this it was proposed that different types of oxygen species (chemisorbed versus surface oxide) are responsible for the differences in reactivity[16]. The structure of the surface also plays a vital role since the size[17, 18] and particle shape[19] of oxide-supported Au nanoparticles have a substantial effect on the reactivity, with rate constants differing by as much as two orders of

magnitude[20]. Also important but controversial is the potential role of subsurface oxygen in the chemistry of coinage metals[21].

It is clear that temperature plays an important role in determining the morphology and ultimately the reactivity of the surface, but most of the theoretical work so far has employed static, zero temperature calculations based on density functional theory. This approach cannot capture the effect of temperature and does not allow for a thorough test of all the possible configurations of oxygen, as it relies only on structures determined *a priori*. Kinetic Monte Carlo (kMC) is a popular theoretical technique to model the dynamical and temperature dependent morphology of a surface[22], although events important to the dynamics of the system need to be known before performing the simulation. Moreover, in kMC the spatial degrees of freedom of the system are typically reduced to a lattice. Ideally, what is needed to capture all relevant effects is a fully atomistic molecular dynamics simulation with accurate forces between nuclei and with realistic conditions (temperature and oxygen concentration).

7.3 Calculations Details

Towards this goal, we perform *ab initio* molecular dynamics simulations (AIMD) in the canonical ensemble[23], with a time step of 3 fs, for the adsorption of oxygen on Au(111) in the framework of density functional theory using the VASP code[24] with the GGA-PW91[25] functional and ultrasoft pseudopotenitals[26-28]. The surface is modeled by a slab consisting of 4 layers in the (111) direction, with a 3x3 primitive unit cell in the lateral directions; the three uppermost layers of the slab were allowed to relax, with the bottom layer fixed at the ideal bulk positions. We consider different temperatures and

coverages of oxygen and obtain the vibration spectra through the velocity autocorrelation function. The calculated spectra are compared to experimental vibrational spectra obtained with high resolution electron energy loss (HREEL)[29].

7.4 Results and Discussion

Two main vibrational features are identified experimentally at 380 cm^{-1} and 580 cm^{-1} (Figure 7.1a) for atomic oxygen deposited by ozone decomposition on Au(111) at a surface temperature of 200 K. At lower coverages only the lower vibrational peak at 380 cm^{-1} is present; the second peak at ~580 cm^{-1} grows as the coverage is increased, starting at ~0.5 ML of oxygen. The second peak dominates near saturation coverage. Recall that the surface is rough on the nanoscale, accounting for the relatively low signal:noise ratio and breadth of the peaks.

We simulated the adsorption of atomic oxygen on Au(111) at three different coverages (0.22, 0.33, and 0.55 ML) and at three different dosing temperatures (200, 500, and 800 K) and calculated the vibrational spectra, Figure 1b. Vibrational spectra are calculated from 20 independent trajectories by first equilibrating each system at the dosing temperature for 6 ps, then cooling to 200 K and running for an additional 6 ps. After changing the temperature to 200 K, 1.5 ps is elapsed to allow the system to reach equilibrium[30], and the velocity autocorrelation function is calculated for the last 4.5 ps of the run. The gold substrate is equilibrated prior to oxygen adsorption for 1 ps starting from random velocities with kinetic energies corresponding to the dosing temperature. Atomic oxygen is then randomly placed, with random velocities corresponding to the dosing temperature, ~3 Å above the equilibrated Au(111) substrate.

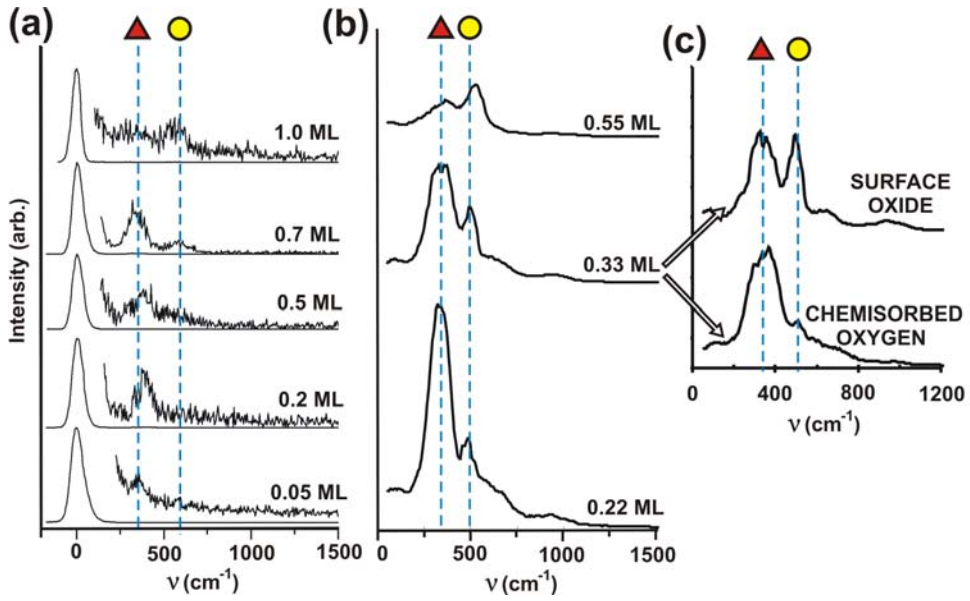

Figure 7.1: (a) HREEL spectra for increasing coverages of atomic oxygen dosed on Au(111) at 200 K. All spectra have been multiplied by a factor of 100. The two main peaks are identified with dotted lines at 364 and 570 cm^{-1} and labeled with a (red) triangle and (yellow) circle, respectively. (b) Calculated vibrational spectra for different coverages of atomic oxygen dosed at 500 K. The lower vibrational peak labeled by a (red) triangle is at 350 cm^{-1} and the second peak labeled by a (yellow) circle is at 500 cm^{-1}. (c) Spectra from 0.33 ML oxygen coverage shown in cases corresponding to simulations that produced chemisorbed oxygen and surface oxide.

The calculated vibrational spectrum and its dependence on oxygen coverage are nearly identical to the experimental results. At 500 K, Figure 7.1b, we observe two vibrational peaks at slightly lower frequencies than experiment, ~350 and ~500 cm^{-1}, with the higher frequency peak increasing in intensity with increasing oxygen coverage. There is a slight shift to higher frequencies for both peaks as the coverage increases; we attribute this shift to the increased oxygen-oxygen interactions due to the higher density

of oxygen. For 0.22 ML of oxygen, the lower frequency peak could shift upwards by as much as ~50 cm^{-1} for oxygen atoms adsorbed in adjacent three-fold sites compared to the case when they are as far away as possible (~ 5Å).

We observe, and subsequently categorize oxygen into three major species on the surface: (1) chemisorbed oxygen, (2) a 2-D surface oxide, and (3) subsurface oxide[31]. Chemisorbed oxygen is characterized as oxygen bound on the top layer of the gold surface and coordinated to three surface gold atoms, shown in Figure 7.2a. The surface oxide contains groups of AuO_2 units where oxygen is bound on opposite sides of a gold atom that is pulled slightly out of the surface, shown in Figure 7.2b. These units can form chains of alternating oxygen and gold atoms generally growing in either straight or perpendicular directions similar to the structure found by Shi et al.[14] who determined this configuration to be the most favorable using static equilibrium DFT thermodynamics calculations. Lastly, the subsurface oxide is characterized by oxygen diffusing anywhere below the top layer of gold atoms, as shown in Figure 7.2c.

To determine the contribution of each species to the total vibrational spectrum we average and group together molecular dynamics runs that produce the same oxygen species. For example, Figure 7.1c shows the vibrational results for 0.33 ML oxygen dosed at 500 K, but split into simulations that result in the chemisorbed oxygen and simulations that produce some surface oxide. A vibrational peak at ~350 cm^{-1} is present in the simulated spectra for both types of species, but the peak at ~500 cm^{-1} is missing in the spectrum for chemisorbed oxygen. This vibrational pattern is the same for different oxygen coverages and dosing temperatures, namely the second higher-frequency peak is not present for chemisorbed oxygen but is present for the surface oxide. There are no

significant differences in the simulated spectra of the surface oxide and the subsurface oxide, suggesting that the higher frequency peak is due to either the surface oxide or the subsurface oxide and not to chemisorbed oxygen.

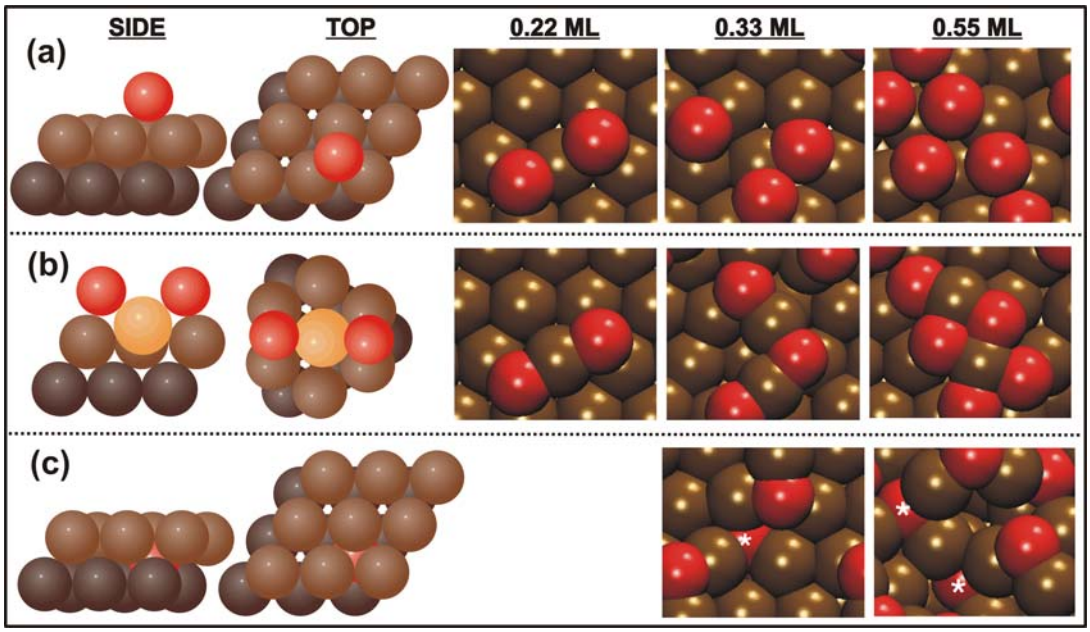

Figure 7.2: Model (left) and examples (right) of the three oxygen species: (a) chemisorbed, (b) surface oxide, and (c) subsurface oxide. A prototypical model of each oxygen type is shown on the left. Dark brown, light brown, yellow, and red spheres represent the second layer of gold, top layer of gold, gold adatoms, and oxygen atoms, respectively. Illustrative examples of each oxygen type at each coverage are shown on the right. Brown and red spheres represent gold and oxygen atoms, respectively. An asterisk labels subsurface oxygen atoms in (c). We did not observe the subsurface oxide below an oxygen coverage of 0.33 ML.

In both the experimental and computational results, as the oxygen coverage increases so does the second vibrational peak. Based on these results, we conclude that chemisorbed oxygen dominates at low coverages of oxygen while the oxide is observed

at higher coverages. Figure 7.3 confirms this conclusion by illustrating the percentage of each oxygen species on the surface at different coverages or dosing temperatures.

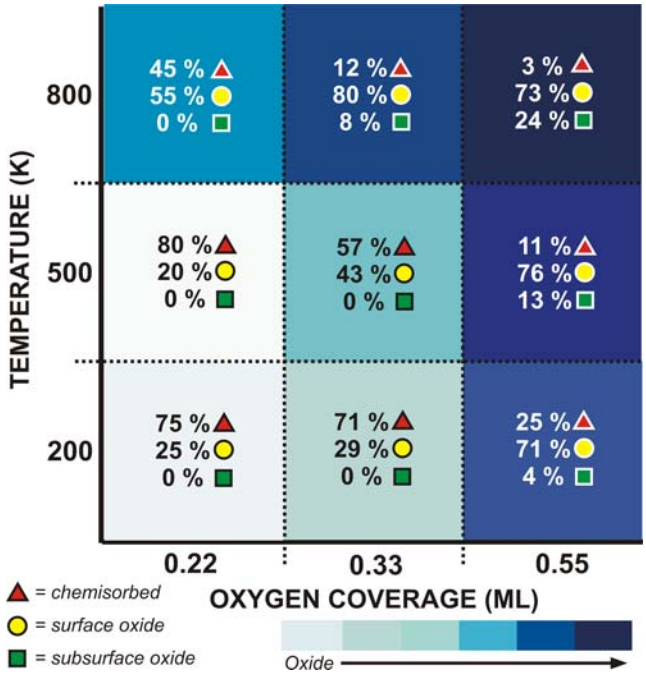

Figure 7.3: Diagram illustrating the percentage of each oxygen type at each dosing temperature and oxygen coverage. Each square is shaded by the amount of oxide character of the surface, calculated by considering the chemisorbed oxygen as the least "oxide-like" and subsurface oxide as the most "oxide-like".

For example, at a low oxygen coverage and dosing temperature (0.22 ML and 200 K) there is a large percentage of chemisorbed oxygen (75%), a smaller percentage of surface oxide (25%), and no subsurface oxide. At a high oxygen coverage and dosing temperature (0.55 ML and 800 K) there is a much larger percentage of surface oxide (73%), and subsurface oxide (24%), and very little chemisorbed oxygen (3%), confirming our conclusion. In previous static DFT calculations, we found that a chemisorbed oxygen vibration is normal to the surface at a frequency similar to this work[32]. Our results also

agree well with previous work based on static DFT calculations, where we found that gold incorporation becomes more favorable at higher coverages of Cl or O[33]. In that case, as the coverage increases the bonding between the adsorbate and gold becomes more covalent in nature, reducing the partial charge on the oxygen which allows oxygen atoms to pack closer together. Presumably the same is true in the present case and could explain the roughening of the surface at higher coverages.

Our results also agree well with previous experimental studies. At each coverage and temperature we considered, there is at least some small amount of surface oxide, see Figure 7.3, consistent with STM observations where there was always some release of gold atoms to form islands on the surface even at low coverages of oxygen[16]. This is especially true for adsorption of oxygen on the "herringbone" reconstruction of Au(111) which contains an extra 4.5% gold atoms in the top layer that can easily be removed by interaction with adsorbates[34, 35]. Our work also supports the previous suggestion that the 2D and 3D islands observed by STM at higher dosing temperatures and coverages are a gold oxide since our calculation, Figure 7.3, suggests that at higher temperatures the surface should be more oxidic in character[36].

7.5 Conclusions

Previous work demonstrated that at lower coverages of oxygen dosed at 200 K, which corresponds to just the presence of the lower vibrational peak in HREELS, Au(111) was the most reactive and selective for oxidation of carbon monoxide as well as other hydrocarbons, and that the surface becomes less reactive at higher dosing temperatures or coverages[15]. We have identified the lower frequency peak in vibrational spectroscopy as corresponding to chemisorbed oxygen from our AIMD simulations and

that this species is dominant at lower coverages and dosing temperatures. This also agrees with our previous work showing that oxygen binds stronger when incorporated with gold adatoms at higher coverages or when bound on steps or vacancies[32]. These conclusions, based on a systematic and unbiased theoretical investigation with AIMD simulations at various temperatures and oxygen coverages, provide fundamental insight into the reactivity of gold by identifying chemisorbed oxygen as the active species for oxidation on Au(111).

Finally, an important consequence of our calculations is the ability to understand the kinetic processes responsible for the formation of the surface and subsurface oxide. The energy barrier, estimated from variations in the total energy, for the formation of the surface oxide is smaller than 0.1 eV, for the formation of sub-surface oxide is in the range of 0.8 – 1.4 eV, and the barrier for chemisorbed oxygen diffusion is in the range of 0.2-0.6 eV. The surface oxide forms when two oxygen atoms diffuse to three-fold sites that share a gold atom in the surface between them, as shown in the 0.22 ML example in Figure 7.2a. This is the dominant but not the sole mechanism, especially at higher temperatures when the surface is very disordered. After this diffusion it takes ~600-1000 fs for the gold atom attached to the two oxygen atoms to lift out of the surface and form the surface oxide, shown in the 0.22 ML example in Figure 7.2b. The process for formation of the subsurface oxide starts with one or several oxygen atoms lifting a surface gold atom, followed by an additional nearby oxygen atom diffusing to fill some of vacancy left behind by the lifted gold atom. This often occurs when the surface oxide (AuO_2) is formed with a third oxygen atom nearby to form the subsurface oxide. A

complete analysis of the kinetics for the formation of the gold oxide will be the subject of future work.

7.5 References and Notes

[1] M. Haruta, *Chem. Rec.* **2003**, *3*, 75.

[2] M. Haruta, M. Date, *Appl. Catal. A-Gen.* **2001**, *222*, 427.

[3] R. Meyer, C. Lemire, S. K. Shaikhutdinov, H. Freund, *Gold Bull.* **2004**, *37*, 72.

[4] M. Haruta, N. Yamada, T. Kobayashi, S. Iijima, *J. Catal.* **1989**, *115*, 301.

[5] T. Hayashi, K.Tanaka, M. Haruta, *J. Catal.* **1998**, *178*, 566.

[6] R. J. H. Grisel, P. J. Kooyman, B. E. Nieuwenhuys, *J. Catal.* **2000**, *191*, 430.

[7] B. W. L. Jang, J. J. Spivey, M. C. Kung, H. H. Kung, *Energy Fuels* **1997**, *11*, 299.

[8] M. A. Chesters, G. A. Somorjai, *Surf. Sci.* **1975**, *52*, 21.

[9] N. D. S. Canning, D. Outka, R. J. Madix, *Surf. Sci.* **1984**, *141*, 240.

[10] J. J. Pireaux, M. Liehr, P. A. Thiry, J. P. Delrue, R. Caudano, *Surf. Sci.* **1984**, *141*, 221.

[11] D.H. Parker, B.E. Koel, *J. Vac. Sci. Technol. A-Vac. Surf. Films* **1990**, *8*, 2585.

[12] M. Mavrikakis, P. Stoltze, J. K. Norskov, *Catal. Lett.* **2000**, *64*, 101.

[13] Z. P. Liu, P. Hu, A. Alavi, *J. Am. Chem. Soc.* **2002**, *124*, 14770.

[14] H. Shi, C. Stampfl, *Phys. Rev. B.* **2007**, *76*, 075327.

[15] S.D. Miller, J.R. Kitchin, *Surf. Sci*. **2008**, *603*, 794.

[16] B. K. Min, A. R. Alemozafar, D. S. Pinnaduwage, X. Deng, C. M. Friend, *J. Phys. Chem. B.* **2006**, *110*, 19833.

[17] M. Valden, X. Lai, D. W. Goodman, *Science* **1998**, *281*, 1647.

[18] M. Valden, S. Pak, X. Lai, D. W. Goodman, *Catal. Lett.* **1998**, *56*, 7.

[19] M. Comotti, W. C. Li, B. Spliethoff, F. Schuth, *J. Am. Chem. Soc.* **2006**, *128*, 917.

[20] N. Lopez, T. V. W. Janssens, B. S. Clausen, Y. Xu, M. Mavrikakis, T. Bligaard, J. K. Norskov, *J. Catal.* **2004**, *223*, 232.

[21] Z. Qu, M. Cheng, W. Huang, X. Bao *J. Catal.* **2005**, *229*, 446.

[22] C. C. Battaile, D. Srolovitz, *Annu. Rev. Mater. Res.* **2002**, *32*, 297.

[23] S. Nose, *Molecular Physics* **2002**, *100*, 191.

[24] G. Kresse, J. Hafner, *Phys. Rev. B.* **1993**, *47*, 558.

[25] J. P. Perdew, Y. Wang, *Phys. Rev. B* **1992**, *45*, 13244.

[26] G. Kresse, J. Hafner, *J. Phys.-Condes. Matter* **1994**, *6*, 8245.

[27] D. Vanderbilt, *Phys. Rev. B.* **1990**, *41*, 7892.

[28] We used a plane-wave cutoff energy of 300.0 eV, an electronic convergence tolerance of 10^{-3} eV, and 2×2×1 Monkhurst-Pack k-point sampling.

[29] HREELS experiments were performed in a stainless steel vacuum chamber with a base pressure of ~ $2x10^{-10}$ Torr. Oxygen covered Au(111) surface was prepared by ozone exposure, as described in detail elsewhere.[16] All were collected at 200 K with a beam energy of 6.91 eV. The typical FWHM of the elastic peak was ~ 70 cm^{-1}

[30] It is known from temperature programmed desorption experiments that the desorption temperature of atomic oxygen from the surface of gold is ~550 K. Because of the time scales that are accessible in the calculations (6 ps), even at a dosing temperature of 800 K, desorption is not observed since we do not reach true equilibrium. However, we do reach a pseudo-equilibrium (as evidenced by the nearly constant energy and other

measurable quantities throughout the simulation) and the higher temperature allows us to model the morphological changes in the time scale accessible by our calculations.

[31] There is not a clear definition in the literature of 'surface oxide' and 'subsurface oxide'. We only use these terms to classify the location of oxygens observed in our simulations. The structure we observe for the subsurface oxide is not the structure of the bulk gold oxide; however, the short timescales accessible in our simulations preclude us from ruling out an oxide structure. Additional work is planned to better understand the bonding and the charge distribution of these different oxygen states.

[32] T.A. Baker, C.M. Friend, E. Kaxiras, *J. Phys. Chem. C.* **2009,** *113*, 3232.

[33] T.A. Baker, C.M. Friend, E. Kaxiras, *J. Chem. Phys.* **2009**, *130*, 084701.

[34] S. Narasimhan, D. Vanderbilt, *Phys. Rev. Lett.* **1992**, *69*, 1564.

[35] B. K. Min, X. Deng, D. S. Pinnaduwage, R. Schalek, C. M. Friend, *Phys. Rev. B.* **2005**, *72*, 4.

[36] Some of the 2D and 3D oxides formed experimentally are ordered. Because of the constraints on the unit cell size in our calculations, we cannot expect to determine the exact structure of these oxides; rather, we may be finding the precursors to their formation.

CHAPTER 8

EFFECTS OF CHLORINE AND OXYGEN COVERAGE ON THE STRUCTURE OF THE AU(111) SURFACE

8.1. Abstract

We investigate the effects of Cl and O coverage on the atomic structure of the Au(111) surface using density functional theory (DFT) calculations. We find that the release and incorporation of gold atoms in the adsorbate layer becomes energetically favorable only at high coverages of either O or Cl (>0.66 ML for O and >0.33 ML for Cl), whereas adsorption without the incorporation of gold is favorable at lower coverages. The bonding between the adsorbate and gold substrate changes significantly with coverage, becoming more covalent (less ionic) at higher Cl and O coverage. This is based on the fact that at higher coverages there is less ionic charge transfer to the adsorbate, while the electron density in the region between the adsorbate and a surface gold atom is increased. Our results illustrate that the O and Cl coverage on Au(111) can dramatically affect its structure and bonding, which are important features in any application of gold involving these adsorbates.

The work was published as an article in *Journal of Chemical Physics*: T. A. Baker, C. M. Friend, E. Kaxiras, **2009**. *130*, 084701.

8.2 Introduction

Gold surfaces play a vital role in all aspects of modern technology and science, from heterogeneous catalysis to nanotechnology[1]. Gold is extensively used as a substrate

for self-assembled monolayers (SAM)[2, 3] in materials science[4], as interconnects in electronic devices[5-7], as a substrate for conducting polymers in chemical sensors[8], and in many different types of biosensors[9, 10]. Gold can be used in plasmonic electronic devices and is an important substrate for surface enhanced Raman spectroscopy[11, 12]. Since such applications rely on some of the unique electronic features of gold, a complete understanding of the gold surface as well as the bonding of adsorbates on gold surfaces is crucial.

The surface morphology of gold can have a significant role in determining its properties. For example, the size[13, 14] and shape[15] of a supported Au nanoparticle has a substantial effect on its catalytic activity: smaller particles (2 – 4 nm in diameter) have much greater catalytic activity than larger ones (20-40 nm in diameter), with rate constants differing by as much as two orders of magnitude[16]. On the surface of gold, the adsorption of electronegative species has been found to affect significantly the morphology of the surface. Adsorbates including NO_2[17], S[18], and CH_3SH[19, 20] can lift gold atoms from the surface. Au(111) may be especially prone to the release of gold atoms due to the 'herringbone' reconstruction which contains an excess of ~4.5% Au atoms compared to the bulk (111) plane, with some of these extra atoms weakly bound at 'elbow' sites[21-23]. The presence of adsorbed molecules can lift the herringbone structure, releasing gold adatoms on the surface[24-26]. The adsorption of atomic oxygen creates small gold islands on the surface[27] which are formed because oxygen can stabilize undercoordinated Au[28]. The morphology of these islands can also affect the reactivity of the surface[29]. Atomic chlorine also releases gold on Au(111), a process which is dynamical in nature and involves many different structures and types of Cl bonding to

Au[30, 31]. Depending on Cl coverage, the surface can exhibit initial release of gold atoms from the herringbone reconstruction, a chemisorbed overlayer, and further release of gold atoms to form a gold chloride layer[32].

In the present work, we study these phenomena which are important for understanding the catalytic properties of the gold surface, using first-principles electronic structure calculations based on density functional theory (DFT). We investigate the energetics of the morphological change of the Au(111) surface upon the adsorption of two different electronegative species, chlorine and oxygen. By examining the electronic charge density and the density of states (DOS) we provide insight into the physical origin of our results, which elucidate recent experimental observations on these systems.

The paper is organized as follows: Section II describes the DFT calculations employed in our work. Section III describes the effect of coverage and gold adatom incorporation on the total energy for adsorption of Cl and O on Au(111), along with the effect of the oxygen chemical potential on the surface free energy. Section IV discusses the observed trends and impacts on bonding by investigating the electronic charge density and DOS for Cl adsorption, followed by Section V, the conclusions.

8.3 Calculational Details

The DFT results were preformed with the VASP code[33] using the GGA-PW91 functional[34] to model electron exchange and correlation. Ultrasoft pseudopotenitals were used with the default plane-wave cutoffs for different elements taken from the GGA ultrasoft-pseudopotential database[35, 36]. We use a 12 layer slab and a $(\sqrt{3}\times\sqrt{3})R30^{\circ}$ surface unit cell to model the Au(111) surface, with the bottom six layers remaining fixed in their bulk positions and the top six layers allowed to relax. The surface supercell does

not capture the herringbone reconstruction, which we expect to not have important effects on the energetics, and which is typically lifted upon adsorption of foreign atoms. The clean Au(111) surface corresponds to a bulk terminated plane. A large vacuum region between the slabs of ~20 Å was used to insure that the dipole induced by the presence of adsorbates on one side of the slab does not create artifacts due to interaction between neighboring unit cells. A Monkhorst-Pack Γ-centered 6×6×1 k-point scheme was used for reciprocal-space sampling. We find that spin polarization has no significant effect on the total-energy comparisons.

Our choice of the PW91 exchange-correlation functional, instead of functionals like PBE and revised-PBE (RPBE), was based on the fact that it provides a better description of Au-Au binding, which is important in addressing the differences in energy between a clean and an adatom-covered gold surface. In general, DFT-GGA calculations underestimate the cohesive energy of metals. We find that the underestimation is most extreme with the RPBE functional: the calculated cohesive energy, using the PW91, PBE, and RPBE functionals are -3.02, -2.99, and -2.38 eV, while the experimental value is -3.81 eV.[37] The same trend was found for the surface energy, calculated using the PW91, PBE, and RPBE functionals: 0.0437, 0.0381, and 0.0153 eV/Å^2, respectively, versus the experimental value of 0.0936 eV/Å^2.[38] Since the PBE and RPBE functionals greatly underestimate the cohesive energy and surface energy, they are likely to give less accurate results for the cost of creating a gold atom or vacancy, compared to the PW91 functional. We provide an estimate of the error introduced by our choice of functional by using different functionals to obtain the relative energies for important structures and assigning the difference in these energies as the uncertainty of the calculation.

In order to provide insight into the physical origin of the results, we calculated the charge associated with specific atoms in selected configurations. There are different approaches to calculating the charge of atoms when using a plane-wave basis, most of them involving integration of the charge in a volume centered at the nucleus of the atom. We used two different methods for integrating the electronic charge: the first method consists of using spheres to integrate the amount of charge around an atom, which is a convenient and physically reasonable approximation. The radius of the sphere is determined by the distance of the minimum value of the electron density between the adsorbate and the nearest surface Au atom. The difference between the integrated density in the adsorbed system and a free adsorbate atom in the gas phase is defined as the net charge. The second method, suggested by Bader, is similar, but more mathematically rigorous: instead of using atom-centered spheres, the density is partitioned into non-overlapping basins defined by surfaces on which the electron density gradient vanishes[39,40]. There are small differences in the charge calculated from the two methods, but the qualitative trends that emerge are the same.

8.4 Results

The first system we considered is the adsorption of 0.33 and 0.67 ML of Cl on Au(111). The adsorption energy for p chlorine atoms is defined relative to the Cl_2 reservoir:

$$E_{\text{Cl-ads}}(p) = E_{\text{Au/Cl}} - E_{\text{s}} - \frac{p}{2} E_{\text{Cl2}} \qquad (8.4.1)$$

where $E_{\text{Au/Cl}}$ is the total energy of the system consisting of the Au surface with p Cl atoms bound on the gold substrate, E_{s} is the energy of the gold substrate, and E_{Cl2} is the energy of the Cl_2 molecule The calculated bond length and binding energy for Cl_2 using the

PW91 functional is 2.02 Å and 2.68 eV respectively, which compares well with the experimental values of 1.99 Å and 2.48 eV[41]. With a different exchange-correlation functional (RPBE[42]), these values are 2.00 Å and 2.54 eV[43].

Experimentally, gold atoms are only incorporated in the adsorbate structure at Cl coverages above 0.33 ML[32]. In order to investigate the energetics for gold incorporation as a function of Cl coverage, we considered the adsorption of chlorine on three different Au(111) substrates: a clean surface and surfaces covered with 0.33 ML and 0.67 ML of Au adatoms. It is important to note that at Cl coverages above 0.33 ML, a wide variety of periodic and aperiodic structures were observed experimentally with scanning tunneling microscopy (STM)[32]. The exact stoichiometry and unit cell dimensions along with clear atomic resolution of the structures could not be determined from these STM studies. Since we are interested in understanding gold incorporation as a function of coverage and not the exact structure at higher coverages, we use the $(\sqrt{3}\times\sqrt{3})R30^\circ$ unit cell as a model for all Cl coverages. We expect that factors such as adsorbate-adsorbate repulsion that lead to Au incorporation will be qualitatively similar in the real and model systems, thus our model can provide insight into the coverage-dependent bonding of adsorbates on the gold surface.

To compare the adsorption of chlorine on each substrate, the total energy is calculated as:

$$E_{\text{tot}}(n,p) = E_{Cl\text{-ads}}(p) + E_{\text{cost}}(n) \tag{8.4.2}$$

where $E_{\text{cost}}(n)$ is the energy cost for creating n gold adatoms:

$$E_{\text{cost}}(n) = E_{\text{s-ad}}(n) - nE_{\text{b}} - E_{\text{s}} \tag{8.4.3}$$

with $E_{s\text{-}ad}(n)$ the total energy of the Au(111) substrate with n adatoms, E_b the energy of a gold atom in the bulk, and E_s, in this case, the energy of the bare Au(111) substrate. This energy cost was calculated for coverages corresponding to 0.33 ML (n=1 in the $(\sqrt{3}\times\sqrt{3})R30^\circ$ unit cell) and 0.67 ML (n=2) of adatoms on the top layer and found to be 0.75 and 0.65 eV, respectively. The cohesive energy of bulk Au is -3.02 eV, the Au-Au dimer cohesion is -2.24 eV, and the Au-Cl pair cohesion is -2.91 eV. Adatom formation and incorporation into a chloride layer can only take place if:

$$E_{Cl\text{-}ads}(p) - E_{tot}(n,p) > 0 \qquad (8.4.4)$$

where $E_{Cl\text{-}ads}(p)$ is the lowest adsorption energy possible for chlorine bound on the clean adatom-free surface and $E_{tot}(n,p)$ is the lowest energy for chlorine on an adatom covered surface.

The energetics of 0.33 ML Cl adsorption on a $(\sqrt{3}\times\sqrt{3})R30^\circ$ unit cell on the three different types of substrates of Au(111) was studied in a previous work[32]. To summarize those results, the system with the lowest energy consists of Cl binding in FCC three-fold sites on the clean surface with an adsorption energy of -0.91 eV (Table I). The adsorption of Cl on adatom-covered Au(111) surfaces was stronger, but not enough to compensate for the cost to create the adatom surface, $E_{cost}(n)$.

By taking into account the cost required to create each surface, it is possible to determine the adsorption species with the lowest energy for the adsorption of 0.67 ML of Cl. The first system we considered is the adsorption of chlorine on the clean adatom-free surface. We find that chlorine binds preferentially on bridge sites, forming a honeycomb pattern on the surface, Figure 8.1a, with an adsorption energy of -0.18 eV per Cl and a Cl-Au distance of 2.60 Å. The repulsive interaction between neighboring chlorine atoms

at a Cl coverage of 0.67 ML weakens the Au-Cl interaction in comparison to the case of 0.33 ML coverage. In the latter case, Cl adsorption prefers a higher coordination to gold (the FCC three-fold site), has a lower adsorption energy (-0.91 eV per Cl), and a slightly smaller Au-Cl length, 2.58 Å.

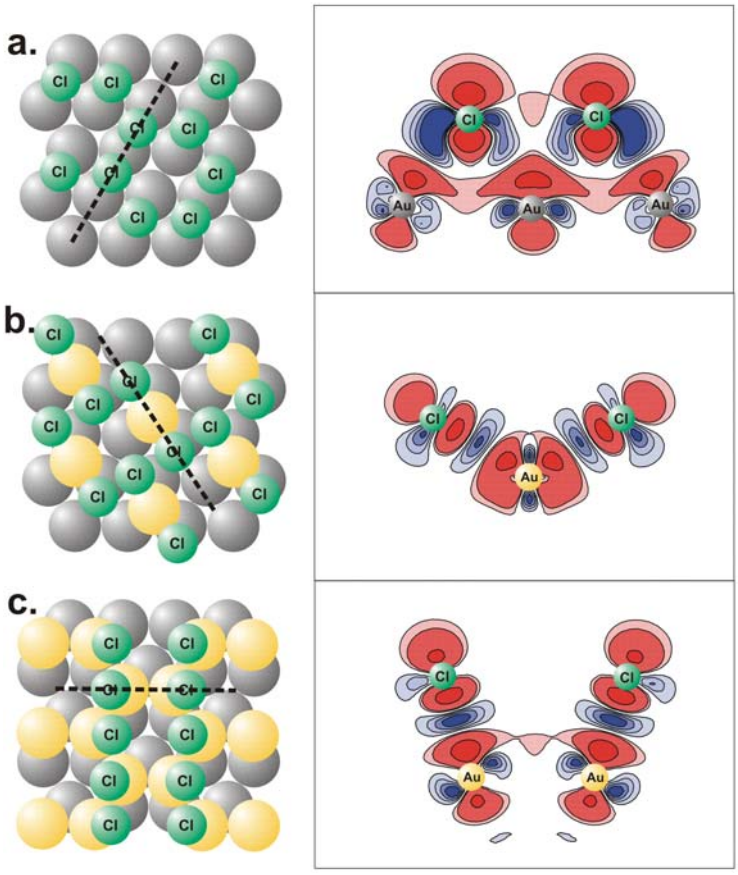

Figure 8.1: Lowest-energy structures (left panels) and charge density difference plots (right panels) of 0.67 ML Cl adsorption on: (a) flat (1x1) surface; (b) Au(111) covered with 0.33 ML Au adatoms; (c) 0.67 ML Au adatoms. The darker gray circles represent the top full layer of gold atoms, lighter yellow circles represent gold adatoms, and small (green) circles represent chlorine atoms. The thick dotted lines on the structural figures on the left show the planes on which the density difference is plotted. Red contours correspond to charge depletion and blue contours to charge accumulation.

We also considered the adsorption energy of chlorine on a surface containing 0.33 ML of gold adatoms. We find that chlorine binds much more strongly to this surface compared to the flat adatom-free surface. The lowest energy configuration has two chlorine atoms bound on top of a gold adatom, on either side and coordinated only to the gold adatom, Figure 8.1b. The adsorption energy for this structure is -0.64 eV per Cl, significantly lower than for the 0.67 ML Cl-coverage on the clean surface. In fact, the adsorption energy is sufficiently lowered to compensate for the cost of creating the Au adatoms, resulting in a surface that is lower in total energy (Table 8.1).

Table 8.1: Summary of total energies, $E_{tot}(n,p)$, defined in Eq.(8.4.2), for two Cl coverages, p (expressed in ML for the $(\sqrt{3}\times\sqrt{3})R30^\circ$ unit cell) on Au(111) with different gold adatom coverages, n. Bold characters indicate the systems with the lowest energy at each chlorine and adatom coverage.

p (ML) / n (ML)	0.33 ML Cl		0.67 ML Cl	
	Site	E_{total} (eV)	Site	E_{total} (eV)
0.00	top	-0.65	bridge	-0.37
	bridge	-0.87		
	HCP	-0.88		
	FCC	**-0.91**		
0.33	top	-0.43	**$AuCl_2$**	**-0.54**
	side	-0.47		
0.67	bridge	-0.81	**half bridge**	**-0.57**
	hollow	-0.24	top	-0.20

The last structure we considered is chlorine adsorbed on 0.67 ML of gold adatoms (equivalent to 0.33 ML of gold vacancies). In this case, the preferred binding site for chlorine is on a "half-bridge site" on the gold atoms that make up the top layer of the surface, Figure 8.1c, in this configuration, Cl is bound directly to one gold atom but in an

off-center position, tilted towards the vacancy and close to what would have been the bridge site of the surface without the vacancy. An alternative structure, with the Cl atom directly on top of the gold atom is substantially higher in energy (Table 8.1). The binding energy for chlorine on the half-bridge site is -0.61 eV per Cl. As in the case of chlorine adsorption on the 0.33 ML adatom-covered surface, the Au-Cl interaction is much stronger and the Au-Cl length is smaller for a surface that contains 0.67 ML adatoms compared to the clean Au(111) surface. The Au-Cl length is 2.60 Å for Cl on a flat surface, but only 2.46 Å on the 0.67 ML adatom-covered surface. When taking into account the cost of creating the adatom-covered surface, chlorine bound at half-bridge sites on the 0.67 ML adatom-covered surface is the lowest energy structure (Table 8.1).

To illustrate that the results above are not just characteristic of the chlorine-gold interaction, but rather they apply generally to electronegative atoms on gold, the same substrates were used to study oxygen adsorption at different coverages. We find that at a coverage of 0.33 ML, oxygen prefers to bind in a FCC three-fold site with an adsorption energy of 0.18 eV. This agrees well with previously published results: an adsorption energy of 0.16 eV was reported using the PW91 functional for an oxygen coverage of 0.25 ML[44]. The adsorption energy can also be defined relative to an oxygen atom instead of an oxygen molecule; using this definition Gajdos et al.[45] reported an adsorption energy of -2.95 eV for a coverage of 0.25 ML, while we find this energy to be -2.84 eV. The overlayer on the clean (adatom-free) surface is the lowest energy structure for 0.33 ML coverage of oxygen (Table 8.2), as was the case for chlorine. The Au-O dimer cohesion energy is -2.57 eV. On the 0.33 ML adatom-covered surface, in contrast to the chlorine adsorption, the adsorption of oxygen is not stronger compared to the adatom-free surface

for 0.33 ML of oxygen. Adsorption on the 0.67 ML adatom-covered surface was slightly stronger (by 0.08 eV) than on the (1x1) clean surface, but this difference is not enough to compensate for the cost of creating the adatoms on the surface.

Table 8.2: Summary of total energies, $E_{tot}(n,p)$ for three O coverages, p, on Au(111) with different gold adatom coverages, n. Notation is the same as in Table I. Energies in brackets are from the PBE functional and are used to estimate the error in Figure 8.3.

p (ML) / n (ML)	0.33 ML O		0.67 ML O		1.00 ML O	
	Site	E_{total} (eV)	Site	E_{total} (eV)	Site	E_{total} (eV)
0.00	**FCC**	**0.16 [0.16]**	**FCC**	**1.13 [1.10]**	bridge	3.45 [3.45]
0.33	top side	1.73 1.86	flat AuO2	1.50 [1.47]	**trigonal pyramid**	**2.64 [2.61]**
0.67	half bridge	0.73 [0.67]	half bridge	1.85		

For 0.67 ML coverage of oxygen, the most stable structure is still the oxygen overlayer without gold incorporation, Figure 8.2a. Due to the repulsion of neighboring oxygen atoms, the 0.67 ML overlayer structure has a higher adsorption energy (0.56 eV per O) compared to the 0.33 ML overlayer (0.16 eV per O). For oxygen adsorption on the 0.33 ML adatom-covered surface, the structure with the lowest energy consists of oxygen bound on either side of the gold adatom, coordinated to both the adatom and the top complete layer of gold atoms, Figure 8.2b. The adsorption energy for this structure is 0.18 eV per O lower than the overlayer, but this difference is not enough to make up for the energy cost of creating the gold adatoms on the surface. The structure with the lowest energy on the 0.67 ML adatom-covered surface has two oxygen atoms bound off-center

from the adatom and interacting with the vacancy below; however, this system is 0.72 eV higher in energy than the overlayer.

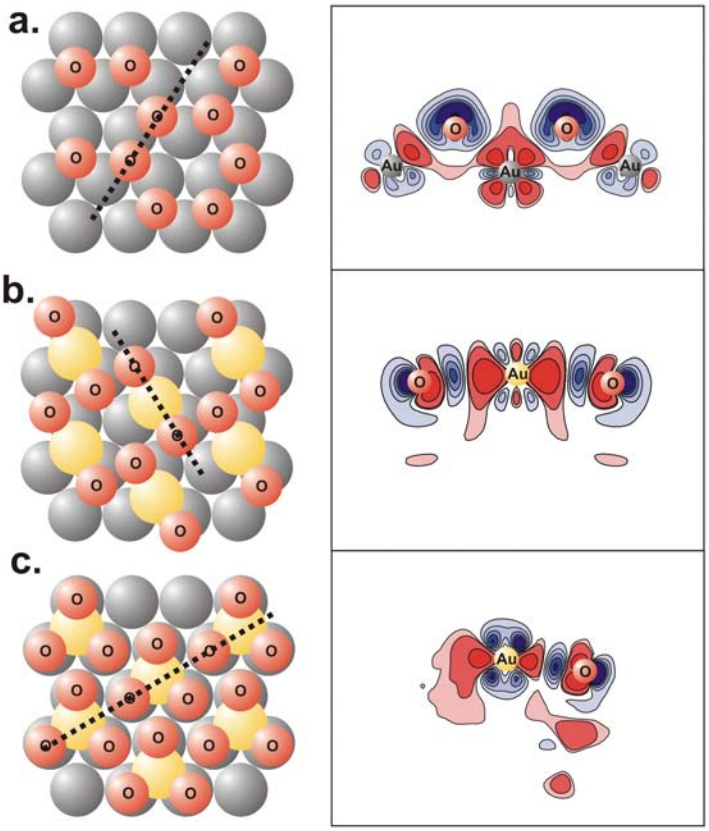

Figure 8.2: Lowest energy structures (left panels) and charge density difference plots (right panels) of: (a) 0.67 ML O adsorption on flat, (1x1) Au(111) surface; (b) 0.67 ML O adsorption on Au(111) surface covered with 0.33 ML adatoms; (c) 1.00 ML O adsorption on 0.33 ML Au adatom-covered Au(111) surface. Symbols are the same as in Figure 8.1, with red for O atoms.

At a coverage of 1.00 ML of oxygen, adatom incorporation becomes energetically favored over formation of the overlayer. The preferred binding site for the 1.00 ML overlayer structure is oxygen on bridge sites, with an adsorption energy of 1.15 eV per O. The 0.33 ML adatom covered gold surface, however, has an adsorption energy of 0.63 eV

per O, which is significantly lower than the overlayer and can easily compensate for the cost of creating the adatom. In this structure, the gold adatom sits on a three-fold site with each oxygen in the plane of the gold adatom and coordinated to both the adatom and the top gold layer, Figure 8.2c.

Experimentally, atomic oxygen is often introduced to the gold using various methods including electron bombardment of condensed NO_2[46], ion sputtering with O_2[47, 48], thermal dissociation of gaseous O_2 using hot filaments[49], and exposure to ozone[50]. Since the source of oxygen in these experimental results is not necessarily oxygen gas but a variety of sources, it is useful to consider the phase diagram of surface free energy as a function of the oxygen chemical potential.

We start with the assumption that the surface is in thermodynamic equilibrium with the separate reference phases at a given temperature T and pressure P. The environment acts as a reservoir where oxygen can adsorb or desorb from the surface without a change in pressure or temperature. The Gibbs free energy $G(T, P, N_{Au}, N_O)$ is the thermodynamic potential required to describe this system. The most stable surface minimizes the surface free energy, $\gamma(T,P)$, defined as:

$$\gamma(T,p) = (1/A)[\, G(T, P, N_{\mathrm{Au}}, N_O) - N_{\mathrm{Au}}\mu_{\mathrm{Au}}(T,P) - N_{\mathrm{O}}\mu_{\mathrm{O}}(T,P)] \qquad (8.4.5)$$

where μ_{Au} and μ_{O} are the chemical potentials of a Au atom and an O atom, N_{Au} and N_{O} are the numbers of these species, and the surface energy has been normalized by dividing by the surface area, A[51-53]. In principle, the Gibbs free energy could be calculated by considering the contributions of vibrational and configurational entropy; in practice these contributions are small and can be neglected allowing the terms to be approximated as DFT total energies[54]. The surface free energy becomes:

$$\gamma_{DFT}(T,P) = (1/A)[\, E(\mathrm{Au/O}) - E(\mathrm{Au}) - N_O\mu_O(T,P)] \qquad (8.4.6)$$

The chemical potential of oxygen could be related to an oxygen pressure and temperature by calculating the translational and rotational partition functions of the gas phase, but for a qualitative phase diagram it suffices to consider the upper and lower bound of the chemical potential[51]. The lowest possible bound of the oxygen chemical potential, which would correspond to an infinitely small pressure of oxygen, is equal to the cost of forming an atomic oxygen atom from the reference reservoir of the molecular solid: $[E(O_{2(s)}) - 2E(O)]/2$, which is also the bond dissociation energy per oxygen atom. A more realistic lower bound is the bond dissociation energy per oxygen atom from oxygen gas. Adsorbing oxygen on the surface at no cost ($\mu_O = 0$) represents the upper bound (high oxygen pressure), therefore the range in chemical potential is:

$$-3.0 \text{ eV} < \mu_O < 0 \qquad (8.4.7)$$

where for consistency in the theoretical results[51] we use the value of $[E(O_{2(g)}) - 2E(O)]/2 \approx -3.0$ eV obtained from our calculations. Figure 8.3 is a plot of the surface free energy as a function of oxygen chemical potential between the two extreme bounds. Oxygen dissociation is not thermodynamically favorable in the small unlabeled region in Figure 8.3 close to the lower bound of the chemical potential. As the oxygen chemical potential increases, a higher oxygen coverage is possible on the surface creating three distinct regions, labeled Ia, Ib, and II in Figure 8.3. The possible error in the calculation due to the choice of exchange-correlation functional is illustrated as a range of values in the chemical potential for the transition between different regions; this was estimated by using two different functionals (PW91 and PBE) to obtain the energy versus chemical potential curves. The structures with the lowest surface free energy in regions Ia

and Ib are the 0.33 ML and 0.67 ML of oxygen coverage without gold adatom incorporation, respectively. The transition between a flat surface and gold incorporation occurs between region I and II when the oxygen coverage with the lowest energy increases from 0.67 ML to 1.00 ML.

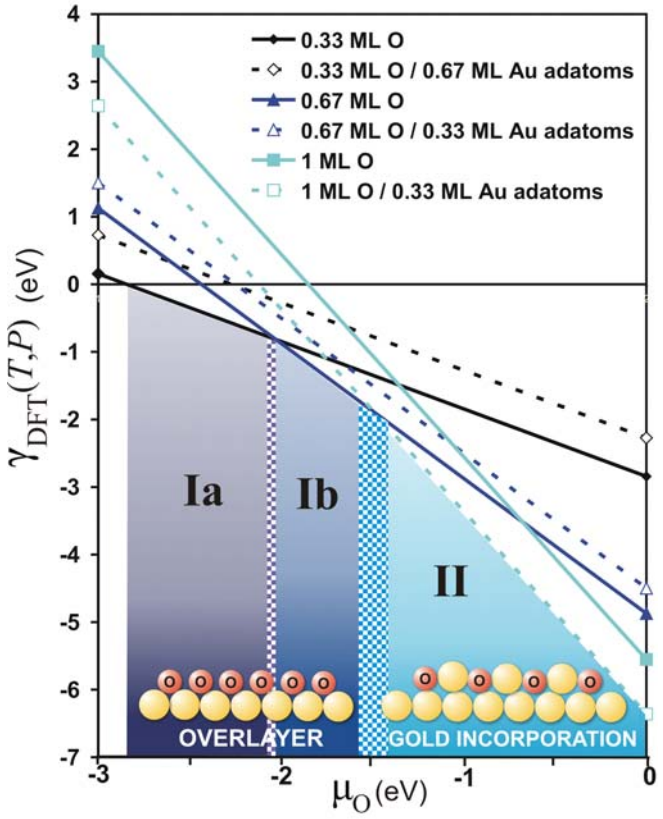

Figure 8.3: Surface free energy, $\gamma_{DFT}(T,P)$ as a function of the oxygen chemical potential, μ_O for different oxygen and gold adatom coverages. The clean surface is represented by a horizontal line at a surface free energy of 0 eV. The transition range in the oxygen chemical potential between regions, representing the error introduced by the choice of exchange-correlation functional, is indicated by checkered-square region.

The surface free energy plot is consistent with the experimental observation that the adsorption of ozone in ultra-high vacuum (UHV) on the Au(111) surface always

results in gold adatoms being released, regardless of oxygen coverage[27]. The experimental chemical potiental[55], -1.05 eV, lies well within region II, where gold adatom incorporation is favorable. This also agrees with Shi et al.[56] who have recently preformed similar calculations using a larger unit cell; they predict that the energetically most favorable configuration is a "surface-oxide-like" layer that has gold incorporated in its structure.

8.5 Discussion

Our results show that the incorporation of Au into an adsorbate layer depends on the coverage of the electronegative atom. At low coverages, Au adatom or vacancy formation is not favorable, while at high coverages defect formation becomes energetically favorable. In general, the adsorbate binds more strongly to a surface containing defects, but the gain in energy due to the stronger binding to the surface does not compensate for the cost of creating the defected surface at low adsorbate coverages. The energy gained from adsorption to a defect-containing surface increases with increasing coverage, which leads to a transition when the energy cost of defect formation can be overcome. This gain in energy at higher coverages is not just the result of adding adsorbate atoms, but rather due to the fact that the gold-adsorbate interaction changes with increasing coverage. To illustrate, at 0.33 ML of chlorine coverage the difference between the adsorption of Cl on a clean surface and on 0.67 ML adatom-covered surface is -0.31 eV per Cl. At 0.67 ML chlorine coverage, a second chlorine atom is added to the $(\sqrt{3}\times\sqrt{3})R30^\circ$ unit cell, but the difference in the total binding energy between chlorine on the flat surface and the 0.67 ML adatom-covered surface is not simply twice the difference at 0.33 ML (-0.62 eV), but larger (-0.86 eV) and adequate to compensate for

the cost of creating the adatom surface (0.65 eV). To account for this effect, there must be differences in the bonding of the adsorbate at different coverages. In the following discussion, we will analyze the density of states (DOS) to identify specifically which states are affected by gold incorporation, and consider charge density plots in an attempt to understand the bonding differences for chlorine at different coverages.

Partial density of states (PDOS) plots provide insight into the ability of chlorine to stabilize adatoms on the gold surface. A comparison of the Au *d*-PDOS of states for the Au(111)-(1x1), the surface containing 0.33 ML of adatoms, and the adatom-covered surface with 0.67 ML Cl, provides insight into bonding changes, Figure 8.4a. As expected, without chlorine adsorbed on the surface, the Au *d* states are higher in energy for the gold adatoms, suggesting that these adatoms are more reactive[57, 58]. With chlorine adsorbed, the gold adatom *d* electronic states are significantly lowered in energy, suggesting that adsorbed Cl can stabilize adatoms that are created on the surface. This explains why the adsorption energy for chlorine at any coverage is lower than the clean surface.

The *p*-PDOS for 0.67 ML Cl on the clean and adatom-covered surfaces indicates that the adsorption of Cl on the adatom-covered surface lowers the energy of Cl, since the *p*-PDOS is generally lower in this case, Figure 8.4b. The same trend is observed for the *s* states of Cl and could explain why the neighboring Cl-Cl distance is smaller on the adatom-covered surface: 2.92 Å on the clean surface versus 2.57 Å on the adatom-covered surface.

Charge density plots of Cl and O on various gold substrates illustrate that the Cl-Au and O-Au bond becomes more covalent with gold incorporation. Figure 8.1 shows the

charge density difference plots for 0.67 ML of Cl on (a) the clean gold surface, (b) the 0.33 ML Au adatom-covered surface and (c) the 0.67 ML Au adatom-covered surface.

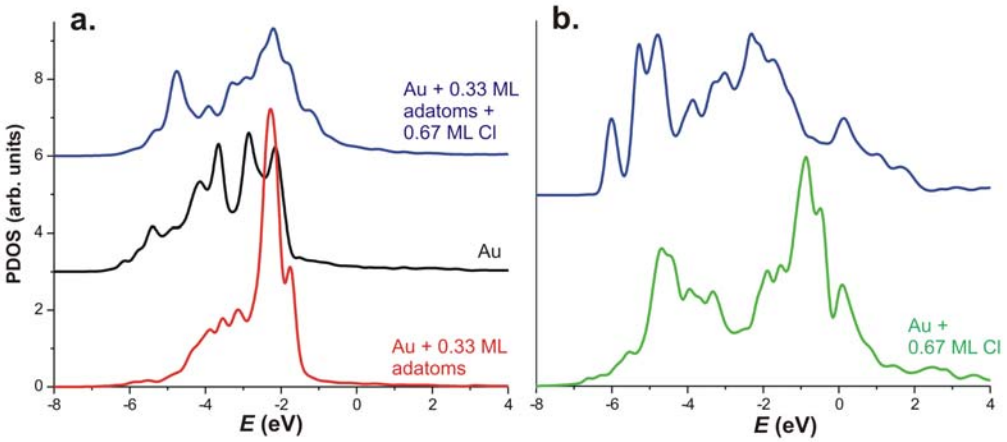

Figure 8.4: (a) Au *d*-PDOS versus energy *E* for the surface gold atom of the clean surface (black), gold adatom for the 0.33 ML adatom-covered surface (red), and gold adatom for the 0.33 ML adatom-covered surface with 0.67 ML Cl (blue). (b) Cl *p*-PDOS versus energy *E* for 0.67 ML of chlorine on the clean surface (green) and 0.33 ML Au adatom-covered surface (blue). The zero of the energy scale is the Fermi level.

The charge density differences are defined as the electron density of the total adsorbed system minus the density of just the Au substrate and Cl atom in the exactly same positions as in the adsorbed system. As mentioned earlier, the overlayer (a) is the highest in energy followed by the 0.33 ML adatom-covered surface (b), with the 0.67 ML adatom-covered surface being the most stable. The charge difference plots illustrate the bonding between Cl and Au on these three surfaces. In previous work, we found that the Cl-Au interaction on the Au(111) surface is mainly covalent in nature[59]. The same is true for these three systems, only in the case of gold incorporation the chlorine atom forms an even stronger covalent bond with the gold substrate. Figure 8.1b and 8.1c illustrates the

accumulation of electron density directly between Cl and Au. The electron density minimum on the line connecting the Cl and Au positions increases as the energy of the system decreases. The density minimum for the clean, 0.33 ML Au adatom-covered, and 0.67 ML Au adatom-covered surface is 0.38, 0.45, and 0.51, respectively. The Au-Cl bond distance follows the same trend, namely: 2.60, 2.51, and 2.46 Å, respectively.

The same trend is also observed for oxygen: as the overlayer coverage increases from 0.33, to 0.67, to 1.00 ML the minimum value of the charge density increases from 0.59, to 0.67, to 0.82 respectively. The system with the lowest energy for 1.00 ML of oxygen contains 0.33 ML of gold adatoms; this O-Au bond has the highest amount of electron density directly along the bond, 1.10. As the coverage increases, the number of gold atoms to which the adsorbate is coordinated decreases. The charge density difference plots (Figure 8.2) illustrate that more electron density is added directly between the adsorbate and gold adatom with increasing coverage, suggesting a stronger covalent interaction similar to the trend observed for Cl. There are some important differences, however, between the Cl and O charge density difference plots. There is less electron density directly between O and Au for 0.67 ML on the adatom-free surface compared to the corresponding Cl case, suggesting the O-Au interaction is more ionic. This could partly be a consequence of oxygen preferring to bind in three-fold sites compared to two-fold sites for Cl. For oxygen adsorption on the adatom-covered surfaces, electron density is added both between the O and Au adatom and on the back side of O, while for Cl electron density is only added directly between Cl and the Au adatom. The electron density accumulation on the back side of the O atom (opposite of the adatom) is attributed to the oxygen binding much closer to the surface than Cl,

preferring higher coordination to Au compared to Cl; this results in bonding not just between oxygen and the adatom, as in the Cl case, but also between O and the underlying gold in the first complete layer.

The charge on the adsorbate also provides evidence that the bonding becomes more covalent with gold incorporation or at higher adsorbate coverages. Table 8.3 contains the charge, calculated using both the sphere and Bader method, for various adsorption systems.

Table 8.3: Summary of calculated charges for different coverages of O and Cl (*p*) on Au(111) with different gold adatom coverages (*n*) . The two different methods of calculating charge are indicated, (A) sphere, or (B) Bader method.

p (ML) / *n* (ML)	0.33 ML Cl		0.67 ML Cl			
	A	B	A	B	A	B
0.00	-0.33	-0.37	-0.33	-0.28		
0.33	-0.20	-0.41	-0.27	-0.20		
	0.33 ML O		0.67 ML O		1.00 ML O	
0.00	-0.54	-0.77	-0.56	-0.70	-0.40	-0.58
0.33	-0.40	-0.59				

The charge changes significantly as a function of the coverage and gold incorporation. Generally, as the coverage of the adsorbate increases or if gold is incorporated into the adsorbate layer, the magnitude of the negative charge decreases. For example, as the oxygen overlayer coverage increases, the charge from the Bader method decreases from -0.77 at 0.33 ML to -0.58 at 1.00 ML. The same is observed for Cl and at the same Cl coverage, gold incorporation lowers the charge. The smaller partial negative charge on the adsorbate may occur partly because the adsorbate is coordinated to fewer gold atoms and these gold atoms have more than one electronegative atom bound to them, so that a

smaller amount of electron density is available to be pulled by the adsorbate atom. These results combined with the charge density plots, indicate that the smaller negative charge is also a result of the increased covalent nature of the adsorbate-Au interaction.

Furthermore, the lower partial negative charge upon gold incorporation should decrease the repulsive interaction between adsorbate atoms on the surface. The adsorption energy per adsorbate atom increases with coverage because of the repulsion between partially negative Cl or O atoms. In many cases, the partial charge on the adsorbate is lower when it is incorporated with gold. The decrease in the charge could help drive gold incorporation since in this case the interatomic repulsion of the adsorbate atoms would be lower.

8.6 Conclusions

Gold is used in a wide variety of applications making it important to have a complete understanding of the interaction of adsorbates with its surface. We used periodic-slab DFT calculations to investigate the energetics of the morphological changes of the Au(111) surface upon the adsorption of two different electronegative species, chlorine and oxygen. We find that gold adatoms can be pulled out of the surface to become part of the absorbate layer. Generally, the Au-adsorbate interaction is stronger for the incorporated gold surface versus the clean surface. At low coverages this stronger interaction cannot compensate for the cost of creating the adatoms on the surface. As the coverage of the adsorbate increases, a transition occurs where the cost for creating adatoms is compensated and the adsorbate system containing incorporated gold atoms becomes lower in energy. Along with these morphological changes, the nature of the Au-adsorbate interaction changes as a function of coverage and gold incorporation. The Au-

adsorbate bonding becomes more covalent with higher coverage or upon the incorporation of gold adatoms, resulting in a smaller adsorbate partial charge with more electron density located directly between the adsorbate and Au. The trends found in this work are qualitatively similar for the adsorption of chlorine and oxygen, but chlorine prefers coordination to fewer surface gold atoms than oxygen; upon adatom incorporation the chlorine is only coordinated to a single gold adatom while oxygen can coordinate with the gold adatom and gold atoms in the top complete layer of gold. Our results are useful in understanding the interaction of chlorine and oxygen with gold, especially in systems where the surface morphology or electronic nature of the surface plays an important role.

8.6 References

[1] K. W. Kolasinski, *Surface Science: Foundations of Catalysis and Nanoscience* [Wiley: New York, **2008**].

[2] P. E. Laibinis, G. M. Whitesides, D. L. Allara, Y. Tao, A. N. Parikh, R. G. Nuzzo, *J. Am. Chem. Soc.* **1991**, *113*, 7152.

[3] A. Ulman, *Chem. Rev.* **1996**, *96*, 1533.

[4] A. Kumar, H. A. Biebuyck, G. M. Whitesides, *Langmuir* **1994**, *10*, 1498.

[5] C. M. Fischer, M. Burghard, S. Rith, K. V. Klitzing, *Appl. Phys. Lett.* **1995**, *66*, 3331.

[6] A. V. Ellis, K. Vijayamohanan, R. Goswami, N. Chakrapani, L. S. Ramanathan, P. M. Ajayan, G. Ramanath, *Nano Lett.* **2003**, *3*, 279.

[7] B. Ozturk, C. Blackledge, B. N. Flanders, D. R. Grischkowsky, *Appl. Phys. Lett.* **2006**, *88*, 073108.

[8] J. Janata, M. Josowicz, *Nature Materials* **2003**, *2*, 19.

[9] J. Liu, Y. Lu, *J. Am. Chem. Soc.* **2003**, *125*, 6642.

[10] Z. Siwy, L. Trofin, P. Kohli, L. A. Baker, C. Trautmann, C. R. Martin, *J. Am. Chem. Soc.* **2005**, *127*, 5000.

[11] E. Ozbay, *Science* **2006**, *311*, 189.

[12] J. Biener, G. W. Nyce, A. M. Hodge, M. M. Biener, A. V. Hamza, S. A. Maier, *Adv. Mater.* **2008**, *20*, 1211.

[13] M. Valden, X. Lai, D. W. Goodman, *Science* **1998**, *281*, 1647.

[14] M. Valden, S. Pak, X. Lai, D. W. Goodman, *Catal. Lett.* **1998**, *56*, 7.

[15] M. Comotti, W. C. Li, B. Spliethoff, F. Schuth, *J. Am. Chem. Soc.* **2006**, *128*, 917.

[16] N. Lopez, T. V. W. Janssens, B. S. Clausen, Y. Xu, M. Mavrikakis, T. Bligaard, J. K. Norskov, J. Catal. **2004**, *223*, 232.

[17] S. M. Driver, T. F. Zhang, D. A. King, *Angew. Chem.-Int. Edit.* **2007**, *46*, 700.

[18] S. Y. Quek, M. M. Biener, J. Biener, J. Bhattacharjee, C. M. Friend, U. V. Waghmare, E. Kaxiras, *J. Phys. Chem. B*. **2006**, *110*, 15663.

[19] P. Maksymovych, D. C. Sorescu, D. Dougherty, J. T. Yates, *J. Phys. Chem. B.* **2005**, *109*, 22463.

[20] L. M. Molina, B. Hammer, *Chem. Phys. Lett.* **2002**, *360*, 264.

[21] S. Narasimhan, D. Vanderbilt, *Phys. Rev. Lett.* **1992**, *69*, 1564.

[22] C. E. Bach, M. Giesen, H. Ibach, T. L. Einstein, *Phys. Rev. Lett.* **1997**, *78*, 4225.

[23] H. Ibach, *J. Vac. Sci. Technol. A-Vac. Surf. Films* **1994**, *12*, 2240.

[24] M. M. Biener, J. Biener, C. M. Friend, *Langmuir* **2005**, *21*, 1668.

[25] H. Ibach, C. E. Bach, M. Giesen, A. Grossmann, *Surf. Sci.* **1997**, *375*, 107.

[26] D. Sander, U. Linke, H. Ibach, *Surf. Sci.* **1992**, *272*, 318.

[27] B. K. Min, X. Deng, D. Pinnaduwage, R. Schalek, C. M. Friend, *Phys. Rev. B*. **2005**, *72*, 4.

[28] J. Biener, M. M. Biener, T. Nowitzki, A. V. Hamza, C. M. Friend, V. Zielasek, M. Baumer, *ChemPhysChem* **2006**, *7*, 1906.

[29] B. K. Min, A. R. Alemozafar, D. Pinnaduwage, X. Deng, C. M. Friend, *J. Phys. Chem. B*. **2006**, *110*, 19833.

[30] N. D. Spencer, R. M. Lambert, *Surf. Sci.* **1981**, *107*, 237.

[31] G. N. Kastanas, B. E. Koel, *Appl. Surf. Sci.* **1993**, *64*, 235.

[32] W. W. Gao, T. A. Baker, L. Zhou, D. S. Pinnaduwage, E. Kaxiras, C. M. Friend, *J. Am. Chem. Soc.* **2008**, *130*, 3560.

[33] G. Kresse, J. Hafner, *Phys. Rev. B*. **1993**, *47*, 558.

[34] J. P. Perdew, Y. Wang, *Phys. Rev. B*. **1992**, *45*, 13244.

[35] D. Vanderbilt, *Phys. Rev. B*. **1990**, *41*, 7892.

[36] G. Kresse, J. Hafner, *J. Phys.-Condes. Matter.* **1994**, *6*, 8245.

[37] C. Kittel, *Introduction to Solid State Physics* [Wiley: New York, 1996].

[38] F. R. Boer, R. Boom, W. C. M. Mattens, A. R. Miedema, A. K. Niessen, *Cohesion in Metal* [North-Holland: Amsterdam, **1988**].

[39] R. F. W. Bader, *Atoms in Molecules: A Quantum Theory* [Oxford Science: Oxford, **1990**].

[40] G. Henkelman, A. Arnaldsson, H. Jonsson, *Comput. Mater. Sci.* **2006**, *36*, 354.

[41] K. P. H. Huber, *Molecular Spectra and Molecular Structure Constant of Diatomic Molecules* [Van Nostrand: New York, **1979**].

[42] B. Hammer, L. B. Hansen, J. K. Norskov, *Phys. Rev. B*. **1999**, *59*, 7413.

[43] P. Broqvist, L. M. Molina, H. Gronbeck, B. Hammer, *J. Catal.* **2004**, *227*, 217.

[44] M. Mavrikakis, P. Stoltze, J. K. Norskov, *Catal. Lett.* **2000**, *64*, 101.

[45] M. Gajdos, J. Hafner, A. Eichler, *J. Phys.-Condes. Matter*. **2005**, *18*, 13.

[46] J. Wang, M. R. Voss, H. Busse, B. E. Koel, *J. Phys. Chem. B.* **1998**, *102*, 4693.

[47] J. M. Gottfried, N. Elghobashi, S. L. M. Schroeder, K. Christmann, *Surf. Sci.* **2003**, *523*, 89.

[48] M. M. Biener, J. Biener, C. M. Friend, *Surf. Sci.* **2005**, *590*, L259.

[49] N. D. S. Canning, D. Outka, R. J. Madix, *Surf. Sci.* **1984**, *141*, 240.

[50] N. Saliba, D. H. Parker, B. E. Koel, *Surf. Sci.* **1998**, *410*, 270.

[51] E. Kaxiras, Y. Baryam, J. D. Joannopoulos, K. C. Pandey, *Phys. Rev. B*. **1987**, *35*, 9625.

[52] G. X. Qian, R. M. Martin, and D. J. Chadi, *Phys. Rev. B*. **1988**, *38*, 7649.

[53] K. Reuter, M. Scheffler, *Phys. Rev. B*. **2003**, *68***,** 045407.

[54] K. Reuter, M. Scheffler, *Phys. Rev. B*. **2001**, *65*, 035406.

[55] J. L. Gole, R. N. Zare, *J. Chem. Phys.* **1972**, *57*, 5331.

[56] H. Shi, C. Stampfl, *Phys. Rev. B.* **2007**, *76*, 075327.

[57] B. Hammer, J. K. Norskov, in *Advances in Catalysis,* Vol. 45, pg 71 [Elsevier: New York, **2000**].

[58] R. Hoffmann, *Rev. Mod. Phys.* **1988**, *60*, 601.

[59] T. A. Baker, C. M. Friend, E. Kaxiras, *J. Am. Chem. Soc.* **2008**, *130*, 3720.

CHAPTER 9

SELECTIVITY SWITCH INDUCED BY DEFECTS: ADSORPTION AND REACTION OF PROPENE ON O-COVERED AU(111)

9.1 Abstract

We investigate the effect of defects, including adatoms, vacancies, and steps, on the adsorption and reaction of propene and atomic oxygen on Au(111), using density functional theory (DFT). The adsorption of propene is stronger on a surface containing defects compared to the flat, bulk-terminated surface, with the largest gain in binding being 0.65 eV on a surface with 1/9 monolayer (ML) of Au adatoms, using the generalized gradient approximation (GGA) for the exchange-correlation functional [0.67 eV when using the local density approximation (LDA) functional]. Charge-density difference plots reveal that there is more depletion of electron density from the carbon-carbon π bond and charge accumulation between the double bond and the gold atom to which the propene is bound on defective surfaces compared to the bulk-terminated surface. We calculate the energy barriers for two competing reactions, namely, allylic hydrogen abstraction by atomic oxygen and oxygen attack of a carbon in the double bond to create an oxametallacycle, using the nudged elastic band method. These reactions are important in determining the selectivity for propene oxidation: allylic H abstraction leads to combustion whereas O addition to form an oxymetallacycle is the first step in the reaction path for propene epoxide formation. A comparison of the energetics of these two pathways on flat and defect-containing Au surfaces indicates that the selectivity will

depend on the nature and prevalence of surface defects. The surface morphology has significant effects on both reactions: for example, in hydrogen abstraction, the reaction barrier on the flat surface is approximately half of the barrier for the surface containing 1/9 ML of adatoms. Both electronic and geometric factors, such as the path and distance the oxygen must travel to meet the allylic hydrogen for abstraction, are important in explaining the reaction barriers trends.

This work is in preparation for submission for publication: T. A. Baker, B. Xu, S. C. Jensen, C. M. Friend, E. Kaxiras.

9.2 Introduction

Understanding the molecular-level mechanism of a heterogeneous catalytic reaction provides the basis for the design of processes and materials with optimized activity and selectivity, a key step towards improved energy efficiency in large-scale synthetic processes. There are many factors that contribute to the reactivity of a metal surface, including its atomic-scale structure. Gold, in particular, has shown promise as a selective oxidation catalyst. Great interest in understanding the reactivity of gold was stimulated by the initial work of Schwank[1] and shortly thereafter, the discovery that nanoscale Au supported on reducible metal oxides were active for the catalytic oxidation[2-4] of CO[5] and propene[6]. These discoveries prompted us to study reactions on O-covered Au(111)[7-9].

In the case of propene oxidation on Au(111)[8], the morphology of the surface may have a substantial role since the presence of atomic oxygen releases gold atoms and stabilizes gold adatoms resulting in a roughened surface[10,11]. The reactivity of this

surface can be tuned by changing the temperature at which oxygen is dosed on the surface. STM studies reveal differences in surface morphology depending on the dosing temperature, suggesting that surface morphology has an impact on the reactivity[9]. Our studies specifically indicate that the local bonding, including that of O atoms, on Au is an important factor in determining reactivity and selectivity, a feature not explored in any previous studies, which have focused on particle size effects.

The role of surface structure and morphology in determining selectivity and activity of gold-based materials is a topic of intense interest. The size and morphology of supported gold particles in heterogeneous catalysts are thought to determine catalytic activity and selectivity[12-17]. Recent model studies have shown that gold nanoparticles on inert materials (such as boron nitride, silicon dioxide, and carbon) can catalyze the oxidation of styrene using molecular oxygen. The activity of these catalysts is strongly dependent on the particle size, with smaller gold particles (~ 1.4 nm in diameter) that have an irregular perimeter being the most active, while larger particles (> 2 nm) that have more regular shapes tend to be inactive[17]. Recent work on the reduction of resazurin on Au nanoparticles, studied by single-molecule techniques, illustrated the importance of surface morphology, distribution of surface sites, and dynamic restructuring on nanocatalysis[15].

Of all the transition metals, gold is especially promising for low temperature selective oxidation. There has been recent focus on complex reactions using Au-based catalysts, specifically the selective oxidation of alkenes[17,18] and alcohols[19-22]. While there is some debate regarding the active species of oxygen and its role in oxidation, atomic oxygen is clearly an active species in single crystal work which servers as a model

system. On these systems atomic oxygen on Au(111) and Au(110) is active for the oxidation of CO[9,23-25] and other olefins, including styrene[7] and propene[8].

The catalysis of propene and other olefins to epoxides is an extremely important reaction because epoxides are extensively used in the chemical industry as an intermediate for many synthetic processes[26]. The oxidation of propene on the surface of gold has been the subject of several theoretical studies[27-34]. Propene oxide is crucial for the production of polyether polyols, propylene glycol, and propylene glycol ethers[35]. While the catalysis of ethene oxide is highly selective on silver heterogeneous catalysts[36], the oxidation of propene is not[37]. The oxidation of propene (Scheme 9.1), proceeds through at least two competing reaction pathways: allylic hydrogen abstraction or oxygen insertion forming intermediary propene oxametallacycle which will lead to the desired epoxide product[8,38]. The first pathway, which is the result of an important difference between ethene and propene, is undesirable because it leads to combustion. The major difference between ethene and propene is the presence of allylic hydrogens, which are attached to a carbon neighboring a C=C bond. These hydrogens are acidic, labile, and can be more easily removed by oxygen bound to the noble metals (Au, Ag, and Cu) because oxygen acts as a Brønsted base. Thus, combustion of propene in the presence of O on Ag, the catalyst used for ethene epoxidation, is favored over epoxidation. For gold or any other metal to be used as a catalyst, allylic hydrogen abstraction must be impeded. The challenge is to determine what can be done to control or tune the favorability of these two reaction pathways.

Theory can provide the guiding principles for understanding the catalytic properties of metals and can therefore be used for the future design of novel catalyts[39].

Advances in modern density functional theory (DFT) and an increase in computational capabilities has made possible accurate calculations for a wide variety of systems important for catalysis. DFT can be used to determine adsorption energies, adsorption and surface structure, charge transfer, bonding characteristics, and to approximate the kinetics of a system. DFT has been successfully applied to describe trends in reactivity for many transition metals and alloys[40]. However, obtaining an accurate understanding of kinetics can be extremely difficult because of the number of factors on which the activity and selectivity depend, including the surface structure. While there exist some successful examples of kinetic studies on defect-free surfaces[41,42], for many catalytic systems the surface structure and the presence of defects significantly affect activity and selectivity, suggesting that predictions using DFT will have to take these features into account.

In this work, we use DFT to calculate the barrier for allylic hydrogen abstraction and oxametallacycle formation of propene by oxygen on the Au(111) surface. We consider defects on the Au(111) surface since the oxygen-covered surfaces of supported gold nanoparticles on metal oxides or single crystal Au(111) in ultra-high vacuum are roughened gold surfaces containing under-coordinated gold atom. Moreover, it has been proposed that these under-coordinated gold atoms are the key to understanding the reactivity of gold[43-45]. We will show that, in general, surface defects (such as steps, surface adatoms, and surface vacancies) significantly affect the adsorption properties of propene on gold. More importantly, we describe in detail the effect of surface morphology on reactivity and its impact on the reaction barrier to allylic hydrogen abstraction by atomic oxygen and the formation of the propene oxametallacycle.

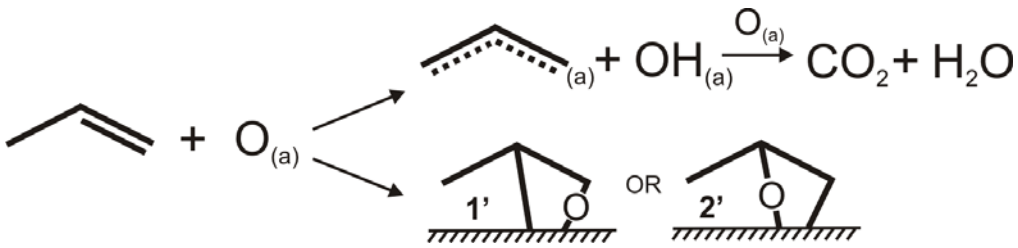

Scheme 9.1: Calculated reactions of propene with adsorbed atomic oxygen on Au(111): allylic hydrogen abstraction to form allyl and hydroxyl (top) and oxygen insertion to form either a primary (1') or secondary (2') oxametallacycle (bottom).

9.3 Calculational Details

For the DFT calculations, we use VASP[46] with the GGA-PW91[47] and LDA functionals[48] to describe electron exchange and correlation. The interaction of propene with the adsorbate-free surface is mainly dispersive (van der Waals) in nature, but the GGA functional typically gives a poor description of this interaction and underestimates binding energies[49]. The LDA functional typically provides better binding energies for dispersive systems. This is not necessarily a result of the LDA functional providing a better physical description of dispersive forces, but is more likely related to the fact that this functional overestimates binding energies[50,51]. Recent attempts have been made to create functionals that can accurately model dispersive forces[52-54], with some success. Herein, we report binding energies calculated using both the GGA and LDA functionals since we are most interested in qualitative trends and relative energies, which we find to be in good agreement between the two functionals.

For calculations using LDA, ultrasoft-pseudopotentials are employed with the default plane-wave cutoffs for different elements taken from the ultrasoft-pseudopotential database[55,56]. Projector augmented wave pseudopotenitals[57] are employed for

calculations using the GGA functional. A 4×4×1 Monkhorst-Pack k-point sampling of reciprocal space is used for the adsorption studies. The surface is modeled by a slab consisting of 4 layers in the (111) direction with a 3×3 supercell of the primitive unit cell in the lateral directions. Only the two uppermost layers of the slab were allowed to relax, with the rest fixed at the ideal bulk positions. The bulk gold positions of the bottom two layers were determined using the calculated lattice constant [4.07 Å using LDA and 4.17Å using GGA], which is in good agreement with the experimental value of 4.08 Å[58]. Reaction barriers were found with the GGA functional using the climbing nudged elastic band method (cNEB)[59-61], with three images between the two fixed end points. In a few cases, the calculation did not converge to a reasonable transition state, which required the use of additional images. To reduce computational costs, these calculations were preformed with a three layer slab, allowing the two uppermost layers to relax with 3×3×1 Monkhurst-Pack k-point sampling. An ensemble of starting points for each reaction was tested. We only report the energy of the pathway with the lowest barrier, defined as the difference in energy between the transition state and the lowest energy configuration from the ensemble of tested starting points.

9.4 Results

Four different gold substrates were used in order to model under-coordinated gold atoms that may be responsible for activating gold: (1) the flat, defect-free (111) surface; (2) a surface with1/9 ML gold adatoms, that is 1 extra Au atom per 3×3 surface unit cell relative to the defect-free surface, which is placed at the FCC three-fold site; (3) a surface with 1/9 ML of vacancy defects, that is 1 Au atom per 3×3 surface unit cell fewer than

the defect-free surface; and (4) a stepped <110>/{1,0,0} Au(211) surface, created by offsetting the lattice vectors by one gold layer, which results in a step and a (3×3) terrace.

The binding strength of propene on each of these surfaces is determined by its adsorption energy defined as:

$$E_{ads} = E_{propene/Au} - E_{Au} - E_{propene} \quad (9.4.1)$$

where $E_{propene/Au}$ is the energy of a propene molecule bound to the gold substrate, E_{Au} is the energy of the gold substrate, and $E_{propene}$ is the energy of a propene molecule in the gas phase. On each gold substrate many different adsorption structures were considered. Symmetry and physical intuition gained from previous calculations helped us reduce the number of binding configurations that we considered, so that every reasonable site was included and the global minimum on the potential energy surface (PES) for each gold substrate has been identified. In some cases, there were minima on the PES with similar energies. These cases will be discussed in more detail but the structure with the lowest energy will be the main focus in this report.

The lowest energy configuration for propene on gold has the carbon-carbon double bond centered over a single under-coordinated gold adatom (see Figure 9.1 and Table 9.1). The adsorption of propene is strongest on an adatom-covered surface and weakens with increasing coordination of the gold atom to which it is bound. The trend in adsorption strength is as follows: defect-free < vacancy < step < adatom (see Table 91). In the most extreme case, adsorption on the adatom-covered surface leads to a binding energy which, compared to the defect-free surface, is lower by 0.65 eV as obtained with the LDA functional [0.67 eV using the GGA functional].

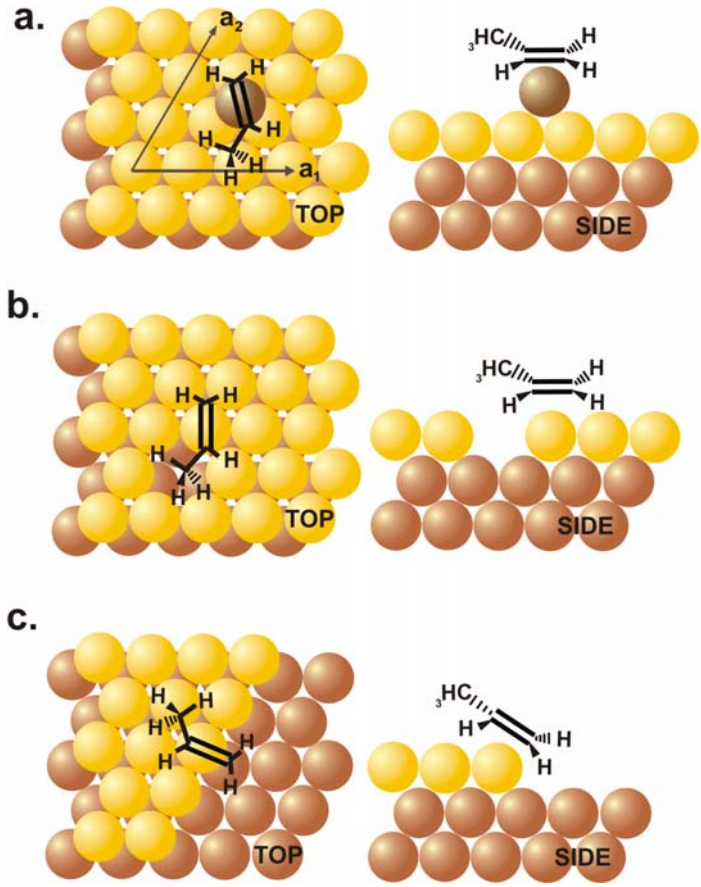

Figure 9.1: Geometries of propene on (a) 1/9 ML adatom covered, (b) 1/9 ML vacancy covered, and (c) stepped gold surfaces.

This increase in binding strength results in a shorter carbon-gold distance. The sp^2 carbon-gold distance is 2.45 Å on the flat surface, but is 2.21 Å for the adatom-covered surface, within the LDA calculation [the corresponding values being 3.07 Å and 2.28 Å for the GGA calculation]; this suggests a stronger electronic interaction with more electron density added between the carbon and gold atoms, allowing the carbon to approach much closer to the gold adatom. On the other defect surfaces, propene prefers adsorption to the gold atom with lowest coordination. In the case of vacancy defects, the

double bond is situated on top of a gold atom neighboring a vacancy. Similarly, propene preferentially binds to the edge atoms of a step. On the flat defect-free surface, all the surface gold atoms have the same coordination so adsorption is equally probable on top of any gold atom on the surface.

Table 9.1: Adsorption energies in eV for propene on the clean and oxygen covered gold substrates.

	Without Oxygen		With Oxygen	
Surface	LDA	GGA	LDA	GGA
flat	-0.72	-0.11	-0.85	-0.21
vacancy	-0.96	-0.20	-1.11	-0.36
step	-1.05	-0.47	-1.21	-0.52
adatom	-1.37	-0.78	-1.51	-0.91

The effect of adsorbed oxygen atoms on propene adsorption was tested on surfaces with and without defects. The adsorption energy for propene is now defined as:

$$E_{ads} = E_{propene/Au/O} - E_{Au/O} - E_{propene} \quad (9.4.2)$$

where $E_{Au/O}$ is the energy of the gold substrate with oxygen at the same location as in the co-adsorbed system, $E_{propene/Au/O}$ is the energy of the total system and $E_{propene}$ is the energy of a single propene molecule in the gas phase. The ideal adsorption sites for oxygen on the different gold substrates have been established in previous work[62]. These preferred configurations were taken as the starting points for our investigation of propene adsorption. Atomic oxygen generally prefers to adsorb on a three-fold hollow site, binding away from an adatom, but neighboring a vacancy. On the stepped surface, binding to the three-fold site at the step edge or at a bridge site hanging over the step edge

are equal in energy. These geometries are obtained by relaxing the forces of all the atoms in the propene, adsorbed oxygen, and top two layers of gold.

The lowest energy configurations correspond to propene and oxygen being in close proximity, yet remaining bound to sites that were preferred when adsorbed individually. This suggests that the interaction between the propene and oxygen is weak relative to the binding strength of each component to the surface. Overall, the adsorption of propene is slightly stronger with the presence of oxygen (Table 9.1). The decrease in adsorption energy is nearly the same for adsorption on all the difference substrates, the average value being 0.14 eV within the LDA calculations [0.13 eV within the GGA]. In general, an oxygen atom binds preferentially near an allylic hydrogen of the propene, except when both the oxygen atom and propene are co-adsorbed on the flat, defect-free surface. In this case, oxygen atoms bind preferentially next to the hydrogen atom of the methylene. However, the difference in energy between this adsorption configuration and oxygen bound next to the allylic hydrogen is quite small (< 0.05 eV).

The only discrepancy between LDA and GGA results in what concerns the lowest energy configuration is for the case where oxygen and propene are co-adsorbed on the surface containing vacancy defects. The lowest energy configuration obtained from the LDA calculation has the C=C double bond centered over the gold atom neighboring the vacancy and the oxygen in a three-fold site neighboring both the vacancy and the allylic hydrogen on the propene. With the GGA functional, the lowest energy configuration corresponds to the oxygen atom at a three-fold site adjacent to the vacancy, while the C=C double bond is centered over a gold atom next to the vacancy. In the resulting arrangement, oxygen sits next to the carbon double-bond. The lowest energy

configuration obtained within the LDA cacluation is only 0.04 eV higher in energy than that obtained when using the GGA functional. Because of the small energy differences and the inherent limitations of DFT, it is likely that propene binds to both of the sites corresponding to the lowest energy configurations obtained with the two different functionals.

We used the climbing nudged elastic band method (cNEB) to find the transition state energies for two pathways: allylic hydrogen abstraction of propene by oxygen and oxametallacycle formation. The reaction of propene on oxygen-covered Au(111) at low temperatures (200 K) and with a low coverage of oxygen (0.3 ML) results in acrolein, acrylic acid, carbon suboxide, and combustion products[8]. While propene is a relatively simple molecule, reactions of propene with oxygen could proceed through a wide variety of mechanisms and intermediates. Scheme 9.1 illustrates that allylic hydrogen abstraction will result in an allyl species on the surface, which is believed to result in undesired combustion. Oxametallacycle formation, on the other hand, leads to the formation of the desired epoxide. In order to study the effect of the surface morphology we choose only to investigate the two important reactions, allylic hydrogen abstraction by oxygen and oxametallacycle formation, because these paths directly probe the competition between combustion and epoxidation.

The reaction barrier in this work is defined as the difference in energy between the lowest energy configuration of the co-adsorbed species and the energy of the transition state found using cNEB. The lowest energy configuration was not always used as the starting point for performing the cNEB, since that configuration may not have the oxygen in close proximity to the allylic hydrogen or double bond. However, the

difference in energy between the lowest energy configuration and that used as the starting configuration was always quite small (<0.1 eV). Various starting and ending points were considered for each surface, but we will discuss here only the pathway with the lowest energy barrier.

Allylic hydrogen abstraction is most facile on the defect-free Au(111) surface and the surface with a vacancy. The calculated barrier for allylic hydrogen abstraction on the defect-free surface is 0.33 eV (Table 9.2), similar to the barrier of 0.30 eV calculated by Torres et al.[28] for hydrogen abstraction on flat O-covered Ag(111).

Table 9.2: Reaction barriers and transition state distances for allylic hydrogen abstraction of propene by oxygen.

Surface	Barrier (eV)	C--O (Å)	C--H (Å)	H--O (Å)
flat	0.33	2.60	1.29	1.31
vacancy	0.33	2.60	1.30	1.30
step	0.73	2.61	1.30	1.33
adatom	0.65	2.60	1.32	1.28

The barriers on the other surfaces with under-coordinated atoms (steps and adatoms), were nearly twice as high (Table 9.2). In all cases atomic oxygen starts in a three fold FCC site in close proximity to an allylic hydrogen. The methyl group rotates so that the allylic hydrogen is pointed toward the oxygen. The transition state contains an allylic hydrogen shared between the carbon and the oxygen atom which is slightly pulled out of its original threefold site to meet with the allylic hydrogen. The ending configuration contains the remaining allyl and an OH group. The starting, transition state, and final configurations for the reaction of propene on the flat, defect-free surface are shown in

Figure 9.2. The reaction pathway and geometry of the transition state is nearly the same on each of the surfaces. Further, the bond distances in all of the transition states are virtually identical (see Table 9.2).

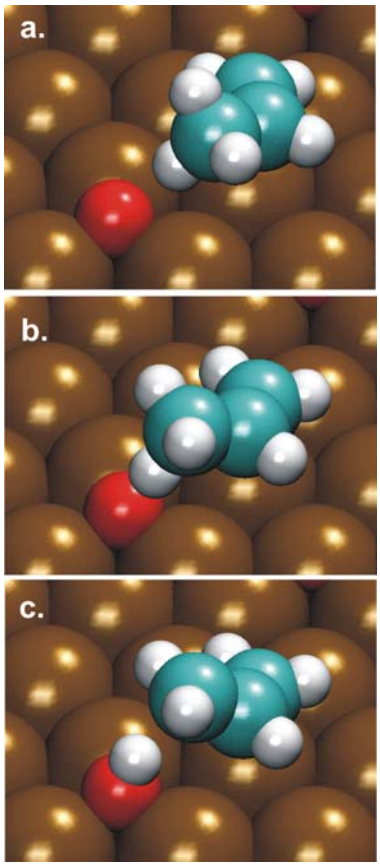

Figure 9.2: The starting (a), transition state (b), and ending point (c) used in the cNEB calculation of allylic hydrogen abstraction by oxygen on the defect free Au(111) surface. Brown, blue, red, and white spheres represent gold, carbon, oxygen, and hydrogen, respectively. The ending point (c.), which is not the structure that is the global minimum since OH is not in its preferred bridging site, is used for the cNEB calculation because of its close proximity to the propene and transition state.

Additionally, we studied the reaction of adsorbed oxygen with propene to form the oxametallacycle species, an intermediate thought to lead to epoxidation. We investigated both possible oxametallacycle configurations with oxygen added to either the primary carbon (labeled 1') or secondary carbon (labeled 2'). The formation of the 2' oxametallacycle is slightly preferred over the formation of the 1' one, since we observed lower barriers and larger gains in energy for the former (Table 9.3).

Table 9.3: Reaction barriers (E_b) and change in energy (ΔE) for forming propyl oxametallacycle with oxygen bonded to either the primary (1') or secondary (2') carbon.

Surface	E_b 1' (eV)	ΔE 1' (eV)	E_b 2' (eV)	ΔE 2' (eV)
flat	0.75	-0.39	0.51	-0.37
vacancy	0.89	-0.20	0.71	-0.31
step	0.82	-0.32	0.62	-0.45
adatom	0.87	0.16	0.65	-0.09

Similar to allylic hydrogen abstraction, we observe differences in the reaction barriers depending on the defects on the gold substrate. However, the magnitudes of these differences are not as large as those observed for hydrogen abstraction (the maximum difference in energy is 0.40 eV for allylic hydrogen abstraction and is 0.21 eV for oxametallacycle formation). The barrier for 2' oxametallacycle formation is lowest on the flat surface (0.51 eV), similar to what was discussed earlier for hydrogen abstraction. In comparison to the flat, defect-free surface, the barrier is higher on the stepped (0.62 eV) and adatom-covered surfaces (0.65 eV), and is the highest on the vacancy-covered surface (0.71 eV). Interestingly, it does not appear that the Brønsted-Evans-Polanyi rule

applies[63], since the reaction barrier (E_b) is not inversely proportional to the total change in energy (ΔE) during the reaction.

9.5 Discussion

Our results indicate that the adsorption of propene is stronger on under-coordinated gold atoms. This gain in energy can be as strong as 0.65 eV when the C=C double bond of propene is bound on top of an adatom compared to adsorption on the flat surface. This agrees well with the work of Chretien et al.[64] who found that propene binds strongest on a gold cluster where the LUMO of the cluster "protrudes most in the vacuum". They found that in most cases this occurs at an under-coordinated gold atom. Similarly, Kokalj et al.[65] found that ethene binds stronger to defects on Ag(001) compared to adsorption on the flat surface. We next elaborate on the physical origin of these findings.

9.5.1. Physical Origin of Adsorption Differences on Defect Au(111)

Charge density difference plots reveal electronic differences in the adsorption of propene in the presence of gold defects and oxygen on the surface. We calculate the difference in electronic density between the combined system (propene adsorbed on the Au(111) surface) and the separate isolated components (free Au(111) surface and free propene molecule) with atomic positions frozen at the optimized surface geometry with respect to the adsorbate. Figure 9.3a shows the charge density difference for propene adsorbed on the flat, defect-free surface; this is the weakest of all the bound systems, showing small changes in the charge density surrounding the propene. As expected by considerations based on organometallic chemistry, the binding of propene to a metal

involves electron donation from the π orbitals of the C=C double bond and donation of electrons from the metal to the anti-bonding π^* orbitals of the double bond, which causes a weakening of the double bond[66]. Experiments have also shown that the double bond of propene binds to gold by π bonding[67,68]. In Figure 9.3a, we observe a depletion of electron density from vertical *p*-like orbitals of the two carbons that make up the C=C double bond. A very small amount of density is added directly between the double bond and the Au atom, which most likely accounts for the slight attraction between propene and the surface. The plot also shows electron density addition to the σ-bond between the two carbon atoms.

Similar qualitative electronic distortions are observed for the adsorption of propene on oxygen-covered Au, Figure 9.3b, however, these distortions are larger compared to those on the flat, defect-free surface. We find that the magnitude of these distortions depends on the location of the oxygen atom relative to the C=C double bond, with distortions being greater for oxygen adsorbed closer to the double bond .

The electronic configuration changes drastically for the adsorption of propene on the Au adatom-covered surface, with the electron density becoming much more localized. This localization of charge occurs almost directly between each of the sp^2–bonded carbons and the Au adatom, resulting in a stronger binding of propene to this surface. The carbon double bond seems to become weaker since its bond length slightly increases from 1.36 Å on the flat, defect-free surface to 1.38 Å on the adatom-covered surface, with values obtained from the LDA functional [the corresponding values from the GGA functional are 1.35 Å and 1.39 Å]. The localization of charge and more drastic electronic

rearrangement are both a result of propene's stronger adsorption on the adatom-covered surface.

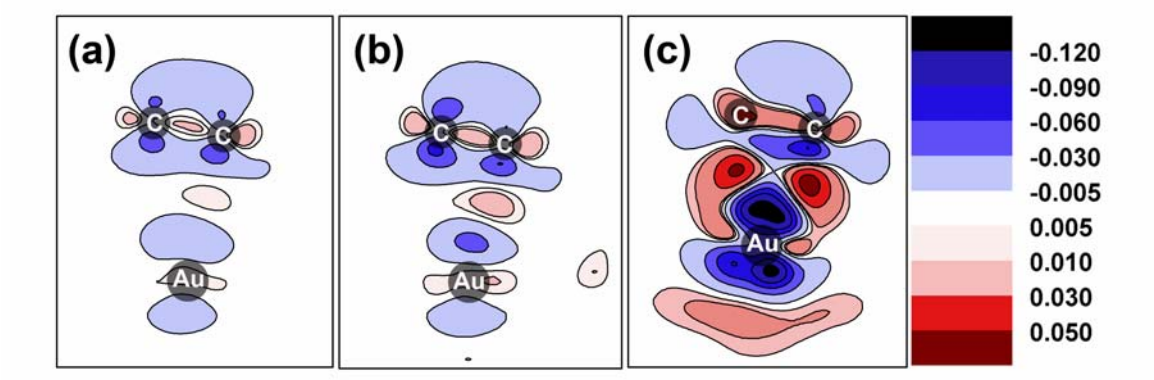

Figure 9.3: Difference charge density contour plots for propene adsorbed on (a) clean, (b) oxygen, and (c) adatom covered gold surfaces calculated using the GGA functional. The plot cuts through the plane that connects two carbons that make the double bond in the propene and the gold atom to which the propene is bound to. In all three cases the carbon on the left is the carbon attached to the methyl group. In (b) the oxygen is neighboring the allylic hydrogen. The labeled Au in (c) is the gold adatom while in (a) and (b) it is a gold atom in the first layer.

9.5.2. Physical Origin of Allylic Hydrogen Abstraction Reactivity Differences on Defect Au(111)

Defects on the gold surface affect both the adsorption strength of propene and the barriers for reaction. An important consequence is that the relative barrier heights for allylic C-H activation versus oxametallacycle formation are switched for the flat, defect-free surface versus the stepped surface. The barrier for allylic hydrogen abstraction is lowest on the defect-free and the vacancy-covered surfaces, while the reaction on the stepped and adatom-covered surfaces involves a barrier at least twice as large. Within

the margin of error expected for calculating reaction barriers, this trend in the barriers could simply be inverse to propene's binding strength. In other words, lower barriers correspond to propene molecules that are bound less strongly to the surface. While this trend may seem to be the simplest and most intuitive explanation for the results obtained, there are other factors responsible for the reactivity trends.

The basicity of the atomic oxygen is generally thought to have a significant impact on its ability to abstract an allylic hydrogen[28] because a stronger base is expected to more easily react with the acidic hydrogen. Oxygen atoms are more electronegative than gold and are expected to pull some electron density from the substrate resulting in a partial negative charge on the oxygen. The measure of the partial negative charge on the oxygen is a crude approximation for its basicity. To estimate the charge on the adsorbed oxygen atom, we use the Bader method which partitions the charge density into non-overlapping basins defined by hyper-surfaces where the electron density gradient vanishes[69,70]. The estimated charge on oxygen atoms is nearly the same on all of the four surfaces we considered (-0.81 e^-). This result is expected since the binding of oxygen on all four of these surfaces is nearly the same; oxygen binds on a three-fold site in all cases. Previous work established that for the adsorption of electronegative atoms on gold, the partial negative charge on the adsorbate decreases only when the number of gold atoms to which the adsorbate atom is bound decreases[71].

The binding strength of oxygen to the surface does not solely explain the observed reaction trends. The stronger the binding of oxygen to the gold surface, the harder it will be to react with hydrogen to form hydroxyls. In previous work, the adsorption of oxygen (at a coverage of 1/16 ML instead of the1/9 ML used herein)[62], was

stronger at the edge of a step or adjacent to a vacancy compared to the flat, defect-free surface. While these results partly follow the proposed trend, the adatom-covered surface is a clear exception. The binding strength of oxygen on the adatom-covered surface is equal to or less (depending on its exact location) than on the flat surface yet the barrier for hydrogen abstraction is over two times higher on the adatom-covered surface in comparison to the flat, defect-free surface.

Changes in the bonding between the methyl carbon and the allylic hydrogen on the different surfaces cannot account for the observed differences in reactivity. The charge density difference plots in Figure 9.3a and Figure 9.3b show some electronic differences between the C=C double bond on the defect-free and the adatom-covered surfaces, but these differences do not extend to the allylic hydrogen. The amounts of electron density between the methyl carbon and allylic hydrogen differ by no more than 0.02 e^- in the four different defect surfaces. The fact that bond distances are similar in the transition states for all four surfaces further suggests that the electronic structure of the reaction pathway is similar for all four cases.

The aforementioned factors all probably affect the reaction of allylic C-H to a small degree. However, the spatial arrangement of the allylic hydrogen of propene with respect to the atomic oxygen is one of the most important factors. During the reaction, both propene and oxygen must distort their equilibrium structures to meet at the transition state. The C-O distance is the same (~2.61 Å) in all of the transition states for the four different surfaces, but is shorter than the relaxed C-O distance which was different on the four surfaces. For example, the equilibrium distance between the methyl carbon and oxygen in the starting configuration on the defect-free surface is 3.42 Å while on the

adatom-covered surface it is 4.59 Å. This distance is also larger for the stepped surface (3.74 Å) and is similar to the adatom surface, which has a much higher barrier for allylic abstraction. The vacancy surface has a smaller starting C-O distance (3.22 Å) and a barrier lower than on the stepped and adatom surfaces, but closer to that on the flat, defect-free surface (0.33 eV).

Our calculations indicate that the oxygen atom moves to a less stable site during reaction with an allylic hydrogen leading to a slight deformation of the gold surface. The energy cost of the distortion is estimated from the difference in energy (ΔE_s) between oxygen adsorbed on the surface in its equilibrium position and oxygen and gold frozen in their positions from the transition state in the absence of propene. The system with atoms frozen in their positions from the transition state is higher in energy due to two reasons. In all cases the oxygen atom moves from a three-fold site to a lower coordination site. The equilibrium coordination for oxygen in OH is on a two-fold site. Therefore, the oxygen would most likely prefer to have lower coordination with the surface atoms because it is gaining a partial bond from hydrogen. Since the transition state in all four cases has nearly the same bond distances and the electronic structures are similar, we assume that this first contribution (the oxygen distortion which is the result of moving from a three-fold to two-fold site) should be the same on all four surfaces. However, depending on the distance and path along which the oxygen must travel to reach the C-O distance in the transition state (~2.61 Å), this could place an extra strain on the oxygen in addition to the first distortion and vary depending on the initial configuration. We find that ΔE_s is 0.19 eV, 0.18 eV, 0.55 eV, and 0.55 eV for the defect-free, vacancy-covered, adatom-covered, and stepped surfaces, respectively. Recall that the barriers on the four

surfaces were 0.33 eV, 0.33 eV, 0.65 eV, and 0.73 eV, respectively, illustrating that the difference in energy between the equilibrium substrate and the substrate frozen in its transition state correlate well with the calculated barriers.

The barrier is not strictly correlated to the distance the oxygen needs to travel but rather to the energy penalty of the process. We compared two different starting configurations for the reaction on the flat, defect-free surface. We find that the starting C-O distance was actually shorter for a reaction that ultimately resulted in a higher barrier. However, the higher barrier could be accounted for by the additional energy cost required to move the oxygen atom to its location in the transition state, ΔE_s. The energy barrier is also most likely correlated to propene distortion, since both the oxygen atom and propene can move to meet at the transition state. For simplicity, we only investigated the energy cost for oxygen distortion to illustrate the correlation to the energy barrier for allylic H abstraction.

9.5.3. Controlling Selectivity

We have modeled two competing pathways for the oxidation of propene on an oxygen covered gold surface. One of the pathways, namely, allylic hydrogen abstraction, is undesired because it leads to combustion. The ability to inhibit this pathway and selectively favor the competing pathway leading to partial oxidation would result in a more effective catalyst. We have shown that reaction barriers can depend on the gold surface structure. A direct consequence of this result is the ability to use the surface structure to tune the catalyst to favor a desired pathway. Figure 9.4 summarizes the energies for allylic hydrogen abstraction and oxametallacycle formation on the defect-

free and stepped surfaces. On the defect-free surface the undesired allylic hydrogen pathway is favored. In contrast, on the stepped surface, the order of barriers is switched, and the barrier for oxametallacycle formation is much lower than that for allylic hydrogen abstraction. Even on a surface that contains steps and terraces, due to the stronger binding of propene to steps, using a simple micro kinetic model (ignoring entropic factors and reverse reactions) it can be shown that the production of the oxametallacycle is favored. From our calculations, we can conclude that a surface with steps and adatoms could eliminate the difference between the energy barriers for the undesired allylic hydrogen abstraction and the desired oxametallacycle formation.

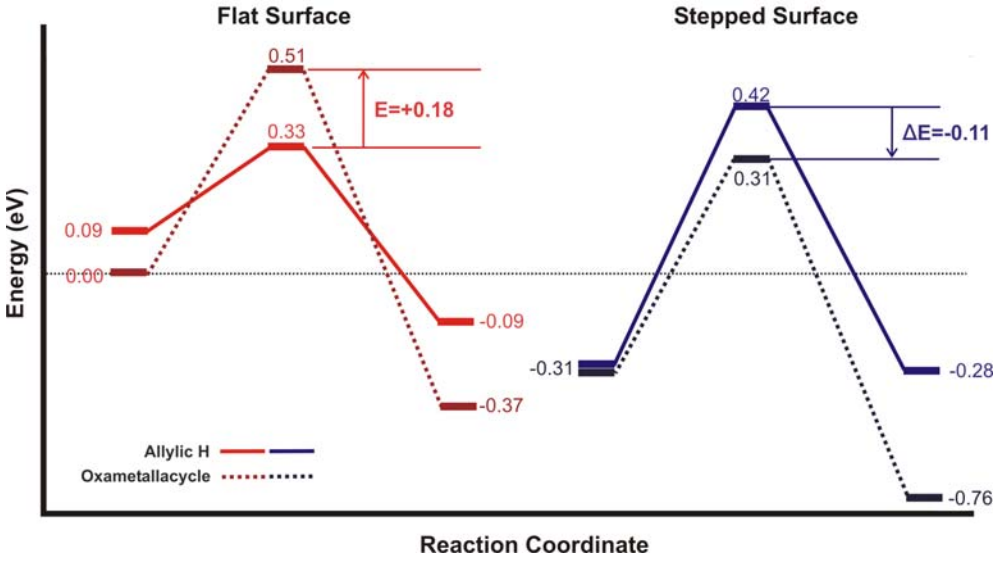

Figure 9.4. Energy diagram illustrating 'selectivity switch' from allylic hydrogen abstraction to oxametallacycle formation for the flat versus stepped gold surfaces. Red and blue represent the flat or stepped surface and solid and dotted lines represent allylic hydrogen abstraction and oxametallacycle formation, respectively.

9.6 Conclusions

We find using density functional theory that the adsorption of propene on Au(111) can change significantly in the presence of defects. Of the different defect surfaces we considered, propene can bind the strongest on a single adatom-covered surface and binds stronger (compared to the flat, defect-free surface) on either vacancy-covered or stepped gold surfaces. Charge density difference plots reveal that the magnitude of the differences in the density, upon adsorption of propene, is greater on the defect-containing surfaces.

More importantly, our results also indicate that the reactivity and selectivity of the gold surface changes with defects. We find that allylic hydrogen abstraction is easiest on the flat surface while the barrier for abstraction is highest on the adatom-covered surface. Our results for allylic hydrogen abstraction indicate that geometric and not electronic factors account for most of the observed differences in the ability of oxygen to abstract an allylic hydrogen. The difference in energy between the equilibrium substrate and the substrate frozen in its transition state configuration, correlates well with the calculated barriers.

Finally, we calculate the possibility to tune the selectivity of gold by changing the surface morphology. Unfavorable allylic hydrogen abstraction, which has a low barrier on the clean surface can be suppressed by creating a surface with steps. From this work alone, we suggest that a stepped surface would lead to more selective oxidation of propene. However, it is important to point out that without doing a complete search of all the possible intermediates and transition states, it is difficult to make exact quantitative predictions regarding the distribution of products for propene oxidation. Nevertheless,

our results clearly indicate that the surface morphology can affect the selectivity of the gold surface, with a stepped surface favoring oxametallacycle formation over allylic hydrogen abstraction. Additional work is currently underway to further investigate oxidation on the four different surfaces considered in the present work.

9.7 References

[1] J. Schwank, *Gold Bull.* **1983**, *16*, 103.

[2] M. Haruta, M. Date, *Appl. Catal. A.* **2001**, *222*, 427.

[3] M. Haruta, *Chem. Rec.* **2003**, *3*, 75.

[4] R. Meyer, C. Lemire, S. K. Shaikhutdinov, H. Freund, *Gold Bull.* **2004**, *37*, 72.

[5] M. Haruta, N. Yamada, T. Kobayashi, S. Iijima, *J. Catal.* **1989**, *115*, 301.

[6] T. Hayashi, K. Tanaka, M. Haruta, *J. Catal.* **1998**, *178*, 566.

[7] X. Y. Deng, C. M. Friend, *J. Am. Chem. Soc.* **2005**, *127*, 17178.

[8] X. Y. Deng, B. K. Min, X. Y. Liu, C. M. Friend, *J. Phys. Chem. B* **2006**, *110*, 15982.

[9] B. K. Min, A. R. Alemozafar, D. Pinnaduwage, X. Deng, C. M. Friend, *J. Phys. Chem. B.* **2006**, *110*, 19833.

[10] J. Biener, M. M. Biener, T. Nowitzki, A. V. Hamza, C. M. Friend, V. Zielasek, M. Baumer, *Chemphyschem* **2006**, *7*, 1906.

[11] B. K. Min, X. Deng, D. Pinnaduwage, R. Schalek, C. M. Friend, *Phys. Rev. B* **2005**, *72*, 4.

[12] N. Lopez, T. V. W. Janssens, B. S. Clausen, Y. Xu, M. Mavrikakis, T. Bligaard, J. K. Norskov, *J. Catal.* **2004**, *223*, 232.

[13] M. Valden, X. Lai, D. W. Goodman, *Science* **1998**, *281*, 1647.

[14] M. Valden, S. Pak, X. Lai, D. W. Goodman, *Catal. Lett.* **1998**, *56*, 7.

[15] W. Xu, J. S. Kong, Y. E. Yeh, P. Chen, *Nature Materials* **2008**, *7*, 992.

[16] D. C. Lim, I. Lopez-Salido, R. Dietsche, M. Bubek, Y. D. Kim, *Angew. Chem. Int. Ed.* **2006**, *45*, 2413.

[17] M. Turner, V. B. Golovko, O. P. H. Vanghan, P. Abdulkin, A. Berenguer-Murcia, M. S. Tikhov, B. F. G. Johnson, R. M. Lambert, *Nature* **2008**, *454*, 981.

[18] M. D. Hughes, Y. J. Xu, P. Jenkins, P. McMorn, P. Landon, D. I. Enache, A. F. Carley, G. A. Attard, G. J. Hutchings, F. King, E. H. Stitt, P. Johnston, K. Griffin, C. J. Kiely, *Nature* **2005**, *437*, 1132.

[19] D. I. Enache, J. K. Edwards, P. Landon, B. Soslona-Espriu, A. F. Carley, A. A. Herzing, M. Watanabe, C. J. Kiely, D. W. Knight, G. J. Hutchings, *Science* **2006**, 362.

[20] A. Abad, C. Almela, A. Corma, H. Garcia, *Tetrahedron* **2006**, *62*, 6666.

[21] S. Biella, M. Rossi, *Chem. Comm.* **2003**, 378.

[22] B. Jorgensen, S. E. Christiansen, M. L. D. Thomsen, C. H. Christensen, *J. Catal.* **2007**, *251*, 332.

[23] D. A. Outka, R. J. Madix, *Surf. Sci.* **1987**, *179*, 351.

[24] J. M. Gottfried, K. Christmann, Elsevier Science Bv, **2004**, pp. 1112.

[25] D. A. Outka, R. J. Madix, *J. Amer. Chem. Soc.* **1987**, *109*, 1708.

[26] J. A. Moulijin, P. W. N. M. van Leeuwen, R. A. Santen, *Catalysis: an integrated approach to homogeneous, heterogeneous and industrial catalysis* [Elsevier: New York, **1993**].

[27] S. Lee, L. M. Molina, M. J. Lopez, J. A. Alonso, B. Hammer, B. Lee, S. Seifert, R. E. Winans, J. W. Elam, M. J. Pellin, S. Vajda, *Angew. Chem. Int. Ed.* **2009**, *48*, 1467.

[28] D. Torres, N. Lopez, F. Illas, R. M. Lambert, *Angew. Chem. Int. Ed.* **2007**, *46*, 2055.

[29] D. Torres, F. Illas, *J Phys. Chem. B* **2006**, *110*, 13310.

[30] A. M. Joshi, N. Delgass, K. T. Thomson, *J. Phys. Chem. B.* **2006**, *110*, 2572.

[31] Y. Shimodaira, H. Kobayaski, *J. Mol. Struct.* **2006**, *762*, 57.

[32] A. M. Joshi, W. N. Delgass, K. T. Thomson, *J. Phys. Chem. C.* **2007**, *111*, 7841.

[33] J. J. Bravo-Suarez, K. K. Bando, J. Q. Lu, T. Fujitani, S. T. Oyama, *J. Catal.* **2008**, *255*, 114.

[34] J. J. Bravo-Suarez, K. K. Bando, T. Akita, T. Fujitani, T. J. Fuhrer, S. T. Oyama, *Chem. Comm.* **2008**, 3272.

[35] T. A. Nijhuis, M. Makkee, B. M. Moulijn, B. M. Weckhuysen, *Ind. Eng. Chem. Res.* **2006**, *45*, 3447.

[36] K. Weisermel, H. J. Arpe, *Industrial Organic Chemistry, 4th Ed.*, [Wiley-VCH: Weinheim, **2003**].

[37] M. Akimoto, K. Ichikawa, E. Echigoya, *J. Catal.* **1982**, *76*, 333.

[38] S. Linic, M. A. Barteau, *J. Am. Chem. Soc.* **2002**, *124*, 310.

[39] J. K. Norskov, T. Bligaard, J. Rossmeisl, C. H. Christensen, *Nature Chemistry* **2009**, *1*, 37.

[40] B. Hammer, J. K. Norskov, *Adv. Catal.* **2000**, *45*, 71.

[41] K. Reuter, D. Frenkel, M. Scheffler, *Phys. Rev. Lett.* **2004**, *93*, 116105.

[42] K. Honkala, A. Hellman, I. N. Remediakis, A. Logadottir, A. Carlsson, S. Dahl, C. H. Christensen, J. K. Norskov, *Science* **2005**, *307*, 555.

[43] T. V. W. Janssens, A. Carlsson, A. Puig-Molina, B. S. Clausen, *J. Catal.* **2006**, *240*, 108.

[44] C. Lemire, R. Meyer, S. K. Shaikhutdinov, H. J. Freund, *Surf. Sci.* **2004**, *552*, 27.

[45] I. N. Remediakis, N. Lopez, J. K. Norskov, *Appl. Catal. A.* **2005**, *291*, 13.

[46] G. Kresse, J. Hafner, *Phys. Rev. B* **1993**, *47*, 558.

[47] J. P. Perdew, Y. Wang, *Phys. Rev. B.* **1992**, *45*, 13244.

[48] W. Kohn, L. J. Sham, *Phys. Rev.* **1965**, *140*, A1133.

[49] H. Rydberg, M. Dion, N. Jacobson, E. Schroder, P. Hyldgaard, S. I. Simak, D. C. Langreth, B. I. Lundqvist, *Phys. Rev. Lett.* **2003**, *91*, 126402.

[50] J. P. Perdew, A. Zunger, *Phys. Rev. B.* **1981**, *23*, 5048.

[51] D. Ceperley, B. J. Alder, *Phys. Rev. Lett.* **1980**, *45*, 566.

[52] W. Kohn, Y. Meir, D. E. Makarov, *Phys. Rev. Lett.* **1998**, *343*, 4153.

[53] Y. Andersson, D. C. Langreth, B. I. Lundqvist, *Phys. Rev. Lett.* **1996**, *76*, 102.

[54] E. Hult, H. Rydberg, B. I. Lundqvist, D. C. Langreth, *Phys. Rev. B.* **1999**, *59*, 4708.

[55] G. Kresse, J. Hafner, *J. Phys.-Conden. Mat.* **1994**, *6*, 8245.

[56] D. Vanderbilt, *Phys. Rev. B.* **1990**, *41*, 7892.

[57] G. Kresse, J. Joubert, *Phys. Rev. B.* **1999**, *59*, 1758.

[58] CRC Handbook of Chemistry and Physics; 77 ed.; D. R. Lide, Ed. [CRC Press: New York, **1996**].

[59] D. Sheppard, R. Terrell, G. Henkelman, *J. Chem. Phys.* **2008**, *128*, 134106.

[60] G. Henkelman, B. P. Uberuaga, H. Jonsson, *J. Chem. Phys.* **2000**, *113*, 9901.

[61] G. Henkelman, H. Jonsson, *J. Chem. Phys.* **2000**, *113*, 9978.

[62] T. A. Baker, C. M. Friend, E. Kaxiras, *J. Phys. Chem. C.* **2009**, *113*, 3232.

[63] C. Wentrup, *Reactive Molecules*, [Wiley: New York, **1984**].

[64] S. Chretien, M. S. Gordon, H. Metiu, *J. Chem. Phys.* **2004**, *121*, 3756.

[65] A. Kokalj, A. D. Corso, S. Gironcoli, S. Baroni, *J. Phys. Chem. B.* **2002**, *106*, 9839.

[66] D. Shriver, P. Atkins, *Inorganic Chemistry* [W.H. Freeman and Company: New York, **1999**].

[67] H. M. Ajo, V. A. Bondzie, C. T. Campbell, *Catal. Lett.* **2002**, *78*, 359.

[68] T. A. Nijhuis, E. Sacaliuc, A. M. Beale, A. M. J. van der Eerden, J. C. Schouten, B. M. Weckhuysen, *J. Catal.* **2008**, *258*, 256.

[69] R. F. W. Bader, *Atoms in Molecules: A Quantum Theory* [Oxford Science, Oxford, **1990**].

[70] G. Henkelman, A. Arnaldsson, H. Jonsson, *Comput. Mater. Sci.* **2006**, *36*, 354.

[71] T. A. Baker, C. M. Friend, E. Kaxiras, *J. Chem. Phys.* **2009**, *130*, 8.

CHAPTER 10

AB INITIO MOLECULAR DYNAMICS INVESTIGATION OF CARBON MONOXIDE OXIDATION ON ATOMIC OXYGEN COVERED AU(111)

10.1 Abstract

Carbon monoxide oxidation on gold surfaces is a complicated but important process in which the activity of gold depends upon many factors including temperature, oxygen coverage, and surface structure. A proper theoretical investigation of this process requires a fully dynamical approach, using quantum mechanical treatment of the electrons and ions. Here, we present such a study of the oxidation of CO on oxygen-covered Au(111) surfaces, using *ab initio* molecular dynamics (AIMD) simulations. On the oxygen-free Au(111) surface at 500 K, CO prefers to bind transiently on top of Au atoms, spending a very small fraction of the total simulation time adsorbed on the surface. CO has much greater probability for adsorption on the oxygen-covered surface, but this probability decreases with oxygen coverage. Our results qualitatively reproduce experimental reactivity trends, namely, the surface activity for CO oxidation decreases with increasing oxygen coverage. We attribute this decrease of activity to two factors: (1) the decrease in the CO adsorption probability as the oxygen coverage increases and (2) the decreasing amount of reactive chemisorbed oxygen with increasing total oxygen coverage.

This work is in preparation to be submitted: T.A. Baker, C.M. Friend, E. Kaxiras.

10.2 Introduction

Since the discovery[1-8] that gold nanoparticles supported on reducible metal oxides are catalytically active for many processes, including CO oxidation[9], there is renewed interest in the potential use of gold as a material for low-temperature selective oxidation catalysis. The detailed understanding of the interaction of oxygen and CO with the Au(111) surface is an important problem because oxidized Au(111) is a model system for understanding chemical processes relevant to heterogeneous catalysis. While the oxidation of CO on gold has been studied extensively both experimentally[10-19] and theoretically[20-38], there are still many unanswered questions regarding the activity of gold. In order to identify the most active type of oxygen and to fully understand the catalytic activity of gold, it is critical to determine the oxygen species and structure that prevail under different conditions. This detailed understanding can contribute toward designing improved gold catalysts.

Min et al.[16] have found that the dosing temperature of ozone to form atomic oxygen on Au(111) has a significant effect on the surface reactivity and selectivity to oxidation. Scanning tunneling microscopy (STM) studies revealed differences in the surface morphology depending on the temperature used for oxidation or the coverage of atomic oxygen. Different types of oxygen (chemisorbed versus a surface oxide) have been suggested as responsible for the differences in reactivity. Liu et al.[25], using density functional theory (DFT) calculations, reported that the energy barrier for CO oxidation depends on the crystal face of the stepped surface. Recently, we also found large differences in the calculated energy barrier, depending on the types of surface defect used, for the reaction of propene with atomic oxygen on Au(111)[39]. Structure also plays

a vital role for oxide-supported Au nanoparticles since the size[40,41] and the particle shape[42] have a substantial effect on the reactivity, with rate constants differing by as much as two orders of magnitude[31]. It is clear the oxygen surface species and surface morphology, which are strongly correlated for the Au-O interaction, play an important role in the reactivity of the gold surface.

The reaction mechanism for CO oxidation is not completely understood. There have been two main proposals for the process of CO oxidation on supported gold nanoparticles: the first scenario assumes that O_2 adsorption is followed by dissociation to form reactive atomic oxygen on the surface, followed by CO adsorption, diffusion, and reaction; in the second scenario, O_2 is activated upon adsorption but is not followed by dissociation, CO adsorbs and diffuses to O_2 to form an OC•••O_2 peroxo-like complex, oxidation occurs, and atomic oxygen is left on the surface. Criticism of the first mechanism is based on the fact that there is no experimental evidence of O_2 dissociation on gold surfaces, on the fact that DFT calculations of O_2 dissociation show a high energy barrier even on small clusters[25,43-45], and on recent work showing the role of molecular O_2 in oxidation[13,46]. Unlike what happens on other transition-metal surfaces, there is no appreciable O_2 dissociation on extended single crystals of gold[15]. As a result, experimental studies use other sources of oxygen to produce atomic oxygen on the surface[47-51]. But for both mechanisms of oxidation, atomic oxygen plays a role in the reaction[52], making it important to understand its interaction and reactivity on gold.

Temperature is an important factor in determining the morphology and ultimately the reactivity of the surface. However, this presents a major problem for theoretical studies and for this reason, past theoretical works of CO oxidation on Au surfaces have

mostly used static, zero-temperature DFT calculations. Kinetic Monte Carlo (kMC) is a popular theoretical technique utilized for modeling the dynamical temperature dependence on the reactivity of a surface[53], but it presumes prior complete knowledge of events important to the dynamics of the system. Furthermore, the spatial degrees of freedom of the system are typically reduced to a simple lattice. For the complicated dynamical interaction of oxygen with gold, it is impossible to know all the important events *a priori* and it is unrealistic to confine these events within the context of a lattice. Ideally, what is needed to capture all relevant effects is a fully atomistic molecular dynamics simulation with accurate forces between ions and under realistic external conditions (temperature and oxygen concentration). Recently, we have developed the ability to use *ab initio* molecular dynamics (AIMD) simulations to model the *dynamic* restructuring of the Au(111) surface due to the adsorption of atomic oxygen, and have obtained results that are in agreement with vibrational spectroscopy experiments[54]. Here, we study the reaction of CO on the oxygen-covered surfaces that we have analyzed in detail, to fully understand the oxidation of CO on Au(111).

We have already studied the adsorption of atomic oxygen at three different coverages, 0.22 of a monolayer (ML), 0.33 ML, and 0.55 ML, and three different temperatures (200 K, 500 K, 800 K). From that study, we found that the morphology and type of oxygen species present on the surface depended on the coverage and dosing temperature, in agreement with experimental results. We categorized oxygen into three different types: chemisorbed oxygen, surface oxide, and sub-surface oxide. These three types represent, respectively, an oxygen atom bound on top of the surface in a three-fold hollow site, an oxygen atom bound to a gold atom which has been pulled out of the

surface, and an oxygen atom buried below the first layer of gold. At low oxygen coverage (< 0.33 ML) or temperature (200 K), the Au(111) surface is smooth and contain mostly chemisorbed oxygen, while higher coverage (> 0.33 ML) or temperature (500 K, 800 K), it is oxidized, containing a higher concentration of surface and sub-surface oxide. By matching calculated vibrational spectra with the experimental results under conditions that produce the most reactive surface for CO and olefin oxidation (low coverage and temperature) we conclude that chemisorbed oxygen was the more reactive types of oxygen for CO oxidation on Au(111). In the present work, we provide a detailed account of CO oxidation on the oxygen-covered Au(111) surface, and confirm our predictions about the nature of the reactive oxygen, by employing AIMD to model the dynamics of CO reaction with atomic oxygen on Au(111).

10.3 Calculational Details

We performed the AIMD simulations in the canonical ensemble[55], with a time step of 2 fs, for the reaction of carbon monoxide with atomic oxygen covered Au(111) in the framework of density functional theory using the VASP code[56] with the GGA-PW91[57] functional and ultrasoft pseudopotenitals[58,59]. We used a plane-wave cutoff energy of 300.0 eV, an electronic convergence tolerance of 10^{-3} eV, and 2×2×1 Monkhorst-Pack reciprocal space (k-point) sampling. The surface is modeled by a slab consisting of 4 layers in the (111) direction, with a 3×3 supercell in the lateral directions; the three uppermost layers of the slab were allowed to relax, with the bottom layer fixed at the ideal bulk positions.

We considered four different oxygen coverages: 0.00 ML, 0.22 ML, 0.33 ML, and 0.55 ML at 500 K. The simulation temperature of 500 K represents an optimal balance of adsorption and reaction, thus minimizing the total simulation time needed to observe important events in the system. The surfaces were prepared as follows[54]: oxygen was randomly placed above an equilibrated Au(111) substrate and the system then simulated at 500 K for 2 ps to allow for adsorption and rearrangement of the surface. To model the reaction of CO with these substrates, one CO molecule (0.11 ML coverage) was introduced to each system with a zero initial velocity, ~3 Å above the surface. At each oxygen coverage, 100 independent runs were performed, with each run lasting 8 ps. All results are obtained after a sufficient equilibrium time. For example, the reported average C-O distance during adsorption of $CO_{(a)}$ was found by averaging the distance at each time step during adsorption, excluding steps that were less than 600 fs after adsorption and before desorption. If the lifetime of $CO_{(a)}$ on the surface was not long enough to provide sufficient statistics (<1600 fs), the MD run was not used for calculating the C-O distance. We defined a process as adsorption (desorption) if the carbon from CO was within (greater than) 2.7 Å of the closest gold atom for a minimum of 300 fs.

10.4 Results

10.4.1 CO adsorption on oxygen-free Au(111)

We first simulated the adsorption of CO on the clean, oxygen-free *p*(3×3)-Au(111) at 500 K. At this temperature, CO should have a very short transient lifetime on

the surface due to its weak adsorption (experimental[60] and theoretical[61] adsorption energies are ~0.4 and 0.34 eV, respectively). For example, experimentally, no measurable adsorption of CO on Au(110)[15] is detected above 125 K or above 100 K on the oxygen-covered Au(111) surface[10]. We observe the same behavior in our simulations: a CO molecule spends only ~7% of the total simulation time adsorbed on the surface. Of the 100 independent runs, each of duration 8 fs, CO adsorbs at some point during the simulation for 40% of the runs, but quickly desorbs spending an average of only 861 fs on the surface resulting in a short overall surface lifetime. It is important not to mistake the calculated 40% adsorption probability with the true experimental sticking probability of CO on Au(111) at 500 K. The sticking probability, defined as the ratio of the adsorption rate to bombardment rate[62], for a molecular beam or a background gas pressure, would have molecules hitting the surface with either a non-zero constant velocity or with a Maxwell-Boltzmann distribution of velocities. In contrast, our simulations are limited to starting CO molecules with a zero initial velocity above the surface so as to increase the probability of adsorption, thus significantly over-estimating the true sticking probability.

We find that CO preferentially binds to top sites on the (1×1)-Au(111) surface, with the carbon interacting with the surface. This is in agreement with experimental[61] and theoretical findings[63], although there are contradictory conclusions in theoretical work suggesting the three-fold site as the most preferred for CO binding[25]. In our work, we find that the C-O bond is slightly elongated during adsorption, with the gas phase C-O bond of 1.144 Å extending to 1.151 Å during adsorption. These bond distances agree remarkably well with past experiments and static DFT calculations. The experimental gas

phase C-O distance[64] is 1.128 Å while the DFT calculated distance is 1.142 Å in the gas phase and 1.149 Å during adsorption[63]. This elongation is due to a slight weakening of the C-O bond, which can be understood as the transfer of electrons from the σ state of CO to the gold surface and back-transfer of electrons from the metal to the π* state of CO[65]. The C-O bond will increase in length as the binding of CO to gold becomes stronger due to surface defects[66].

Prior experimental work shows that CO lifts the $22\times\sqrt{3}$ herringbone reconstruction of gold[67]. Due to the limitation of the supercell size that can be handled within our DFT calculations, it is impossible to model the herringbone reconstruction in our simulations. We do, however, observe evidence of the ability of CO to lift Au from the top surface layer of the (1×1)-Au(111). The gold atom to which CO is bound is slightly lifted out of the surface by an average distance of 0.57 Å compared to the remaining gold atoms in the top layer of the surface. In several instances in the simulations, the CO completely lifts a gold atom out of the surface. In these cases the Au-C bond is much shorter, suggesting a stronger interaction, in agreement with previous DFT and experimental studies in which CO adsorption was found to be stronger on under-coordinated gold atoms, including adatoms and step edges[31,63,66]. The lifting of the herringbone reconstruction is not surprising, as it is also seen in the case of adsorption of many molecules on the Au(111)[68-70] surface, and it can be partly attributed to the increase in binding between the adatom and CO.

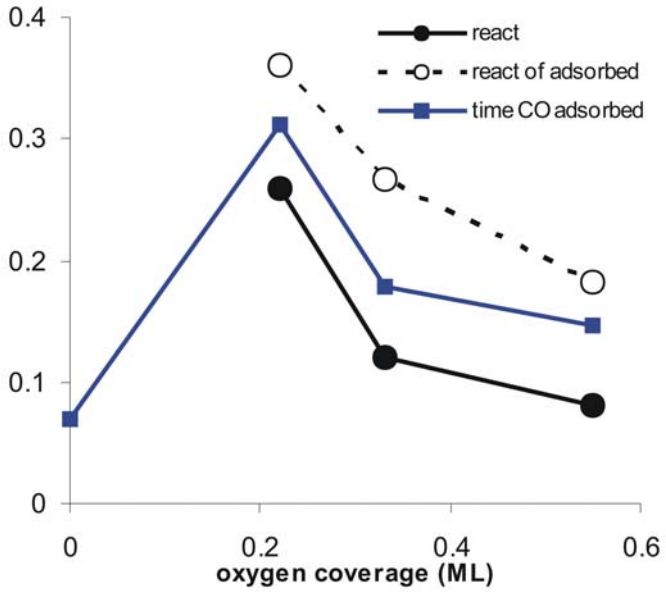

Figure 10.1: As a function of oxygen coverage, the ratio of time a CO molecule spends adsorbed on the Au(111) surface (blue squares connected by solid blue line), the ratio of MD runs that resulted in the oxidation of CO to CO_2 (solid black circles connected by solid line), and the ratio of MD runs that resulted in CO_2 in which CO adsorbed on the surface (open black circles connected by dotted line).

10.4.2 CO adsorption on oxygen-covered Au(111)

We next considered CO adsorption and oxidation to CO_2 on an oxygen-covered Au(111) surface at 500 K, at three different oxygen coverages: 0.22 ML, 0.33 ML, and 0.55 ML. We observed varying degrees of adsorption and reactivity, as a function of the coverage. Compared to adsorption on the oxygen-free surface, CO spends a longer time bound to the surface, however, the adsorption lifetime decreases with increasing oxygen coverage (Figure 10.1). Earlier theoretical[54] and experimental[71] work has shown that with increasing oxygen coverage, the gold surface becomes rough and therefore consists

of a higher concentration of under-coordinated surface gold atoms. This should increase the binding strength leading to more adsorption. In fact, by analyzing the average bond length of the carbon atom within CO to the gold atom on the surface to which it is bound, we observe a systematic decrease in the bond length with increasing oxygen coverage (shown in Figure 10.2), suggesting that CO adsorption is stronger on the rougher surface. However, at O coverage greater than 0.22 ML, we observe a decrease in the CO surface lifetime, in agreement with previous experimental observations[17]. This suggests that while the binding of CO to the surface is stronger at higher oxygen coverage, the additional adsorbed oxygen is blocking sites for adsorption.

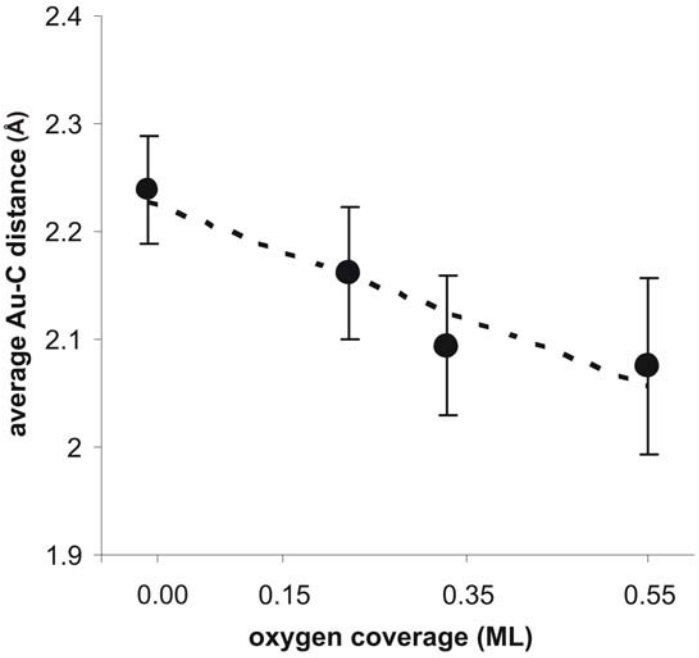

Figure 10.2: Average Au-$C_{(CO)}$ distance for adsorbed CO as a function of oxygen coverage

The preferred binding site for CO on the oxygen-covered Au(111) surface is the top site of a gold atom with the CO molecule binding perpendicular to the surface, similar

to what is observed on the clean surface. This is especially true for low oxygen coverage (< 0.33 ML). Figure 10.3 and Table 10.1 illustrate the observed binding sites and distribution of these sites at each coverage. At higher coverage, the number of binding sites around the surface oxide increases, a direct result of the fact that the surface oxide is the more prevalent oxygen type at these conditions. A transition in CO adsorption sites occurs, changing from sites A and C to site D (see Figure 10.3), as the oxygen coverage increases from 0.33 ML to 0.55 ML. This corresponds to a change in adsorption from around the AuO_2 surface oxide complex to the site on top of the surface oxide; this is most likely the result of site blocking around the surface oxide complex by oxygen, which leaves only the top of the complex as available binding sites. We again find that CO pulls gold atoms out of the top surface layer, same as on the clean surface. This is especially true for one binding site, defined as site E (Figure 10.3), in which a CO molecule binds on a gold atom which is also bound to an adsorbed oxygen atom. Upon adsorption, this gold atom is lifted from the surface creating a chain starting with the adsorbed oxygen, a gold adatom, the carbon of the CO, and finally the oxygen from the CO. This configuration had many variations depending on the type of oxygen surrounding the chain, and it is clear from the wide variation of systems we observed that the co-adsorbed system is quite complex and dynamical in nature.

In many of the simulations we observe the reaction of an adsorbed CO with atomic oxygen to produce CO_2. Since the interaction of CO_2 with the surface is extremely weak, CO_2 desorbs from the surface upon formation[10]. Min et al.[16] have shown that the reactivity of CO with the surface depends on the oxygen coverage. They find for an Au surface created by dosing ozone at 200 K that the most reactive coverage is ~0.5

ML, with the reactivity decreasing almost linearly with coverage, for either higher or lower oxygen coverage.

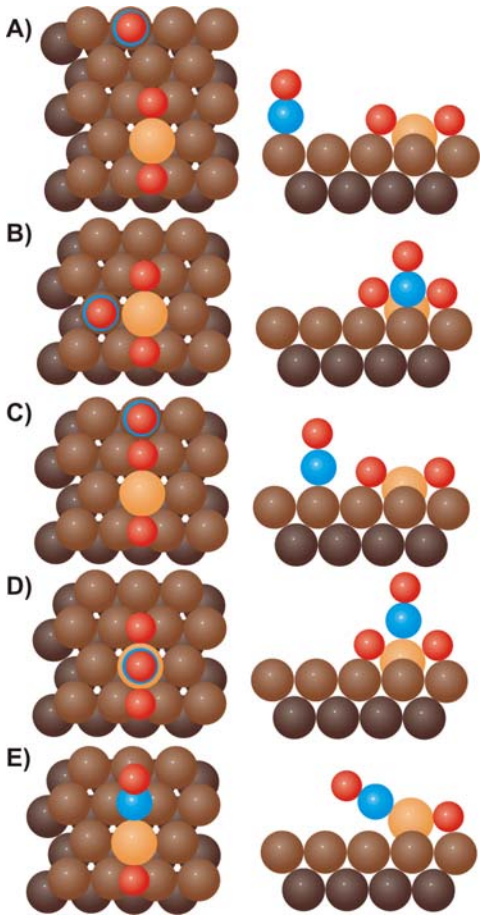

Figure 10.3: Model of adsorption sites for CO on the oxygen covered surface. In site E, a CO molecule binds on the same gold atom opposite an oxygen atom adsorbed on the surface causing the gold atom to be lifted from the surface with the CO not bound perpendicular to the surface. Brown, gold, blue, and red spheres represent the first layer of gold atoms, a gold adatom lifted out of the first layer of the surface, a carbon atom, and oxygen atom, respectively. Note that the figure only serves as a guide for classification. Since we performed atomistic dynamical simulations, we observed small variations and combinations of these structures.

Table 10.1: Ratio of CO adsorption sites at each coverage. The sites are illustrated in Figure 10.3.

CO site	0.22 ML	0.33 ML	0.55 ML
A	0.63	0.24	0.25
B	0.17	0.11	0.16
C	0.21	0.47	0.00
D	0.00	0.02	0.52
E	0.01	0.16	0.07

Table 10.2: Ratio of reaction pathways at each coverage. The capital letter of each reaction signifies the starting adsorption site (Figure 10.3) and the subscript numbers refer to each different reaction. Examples of each reaction are illustrated in Figure 10.4.

reaction	0.22 ML	0.33 ML	0.55 ML
A_1	0.77	0.42	0.00
A_2	0.08	0.08	0.50
B_1	0.04	0.00	0.00
C_1	0.12	0.17	0.00
E_1	0.00	0.33	0.00
E_2	0.00	0.00	0.50

Qualitatively, the behavior is the same (see Figure 10.1); however, the reactivity is highest at 0.22 ML oxygen coverage, with about 26% of the independent simulation runs resulting in oxidation. The reactivity decreases to 12% at 0.33 ML and to 8% at 0.55 ML of atomic oxygen coverage. In previous work, we found that experimental vibrational results at ~0.5 ML O-covered Au(111) closely match the theoretical results at

~0.2 ML, suggesting agreement between experimental and theoretical results for the most reactive coverage.

An ensemble of oxidation reaction pathways exist, with all reactions following the Langmuir-Hinshelwood mechanism in which CO adsorption is followed by subsequent reaction, in agreement with experimental observations. Lazaga, et al.[10] found a negative activation energy for CO oxidation on Au(111) that was independent of oxygen coverage or CO pressure. This result ruled out the possibility of a single elementary reaction step, indicating that CO oxidation does not proceed via an Eley-Rideal mechanism. Reactions that involve a chemisorbed oxygen atom proceed through mainly one pathway, labeled A_1 in Figure 10.4. In this pathway a CO molecule is bound on top of a gold atom neighboring a three-fold site. During the reaction, the CO molecule diffuses into the bridge site and towards the oxygen, while at the same time the O atom moves towards the CO through the same two-fold site. The C of the CO molecule meets the absorbed oxygen atom forming CO_2 which then desorbs from the surface. CO oxidation was studied in a number of static DFT calculations; Su et al.[24] found a barrier of 0.29 eV for the oxidation on the Au(111) surface, while Liu et al.[25] found a barrier of 0.25 eV for the same reaction on the Au(221) surface. In both studies the reaction takes place at step edges, in agreement with our findings, that is, reactions take place with high probability at defect sites with low coordination. A second, less frequent pathway for CO reaction with chemisorbed oxygen, labeled A_2 in Figure 10.4, occurs when CO binds to the same gold atom to which an adsorbed oxygen is bound in a three-fold site. The reaction following adsorption is fast due to the instability of the system and because the CO molecule can easily find the adsorbed oxygen atom. Oxidation pathways involving an

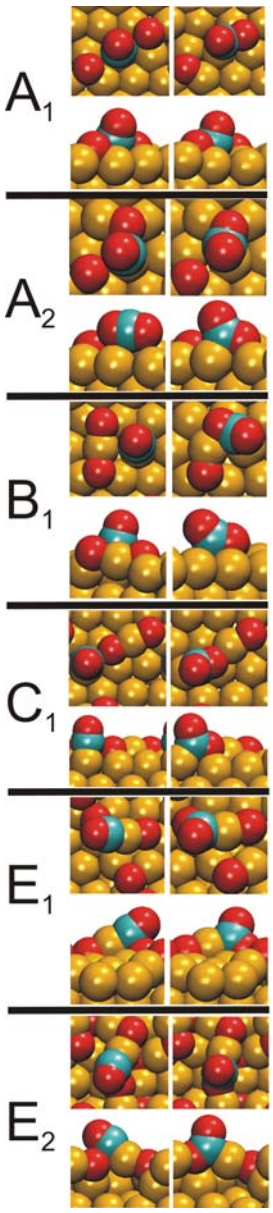

Figure 10.4: Snapshots (top and side views) of reaction pathways for CO oxidation to CO_2 on oxygen covered Au(111) surfaces. Reaction E_1 and E_2 differ in that CO reacts with a chemisorbed oxygen in the former, while CO reacts with a surface oxide in the latter. Yellow, blue, and red spheres represent gold, carbon, and oxygen atoms, respectively. These defined reaction pathways are used in Table 10.2.

adsorbed surface oxide complex are initiated in the easiest way from adsorption site C (see Figure 10.3). A reaction occurs when the CO molecule diffuses towards the adsorbed oxygen. Other reactions involve adsorption site E and occur when the carbon reacts with chemisorbed oxygen (E_1) or the surface oxide or subsurface oxygen (E_2). Table 10.2 lists the ratio of each reaction pathway by coverage. At lower oxygen coverage, reaction pathways involving chemisorbed oxygen (A_1 and A_2 in Figure 10.4) are dominant, while at higher coverage, reactions with the subsurface oxide and other complicated pathways occur, as discussed in more detail in the next section.

10.5 Discussion

Using AIMD, we have observed the reaction of CO with atomic oxygen to form CO_2 on the Au(111) surface. In accordance with past experimental and theoretical work, we observe a reactivity difference depending on the surface structure and oxygen coverage. We find the most reactive surface to be the one with 0.22 ML of oxygen, in mostly chemisorbed form. We suggest that there are two main factors that control the reactivity of CO on the Au(111) oxygen-covered surface: first, the ability of CO to adsorb on the surface, and second, the type of the adsorbed oxygen, including chemisorbed oxygen and surface oxide.

Since the reaction follows the Langmuir-Hinshelwood mechanism, adsorption of CO is an important first step to reaction. We find a strong correlation between the ratio of the CO surface lifetime and the rate of oxidation. Despite the stronger CO adsorption at higher oxygen coverage, due to site blocking, the CO spends less time adsorbed on the surface. Since CO spends less time on the surface, there is less probability to react, leading to a lower oxidation rate.

It is important to understand the role of the type of oxygen involved in the reaction, that is, whether oxygen is chemisorbed, or takes the form of a surface or sub-surface oxide. The average time to reaction after adsorption on the 0.22 ML, 0.33 ML, and 0.55 ML oxygen-covered surfaces are all nearly the same: 1688, 1491, and 1553 fs, respectively. This may suggest that reactivity is generally insensitive to the type of oxygen present on the surface, even though a higher coverage increases the probability for CO to find an oxygen atom to react. However, it implausible that a sub-surface oxygen atom buried under the first layer of gold could react to form CO_2 as easily as an a surface oxygen atom. The reaction energy barriers and the availability to attack would significantly differ in these two extreme cases. Indeed we find that the rate of oxidation for the systems in which CO adsorbs decreases with increasing oxygen coverage (see Figure 10.1), suggesting that the CO adsorption rate alone cannot explain all reactivity trends. Furthermore, the reaction rate still decreases as function of coverage even if the reaction probability is normalized by the fraction of time CO spends adsorbed on the surface. The oxygen type contributing most to oxidation involves chemisorbed oxygen atoms: Table 10.3 breaks down the oxygen type present at 0.22 ML and 0.33 ML of oxygen and the oxygen type that participates in the reaction at each coverage. At either oxygen coverage, the chemisorbed oxygen contributes to the majority of the oxidation reactions. For 0.22 ML of oxygen coverage, initially 80% of the surface is covered with chemisorbed oxygen while 20% is covered in surface oxide. However, of the oxygen type responsible for oxidation, 86% is chemisorbed oxygen. The same is true for 0.33 ML of oxygen coverage: the surface is covered with 60% of chemisorbed oxygen, yet chemisorbed oxygen makes up 83% of the reactive atoms, illustrating that the

chemisorbed oxygen is the most reactive type on the surface. Interestingly, the absolute number of chemisorbed oxygen on the surface is comparable at 0.22 ML and 0.33 ML of oxygen coverage, even though the ratio of chemisorbed oxygen to surface oxide is much higher at 0.22 ML.

Table 10.3: Ratio of chemisorbed oxygen and surface oxide on the surface before CO oxidation (surface species) and the oxygen species consumed during oxidation (reactive oxygen) on 0.22 ML and 0.33 ML oxygen covered Au(111).

	0.22 ML		**0.33 ML**	
	surface species	reactive oxygen	surface species	reactive oxygen
chemisorbed	0.80	0.88	0.60	0.83
surface oxide	0.20	0.12	0.40	0.17

Our results clearly indicate that chemisorbed oxygen is the most reactive type. The decrease in reactivity from 0.22 ML to 0.33 ML of oxygen coverage may depend on factors other than CO adsorption rates. The ability for CO and O to diffuse on the surface may also be important because molecules must meet in order to react. Our calculations show that at higher oxygen coverage (> 0.33 ML) on Au(111), there are more under-coordinated gold atoms leading to stronger CO adsorption and a rougher surface which slows diffusion. This effect could be another reason for the observed slower reaction rates at higher oxygen coverage. In contrast, experimental STM images for higher coverage of atomic oxygen on Au(111) suggest the surface has mobile species[49,71], a good indication that diffusion readily occurs and should not be a large factor affecting

reactivity. Such factors are difficult to capture in our simulations due to the limitations of AIMD in accessing long-time and -length diffusion processes.

10.6 Conclusions

Realistic simulation of catalytic reactions on surfaces is an important endeavor that requires very substantial computational resources. Generally, two key factors need to be taken into consideration when simulating such systems: the ability to accurately describe the important characteristics of the system (such as the forces between nuclei, charge transfer, etc.) and the need to minimize the computational cost of the simulation so that the dynamics of the system can be modeled for long time scales. Coarse-grained and lattice based methods, such as kMC, are capable of investigating processes over a long time scale but these methods must simplify the complicated electronic and ionic system using approximations, or reduce the dimensionality of the fully atomistic system to a lattice. For systems as complicated as the interaction of oxygen on gold, neither of these approximations is acceptable, because over-simplifying the system features makes the simulation unreliable. To avoid this problem, we have used a fully atomistic simulation with forces between nuclei accurately calculated using DFT. This level of accuracy is computationally costly, resulting in dynamical runs that extend only for ~10 ps. Nevertheless, a number of useful conclusions can be obtained from these simulations.

The oxidation of CO on Au(111) is a prototypical model system for *ab initio* molecular dynamics simulations, due to its inherent interest, involving a representative simple molecule that can be oxidized and an originally inert solid surface on which atomic-scale features can play an important role in reactivity. We carried out an extensive

study of this system, using AIMD simulations. We find the highest rate of CO oxidation for 0.22 ML of oxygen coverage, with decreasing activity at the other two oxygen-coverage conditions we considered, 0.33 ML and 0.55 ML. The difference in reactivity that we found is most likely due to two factors: the type of oxygen atoms present on the surface during reaction and the ability of CO to adsorb on the surface. We have identified chemisorbed oxygen as the most reactive type of oxygen atoms. Furthermore, we observe a decrease in the adsorption probability for CO with increasing oxygen coverage. Despite the increase in the strength of CO adsorption with increasing oxygen coverage, the decrease in the probability for CO adsorption results in lower CO surface lifetimes leading to a decrease in reactivity.

10.7 References

[1] M. Haruta, *Chem. Rec.* **2003**, *3*, 75.

[2] M. Haruta, M. Date, *Appl. Catal. A-Gen.* **2001**, *222*, 427-437.

[3] R. Meyer, C. Lemire, S. K. Shaikhutdinov, H. Freund, *World Gold Council* **2004**, 72.

[4] M. Haruta, N. Yamada, T. Kobayashi, S. Iijima, *J. Catal.* **1989**, *115*, 301-309.

[5] T. Hayashi, K. Tanaka, M. Haruta, *J. Catal.* **1998**, *178*, 566-575.

[6] R. J. H. Grisel, P. J. Kooyman, B. E. Nieuwenhuys, *J. Catal.* **2000**, *191*, 430-437.

[7] B. W. L. Jang, J. J. Spivey, M. C. Kung, H. H. Kung, *Am. Chem. Soc.* **1997**, p 299-306.

[8] D. Thompson, *Gold Bull.* **2000**, *33*, 40-40.

[9] M. Haruta, T. Kobayashi, H. Sano, N. Yamada, *Chem. Lett.* **1987**, 405-408.

[10] M. A. Lazaga, D. T. Wickham, D. H. Parker, G. N. Kastanas, B. E. Koel, *ACS Symp. Series* **1993**, *523*, 90-109.

[11] B. K. Min, C. M. Friend, *Chem. Rev.* **2007**, *107*, 2709-2724.

[12] J. Kim, E. Samano, B. E. Koel, *J. Phys. Chem. B* **2006**, *110*, 17512-17517.

[13] J. D. Stiehl, T. S. Kim, S. M. McClure, C. B. Mullins, *J. Am. Chem. Soc.* **2004**, *126*, 13574-13575.

[14] J. M. Gottfried, K. Christmann, *Elsevier Science Bv* **2004**, p 1112-1117.

[15] D. A. Outka, R. J. Madix, *Surf. Sci.* **1987**, *179*, 351-360.

[16] B. K. Min, A. R. Alemozafar, D. Pinnaduwage, X. Deng, C. M. Friend, *J. Phys. Chem. B* **2006**, *110*, 19833-19838.

[17] R. A. Ojifinni, N. S. Froemming, J. Gong, M. Pan, T. S. Kim, J. M. White, G. Henkelman, C. B. Mullins, *J. Am. Chem. Soc.* **2008**, *130*, 6801-6812.

[18] T. S. Kim, J. Gong, R. A. Ojifinni, J. M. White, C. B. Mullins, *J. Am. Chem. Soc.* **2006**, *128*, 6282-6283.

[19] B. Yoon, H. Hakkinen, U. Landman, A. S. Worz, J. M. Antonietti, S. Abbet, K. Judai, U. Heiz, *Science* **2005**, *307*, 403-407.

[20] P. Broqvist, L. M. Molina, H. Gronbeck, B. Hammer, *J. Catal.* **2004**, *227*, 217-226.

[21] L. M. Molina, M. D. Rasmussen, B. Hammer, *J. Chem. Phys.* **2004**, *120*, 7673-7680.

[22] L. M. Molina, B. Hammer, *Phys. Rev. B* **2004**, *69*, 155424.

[23] R. Coquet, K. L. Howard, D. J. Willock, *Chem. Soc. Rev.* **2008**, *37*, 2046.

[24] H. Y. Su, M .M. Yang, X. H. Bao, W. X. Li, *J. Phys. Chem. C* **2008**, *112*, 17303-17310.

[25] Z. P. Liu, P. Hu, A. Alavi, *J. Am. Chem. Soc.* **2002**, *124*, 14770-14779.

[26] A. Prestianni, A. Martorana, I. Ciofini, F. Labat, C. Adamo, *J. Phys. Chem. C* **2008**, *112*, 18061-18066.

[27] J. L. C. Fajin, M. Cordeiro, J. R. B. Gomes, *J. Phys. Chem. C* **2008**, *112*, 17291-17302.

[28] Y. Chen, P. Crawford, P. Hu, *Catal. Lett.* **2007**, *119*, 21-28.

[29] C. M. Wang, K. N. Fan, Z. P. Liu, *J. Am. Chem. Soc.* **2007**, *129*, 2642-2647.

[30] R. Ganesh, S. Pala, F. Liu, *J. Chem. Phys.* **2006**, *125*, 5.

[31] N. Lopez, T. V. W. Janssens, B. S. Clausen, Y. Xu, M. Mavrikakis, T. Bligaard, J. K. Norskov, *J. Catal.* **2004**, *223*, 232-235.

[32] C. J. Zhang, P. Hu, *J. Am. Chem. Soc.* **2000**, *122*, 2134-2135.

[33] L. M. Molina, A. Lesarri, J. A. Alonso, *Chem. Phys. Lett.* **2009**, *468*, 201-204.

[34] L. M. Liu, B. McAllister, H. Q. Ye, P. Hu, *J. Am. Chem. Soc.* **2006**, *128*, 4017-4022.

[35] Z. P. Liu, S. J. Jenkins, D. A. King, *Phys. Rev. Lett.* **2004**, *93*, 156102.

[36] Z. P. Liu, X. Q. Gong, J. Kohanoff, C. Sanchez, P. Hu, *Phys. Rev. Lett.* **2003**, *91*, 266102.

[37] S. Kandoi, A. A. Gokhale, L. C. Grabow, J. A. Dumesic, M. Mavrikakis, *Catal. Lett.* **2003**, *93*, 93.

[38] I. N. Remediakis, N. Lopez, J. K. Norskov, *Angew. Chem. Int. Ed.* **2005**, *44*, 1824.

[39] T. A. Baker, B. Xu, C. M. Friend, E. Kaxiras, *unpublished* **2009**.

[40] M. Valden, X. Lai, D. W. Goodman, *Science* **1998**, *281*, 1647-1650.

[41] M. Valden, S. Pak, X. Lai, D. W. Goodman, *Catal. Lett.* **1998**, *56*, 7-10.

[42] M. Comotti, W. C. Li, B. Spliethoff, F. Schuth, *J. Am. Chem. Soc.* **2006**, *128*, 917-924.

[43] Y. Xu, M. Mavrikakis, *J. Phys. Chem. B* **2003**, *107*, 9298.

[44] B. Yoon, H. Hakkinen, U. Landman, *J. Phys. Chem. A* **2003**, *107*, 4066.

[45] G. Mills, M. S. Gordon, H. Metiu, *J. Chem. Phys.* **2003**, *118*, 4198.

[46] J. D. Stiehl, T. S. Kim, S. M. McClure, C. B. Mullins, *J. Am. Chem. Soc.* **2004**, *126*, 1606.

[47] J. Wang, M. R. Voss, H. Busse, B. E. Koel, *J. Phys. Chem. B* **1998**, *102*, 4693-4696.

[48] J. M. Gottfried, N. Elghobashi, S. L. M. Schroeder, K. Christmann, *Surf. Sci.* **2003**, *523*, 89-102.

[49] M. M. Biener, J. Biener, C. M. Friend, *Surf. Sci.* **2005**, *590*, L259-L265.

[50] N. D. S. Canning, D. Outka, R. J. Madix, *Surf. Sci.* **1984**, *141*, 240-254.

[51] N. Saliba, D. H. Parker, B. E. Koel, *Surf. Sci.* **1998**, *410*, 270-282.

[52] X. Y. Deng, B. K. Min, A. Guloy, C. M. Friend, *J. Am. Chem. Soc.* **2005**, *127*, 9267-9270.

[53] C. C. Battaile, D. J. Srolovitz, *Annu. Rev. Mat. Res.* **2002**, *32*, 297.

[54] T. A. Baker, B. Xu, X. Liu, C. M. Friend, E. Kaxiras, submitted to *J. Phys. Chem. C.* **2009**.

[55] S. Nose, *Mol. Phys.* **2002**, *100*, 191.

[56] G. Kresse, J. Hafner, *Phys. Rev. B.* **1993**, *47*, 558-561.

[57] D. Vanderbilt, *Phys. Rev. B.* **1990**, *41*, 7892-7895.

[58] G. Kresse, J. Hafner, *J. Phys.-Condens. Mat.* **1994**, *6*, 8245-8257.

[59] J. P. Perdew, Y. Wang, *Phys. Rev. B* **1992**, *45*, 13244-13249.

[60] G. S. Elliott, University of California, San Diego, **1988**.

[61] L. Piccolo, D. Loffreda, F. J. Ladete Santos Aires, C. Deranlot, Y. Jugnet, P. Sautet, J. C. Bertolini, *Surf. Sci.* **2004**, *566-568*, 995.

[62] D. A. King, M. G. Wells, *Surf. Sci.* **1972**, *29*, 454-&.

[63] M. Mavrikakis, P. Stoltze, J. K. Morskov, *Catal. Lett.* **2000**, *64*, 101.

[64] CRC Handbook of Chemistry and Physics; 77 ed.; D. R. Lide, Ed. [CRC Press: New York, **1996**].

[65] D. Shriver, P. Atkins, *Inorganic Chemistry* [W.H. Freeman and Company: New York, **2003**].

[66] D. Loffreda, P. Sautet, *J. Phys. Chem. B.* **2005**, *109*, 9596.

[67] K. F. Peters, P. Steadman, H. Isern, J. Alvarez, S. Ferrer, *Surf. Sci.* **2000**, *467*, 10.

[68] S. Narasimhan, D. Vanderbilt, *Phys. Rev. Lett.* **1992**, *69*, 1564-1567.

[69] C. E. Bach, M. Giesen, H. Ibach, T. L. Einstein, *Phys. Rev. Lett.* **1997**, *78*, 4225-4228.

[70] H. Ibach, C. E. Bach, M. Giesen, A. Grossmann, *Surf. Sci.* **1997**, *375*, 107-119.

[71] B. K. Min, X. Deng, D. Pinnaduwage, R. Schalek, C. M. Friend, *Phys. Rev. B* **2005**, *72*, 4.

[72] T. Kizuka, N. Tanaka, *Phys. Rev. B* **1997**, *56*, 10079.

[73] B. Pauwels, G. Van Tendeloo, W. Bouwen, L. T. Kuhn, P. Lievens, H. Lei, M. Hou, *Phys. Rev. B* **2000**, *62*, 10383.

[74] P. M. Ajayan, L. D. Marks, *Nature* **1989**, *338*, 139.

[75] R. J. H. Grisel, B. E. Nieuwenhuys, *J. Catal.* **2001**, *199*, 48.

[76] A. Sanchez, S. Abbet, U. Heiz, W. D. Schneider, H. Hakkinen, R. N. Barnett, U. Landman, *J. Phys. Chem. A.* **1999**, *103*, 9573.

APPENDIX A

A PATHWAY FOR NH ADDITION TO STYRENE PROMOTED BY GOLD

A.1 Abstract

Addition of NH across the double bond of styrene was observed on Au(111) covered with NH_x groups. This is the first time that a heterogeneous reaction has been *discovered* in studies of a single-crystal without previously being reported on a high-surface area catalyst. Chemisorbed atomic oxygen is used to induce ammonia dissociation, which successfully produces NH_x on the gold surface. The product of styrene and NH_x on Au(111) is tentatively identified as 2-phenylaziridine, based on the quantitative analysis of mass spectrometer fragmentations collected in the experiments.

This work was published in *Angewandte Chemie – International Edition*: X.Y. Deng, T. A. Baker, C.M. Friend, **2006**, *45*, 7075.

A.2 Introduction

Gold-based heterogeneous catalysts have surprising potential for low-temperature oxidation processes[1-4], including alcohol oxidation[5-8], direct synthesis of hydrogen peroxide[9,10], CO oxidation[11,12], and olefin epoxidation[11,13]. These systems have potential for a substantial positive impact on the environment and economy because of their high selectivity and also the low temperature at which they operate[14]. Hence, a substantial

amount of effort has been directed to further improve the performance of heterogeneous gold catalysts and to understand the origin of their catalytic activity[15-18].

Herein, we investigate the addition of NH to styrene using heterogeneous Au because of the potential importance of these three-membered N-containing rings in organic synthesis as a building block for biologically active molecules and for use in antitumor and antibiotic applications[19-21]. Previously, we demonstrated that the Au(111) surface promotes oxidation reactions that also occur on catalysts with high surface areas at higher pressure, once oxygen has been adsorbed onto the surface[22], thereby establishing that Au(111) is a good model for understanding the molecular-level detail of heterogeneous Au-based oxidation catalysis. Hence, reactions that occur on Au(111) provide a guide for the type of reactions that may be induced by heterogeneous gold catalysts.

Nitrene addition to styrene is promoted by a gold surface, which indicates that such reactions should be possible with heterogeneous Au catalysts. To our knowledge, this is the first report of gold-catalyzed functionalization of an olefin with NH in a heterogeneous system, which may have advantages and mechanistic differences when compared to aziridination in solution[23,24], or in other methods of activating ammonia for amination[25].

Aziridines are structurally analogous to epoxides and may be formed by addition of a nitrene group to the olefin. Recently, we showed that oxidized Au(111) promotes styrene epoxidation[22]. This observation motivated us to explore the analogous aziridination of styrene on Au(111). Indeed, aziridination of styrene does occur on Au(111) covered with NH_x. By precovering the surface with NH, we are able to study the

elementary steps important in catalytic processes. This is a well-established approach for studying other reactions important in catalysis using the tools of surface science[26-28].

A.3 Experimental Details

All experiments were performed in a stainless-steel ultrahigh-vacuum chamber with a base pressure of $<1\times10^{-10}$ Torr, as described previously[29]. The chamber was equipped with a quadrupole mass spectrometer (UTI model 100C) which was used for temperature-programmed reaction spectroscopy (TPRS), an Auger electron spectrometer (AES), and low-energy electron diffraction optics (LEED).

The Au(111) surface was prepared by cycles of sputtering of Ar^+ ions (1000 eV, 1.3 Å) at 300 K, followed by annealing at 900 K for 5 min, and then at 700 K for 30 min. This procedure was repeated until no impurities were detected using AES.

Ozone was produced by electrical discharge and was trapped in silica gel (3-8 mesh, Fisher Scientific Co.) at -78 C^o using a mixture of dry ice and ethanol. The Au(111) surface at 200 K was exposed to O_3, with a pressure rise of 1×10^{-8} Torr over 20 s, which resulted in an approximate 0.2 ML. The resulting oxygen atom coverage was determined by comparing the integrated area of the O_2-desorption peak relative to a saturation coverage (ca. 1 ML) which had been determined previously[30,31]. Following the deposition of oxygen, the surface was exposed to NH_3 (Matheson, anhydrous grade) or $^{15}NH_3$ (Cambridge Isotope Laboratories, 98 %). The NH_3 was deposited at 190 K for 2 min with a pressure rise of 1×10^{-10} Torr. Finally, styrene (Alfa Aesar, 99.5 %) was deposited at 150 K for 30 s with a pressure rise of 1×10^{-10} Torr and was used after cycles of freeze-pump-thaw purification, with the purity checked by mass spectrometry.

All temperature-programmed reaction spectra (TPRS) were taken by a computer-controlled UTI 100c mass spectrometer, as described in detail previously[32]. The crystal was biased at -100 V during the collection of temperature-programmed reaction data, so as to avoid an electron-induced reaction from the mass-spectrometer filament. The temperature was measured with a K-type (Chromega/Alomega) thermocouple and radiative heating was used to achieve the temperature ramp to 650 K. The heating rate for TPRS was relatively linear, in the range 150-600 K with an average of about 6 K s^{-1}.

A.4 Results and Discussion

Reactive NH_x (x=1,2) species are formed from the reaction of NH_3 with chemisorbed oxygen on Au(111) (Figure A.1). By selecting the appropriate conditions, we are able to remove all the oxygen through the evolution of water. In temperature-programmed reaction experiments, water is evolved at 210 K if NH_3 is exposed to O-covered Au(111) at 110 K; however, when dosed with an excess of ammonia and the surface maintained at 190 K, the oxygen is removed through water evolution (Figure A.1a,b). Notably, ammonia does not react on the clean Au(111) surface, but desorbs molecularly at 155 K (data not shown). The NH_x formed on the surface undergoes disproportionation upon heating (Figure A.1). Molecular ammonia desorbs from the surface at 160 K. A second NH_3 peak at 210 K is ascribed to the reformation of NH_3 from disproportionation of NH_x species. Adsorbed nitrogen atoms are also formed, which ultimately lead to N_2 formation at 425 K. No H_2 is evolved; rather hydrogen is removed either as water during formation of NH_x or by reformation of NH_3. All these observations show that NH bonds are activated by the reaction of ammonia with oxygen-covered

Au(111), analogous to reactions reported previously on Ag and Cu surfaces[33-35], and to recent reports for Au(111) oxidized using an oxygen plasma[36].

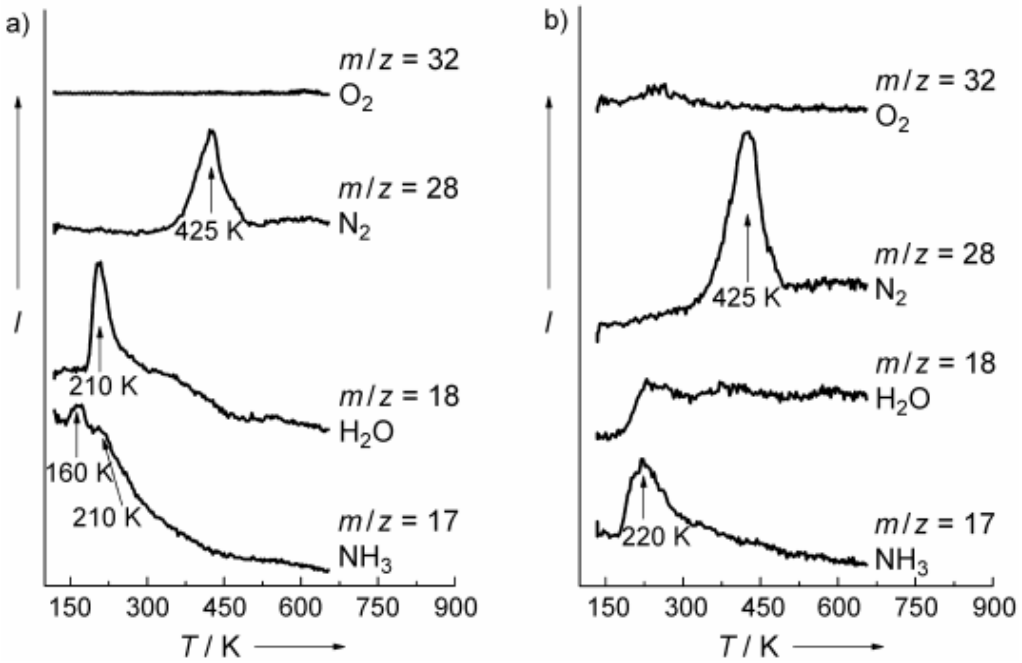

Figure A.1: Temperature-programmed reaction spectra following the adsorption of NH_3 on O-covered Au(111) (θ_O=0.2 ML). When NH_3 is exposed to the O-covered surface at 110 K (a), all oxygen reacts with N-H bonds to form water on heating above 175 K. Exposure of NH_3 to the same surface at 190 K (b) leads to removal of all oxygen as water, so as to generate a surface which contains mainly adsorbed NH_x. The NH_x disproportionates to evolved gaseous NH_3 and adsorbed N upon heating to higher temperatures. The adsorbed nitrogen atoms combine to form N_2 at 425 K. The oxygen-covered surface was prepared by O_3 decomposition at 200 K. *I* = mass spectroscopy intensity.

All adsorbed oxygen is converted into water through the reaction with N-H bonds. Water is the only oxygen-containing species detected upon heating; NO, N_2O, and NO_2

are not detected (data not shown). Furthermore, there is no detectable formation of O_2, which would occur at around 550 K from oxygen-atom recombination if there were residual adsorbed oxygen present. The reactivity of the oxygen layer towards NH_3 and other species depends on the method used for oxidation.

To accumulate NH_x and remove OH and H_2O, as well as molecular NH_3 from the surface, we exposed the oxygen-covered Au(111) surface (θ_O=0.2 monolayer (ML)) to a larger dose of NH_3 at 190 K (a temperature that is high enough to prevent adsorption of molecular NH_3 and low enough to keep NH_x on the surface; Figure A.1b). After this treatment, NH_3 reformation from NH_x, was observed as a peak at 220 K and N_2 formation at 425 K. Water formed from the reaction of NH_3 with oxygen desorbs from the surface during the reaction and therefore there is no well-defined H_2O peak - only an increased water background was observed. This desorption is concomitant with ammonia desorption, possibly because of the displacement of water by ammonia from other surfaces. Since this method exclusively produces NH_x on the surface, it was used in all experiments described later.

Addition of NH to styrene was observed following the reaction of styrene on Au(111) covered with NH_x at 150 K (Figure A.2). Specifically, a product with a parent ion at m/z=119 and the most intense peak at m/z=118 was evolved at 390 K and tentatively identified as 2-phenylaziridine. A small amount of H_2O was also produced in the reaction, possibly because of the presence of some residual oxygen on the surface following exposure to ammonia. Notably, no oxygen-addition products (CO, CO_2, epoxide, or organic acids) were detected. Remaining styrene desorbed from the surface at 200 K (multilayers) and 285 K (monolayer). A residue containing carbon and nitrogen

remained on the surface after reaction of styrene and NH_x. NO and CO_2 were produced after exposing the residue on the surface to ozone and subsequent heating. The fact that NO was produced from post-oxidation of the residue, but no N_2 was observed after reaction of styrene with NH_x, indicates that the nitrogen is bound to carbon in the residue.

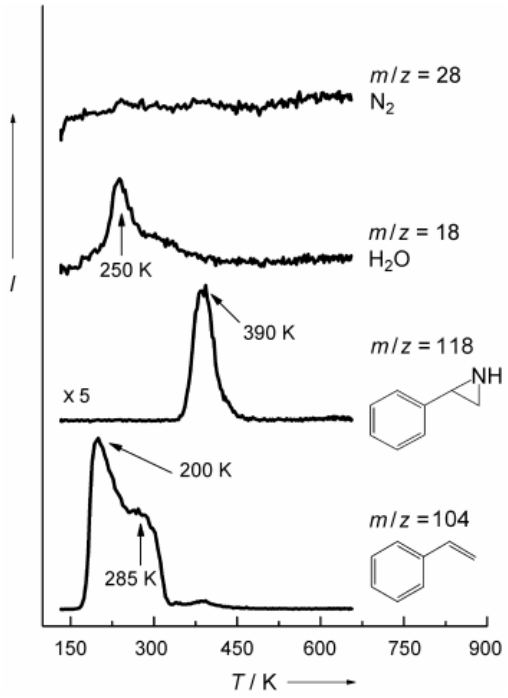

Figure A.2. Temperature-programmed reaction spectra following the adsorption of styrene on NH_x-covered Au(111) at 150 K. The reaction yields 2-phenylaziridine (390 K), exclusively. Neither oxidation nor nitrilation products were observed. Some residual oxygen reacts with NH_x and forms H_2O at 250 K. No N_2 desorption was observed, which indicates a high overall activity since all the NH_x has been consumed in the reaction.

We unequivocally established that the product formed at 390 K contains nitrogen by using $^{15}NH_3$ as our starting reagent (Figure A.3). The parent ion shifts from *m*/*z*=119 to 120 when the reaction of styrene on the surface covered with $^{15}NH_x$ was performed. Notably, a shift of the *m*/*z* signal by +1 is also observed for all the observed mass

fragments which contain nitrogen; for example, the most intense fragmentation [*M*-1] shifts from *m*/*z*=118 to 119.

The stoichiometry (C_8H_9N) of the product was determined from the parent ion signal (*m*/*z*=119) in conjunction with the shifts in the signals found in the experiments using $^{15}NH_3$. The intensities of the major fragmentation ions of the product from the experiment using our mass spectrometer were compared with the literature values of selected ion intensities of isomers with C_8H_9N stoichiometry (Table A.1). The use of literature values to eliminate possible products based on the yields of the fragment ions is validated by the good agreement with the measured intensities of the fragment ions of indoline.

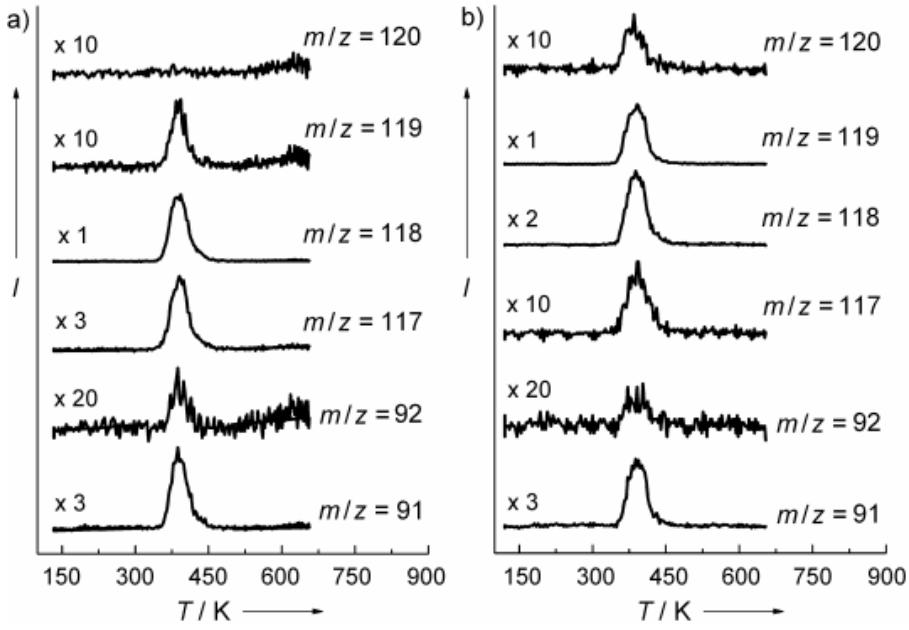

Figure A.3: Mass spectrometer fragmentations of 2-phenylaziridine from the reaction of styrene on a Au(111) surface covered with a) $^{14}NH_x$ or b) $^{15}NH_x$. The shift of +1 for the parent ion (*m*/*z* 119 to 120), as well as the most intense peak (*m*/*z* 118 to 119) when using $^{15}NH_3$, is a strong indication that the product contains nitrogen.

We assign the product formed in the reaction as 2-phenylaziridine based on analysis of its fragmentation pattern (Table A.1). The fragments of the product we observed do not match any of those C_8H_9N isomers cited by the National Institute of Standards and Technology (NIST). In addition, the presence of the *m*/*z*=91 fragment and the absence of a mass shift for this fragment when $^{15}NH_3$ was used as the source of nitrogen is compelling evidence that the product has a benzyl group ($C_6H_5CH_2$-), which is consistent with the 2-phenylaziridine structure. Furthermore, this result rules out *N*-phenyl aziridines and the imine, $C_6H_5C(CH_3)$=NH as the product because the strong *m*/*z*=91 signal contains nitrogen in this isomer. Although the mass spectrum for 2-phenylaziridine is not available from the NIST database for direct comparison, our observations all strongly point to it being the product. The other imine $C_6H_5CH_2C(H)$=NH cannot be completely ruled out.

Table A.1: Mass spectrometer fragmentation patterns of 2-phenylaziridine from the reaction of styrene on a Au(111) surface covered with NH_x and also reactions of isomers with C_8H_9N stoichiometry.

m/*z*	2-Phenyl-aziridine 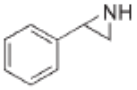	Indoline[a] 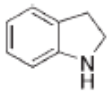	*N*-Phenyl-aziridine[b] 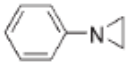	4-Amino-styrene[b] 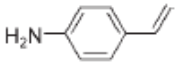
91	40	45 (30)	(100)	(24)
92	3	5 (3)	(10)	(5)
117	36	45 (29)	(0)	(15)
118	100	100 (100)	(9)	(58)
119	6	50 (63)	(40)	(100)
120	0	4 (6)	(4)	(8)

[a]These data rule out the possibility of the product being indoline, *N*-phenylaziridine, or 4-aminostyrene. [b] The numbers in the parentheses were obtained from the NIST database.

A.5 Conclusions

We suggest that the formation of 2-phenylaziridine is the result of the transfer of NH to styrene on Au(111) by analogy with the corresponding epoxidation reaction on this surface[22]. Spectroscopic studies are underway to identify the NH_x species present on the surface during reaction. We will show in a subsequent report that styrene nitrilation (forming benzo- and benzyl nitrile) occurred only when nitrogen atoms were pre-adsorbed on Au(111)[37]. This observation indicates that the presence of NH_x (NH and/or NH_2), not nitrogen atoms, is necessary for aziridination.

Our results indicate that 2-phenylaziridine is formed from the Au-promoted reaction of styrene and NH_x. In this reaction, oxygen is used to activate the NH_3 and to form NH_x species on the surface. By adjusting the preparation conditions, oxygen is consumed by the NH_3 and forms H_2O, which desorbs, and NH_x remains exclusively on the Au(111) surface.

The aziridination of organic molecules is generally a complex process usually promoted by a homogeneous catalyst[24]. Our study clearly shows the promise of the aziridination of a C=C bond by using a heterogeneous gold system, which may provide a convenient and more efficient route. The key features are the N-H bonds so as to form the desired nitrene and a C=C bond. Notably, the temperature needed for this process is low, which is significant for the selective synthesis of molecules important in the pharmaceutical industry. Nevertheless, there are still unanswered questions including the identification of the product by other means to completely rule out other products like imines, the generality of the process for more complex nitrenes and olefins, the degree of selectivity, whether these reactions can be carried out stereoselectively, and whether this

process can be carried out catalytically. Although this study was carried out using a single crystal and under ultrahigh-vacuum conditions, it is reasonable that this pathway would also apply for high-pressure conditions using supported nanoscopic Au clusters, especially since the related oxidation reactions on gold occur under both low- and high-pressure conditions.

A.6 References

[1] G. C. Bond, D. T. Thompson, *Catal. Rev. Sci. Eng.* **1999**, *41*, 319.

[2] Q. Fu, H. Saltsburg, M. Flytzani-Stephanopoulos, *Science* **2003**, *301*, 935.

[3] J. E. Bailie, G. J. Hutchings, *Chem. Commun.* **1999**, 2151.

[4] C. Mohr, H. Hofmeister, M. Lucas, P. Claus, *Chem. Ing. Tech.* **1999**, *71*, 869.

[5] S. Biella, L. Prati, M. Rossi, *Inorg. Chim. Acta* **2003**, *349*, 253.

[6] S. Biella, L. Prati, M. Rossi, *J. Catal.* **2002**, *206*, 242.

[7] S. Carrettin, P. McMorn, P. Johnston, K. Griffin, C. J. Kiely, G. J. Hutchings, *Phys. Chem. Chem. Phys.* **2003**, *5*, 1329.

[8] D. I. Enache, J. K. Edwards, P. Landon, B. Soslona-Espriu, A. F. Carley, A. A. Herzing, M. Watanabe, C. J. Kiely, D. W. Knight, G. J. Hutchings, *Science* **2006**, *311*, 362.

[9] P. Landon, P. J. Collier, A. J. Papworth, C. J. Kiely, G. J. Hutchings, *Chem. Commun.* **2002**, 2058.

[10] P. Landon, P. J. Collier, A. F. Carley, D. Chadwick, A. J. Papworth, A. Burrows, C. J. Kiely, G. J. Hutchings, *Phys. Chem. Chem. Phys.* **2003**, *5*, 1917.

[11] M. Haruta, *Catal. Today* **1997**, *36*, 153.

[12] G. C. Bond, D. T. Thompson, *Gold Bull.* **2000**, *33*, 41.

[13] T. Hayashi, K. Tanaka, M. Haruta, *J. Catal.* **1998**, *178*, 566.

[14] C. T. Campbell, *Science* **2004**, *306*, 234.

[15] M. Valden, X. Lai, D. W. Goodman, *Science* **1998**, *281*, 1647.

[16] M. S. Chen, D. W. Goodman, *Science* **2004**, *306*, 252.

[17] B. Yoon, H. Hakkinen, U. Landman, A. S. Worz, J. M. Antonietti, S. Abbet, K. Judai, U. Heiz, *Science* **2005**, *307*, 403.

[18] M. D. Hughes, Y. J. Xu, P. Jenkins, P. McMorn, P. Landon, D. I. Enache, A. F. Carley, G. A. Attard, G. J. Hutchings, F. King, E. H. Stitt, P. Johnston, K. Griffin, C. J. Kiely, *Nature* **2005**, *437*, 1132.

[19] K. Dvorakova, C. M. Payne, M. E. Tome, M. M. Briehl, T. McClure, R. T. Dorr, *Biochem. Pharmacol.* **2000**, *60*, 749.

[20] F. Brown, *Vaccine* **2001**, *20*, 322.

[21] T. B. Sim, S. H. Kang, K. S. Lee, W. K. Lee, H. Yun, Y. K. Dong, H. J. Ha, *J. Org. Chem.* **2003**, *68*, 104.

[22] X. Deng, C. M. Friend, *J. Am. Chem. Soc.* **2005**, *127*, 17178.

[23] D. A. Evans, M. M. Faul, M. T. Bilodeau, *J. Am. Chem. Soc.* **1994**, *116*, 2742.

[24] P. Müller, C. Fruit, *Chem. Rev.* **2003**, *103*, 2905.

[25] J. Zhao, A. S. Goldman, J. F. Hartwig, *Science* **2005**, *307*, 1080.

[26] J. M. Gottfried, K. Christmann, *Surf. Sci.* **2004**, *566*, 1112.

[27] J. T. Roberts, A. J. Capote, R. J. Madix, *Surf. Sci.* **1991**, *253*, 13.

[28] J. T. Roberts, R. J. Madix, *J. Am. Chem. Soc.* **1988**, *110*, 8540.

[29] M. K. Weldon, C. M. Friend, *Surf. Sci.* **1994**, *310*, 95.

[30] N. Saliba, D. H. Parker, B. E. Koel, *Surf. Sci.* **1998**, *410*, 270.

[31] B. K. Min, A. R. Alemozafar, D. Pinnaduwage, X. Deng, C. M. Friend, *J. Phys. Chem. B.* **2006**, *110*, 19833.

[32] L. J. Deiner, J. G. Serafin, C. M. Friend, S. G. Weller, J. A. Levinson, R. E. Palmer, *J. Am. Chem. Soc.* **2003**, *125*, 13252.

[33] B. Afsin, P. R. Davies, A. Pashuski, M. W. Roberts, *Surf. Sci.* **1991**, *259*, L724.

[34] X. C. Guo, R. J. Madix, *Surf. Sci.* **2002**, *501*, 37.

[35] B. Afsin, P. R. Davies, A. Pashusky, M. W. Roberts, D. Vincent, *Surf. Sci.* **1993**, *284*, 109.

[36] J. Gong, R. A. Ojifinni, T. S. Kim, J. M. White, C. B. Mullins, *J. Am. Chem. Soc.* **2006**, *128*, 9012.

[37] X. Deng, C. M. Friend, unpublished results.

APPENDIX B

TRANSIENT HYDROXYL FORMATION FROM WATER ON OXYGEN-COVERED AU(111)

B.1 Abstract

We present evidence for the formation of transient hydroxyls from the reaction of water with atomic oxygen on Au(111) and investigate the effect of adsorbed oxygen on the hydrogen bonding of water. Water is evolved in peaks at 175 K and 195 K in temperature programmed reaction experiments following adsorption of water on oxygen-covered Au(111). The peak at 175 K is ascribed to sublimation of multilayers of water whereas the peak at 195 K is associated with oxygen-stabilized water or a water-hydroxyl surface complex. Infrared reflection absorption spectra are consistent with the presence of molecular water over the entire range of coverages studied, indicating that isolated, stable hydroxyls are not formed. Isotopic exchange of adsorbed 16O with H218O following adsorption and subsequent temperature programmed reaction, however, indicates transient OH species are formed. The extent of oxygen exchange was considerable—up to 70%. The degree of oxygen exchange depends on the initial coverage of oxygen, the surface temperature when preparing oxygen adatoms, and the H218O coverage. The hydroxyls are short-lived, forming and disproportionating multiple times before water desorption during temperature-programmed reaction. It was also found that chemisorbed oxygen is critical in the formation of hydroxyls and stabilizing water, whereas gold oxide does not contribute to these effects. These results

identify transient hydroxyls as species that could play a critical role in oxidative chemical reactions on gold, especially in ambient water vapor. The crystallinity of adsorbed water also depended on the degree of surface ordering and chemical modification based on scanning tunneling microscopy and infrared spectra. These results demonstrate that oxidation of interfaces has a major impact on their interaction with water.

This work was published as an article in *Journal of Chemical Physics:* R. G. Quiller, T. A. Baker, X. Deng, M. E. Colling, B. K. Min, and C. M. Friend **2008**, *129*, 064702.

B.2 Introduction

Water plays an important role in a variety of chemical phenomena that occur on metal surfaces including catalytic reactions such as the water-gas shift reaction[1-4], hydrocarbon oxidation[5,6], and hydrogenation reactions[7]. Understanding the interaction of water with oxygen on metal surfaces, in particular Au, is also of broad fundamental interest because of the possible role of water in liquid phase systems, such as catalysis[8-12], electrochemistry[13], and the performance of biocompatible surfaces[14]. In heterogeneous catalysis, it is known that moisture enhances the performance of Au nanoparticles supported on TiO_2 by increasing the activity for CO oxidation[15,16] and decreasing the rate of deactivation for propene epoxidation[17].

The recent surge of interest in the investigation of water[18,19] has prompted questions of general interest such as whether or not water is ordered by metal surfaces and how the wetting behavior depends on the chemical modification of the surface. This behavior is important for a variety of applications including biointerfaces. For example, molecular dynamics simulations show that diamond (111) modified by Na^+ can stabilize

the dipole interaction of ice with the surface[20]; this allows the stabilization of ice multilayers at body temperature, which has biocompatibility-enhancing implications for wear-resistant medical coatings[20]. Wetting behavior of surfaces also strongly depends on modification by oxygen[21,22]. For instance, on Cu(110) wetting is controlled by the presence of OH, which in turn anchors water adsorption via lateral hydrogen bonding resulting in a mixed OH and water layer at near-ambient conditions of water[23,24]. In contrast, Cu(111), which has a higher barrier to water dissociation, remains adsorbate-free under the same conditions[23]. On Pt(111), OH is stabilized by water and it was found that both OH and stabilizing water are more strongly bound than water alone[25].

In order to investigate the nature of these effects, and more specifically, the interaction of water with oxygen-covered gold, the Au(111) surface was used as a model. We chose this system in part because water was shown to enhance the rate of CO oxidation on Au(111) containing atomic oxygen[26-28]. Kim et al. demonstrated that oxygen originating from water was incorporated into the CO_2 produced, and that the presence of water increased the CO_2 production rate even when no metal oxide support was present. Recently, Ojifinni et al. found that hydroxyls readily form from oxygen-scrambling experiments involving $H_2{}^{18}O$ on an oxygen-covered Au(111) surface prepared using a RF generator to dose atomic oxygen[28]. Although DFT results suggest that two hydroxyls are not thermodynamically stable compared to a water molecule interacting with atomic oxygen on Au(111)[29,30], the difference in energies of these states, 0.05 eV, is sufficiently small that rapid and reversible OH formation is expected and favorable even at 45 K[28]. These calculations did not address the interactions between OH formed from dissociation and neighboring water molecules. Earlier studies using X-ray

photoelectron spectroscopy (XPS) did not provide evidence of a stable hydroxyl species when water is adsorbed on oxygen-covered Au(111)[31]. The work described herein investigates conditions necessary for the formation of transient OH species which are most likely stabilized by hydrogen bonding to neighboring water molecules and illustrates that the surface roughness and the presence of oxygen adatoms affects intermolecular interactions.

B.3 Experimental Details

Experiments were performed in three separate ultrahigh vacuum chambers with base pressures < 4×10^{-10} torr. One chamber is equipped with a quadrupole mass spectrometer (Pfeiffer Prisma QMS 200), an Auger electron spectrometer (Varian model 981-2607), and low-energy electron diffraction (LEED) optics (Princeton Research Instruments model PRI-179). The second chamber is equipped with a quadrupole mass spectrometer (Pfeiffer Prisma QMS 200), an Auger electron spectrometer (Perkin Elmer model 15-155), and LEED optics (Physical Electronics model 15-180) and is interfaced with a Fourier transform infrared spectrometer (Thermo Nicolet 670). Scanning tunneling microscopy (STM) experiments were performed in an ultrahigh vacuum chamber with base pressure ~2×10^{-10} torr, with separate compartments for sample preparation and characterization[32]. The system was equipped with a STM (RHK SPM 100), LEED optics, an Auger electron spectrometer (PRI 179), and a mass spectrometer (Balzers QME 200). The Pt/Ir scanning tip was cleaned in vacuum using field evaporation (300 V, 3.8-4.0 × 10^{-6} A, 15 minutes) on a separately mounted gold single crystal. Atomically resolved Au(111)-(1 × 1) was used to calibrate scan dimensions.

The surface of the Au(111) crystal was prepared using the established method[33,34] of cycles of Ar^+ bombardment followed by annealing at 900 K for 5 minutes and 700 K for 60 minutes. This procedure is repeated until no impurities are detected by Auger electron spectroscopy (AES) and satellite spots characteristic of the herringbone reconstruction were obtained in LEED[34,35].

Atomic oxygen-covered Au(111) was prepared by exposing the crystal to ozone at 200 K with a direct doser using a method previously described[32,36]. The surface coverage of atomic oxygen was determined by comparing the area of the O_2 desorption peak to the area obtained at the saturation coverage (~1 ML)[32,36]. The roughened Au(111) surface without oxygen was prepared by exposing the 0.2 ML oxygen-covered surface to CO at 200 K using a direct doser with a background pressure rise of 2.5×10^{-8} torr for 10 minutes. This was sufficient to react away all surface oxygen so that no oxygen would be detected with the mass spectrometer when heated. This procedure is known to preserve the surface's roughened morphology[37] and was confirmed using STM.

Distilled H_2O and $H_2{}^{18}O$ (Cambridge Isotope Laboratories, 97% atomic purity) were purified using freeze-pump-thaw cycles, and the purity was confirmed using mass spectroscopy by condensing multilayers on the crystal and subsequently subliming the multilayer while monitoring with mass spectrometry. During $H_2{}^{18}O$ dosing, the inlet consisted of 80% $H_2{}^{18}O$ and ~20% $H_2{}^{16}O$, which is accounted for in our analysis. The rise in chamber pressure during directed water dosing was 1×10^{-10} torr; direct dosing exposures were calibrated by comparing desorption spectra from Au(111) following water dosing from a controlled background pressure. The enhancement factor due to

direct dosing was estimated to be ~150. All water exposures were performed at a crystal temperature of 145 K, which is below the desorption temperature of molecular water.

Temperature programmed desorption (TPD) data were acquired with a computer-interfaced Pfeiffer Prisma QMS 200 mass spectrometer. The crystal was biased at –70 V during data collection to prevent any electron-induced reactions from the mass spectrometer's filament. Temperature was measured with a K-type chromel/alumel thermocouple. Resistive heating with a tantalum wire was used to obtain an average heating rate of ~2.4 K/s between 120 K and 600 K. In order to deconvolute multiple water desorption peaks, integrated intensities were approximated by subtracting the temperature programmed desorption curve for multilayer water on clean Au(111) from the corresponding spectrum on the oxygen-covered surface, fitting the resulting spectra with a Gaussian function and subsequently integrating the function.

Reflection-absorption infrared spectroscopy (RAIRS) data were recorded using a Thermo Nicolet MCT-A semiconductor photodiode detector. Background spectra were acquired at 120 K after first heating to 600 K to desorb all water and oxygen. Three sets of 600 scans were coadded for each experiment with a resolution of 4 cm^{-1}.

B.4 Results and Discussion

Water desorbs from clean Au(111) in a single, zero-order peak[38,39] (Figure B.1a). This peak shifts from 167 K to 178 K with increasing water exposure[39,40] in the range studied, 0.3 L to 1.0 L, and shows no distinguishing characteristics separating submonolayer and multilayer coverages.

A new water peak in addition to the peak at ~175 K is observed at 195 K when Au(111) is oxidized at 200 K and subsequently exposed to water at 145 K (Figure B.1b),

in agreement with other studies[28]. The maximum intensity of the 195 K water peak depends on the initial oxygen coverage (Figure B.1 inset). The amount of water in the 195 K peak rises with increasing oxygen coverage, up to ~0.2 ML; thereafter, it decreases as a function of increasing oxygen coverage. At an oxygen coverage of 0.58 ML, there is no discernible water peak at 195 K. The dependence of the 195 K water peak on oxygen coverage indicates a strong interaction (possibly a reaction) between water and adsorbed oxygen. The possibility of OH desorption was ruled out because the *m/z* = 18:17 ratio for the water peaks on the oxygen-covered surface matched the *m/z* = 18:17 ratio on the clean surface, which we measured to be ~2.3 with our mass spectrometer. O_2 desorption occurs at 535 K and the amount of oxygen remains the same, regardless of water exposure, confirming that water reversibly desorbs at low temperature without affecting the surface oxygen coverage.

The appearance of the water desorption peak at 195 K associated with the presence of O atoms on the surface depends strongly on the conditions used to oxidize the surface. Specifically, the 195 K water desorption peak was absent when the surface was oxidized at 400 K (Figure B.1c). This is true for all oxygen coverages studied: 0.09 ML, 0.20 ML, 0.38 ML, and 0.81 ML. Furthermore, the 195 K peak is absent for oxygen coverages above 0.53 ML even for oxidation carried out at 200 K.

Previous studies have shown that the morphology of the surface and the local bonding of oxygen depend on the conditions used to prepare the surface[32,34,36,37,41-44]. There are at least two distinct oxygen moieties present following ozone decomposition on Au(111) based on XPS[32] and high resolution electron energy loss spectroscopy (HREELS)[36]. Min et al. identified these states as chemisorbed oxygen and gold oxide.

Chemisorbed oxygen (529.1 eV binding energy) associated with a disordered surface[37] was observed in XPS at low oxygen coverages for ozone decomposition at 200 K, while gold oxide—i.e. an ordered 2-D structure—signified by an O 1s binding energy of 530.1 eV is predominant at oxygen coverages > 0.5 ML and when ozone is decomposed on the surface at 400 K[37].

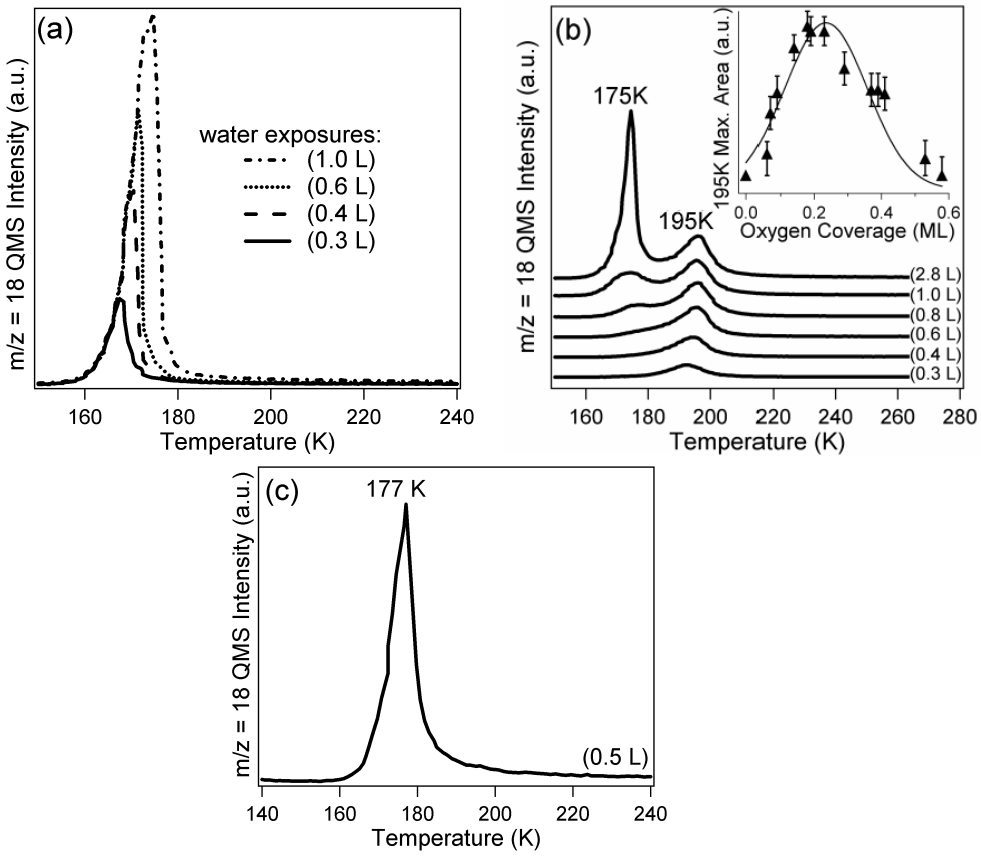

Figure B.1: Temperature programmed desorption spectra obtained after water adsorption on (a) clean Au(111) and Au(111) containing 0.2 ML of oxygen atoms formed by exposure to ozone at (b) 200 K and (c) 400 K. Water exposures were dosed at 145 K and are listed in parentheses. The inset shows the maximum integrated intensity of the 195 K peak as a function of oxygen surface coverage. Water exposures for data

corresponding to points in the inset were 6.4 L, which was sufficient to saturate the 195 K peak. The solid line is a guide to the eye.

In addition, the morphology of the surfaces created at 200 vs. 400 K is substantially different. Oxidation induces release of Au atoms from the surface under all conditions (Figure B.2a,b)[37]. After oxidation at 200 K, there is a preponderance of small (2-5 nm diameter) Au particles (Figure B.2a)[41]. A gold oxide phase is associated with the rough morphology and the development of pits and islands are observed for oxygen coverages approaching 1 ML[37]. Larger particles with regions of atomic-scale order in a rectangular structure are formed upon oxidation at 400 K (Figure B.2b)[32]. Similar ordering and the agglomeration of the gold oxide phase is accomplished by annealing low coverages of oxygen on the Au(111) surface to 400 K.

Detailed studies of the water desorption peaks were performed for an oxygen coverage of 0.2 ML after oxidation at 200 K in order to gain more insight into the bonding of water with the oxygen-covered Au (Figure B.1b). The 195 K peak develops first for low water exposure. As the water exposure is increased beyond ~0.6 L, the 195 K peaks saturates and the 175 K peak begins to appear. Above this exposure, the 175 K peak continues to grow linearly and does not saturate up to the maximum water dose studied, 6.4 L. The 195 K peak retains essentially the same shape for exposures beyond ~0.6 L and only shows an apparent intensity increase due to overlap with the trailing edge of the 175 K peak.

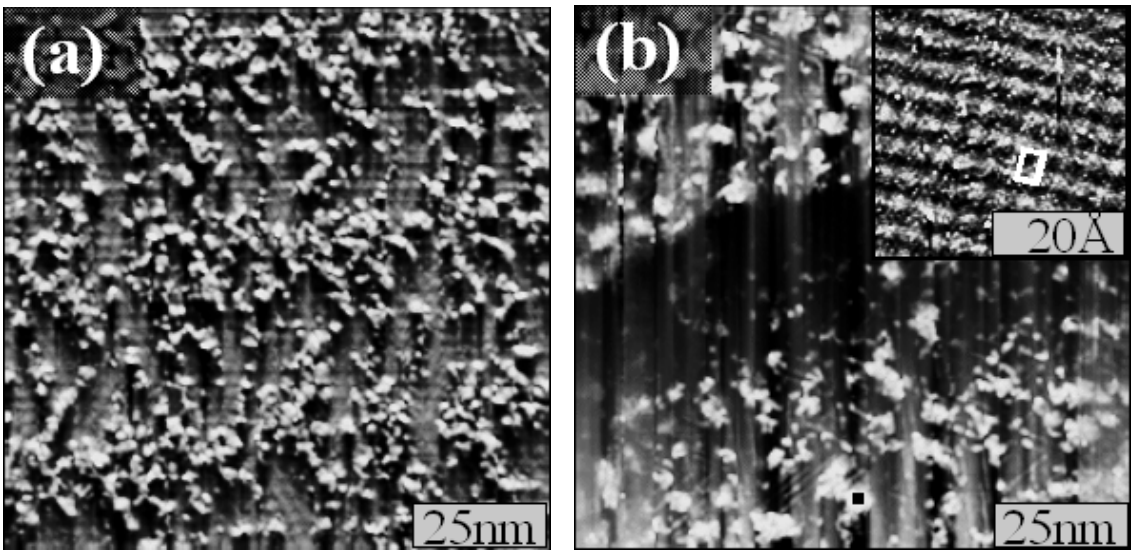

Figure B.2: STM scan of Au(111) (a) exposed to 5×10^{-8} torr of ozone at 200 K for 10 minutes, and (b) exposed to 5×10^{-8} torr of ozone at 400 K for 5 minutes. The inset shows atomically-resolved features of the region marked by a black box. Note the square unit cell marked in white, which indicates the island must contain oxygen. The areas adjoining the islands in (b) were covered by the Au(111)-(1 × 1). All STM scans were obtained at 200 K in constant height mode (U_s = 85 mV and I = 0.79 nA).

The water desorption peak at 195 K has two possible origins. Oxygen might stabilize water molecules on the surface via hydrogen bonding, thereby increasing the strength of interaction and increasing the desorption temperature from ~175 K to 195 K. The formation of stable H_2O-O complexes has previously been proposed to account for this temperature upshift[28]. Water stabilization due to chemisorbed oxygen is observed, for example, on the Ru(0001)-(2 × 2)-O surface as compared to the clean surface[45]. Alternatively, water may react with adsorbed oxygen to form adsorbed hydroxyl ($H_2O_{(a)} + O_{(a)} \rightarrow 2OH_{(a)}$) with disproportionation of hydroxyl species ($2OH_{(a)} \rightarrow H_2O_{(a)} + O_{(a)}$) occurring upon heating to ~195 K. It is possible that hydroxyls formed on the surface

may hydrogen bond to molecular water, forming stabilized $(H_2O)_n\cdots(OH)$ complexes. Theoretical[46-49] and experimental[25] studies have found that this type of stabilization occurs on Pt(111) where the $OH\cdots H_2O$ hydrogen bond is 0.2 eV stronger than the $H_2O\cdots H_2O$ hydrogen bond, creating a stabilization of the dissociated state. Similar behavior has been reported on Pd(111)[50].

The small difference in the water desorption temperature, ~20 K, for the 195 K state relative to water desorption from clean Au(111) is similar to shifts reported for water interaction via hydrogen bonding to oxygen on several other metal surfaces, such as Ag(110)[51] and Cu(110)[52]. In these cases, the presence of oxygen leads to shifts in the desorption peaks of 30 K or less relative to water desorbing from the corresponding clean surface or to sublimation of water multilayers. On the other hand, water evolved from OH disproportionation on surfaces including Ag(110)[51], Cu(110)[52], Cu(100)[53], and Pd(100)[54] generally exhibits a much larger temperature difference, 55 – 80 K, from molecular water desorption states.

Isotopic exchange experiments, however, provide unambiguous evidence for the formation of hydroxyl species. Reaction of $H_2{}^{18}O$ on Au(111) containing 0.14 ML ^{16}O results in oxygen exchange in agreement with recent studies by Kim et al[26-28]. Specifically, $^{16}O_2$, $^{16}O^{18}O$, and $^{18}O_2$ were detected in a peak at 535 K characteristic of oxygen recombination on Au(111)[36,55] (Figure B.3). This result unequivocally shows that hydroxyls form, at least transiently, from the reaction of water with oxygen on the surface:

$$H_2{}^{18}O_a + {}^{16}O_a \leftrightarrow {}^{16}OH_a + {}^{18}OH_a \leftrightarrow H_2{}^{16}O_a + {}^{18}O_a$$

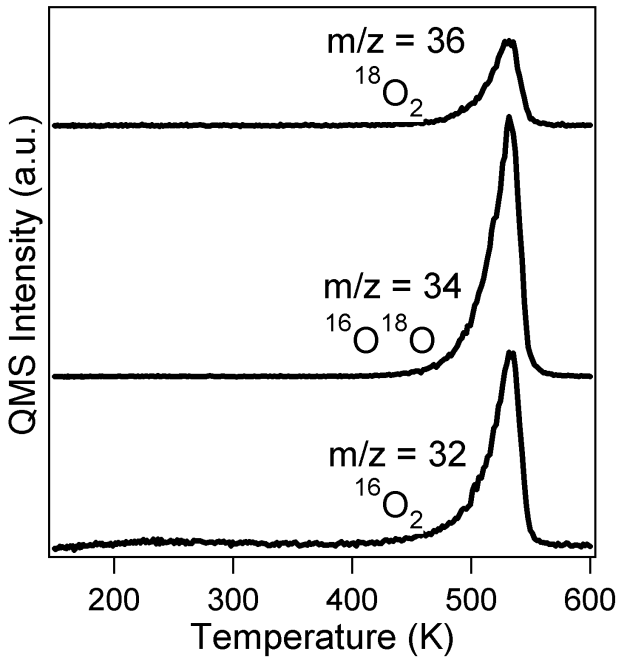

Figure B.3. Temperature programmed desorption spectra following adsorption of a mixture of $H_2{}^{18}O$ and $H_2{}^{16}O$ (4:1 ratio, respectively) on oxygen-covered Au(111) (θ_O = 0.2 ML). The oxygen-covered surface was prepared at 200 K. 2.4 L of the water mixture was exposed to the surface at 145 K.

The amount of ^{18}O evolved in the 535 K oxygen peaks versus initial ^{16}O coverage (Figure B.4) follows the same trend that was found for the maximum integrated area of the 195 K water peak; the amount of ^{18}O evolved as molecular oxygen increases with initial oxygen coverage up to ~0.2 ML and then decreases with further increases in oxygen coverage. Since only relatively small amounts of ^{18}O evolve for larger oxygen coverages and we found that a negligible amount of ^{18}O evolves when the oxygen-covered surface is prepared at 400 K, this indicates that chemisorbed oxygen, not gold oxide, is the active oxygen moiety for hydroxyl formation.

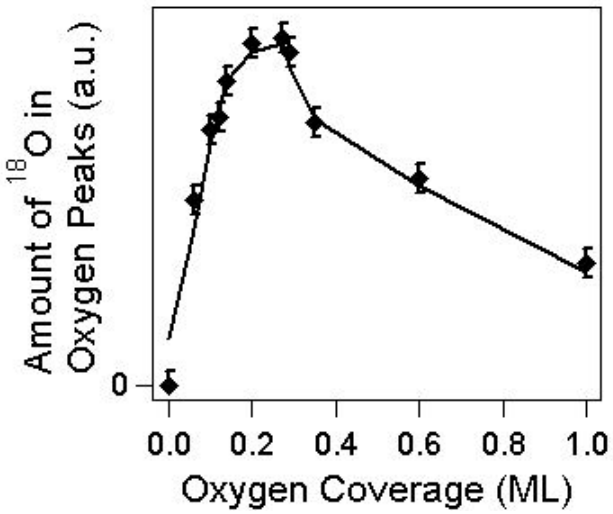

Figure B.4. The relative amount of ^{18}O in the oxygen peaks that evolve during temperature programmed desorption versus initial ^{16}O coverage when the ^{16}O-covered surface is exposed to 2.4 L of a mixture of $H_2{}^{18}O$ and $H_2{}^{16}O$ (4:1 ratio, respectively) at 145 K. The ^{16}O-covered surface was prepared at 200 K. The solid line is a guide to the eye.

The *m/z* = 20 (parent ion for $H_2{}^{18}O$) to *m/z* = 18 (parent ion for $H_2{}^{16}O$) ratio for each of the water desorption peaks when $H_2{}^{18}O$ is condensed on ^{16}O-covered Au(111) shows that water formed from the disproportionation of hydroxyls containing oxygen originating from the surface is evolved in both the 175 K and 195 K peaks (Figure 3.5a). The ratios of $H_2{}^{18}O$: $H_2{}^{16}O$ are 2.3:1 ± 0.2 and 2.1:1 ± 0.2 for the 175 K and 195 K water peaks, respectively, when 1.0 L of a mixture of $H_2{}^{18}O$ and $H_2{}^{16}O$ is condensed on 0.14 ML ^{16}O-covered Au(111). The ratio of $H_2{}^{18}O$: $H_2{}^{16}O$ in water itself is ~4:1 as determined by condensation on and subsequent desorption from clean Au(111) (Figure B.5b); therefore, it is evident that there is an increased amount of $H_2{}^{16}O$ in *both* water peaks for the oxygen-covered surface. The difference in the evolved $H_2{}^{18}O$: $H_2{}^{16}O$ ratio

from the ratio in the water inlet is less pronounced with increasing exposure. For example for an exposure of 2.4 L on 0.14 ML ^{16}O-covered Au(111), the ratios are 3.0 ± 0.2 and 2.4 ± 0.2 for the 175 K and 195 K peaks, respectively. These data strongly indicate that there is rapid formation of OH from water and vice versa, leading to isotopic mixing between condensed water and surface oxygen. It is in agreement with Ojifinni et al. who explained their observation of water containing oxygen originating from the surface by the rapid surface diffusion of OH for temperatures above 75 K[28].

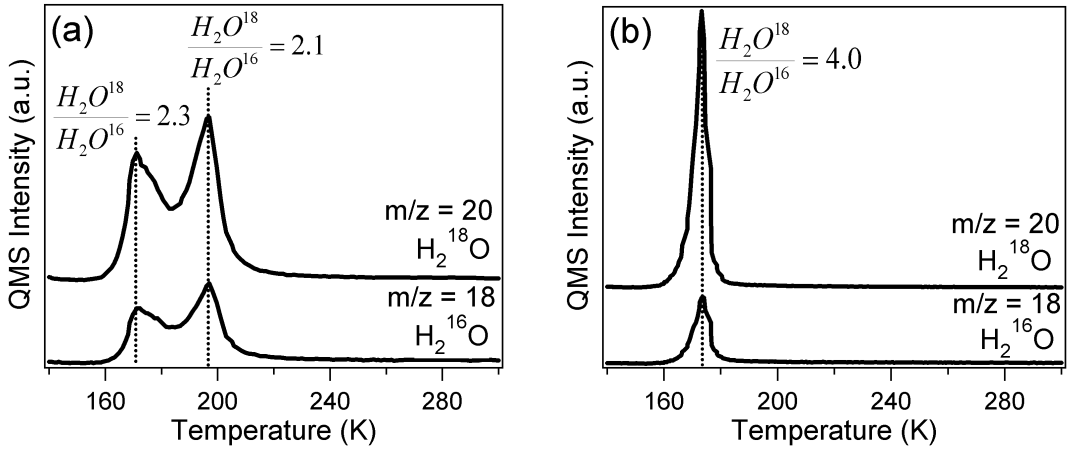

Figure B.5. Temperature programmed desorption spectra for 1.0 L of a mixture of $H_2{}^{18}O$ and $H_2{}^{16}O$ (4:1 ratio, respectively) condensed on (a) oxygen-covered Au(111) (θ_O = 0.14 ML) and (b) clean Au(111) at 145 K. The oxygen-covered surface was prepared at 200 K. The ratio of *m/z* = 20 to *m/z* = 18 in (a) was 2.3 for the 175 K peak and 2.1 for the 195 K peak. The ratio of *m/z* = 20 to *m/z* = 18 for the 175 K peak in (b) was 4.0.

Conclusive evidence that the surface hydroxyls are transient or form stabilized water-hydroxyl complexes comes from analyzing the percentage of ^{18}O in the oxygen peaks evolving at 535 K (Figure B.6). If the adsorbed oxygen quantitatively reacts with the water, equal amounts of ^{18}OH and ^{16}OH would be formed on the surface and,

accordingly, the percent of ^{18}O in the adsorbed oxygen remaining after hydroxyl disproportionation can be as high as 50% if we assume the hydroxyls disproportionate randomly and if all of the surface oxygen is chemisorbed. (Isotope effects for the recombination of ^{18}OH vs. ^{16}OH should be negligible.) The percentage of ^{18}O evolving as molecular oxygen was calculated after reacting an excess of $H_2{}^{18}O$ (2.4 L) with oxygen-covered surfaces with varying oxygen coverages prepared at 200 K. Amounts of ^{18}O evolving in molecular oxygen during heating were as high as 70%, which approached the maximum possible exchange, 80%, which corresponds to exchange of all surface oxygen based on the ratio of $H_2{}^{18}O$ to $H_2{}^{16}O$ in the doser.

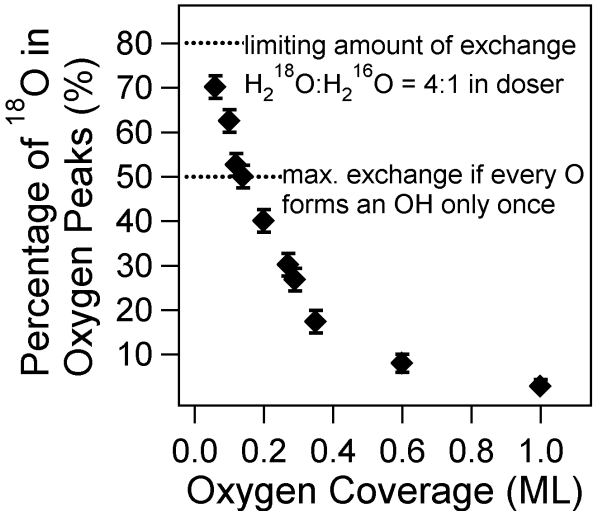

Figure B.6. Percentage of ^{18}O evolved in the oxygen peaks versus oxygen coverage when a mixture of $H_2{}^{18}O$ and $H_2{}^{16}O$ (4:1 ratio, respectively) is condensed on ^{16}O-covered Au(111). The oxygen-covered surface was prepared at 200 K. 2.4 L of the water mixture was exposed to the surface at 145 K.

This indicates that OH formation and disproportionation must be occurring on the surface multiple times, with an average of at least three exchange events occurring for a given

oxygen species (determined by assuming disproportionation occurs randomly, all surface ^{16}O is reactive at coverages < 0.2 ML, and a fraction of ^{16}O based on XPS O 1s peak intensities[32] is reactive for larger coverages). Additionally, this confirms that the 195 K water desorption peak is not due to simple disproportionation of isolated OH; rather it is due to oxygen-stabilized water or a water-hydroxyl surface complex.

RAIRS studies were performed in order to identify and probe the surface species present and their intermolecular interactions when water is adsorbed on the clean and oxygen-covered surface. The HOH bending mode at 1653 cm^{-1} and the OH stretch of bulk ice at 3365 cm^{-1} with a smaller peak at 3456 cm^{-1} were observed following adsorption of water on *clean* Au(111)[40] (Figure B.7a). The shape of the bulk ice OH stretch is characteristic of crystalline ice, which was expected based on our water adsorption temperature, 145 K, in accordance with Wang et al.[56] who characterized water on Au(111) using infrared spectroscopy and found that amorphous ice films deposited at 86 K underwent an amorphous-to-crystalline phase transition at ~120 K, which was evident in the shape of the bulk ice OH stretch. The complex shape of this mode is attributed to multiple factors including intermolecular interactions, bond length distribution, and vibrational lifetime[57]. In our work, water was adsorbed well above the amorphous-to-crystalline phase transition, but in contrast to previous observations, a small non-hydrogen bonded "free" OH stretch at 3691 cm^{-1} was also observed in our spectra. This stretching mode increased slightly in magnitude with water coverage, but remained small. The observation of this feature was not previously reported under these conditions[56].

When oxygen was preadsorbed on the surface, the HOH bending mode, the bulk ice OH stretch, and the "free" OH stretch were again observed for all coverages investigated, indicating the presence of molecular water (Figure B.7b).

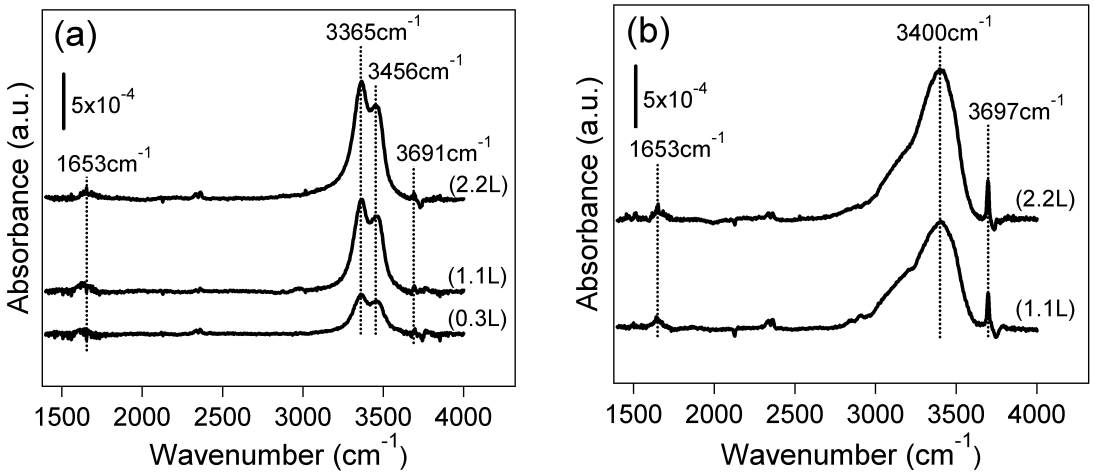

Figure B.7. Infrared (RAIRS) spectra acquired after water adsorption on (a) clean Au(111) and (b) 0.2 ML oxygen-covered Au(111). Water was dosed for the exposures shown in parentheses at 145 K. All spectra were acquired at 120 K. Background spectra were acquired after flashing the sample to 600 K and subsequent cooling to 120 K. The baseline was corrected. Features that were close to noise-level in the range, 3730 - 3745 cm^{-1} and 2330 - 2365 cm^{-1}, were present for all RAIRS experiments and did not vary with surface treatment. The former feature is assigned to the asymmetrical stretch of OH for water in the vapor phase[58], which is the mode with the largest intensity for water vapor, and is attributed to contamination in the purge gas along the infrared beam's path external to the ultrahigh vacuum chamber. The latter feature is assigned to CO_2 gas[59] due to a small carbon dioxide impurity in the purge gas.

The primary differences in the spectra for water adsorption on the clean Au(111) surface and on the oxygen precovered surface are the shape of the bulk ice OH stretch and the intensity of the "free" OH stretch, which is enhanced for the oxygen-covered surface. Notably, an asymmetric peak at 3400 cm^{-1} for the oxygen-covered surface replaces the peaks at 3365 cm^{-1} and 3456 cm^{-1} for the bulk ice OH stretch on clean Au(111). The shape of the bulk ice OH stretch and presence of the "free" OH stretch is characteristic of amorphous ice[56,57] and indicates an effect on the long-range intermolecular coupling forces. The overall shift to higher frequency of the bulk ice OH stretch is indicative of longer O-O bond distances[57], suggesting water's interaction with surface oxygen results in weaker $H_2O\cdots H_2O$ hydrogen bonding. The enhanced "free" OH stretch seen in RAIRS can be attributed to non-hydrogen bonded OH groups dangling into vacuum[56].

These effects are primarily attributed to the presence of surface oxygen, not the moiety of the oxygen or the roughening of the Au(111) surface due to ozone decomposition and the release of Au atoms from the surface[37]. When water is condensed on the Au(111) surface with a low coverage, < 0.3 ML, of oxygen that was annealed to 400 K for 5 minutes, which results in an ordered 2-D surface gold oxide, the infrared spectra are qualitatively very similar to spectra associated with the surface without annealing (Figure B.8); the nature of the bulk ice OH stretch is amorphous and a strong "free OH" stretch is present. When water is exposed to the roughened Au(111) surface without oxygen (Figure B.9a,b), the "free OH" stretch is observed but there are only minor differences in the bulk ice OH stretch from the crystalline ice shape observed for water on clean Au(111) (Figure B.9c). Notably, the peak at 3456 cm^{-1} is less pronounced and appears as a shoulder on the peak at 3367 cm^{-1}. It is clear that roughening the

Au(111) surface influences the hydrogen bonding of water to some extent; however, the spectrum most closely resembles that of crystalline ice on the flat, clean Au(111) surface. Thus, we primarily attribute differences in the spectra on the oxygen-covered surfaces from the flat, clean Au(111) surface to differences in hydrogen bonding when oxygen is present, and not the oxygen moiety or surface roughness.

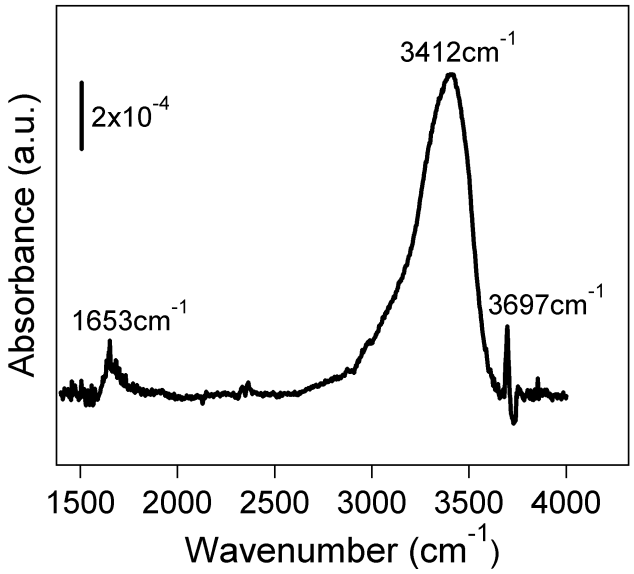

Figure B.8. Infrared (RAIRS) spectrum acquired after exposing a 0.2 ML oxygen-covered Au(111) surface that had been annealed to 400 K for 5 minutes to 2.2 L of water at 145 K. The spectrum was acquired at 120 K. The background spectrum was acquired after flashing the sample to 600 K and subsequently cooling to 120 K. The baseline was corrected. The features in the range, 3730 - 3745 cm^{-1} and 2330 - 2365 cm^{-1} are attributed to impurities in the purge gas external to the ultrahigh vacuum chamber due to vapor phase water[58] and CO_2[59], respectively.

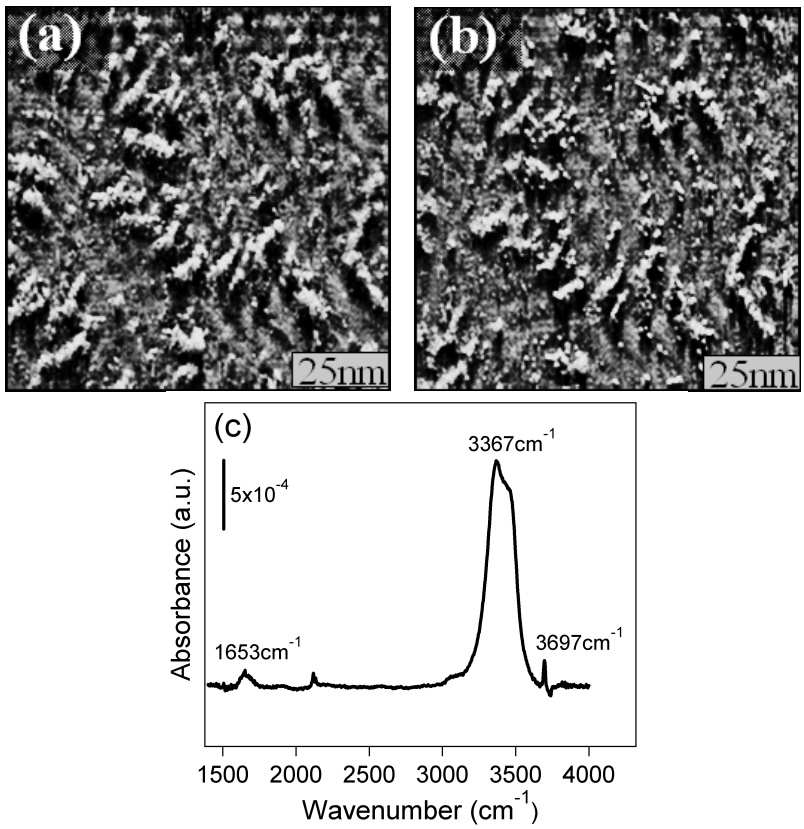

Figure B.9. STM scans of oxygen-covered Au(111) surfaces prepared at 200 K before (a) and after (b) exposure to $CO_{(g)}$ at 200 K with a background pressure rise of 1×10^{-8} torr for 5 minutes. The exposures were sufficient to react away all of the surface $O_{(a)}$. All STM scans were obtained at 200 K in constant height mode (U_s = 85 mV and I = 0.79 nA). (c) The corresponding infrared spectrum for 2.2 L water condensed at 145 K on the roughened Au(111) surface without oxygen. The spectrum was acquired at 120 K. The background spectrum was acquired after flashing the sample to 600 K and subsequently cooling to 120 K. The baseline was corrected. The feature in the range, 3730 - 3745 cm^{-1}, is assigned to a contamination in the purge gas external to the ultrahigh vacuum chamber due to vapor phase water[58]. There is also a set of small peaks at 2119 cm^{-1} and 2133 cm^{-1}, which is due to linear adsorption of residual CO on the crystal while cooling the surface to acquire infrared spectra[60,61].

Our data do *not* provide evidence for species with O-O bonds, e.g. HOO; however, as our signal-to-noise diminished significantly below 1000 cm^{-1}, the frequency range expected for the O-O stretch of peroxo based on studies of Pt(111)[62,63] and polycrystalline Ag[64], we cannot unequivocally rule out such a species. Consistent with the $H_2{}^{18}O$ oxygen-exchange experiments, RAIRS does not provide evidence for the existence of stable, isolated hydroxyl species for exposures as low as ~0.05 L, which would have a sharp peak at ~3600 cm^{-1}. These RAIRS data taken alone, however, cannot rule out the possibility of isolated hydroxyls at coverages below 0.05 ML, because our signal-to-noise ratio is insufficient to detect species at such low coverages. It is also known that the presence of water suppresses the hydroxyl OH stretch due to hydrogen bonding[65], leaving the possibility for hydroxyls hydrogen bonded to water.

Our results suggest a possible water-hydroxyl surface complex analogous to the water-hydroxyl mixed phase on Pt(111)[25,66]. On Pt(111) OH will decompose with a low activation energy via $2OH_{(ads)} \rightarrow O_{(ads)} + H_2O_{(ads)}$ unless stabilized by water[46,47]. The optimum stoichiometry for the mixed phase is 2:1 for water and atomic oxygen, respectively, corresponding to saturation of a Pt(111)-(2 × 2)-O surface with water[25]. LEED-IV structure analysis showed the resulting overlayer consists of hexagonal rings of hydrogen bonded oxygen atoms[67]. The stabilization of the mixed phase is manifested as an increase in the desorption temperature of water by ~40 K when compared to water on the bare surface[68]. In accordance with our infrared spectra, no vibrational modes corresponding to hydroxyls are observed. In fact, the saturated mixed phase on Pt(111) does not have measurable adsorption in the bulk ice OH stretch, the "free" OH stretch, or

the H_2O bending mode; this is a result of the flat lying geometry of the water-hydroxyl mixed phase[68].

Similarly, a water-hydroxyl mixed phase was recently reported on Pd(111) from the reaction of chemisorbed oxygen and water with nearly identical behavior to the Pt(111) surface[50]. Clay et al. found that the most stable water-hydroxyl mixed phase contained 0.67 monolayers of oxygen formed via $3H_2O + O \rightarrow 2(H_2O + OH)$ and had $(\sqrt{3} \times \sqrt{3})R30^{\circ}$ periodicity. Stabilization of the mixed phase was evident by OH recombining and water desorbing at a temperature 20 K higher than the desorption temperature of pure water on Pd(111)[50].

Our work clearly indicates that the behavior of water at Au interfaces is affected by oxidation and roughness. It was determined that hydrogen bonding of water to oxygen adatoms results in short-lived OH species, which interact with water; it is possible that this interaction results in a water-hydroxyl mixed phase in analogy to what is observed on Pt(111) and Pd(111). The enhancement in the CO oxidation rate previously observed when water is adsorbed on an atomic oxygen-covered Au(111) surface[26-28] is still not clearly understood and warrants further study to account for complex hydrogen bonding interactions.

B.5 Conclusions

The interaction of water with atomic oxygen on Au(111) was investigated using TPD and RAIRS. The reaction of $H_2{}^{18}O$ with surface ^{16}O resulting in oxygen exchange conclusively showed that hydroxyls are formed. The extent of exchange, which was up to 70%, indicated that the hydroxyls are interacting with water or transient, forming and disproportionating multiple times on the surface. Water containing exchanged oxygen

was present in both the 175 K water peak and the 195 K water desorption peaks. These results are corroborating evidence that the 195 K water desorption peak is not due to the disproportionation of isolated, stable hydroxyls, but rather oxygen-stabilized water or a water-hydroxyl surface complex.

RAIRS spectra further support the transient nature of the hydroxyls, indicating that molecular water is present on the surface for all water exposures investigated, possibly hydrogen bonded to hydroxyl species and suppressing their OH stretch. RAIRS and STM also characterized the effect of preadsorbed oxygen and surface roughening on water's intermolecular interactions. The presence of chemisorbed oxygen and gold oxide each resulted in a change in shape from crystalline to amorphous for the bulk ice OH stretch, and a substantial enhancement of the "free" OH stretch signaling a reduction in the number of OH bonds contributing to hydrogen bonding. Surface roughening had a much less significant affect on hydrogen bonding but did alter the shape of the bulk ice OH stretch, and the presence of the "free" OH stretch indicated contributions from water molecules that were not fully coordinated.

In conjunction with previous XPS studies[32], it is concluded that chemisorbed oxygen plays a key role in water's interaction with Au(111). It was found that chemisorbed oxygen is responsible for transient hydroxyl formation and for the stabilization of water during TPD, while gold oxide, which is prevalent at high oxygen coverages and is associated with the ordered surface formed by annealing at 400 K, does not contribute to these effects. These results help identify transient hydroxyls as possibly playing an important role in oxidation reactions on gold in the presence of oxygen and water. It suggests that both water and hydroxyls must be considered in, e.g. CO

oxidation on Au(111), but it does not answer previous mass balance concerns regarding hydrogen when CO oxidation on oxygen-covered Au(111) is enhanced by water[26,28,69]. Our results also indicate that water's interaction and ordering at, e.g. biocompatible interfaces, can be significantly affected by surface roughness and chemical modification.

B.6 References

[1] Z.-P. Liu, S. J. Jenkins, D. A. King, *Phys. Rev. Lett.* **2005**, *94*, 196102/1-196102/4.

[2] D. Andreeva, V. Idakiev, T. Tabakova, L. Ilieva, P. Falaras, A. Bourlinos, A. Travlos, *Catal. Today* **2002**, *72*, 51-57.

[3] Q. Fu, H. Saltsburg, M. Flytzani-Stephanopoulos, *Science* **2003**, *301*, 935-938.

[4] J. A. Rodriguez, Ma, S.; Liu, P.; Hrbek, J.; Evans, J.; Pérez, M. *Science* **2007**, *318*, 1757-1760.

[5] A. L. Marsh, J. L. Gland, *Catal. Lett.* **2004**, *93*, 165-170.

[6] J. T. Ranney, S. R. Bare, J. L. Gland, *Catal. Lett.* **1997**, *48*, 25-29.

[7] J. A. S. Don, J. F. Joseph, *Faraday Discuss. Chem. Soc.* **1981**, *72*, 145-156.

[8] A. Corma, V. Fornés, S. Iborra, M. Mifsud, M. Renz, *J. Catal.* **2004**, *221*, 67-76.

[9] E. Maerten, S. Cabrera, A. Kjærsgaard, K. A. Jørgensen, *J. Org. Chem.* **2007**, *72*, 8893-8903.

[10] M. Lazar, R. J. Angelici, *J. Am. Chem. Soc.* **2006**, *128*, 10613-10620.

[11] B. Zhu, R. J. Angelici, *J. Am. Chem. Soc.* **2006**, *128*, 14460-14461.

[12] B. Zhu, R. J. Angelici, *Chem. Commun.* **2007**, *21*, 2157-2159.

[13] A. B. Anderson, *Electrochim. Acta* **2002**, *47*, 3759-3763.

[14] Y. Arima, H. Iwata, *Biomaterials* **2007**, *28*, 3074–3082.

[15] M. Daté, M. Haruta, *J. Catal.* **2001**, *201*, 221-224.

[16] M. Daté, M. Okumura, S. Tsubota, M. Haruta, *Angew. Chem. Int. Ed.* **2004**, *43*, 2129-2132.

[17] T. A. Nijhuis, B. M. Weckhuysen, *Chem. Commun.* **2005**, 6002-6004.

[18] M. A. Henderson, *Surf. Sci. Rep.* **2002**, *46*, 1-308.

[19] P. G. Sennikov, S. K. Ignatov, O. Schrems, *ChemPhysChem* **2005**, *6*, 392 – 412.

[20] A. D. Wissner-Gross, E. Kaxiras, *Phys. Rev. E* **2007**, *76*, 020501.

[21] R. Wang, L. Cong, M. Kido, *Appl. Surf. Sci.* **2002**, *191*, 74-84.

[22] S. P. Liaw, *Datong Xuebao* **1989**, *19*, 1-5.

[23] S. Yamamoto, K. Andersson, H. Bluhm, G. Ketteler, D. E. Starr, T. Schiros, H. Ogasawara, L. G. M. Pettersson, M. Salmeron, A. Nilsson, *J. Phys. Chem. C* **2007**, *111*, 7848-7850.

[24] K. Andersson, G. Ketteler, H. Bluhm, S. Yamamoto, H. Ogasawara, L. G. M. Pettersson, M. Salmeron, A. Nilsson, *J. Phys. Chem. C.* **2007**, *111*, 14493-14499.

[25] T. Schiros, L.-Å. Naslund, K. Andersson, J. Gyllenpalm, G. S. Karlberg, M. Odelius, H. Ogasawara, L. G. M. Pettersson, A. Nilsson, *J. Phys. Chem. C.* **2007**, *111*, 15003-15012.

[26] T. S. Kim, J. Gong, R. A. Ojifinni, J. M. White, C. B. Mullins, *J. Am. Chem. Soc.* **2006**, *128*, 6282-6283.

[27] J. Gong, R. A. Ojifinni, T. S. Kim, J. D. Stiehl, S. M. McClure, J. M. White, C. B. Mullins, *Top. Cat.* **2007**, *44*, 57-63.

[28] R. A. Ojifinni, N. S. Froemming, J. Gong, M. Pan, T. S. Kim, J. M. White, G. Henkelman, C. B. Mullins, *J. Am. Chem. Soc.* **2008**, *130*, 6801-6812.

[29] G.-C. Wang, S.-X. Tao, X.-H. Bu, *J. Catal.* **2006**, *244*, 10-16.

[30] S. Kandoi, A. A. Gokhale, L. C. Grabow, J. A. Dumesic, M. Mavrikakis, *Catal. Lett.* **2004**, *93*, 93-100.

[31] M. A. Lazaga, D. T. Wickham, D. H. Parker, G. N. Kastanas, B. E. Koel, *ACS Sym. Ser.* **1993**, *523*, 90-109.

[32] B. K. Min, A. R. Alemozafar, D. Pinnaduwage, X. Deng, C. M. Friend, *J. Phys. Chem. B* **2006**, *110*, 19833-19838.

[33] M. A. Van Hove, R. J. Koestner, P. C. Stair, J. P. Biberian, L. L. Kesmodel, I. Bartos, G. A. Somorjai, *Surf. Sci.* **1981**, *103*, 189-217.

[34] B. K. Min, X. Y. Deng, D. S. Pinnaduwage, R. Schalek, C. M. Friend, *Phys. Rev. B.* **2005**, *72*, 121410.

[35] M. A. Van Hove, R. J. Koestner, P. C. Stair, J. P. Biberian, L. L. Kesmodel, I. Bartos, G. A. Somorjai, *Surf. Sci.* **1981**, *103*, 218-238.

[36] N. Saliba, D. H. Parker, B. E. Koel, *Surf. Sci.* **1998**, *410*, 270-282.

[37] B. K. Min, A. R. Alemozafar, M. M. Biener, J. Biener, C. M. Friend, *Top. Catal.* **2005**, *36*, 77-90.

[38] B. D. Kay, K. R. Lykke, J. R. Creighton, S. J. Ward, *J. Chem. Phys.* **1989**, *91*, 5120-5121.

[39] J. Wang, M. R. Voss, H. Busse, B. E. Koel, *J. Phys. Chem. B.* **1998**, *102*, 4693-4696.

[40] S. Sato, D. Yamaguchi, K. Nakagawa, Y. Inoue, A.Yabushita, M. Kawasaki, *Langmuir* **2000**, *16*, 9533-9538.

[41] B. K. Min, C. M. Friend, *Chem. Rev.* **2007**, *107*, 2709-2724.

[42] J. M. Gottfried, N. Elghobashi, S. L. M. Schroeder, K. Christmann, *Surf. Sci.* **2003**, *523*, 89-102.

[43] J. M. Gottfried, K. J. Schmidt, S. L. M. Schroeder, K. Christmann, *Surf. Sci.* **2002**, *511*, 65-82.

[44] J. M. Gottfried, K. J. Schmidt, S. L. M. Schroeder, K. Christmann, *Surf. Sci.* **2003**, *525*, 197-206.

[45] P. Cabrera-Sanfelix, D. Sánchez-Portal, A. Mugarza, T. K. Shimizu, M. Salmeron, A. Arnau, *Phys. Rev. B.* **2007**, *76*, 205438.

[46] A. Michaelides, P. Hu, *J. Chem. Phys.* **2001**, *114*, 513-519.

[47] A. Michaelides, P. Hu, *J. Am. Chem. Soc.* **2001**, *123*, 4235-4242.

[48] G. S. Karlberg, G. Wahnstrom, *Phys. Rev. Lett.* **2004**, *92*, 136103.

[49] G. S. Karlberg, G. Wahnstrom, *J. Chem. Phys.* **2005**, *122*, 194705.

[50] C. Clay, L. Cummings, A. Hodgson, *Surf. Sci.* **2007**, *601*, 562-568.

[51] E. M. Stuve, R. J. Madix, B. A. Sexton, *Surf. Sci.* **1981**, *111*, 11-25.

[52] K. Bange, D. E. Grider, T. E. Madey, J. K. Sass, *Surf. Sci.* **1984**, *137*, 38-64.

[53] T. Sueyoshi, T. Sasaki, Y. Iwasawa, *J. Phys. Chem. B* **1997**, *101*, 4648-4655.

[54] E. M. Stuve, S. W. Jorgensen, R. J. Madix, *Surf. Sci.* **1984**, *146*, 179-198.

[55] X. Deng, B. K. Min, A. Guloy, C. M. Friend, *J. Am. Chem. Soc.* **2005**, *127*, 9267-9270.

[56] J. Wang, B. E. Koel, *Surf. Sci.* **1999**, *436*, 15-28.

[57] F. Bensebaa, T. H. Ellis, *Prog. Surf. Sci.* **1995**, *50*, 173-185.

[58] D. Eisenberg, W. Kauzmann, *The structure and properties of water*; [Oxford University Press: New York, **1969**].

[59] S. Meyer, F. Temps, *Int. J. Chem. Kinet.* **2000**, *32*, 136-145.

[60] T. Zhang, Z.-P. Liu, S. M. Driver, S. J. Pratt, S. J. Jenkins, D. A. King, *Phys. Rev. Lett.* **2005**, *95*, 266102-266105.

[61] J.-D. Grunwaldt, A. Baiker, *J. Phys. Chem. B* **1999**, *103*, 1002-1012.

[62] K. Gustafsson, S. Andersson, *J. Chem. Phys.* **2004**, *120*, 7750-7754.

[63] K. Gustafsson, S. Andersson, *J. Chem. Phys.* **2004**, *121*, 8532-8536.

[64] X.-D. Wang, W. T. Tysoe, R. G. Greenler, K. Truszkowska, *Surf. Sci.* **1991**, *258*, 335-345.

[65] D. H. Kang, C. M. Friend, *Langmuir* **2004**, *20*, 11443-11449.

[66] G. S. Karlberg, F. E. Olsson, M. Persson, G. Wahnstrom, *J. Chem. Phys.* **2003**, *119*, 4865-4872.

[67] G. Held, C. Clay, S. D. Barrett, S. Haq, A. Hodgson, *J. Chem. Phys.* **2005**, *123*, 064711.

[68] C. Clay, S. Haq, A. Hodgson, *Phys. Rev. Lett.* **2004**, *92*, 046102.

[69] X.-Q. Gong, P. Hua, R. Raval, *J. Chem. Phys.* **2003**, *119*, 6324-6334.

APPENDIX C

PHENOL FORMATION FROM CYCLOHEXENE: A DFT MECHANISTIC STUDY

C.1 Abstract

It was found experimentally (X. Liu and C.M. Friend) that the highly selective oxidation of cyclohexene on oxygen covered Au(111) occurs via two distinctive pathways: Brønsted acid-base reaction between allylic hydrogens and surface oxygens and direct oxygen insertion into an allylic C-H bond. It was also proposed that surface-mediated keto-enol tautomerization occurs in the last step of phenol formation. To confirm this last step we calculate the energy barrier, using density functional theory, for two different possible reaction pathways in the final step of phenol formation: (a) β-H transfer and (b) keto-enol tautomerization. These pathways were tested using both the climbing nudged elastic band method (cNEB) and the constrained minimization technique (CM). We find that both the starting intermediate and transition state for keto-enol tautomerization is much lower in energy than β-H transfer, confirming the experimental results.

This work will be combined with experimental results and submitted for publication: X. Liu, T. A. Baker, E. Kaxiras, C. M. Friend.

C.2 Introduction

The oxidation of olefins is of fundamental importance in heterogeneous catalysis. Model studies on single-crystal surfaces provide important insight into the atomic-level

mechanism for such processes[1-3]. Gold has recently attracted a great deal of attention with selective oxidation of olefins being one of the most investigated reaction classes[4, 5].

Among the transition metals, only silver is an effective catalyst for selective partial oxidation since Pt, Pd, Rh, and Ir all lead to combustion. The primary motivation for investigating olefin oxidation by gold is the potential for selective oxidation of olefins with allylic C-H bonds. On silver, reactions between atomic oxygen and adsorbed organic species that have acidic bonds (R-H) are well described as Brønsted acid-base processes (in terms of their gas-phase acidities)[2,6]. Though this property has been exploited for selective oxidation, olefins containing acidic *allylic* C-H bonds generally combust on silver because allylic hydrogens are labile. An exception to this rule is the oxydehydrogenation of cyclohexene, a gas-phase acid with allylic C-H bonds. The reaction yields benzene, formed as a result of the sequential scission of four separate C-H bonds, starting from the acidic allylic C-H[6] bond.

Experimental work (performed by Xiaoying Liu and Cynthia M. Friend, unpublished) shows the selective insertion of atomic oxygen adsorbed on Au(111) into allylic C-H bonds of cyclohexene—a pathway that is not observed on silver. Conversion of cyclohexene has been employed as a benchmark reaction for testing the catalytic behavior of a variety of materials[7-10], and their results provide insight into the performance of gold for partial oxidation reactions. Analogous to the oxidation reaction on Ag(110)[2, 6], benzene is produced from allylic C-H bond activation on oxidized Au(111). However, this oxygen insertion pathway, which appears unique to gold, yields 2-cyclohexene-1-one, 2-cyclohexene-1,4-dione, and phenol from the reaction of cyclohexene on oxidized Au(111)—none of which have been reported for the reaction on

silver and none of which occur on any other clean metal surfaces. Further, Liu and Friend found evidence for a surface-mediated internal keto-enol tautomerization in the last step of phenol production, the first report of such a surface-mediated process. Density funtional theroy calculations performed in this work help confirm this step.

C.3 Calculational Details

DFT results were obtained using the VASP code[11] with the GGA-PW91[12] functional to model electron exchange and correlation. Projector augmented wave pseudopotentials are employed with the default plane-wave cutoffs for different elements taken from the GGA pseudopotential database[13] and a 5x5x1 Monkhorst-Pack k-point sampling was used. The surface was modeled by a slab consisting of 4 layers in the (111) direction, with a 3x3 primitive unit cell in the lateral directions; only the two uppermost layers of the slab were allowed to relax, with the rest fixed at the ideal bulk positions. The bulk positions were taken from the calculated lattice constant of 4.17 Å which is in good agreement with the experimental value of 4.08 Å[14].

Two different methods for finding transition states (TS) are used: climbing nudged elastic band method (cNEB)[15-17] and constrained minimization (CM)[18]. The nudged elastic band method consists of using an initial and final state with points (images) in between connected by spring forces. Upon relaxing each image with the spring forces imposed, the images should lie on the minimum energy path (MEP). The saddle point on the potential energy surface (PES) is found after initially converging the points and then "climbing" the highest energy image to the top of the MEP. In this work, 3 images were used. In the CM technique an appropriate bond distance between the reactants is chosen as the reaction coordinate and kept frozen at several values while the

rest of the system is allowed to relax. The TS corresponds to the maximum along the reaction coordinate.

C4. Results and Discussion

The TS of two pathways leading to the formation of phenol were found in this work: (a) β-H transfer and (b) tautomerization (Figure C.1). For each starting intermediate, many different configurations were tested to find the system with the lowest energy to serve as the starting point for the cNEB method. The corresponding configuration for each case is shown in Figure C.2.

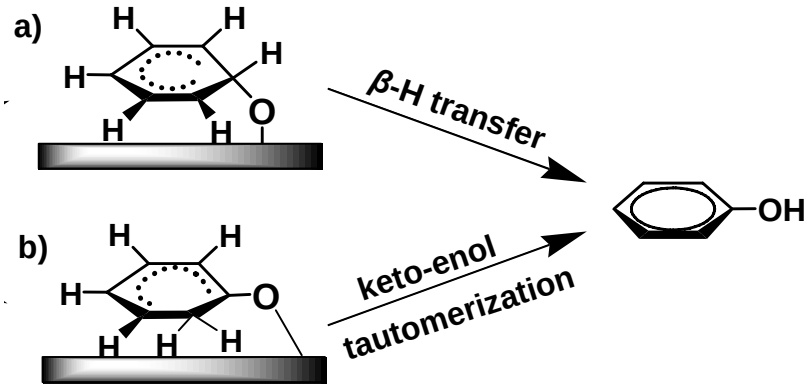

Figure C.1: The starting intermediates and final product (phenol).

Both reaction mechanisms were tested with cNEB and CM. Unfortunately, the β-H transfer mechanism did not converge using NEB and as a result we were forced to rely on the CM technique. To determine the TS with the CM technique, we choose two different groups of atoms to be held fixed. This group, however, created a 'jump' in which the β-hydrogen did not smoothly transfer from the carbon to the oxygen, possibly missing the true TS. In the second case, the carbon-oxgyen bond was held constant along with the β-hydrogen involved in the transfer, which was linearly extrapolated between its

starting and ending point. Fixing these atoms produced a much smother transition, but since more atoms were constrained it is possible that this result could overestimate the energy barrier. It should be safe to conclude, however, that the true TS energy lies in between the results found from these two methods. The energy at different points along the reaction coordinate is shown in Figure C.3 for the two cases, with the point with the highest energy being the TS.

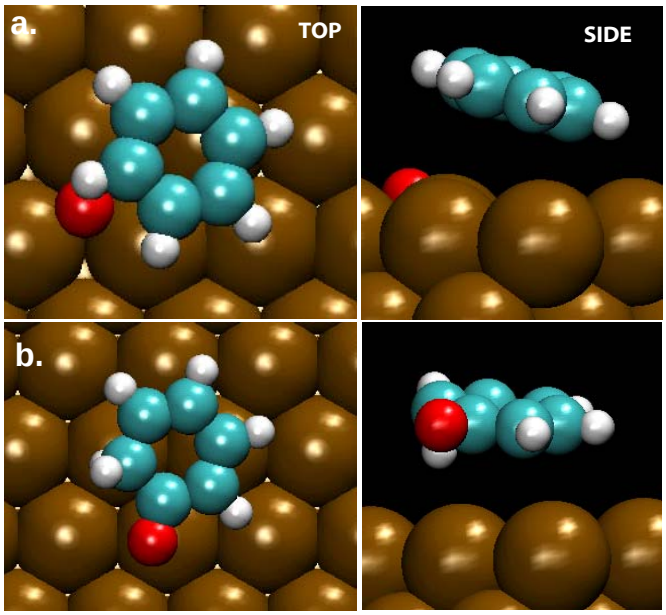

Figure C.2: Starting configurations for phenol formation for (a) β-H transfer and (b) tautomerization mechanisms. Larger brown circles represent gold atoms and the smaller red, white, and blue circles represent oxygen, hydrogen, and carbon, respectively.

The energy barrier (versus the energy of the starting intermediate) for constraining just the oxygen and carbon and with all three atoms fixed is 1.52 eV and 3.03 eV respectively. As expected, the TS energy is higher when H is constrained. The geometry of the TS found with carbon, hydrogen, and oxygen held constant is shown in Figure C.4a. The same procedure is performed for the tautomerization reaction; the

barrier when keeping the oxygen and transferring H fixed and for keeping the oxygen and both hydrogens fixed is 1.71 eV and 2.04 eV, respectively.

The TS for tautomerization was also found using cNEB. The energy barrier was found to be 1.87 eV and its geometry is shown in Figure C.4b. The energy and geometry of the TS agree well with past theoretical results. Gomez et. al[19] found the gas-phase barrier to be 2.31 eV with the total energy change of -0.83 eV at the CASPT2(8,8)/cc-pVDZ level.

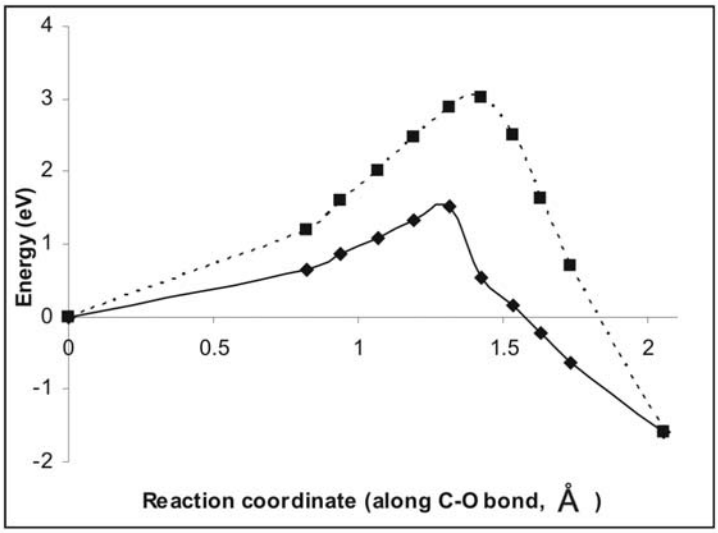

Figure C.3: Energy along the reaction coordinate using the constrained minimization technique for the β-H transfer mechanism. The oxygen and closest carbon is held fixed for the solid black curve, and the oxygen, carbon, and β-hydrogen are held fixed for the dashed curve.

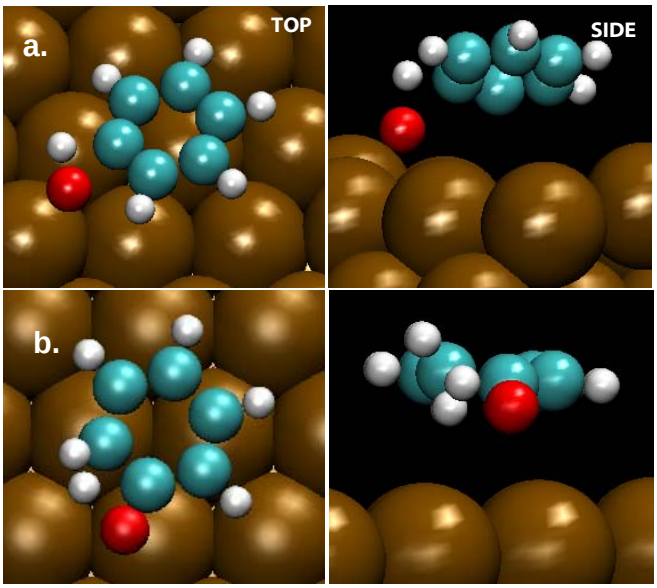

Figure C.4: Model of TS for (a) β-H transfer and (b) tautomerization. Larger brown circles represent gold atoms and the smaller red, white, and blue circles represent oxygen, hydrogen, and carbon, respectively.

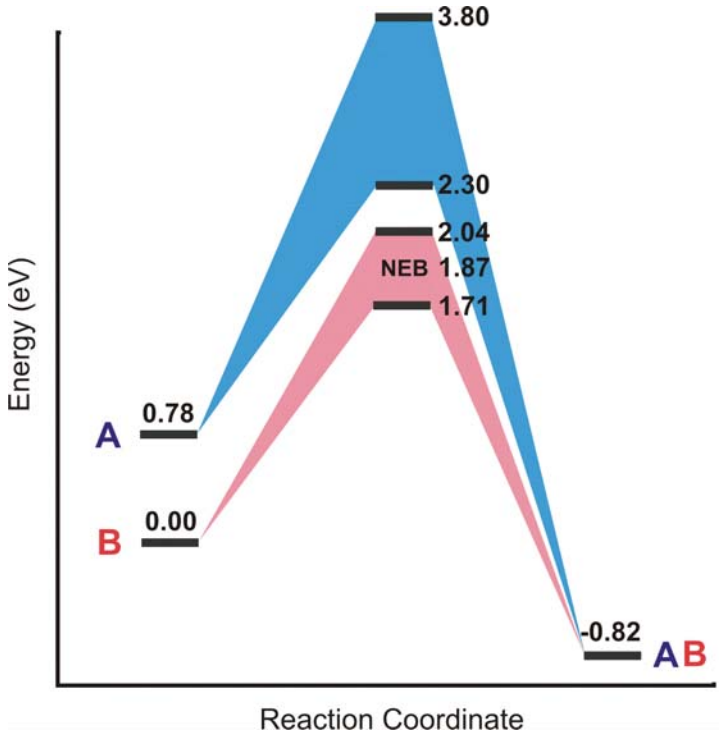

Figure C.5: Energy diagram for the two different reaction mechanisms: (A) β-H transfer and (B) tautomerization. A range of transition state energies is shown depending on the atoms held fixed during the constrained minimization technique. The transition state

energy found using nudged elastic band method (NEB) is also shown for the tautomerization reaction.

C.5. Conclusions

Density functional theory calculations were used to determine the transition state for two different mechanisms in the final step of cyclohexene oxidation in forming phenol. It was found that the starting intermediate and the transition state is lower in energy for tautomerization compared to β-H transfer (Figure C.5) indicating that tautomerization should be the preferred mechanism for phenol formation.

C.6 References

[1] E. M. Stuve, R. J. Madix, *Surf. Sci.* **1985**, *160*, 293-304.

[2] R. J. Madix, J. T. Roberts, in *Surface Reactions, Vol. 34*, 1 ed. Ed.: R. J. Madix, [Springer-Verlag: Berlin Heidelberg, **1994**].

[3] X. Xu, C. M. Friend, *J. Am.Chem.Soc.* **1990**, *112*, 4571-4573.

[4] T. Hayashi, K. Tanaka, M. Haruta, *J. Catal.* **1998**, *178*, 566-575.

[5] M. D. Hughes, Y. J. Xu, P. Jenkins, P. McMorn, P. Landon, D. I. Enache, A. F. Carley, G. A. Attard, G. J. Hutchings, F. King, E. H. Stitt, P. Johnston, K. Griffin, C. J. Kiely, *Nature* **2005**, *437*, 1132-1135.

[6] J. T. Roberts, R. J. Madix, *Surf. Sci.* **1990**, *226*, L71-L78.

[7] H. Kochkar, F. Figueras, *J. Catal.* **1997**, *171*, 420-430.

[8] T. Yamakawa, T. Fujita, S. Shinoda, *J. Mol. Catal.* **1991**, *66*, 321-327.

[9] K. Sato, M. Aoki, R. Noyori, *Science* **1998**, *281*, 1646-1647.

[10] M. Rozwadowski, J. Datka, M. Lezanska, J. Wloch, K. Erdmann, J. Kornatowski, *Phys. Chem. Chem. Phys.* **2001**, *3*, 5082-5086.

[11] G. Kresse, J. Hafner, *Phys. Rev. B.* **1993**, *47*, 558.

[12] J. P. Perdew, Y. Wang, *Phys. Rev. B.* **1992**, *45*, 13244.

[13] G. Kresse, J. Joubert, *Phys. Rev. B.* **1999**, *59*, 1758.

[14] CRC Handbook of Chemistry and Physics; 77 ed.; D. R. Lide, Ed. [CRC Press: New York, **1996**].

[15] D. Sheppard, R. Terrell, G. Henkelman *J. Chem. Phys.* **2008**, *128*, 134106.

[16] G. Henkelman, B.P. Uberuaga, H. Jónsson, *J. Chem. Phys.* **2000**, *113*, 9901.

[17] G. Henkelman, H. Jónsson, *J. Chem. Phys.* **2000**, *113*, 9978.

[18] A. Alavi, P. Hu. T. Deutsch, P.L. Silvestrelli, J. Hutter. *Phys Rev. Lett.* **1998**, *80* 3650.

[19] I. Gomez, E. Rodriguez, M. Reguero, *J. Mol. Struct: THEO CHEM.* **2006**, *767*, 11.